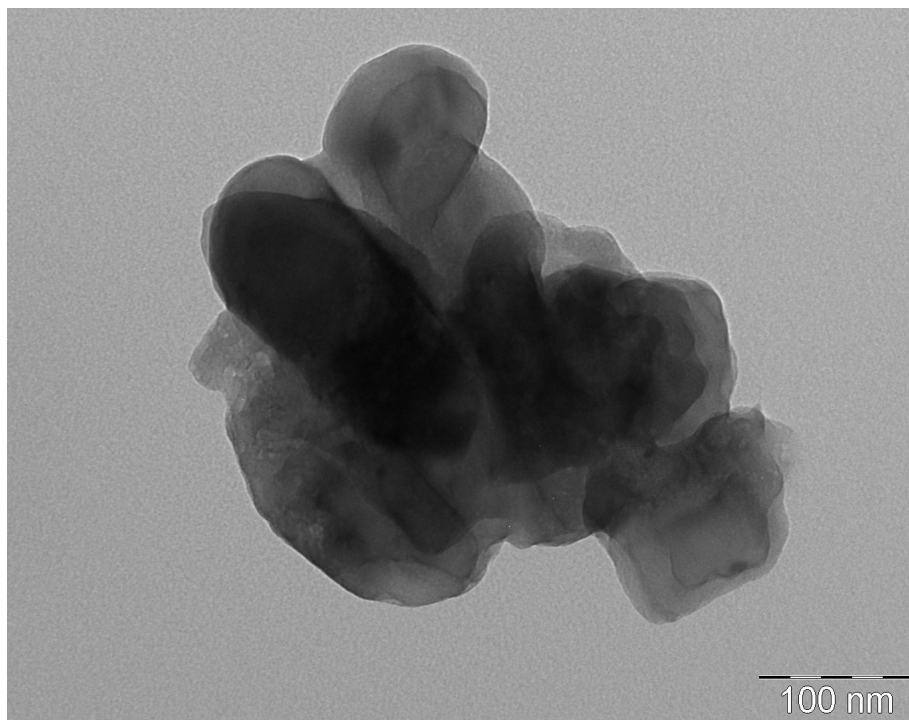




Automotive Brake Materials: Characterization of Wear Products and Relevant Mechanisms at High Temperature

Piyush Chandra Verma



February 23, 2016

Automotive Brake Materials: Characterization of Wear Products and Relevant Mechanisms at High Temperature

Piyush Chandra Verma

E-mail: piyushchandraverma@unitn.it, piyushchandraverma@gmail.com

Approved by:

Prof. Giovanni Straffelini, Advisor
Department of Industrial Engineering
University of Trento, Italy.

Ph.D. Commission:

Prof. Stefano Gialanella,
Department of Industrial Engineering
University of Trento, Italy.

Prof. Ulf Olofsson
Department of Machine Design, School of
Industrial Technology and Engineering
*Royal Institute of Technology (KTH)
Stockholm, Sweden.*

Prof. Maurizio Valle
DITEN - Department of Naval, Electrical,
Electronic and Telecommunications
Engineering,
University of Genova, Italy.

University of Trento,
Department of Industrial Engineering

February 2016

University of Trento - Department of Industrial Engineering
Doctoral Thesis

Piyush Chandra Verma - 2016
Published in Trento (Italy) – by University of Trento

Dedicated with extreme affection and gratitude to:

*My loving family and
my jaan master Aarav Verma*

Abstract

Wear is an ubiquitous phenomenon affecting an extremely wide number of technological system, often determining their premature failure. In this regard, wear and friction behavior of friction materials and the characterization of wear debris from brake disc system is an important step to understand the dominant wear mechanisms active in a given tribological system, in order to improve its performances and to increase the expected lifetime. In the thesis, four tribological task has been performed, under the code name *Case I, II, III & IV*. This thesis present the work on the development of a characterization methodology of a wear debris from brake pad-disc system, M1 and M2 friction materials at elevated temperatures and study of the wear and frictional behavior of a heat treated cast iron disc.

In *Case I*, the dry sliding behavior of two friction materials (M1 & M2) have been investigated. The sliding tests were carried out on a pin-on-disc test rig, using a cast iron disc as a counterface, under mild conditions (the applied nominal pressure was 2 MPa and the sliding speed was 3.14 m/s). The results shows that friction material M2 is characterized by a lower friction coefficient than friction material M1, and the friction coefficient is stable during the test. In addition, friction material M2 shows a lower wear rate than M1. The results were explained by considering the characteristics of the friction layer that is established during the test. On the bases of the experimental observations, the lower friction and wear of friction material M2 was attributed to the formation a quite uniform and well compacted friction layer, due to the presence of ingredients, such as Zr oxides, able to form small particles during sliding that are compacted and held together by the presence of metallic ingredients, such as copper. The absence of Zr-oxides in the formulation of M1 friction material and the presence, in their place, of hard and abrasives Mg, Zn and Al-oxides, impeded the formation of wide covering friction layer, increasing friction and wear. The different frictional properties of the brake pads determine their driving performances, and the different wear behavior determine their in-service deterioration and also their attitude to emit particulate matter in the environment, which is nowadays a concern of increasing importance.

Under the *Case II*, a streamline characterization protocol for wear debris emitted under wear testing conditions (*Case I - M1 friction material*) used for disc brake assemblies is presented. An important aspect of the experimental test methodology concerns the powder collection methodology on different substrates: aluminum foil, for a gravitational integral collection, and polycarbonate filters of an ELPI+ impactor equipment, on which particles are selectively trapped, according to their average size. The protocol is based on the application of different materials characterization tools, like scanning electron microscopy (SEM), energy dispersive X-ray spectroscopy (EDXS), X-ray diffraction (XRD), transmission electron microscopy (TEM) and selected area electron diffraction (SAED). The deliberate aim of the study was to identify suitable selection parameters, like specimen availability and average particle size, for an effective and smart application of the mentioned experimental techniques so to optimize testing times and obtain statistical reliable results. The proposed characterization approach could be profitably employed also in other contexts, like environmental and health monitoring, as far as particulate matter, even from other sources than brake systems, is concerned. We extended the work in *Case I* by investigating further wear mechanisms of M1 & M2 pins at elevated temperatures i.e., 170°C, 200°C, 250°C, 300°C and 350°C, under *Case III*. The results showed a

clear evolution of frictional parameters with temperature. For M1, the working temperature were 155°C, 200°C, 250°C and 300°C, the absence of frictional parameters with temperature and wear behavior of M1 is higher than M2 with one degree higher order of magnitude. Wear tracks on the discs form from the piling up of wear fragments produced both by the tribo-oxidation of the disc itself and from the wearing out of the pin materials. This accumulation of wear debris on the disc surface nearly compensate for the weight loss associated with disc wear. The observed tribological behaviour is very much influenced by the thermal degradation of the phenolic binder of the friction material. The thermal decomposition kinetics was confirmed by thermogravimetric analyses, conducted on purpose on the pin material, and by Raman spectroscopy results, that confirmed the presence of carbonaceous products on the worn out pin surface. For M2, the working temperature were 170°C, 200°C, 250°C, 300°C and 350°C, above 170°C a transition from mild to severe wear was observed. Correspondingly, the friction layers, in particular, the secondary plateaus, which develop on the pins and disc surface during sliding displayed quite different features, as proved by electron microscopy observations and X-ray spectroscopy analyses. As concerns the pins, at 25°C and 170°C, the friction layer consists of primary and well compacted secondary plateaus. At 200°C and above, a progressive reduction of the pin surface coverage by the secondary component of the friction layer and a corresponding thinning of this component are observed. Secondary plateaus are barely present on the samples tested at 350°C. Although referring to rather extreme conditions and simplified sliding conditions, the results obtained in this study provide useful indications on the role that the thermal stability of the organic component may have in determining wear rate in brake systems in which the temperature rise may be induced by actual operational conditions.

The *Case IV* work aims at illustrating the role of conventional heat-treatments on the friction and wear behavior of the above system. Wear rates of both disc and M2 friction material were reduced by almost one order of magnitude when the disc is preliminarily heat-treated and then grinded to remove the surface decarburized layer that forms during the adopted treatment cycle. Heat-treatment and heat-treatment plus ground results in the reduction of the friction coefficient, which was comparatively low for the grounded samples (grinded to remove the surface decarburized layer). The friction and wear behavior along with the contact temperature evolutions were rationalized according to the materials characteristics and the observed wear mechanisms.

Keywords:

Wear testing; debris collection; electron microscopy; single particle analysis; X-ray diffraction; energy dispersive X-ray spectroscopy; wear mechanisms; high temperature wear tests; friction coefficient; severe wear; mild wear; brake materials; degradation phenolic resin; brake systems; sliding wear; friction; contact temperature; cast iron; heat-treatment.

Acknowledgments

The present study was carried out at the Department of Industrial Engineering of the University of Trento during the years 2013–2015. For that, I am grateful to my supervisor, Prof. Giovanni Straffelini, for introducing me to the fascinating and wonderful world of *Friction and Wear* of brake materials and their valuable guidance and support throughout this PhD work. I always felt a real research joy working under him. I am also grateful to Prof. Stefano Gialanella for his characterization classes and his valuable comments, guidance and motivation, during my PhD and believed in me more than I did myself.

A word of thanks to TEM training by Dr. Gloria Ischia and SEM training by Dr. Lorena Maines have been very helpful to carry out this work.

I am also grateful to Prof. Luca Lutterotti for giving me in depth knowledge of XRD and MAUD software. My special thanks are extended to Dr. Rodica Ciudin for all the fruitful discussions on characterization work and SEM lab. work undertaken together.

I would like to express my very great appreciation to Ing. Guido Perricone, Ing. Andrea Bonfanti, Dr. Ibrahim Metinoz, Dr. Vlastimil Matejka, Ing. Mattia Alemani and all research team member out there in Brembo S.p.A R&D laboratory, who made my one week in Brembo S.p.A. a fruitful learning experience.

I express my grateful to Ing. Luca Menapance for helping me always in my thesis and for all funny and valuable discussions that we always made. Thank you! Luca.

In addition, I wish to express my thanks to Prof. Pranesh Aswath, Associate Dean of University of Texas at Arlington (U.S.A.), who gave me opportunity to use his wonderful material science and engineering characterization laboratory and many thanks to all researchers and staff members of UTA. A special thanks to Mr. Vibhu sharma and Mr. Vinay sharma and their friend circle, who made my stay in US unforgettable and pleasant.

Prof. Rajesh Prasad for being a great motivator during his one month research visit in UNITN.

My parents, loving siblings and master Aarav, who always been a true motivation and inspiration.

A lot of people need to be acknowledged also if they did not directly contributed to this research project. They indeed contributed to keep my motivation high, improve myself as a human being and as a researcher and made my life in these past years very pleasant. I would like to say thank you to Dr. Kiran Naik, Dr. Anshu, Dr. Pradnyesh satardekar, Dr. Pradeep Warriar, Dr. Rajesh Pandiyan, Dr. Pushkar Patil, Dr. Subrata Kumar Ghosh, Dr. Prasanta Jana, Dr. Parveen Kumar, Dr. Maitreyi Sur, Dr. Sri Ram, Dr. Raju Edla, Dr. Sanjay Thorat, Dr. Sergey Verlinski, Swati Singh, Arpana Singh, Narges Ataollahi, Pablo Vinicius Lia Fook, Bochra Negri, Babak Omranpour and many more for all their love, support and care. Love you all and thank you so much UNITN.

The research leading to all results in this thesis has achieved funding from the European Union Seventh Framework Programme (FP-PEOPLE-2012-IAPP) under the Rebrake Project, grant agreement no. 324385 (www.rebrake-project.eu).

Piyush Chandra Verma

List of Tables

Table 2.1.1: *Generally classification of brake pads based on metal content and coefficient of friction.*

Table 2.1.2: *General chemical analysis of different forms of disc materials.*

Table 3.1.1: *General features of friction materials ingredients.*

Table 4.1.1: *Different type of braking condition in disc brake system.*

Table 5.1.1: *Brake wear PM and human health effects – summary table.*

Table 6.1.1: *List of problem defined in the thesis and test highlight.*

Table 7.1.1: *Experimental composition measured by X-ray fluorescence spectroscopy (XRF) for M1 & M2 frictional materials.*

Table 7.1.2: *Stoichiometries of the various compounds present in M1 & M2 frictional materials.*

Table 7.3.1: *Characteristic features of Poly Carbonate Filter.*

Table 7.3.2: *List of different stages of ELPI+ with total particle number and total mass (Case II, PC filters-1.39MPa, 13.0m/s).*

Table 7.4.1: *Comparison of two different mode of XRD operation.*

Table 7.4.2: *The following diffraction instrument calibration setup used in MAUD software.*

Table 8.1.1: *Friction and wear data of M1 & M2 frictional materials.*

Table 8.2.1: *Impactor stage specification. For each stage, corresponding to different aerodynamic diameters (D_i), the total number of collected particles and the relevant mass density is measured.*

Table 8.2.2: *List of different phases present in M1-AF and different stages of polycarbonate filter.*

Table 8.2.3: *PC-8 stage_12 sample. Quantitative analyzes of the EDXS data taken from the spectra in Fig.8.4.15.*

Table 8.2.4: *Summary indications about the experimental protocol for wear debris characterization emerging from the present study. ✓ : indicates that the technique can be profitably employed; ✗: unsuitable techniques; ?: TEM observations can be conducted in principle, although imaging may result quite problematic owing to the excessive average thickness of the particles.*

Table 8.3.1: *Wear rates, Average pin temperature and friction coefficient of the M1 and M2 pins at different temperatures.*

Table 8.3.2 : *Quantitative crystallographic analysis results obtained for M1 pin.*

Table 8.4.1: *Average pin temperature and friction coefficient attained after 4000m of sliding.*

Table 8.4.2: *Wear rates of the pin and the discs.*

Table 8.4.3: *Treated disc surface hardness.*

Table 8.4.4: *Chemical composition of the friction layer based on EDXS.*

Table 9.1.1: *Major results highlights of each one of the tribological Cases.*

List of Figures

- Figure 1.5.1:** layout of the main goals of the thesis.
- Figure 2.1.1:** A simple solid body sliding on a surface.
- Figure 2.2.1:** Schematic diagram of disc brake system.
- Figure 2.2.2:** A commercial brake pad friction material.
- Figure 4.3.1:** Mechanisms of abrasive wear: microcutting, fracture, fatigue and grain pull-out.
- Figure 4.3.2:** Two and three-body modes of abrasive wear.
- Figure 4.4.1:** Schematic of the contact situation between an organic friction material and a brake disc and formation of compacted plateaus.
- Figure 4.4.2:** Influence of contact temperature on the wear rate of a friction material.
- Figure 4.4.3:** Schematization of the influence of sliding parameters on the braking conditions.
- Figure 4.4.4:** Summary of the basic wear mechanisms in braking systems.
- Figure 5.1.1:** Schematic representation of the size distribution of atmospheric particles.
- Figure 5.2.1:** The correlation between the proportion of affected population and severity of human health risk associated to exposure to atmospheric particulate matter.
- Figure 6.1.1:** The flow-chart of tribological results of two friction materials.
- Figure 6.2.1:** The flow-chart of the characterization methodology.
- Figure 6.3.1:** High temperature wear test rig.
- Figure 6.4.1:** Highlighting the reason for the heat treatment of the cast iron disc.
- Figure 7.1.1:** Brake pad pins from different frictional materials, M1 and M2.
- Figure 7.1.2:** Microstructure of virgin brake pad materials (a) M2 brake pad where **A:** Potassium titanate fibre, **B:** Tin sulfide and **C:** Resin binder (b) M1 brake pad in which **A:** Steel fiber, **B:** Magnesium oxide, **C:** Tin sulfide and **D:** Area rich in Fe, Mg, Ca and Zn.
- Figure 7.2.1:** a) Optical image of the small cast iron disc, used in case III & IV b) Optical image of the big cast iron disc, used in case I & II, c) Microstructure of the grey cast iron, d) microstructure after etching with 2% Nital + 2% Picral (50-50 vol%).
- Figure 7.3.1:** Simple pin-on-disc machine fundamentals.
- Figure 7.3.2:** Schematic of the test equipment [Olofsson et al., 2009]. **A:** Room air; **B:** Fan; **C:** Flow rate measurement; **D:** Filter; **E:** Flexible tube; **F:** Inlet for clean air, measurement point; **G:** Closed box (Chamber); **H:** Pin-on-disc machine; **N:** Air inside box, well mixed; **J:** Air outlet, measurement points; **L:** Dead weight; **M:** Rotating disc sample; **I:** Pin Sample.
- Figure 7.3.3:** ELPI+ particle collection instrument (a) and (b). Polycarbonate filters with collected particles, (c). Scheme of working principles, (d).
- Figure 7.3.4:** Pin-on-disc equipment with aluminum foil for collecting of wear debris.
- Figure 7.3.5:** Real time and schematic closed loop feedback high temperature wear test setup.
- Figure 7.3.6:** a) Low temperature Pin-on-disc: Frictional heating system with 140mm diameter cast iron disc used in case I. b) High Temperature Pin-on-disc: External heating system with 63.1 mm diameter cast iron disc used in case III.
- Figure 7.3.7:** Infrared camera images of high temperature pin-on-disc at different temperature.
- Figure 7.3.8:** Shows time lag of heating between the heating coils, adapter and cast iron disc.
- Figure 7.3.9:** Tribo-oxidation of cast iron at different high temperature test.
- Figure 7.3.10:** Pin holder with two holes for chromel-alumel-type thermocouples.
- Figure 7.3.11:** Diagram showing T_{sup} which is resultant linear gradient of T_1 and T_2 .
- Figure 7.4.1:** IPD 3000 Diffractometer.
- Figure 7.4.2:** IPD 3000 Diffractometer: transmission mode configuration.
- Figure 7.4.3:** Two different configurations of operation for XRD analyses.
- Figure 7.4.4:** Imaging plate X-ray screen detector / Diffraction pattern of Si standard powder.

Figure 7.4.5: *Different size of incoming X-Ray beam collimators.*

Figure 7.4.6: a) D8 diffractometer, b) position of sample holder, c) Sample holder with M1 brake pad pin.

Figure 7.4.7: *Carbon coating apparatus.*

Figure 7.4.8: *Carbon sputtered samples for SEM observation. In this case, a graphite disc substrate was also present on each SEM stub.*

Figure 7.4.9: *Switching valve for high vacuum (HV) or low vacuum (LV=ESEM) SEM operational modes.*

Figure 7.4.10: a) *Ultrasonic bath. Beaker containing ethanol and small piece of filter. b) TEM instrument with EDXS.*

Figure 7.4.11: a) *A thermo scientific DXR Raman spectrometer, b) wear debris Raman analysis, c) worn pin surface Raman analysis.*

Figure 8.1.1: *Coefficient of frictional of M1 and M2 at 25°C temperature*

Figure 8.1.2 : *Shows the height loss difference and weight loss difference between the two brake pad.*

Figure 8.1.3: *SEM images of the M2 brake pad worn surfaces rubbed against cast iron rotating disc.*

Figure 8.1.4: (a) *Energy dispersive X-ray spectroscopy analysis of the third layer formed on the worn surface of M2 brake pad pin when tested against rotating cast iron disc.*

Figure 8.1.5: *SEM images of the M1 brake pad worn surfaces rubbed against cast iron rotating disc.*

Figure 8.1.6: *Energy dispersive X-ray spectroscopy analysis of the third layer formed on the worn surface of M1 pin when tested against rotating cast iron disc at different location named 1 & 2.*

Figure 8.1.7: (a) *Nano wear debris particle of M2 brake pad. (b) Process diffraction – identification of iron oxide and zirconium oxide as a major phases present in fig. 8.1.6a. (c) EDX analysis of fig.8.1.6a M2 brake pad wear debris. (d) Electron diffraction patterns (SAED) corresponding to nanocrystalline wear debris fig.8.1.6a. The diffraction pattern shows concentric rings corresponding to Fe_2O_3 , Fe_3O_4 and ZrO_2 .*

Figure 8.1.8: *X-ray diffraction of M2 brake pad's wear debris powder (bulk) placed in a 0.5 mm capillary tube diffracted in transmitted mode.*

Figure 8.1.9: (a) *Nano wear debris particle of M1 brake pad. (b) Process diffraction – identification of mixed phase of magnesium oxide, tin oxide and iron oxide as a major phases present in fig. 8.1.8a. (c) EDX analysis of fig. 8.1.8a M1 brake pad wear debris. (d) Electron diffraction patterns (SAED) corresponding to nanocrystalline wear debris fig. 8.1.8a. The diffraction pattern shows concentric rings corresponding to Fe_3O_4 , SnO_2 and MgO .*

Figure 8.1.10: *X-ray diffraction of M1 brake pad's wear debris powder (bulk) placed in a 0.5 mm capillary tube diffracted in transmission mode.*

Figure 8.1.11: *Wear mechanism involved in dry sliding of friction materials (M2 & M1) at higher temperatures.*

Figure 8.2.1: *Experimental imaging plate XRD ring pattern of AF-M1 sample.*

Figure 8.2.2: *Experimental (blue dots) and modelled (continuous black line) XRD spectrum patterns of AF-M1 sample. Main diffraction peaks of identified phases are marked in the graph.*

Figure 8.2.3: (a) *Experimental imaging plate XRD ring pattern of stage_12 of PC-M1. (b) Experimental (blue dots) and modeled (continuous black line) XRD spectrum patterns of stage_12 of PC-M1. Main diffraction peaks of identified phases are marked in the graph.*

Figure 8.2.4: *Experimental (blue dots) and modelled (continuous black line) XRD spectrum patterns of stage_15 of PC-M1 sample. Main diffraction peaks of identified phases are marked in the graph.*

Figure 8.2.5: *X-ray diffraction spectrum of powders collected on polycarbonate filters.*

Figure 8.2.6: *SEM images of pin-on-disc wear debris of AF-8.*

Figure 8.2.7: *EDAX spectrum (a) ultrafine particle of fig.8.2.6a, (b) full frame of coarser particles of fig.8.2.6c.*

Figure 8.2.8: *SEM Images showing different stages of PC-8.*

Figure 8.2.9: *EDAX spectrum (a) agglomerated particles of fig.8.2.8a, (b) full frame of coarser particles of fig.8.2.8e.*

Figure 8.2.10: *Average elemental wt % of different stages of polycarbonate filters and aluminum foil.*

Figure 8.2.11: *TEM image (a) and relevant SAED of sample AF-M1. (c) Process Diffraction analysis of the same SAED pattern showing the imaged particles contain iron (red) and magnesium (green) oxides.*

Figure 8.2.12: (a) *TEM image of stage_03 of PC-M1. SAED of the same field of view as fig.8.2.12(a). (e) Process Diffraction of the airborne particle of stage_03 of PC-M1 showing Fe_2O_3 phase. (c) TEM image of stage_12 of PC-M1.*

SAED of the same field of view as fig. 8.2.12 (c). (f) Process Diffraction of the airborne particle of of stage_12 of PC-M1 showing Fe_2O_3 phase.

Figure 8.2.13: SAED (left) and XRD (right) patterns for PC-M1 stage_12 sample. In the SAED in green reference lines for Fe_2O_3 . As concerns the XRD pattern, the main diffraction peaks of identified phases are marked.

Figure 8.2.14: Intersection diagram for SAED and XRD results of sample PC-M1 stage_12 sample.

Figure 8.2.15: PC-8 stage_12 sample TEM (left) and SEM (right) wear debris and relevant EDX spectra. In both spectra the main detected elements are indicated. Gold lines in EDXS-TEM spectrum are due to carbon coated gold grid used for sample preparation.

Figure 8.3.1: TGA curves of friction materials M1 & M2 in air.

Figure 8.3.2: Evolution of the friction coefficient of M2 & M1 friction materials. extrapolated contact temperature of pins measured by thermocouple at 6mm and at 4mm.

Figure 8.3.3: Specific wear behaviour of M1 and M2 friction materials pin at different temperatures.

Figure 8.3.4: SEM of worn surfaces of M2 (part-I) and M1(part-II) friction materials pins at different elevated temperature.

Figure 8.2.5: Average elemental composition of wear debris on M2 & M1 worn pin surfac-planar view.

Figure 8.3.6: Raman spectra of decomposed phenolic resin at different temperatures.

Figure 8.3.7:(a) Lorentzian curve fit for the deconvoluted Raman spectra of black carbonaceous product of high temperature frictional test at 25°C, (b) 250°C and (c) 300°C.

Figure 8.3.8: SEM observation of disc surface of M2 (part-I) and M1(part-II) at different temperatures.

Figure 8.3.9: Average elemental composition of wear debris on M2(a) & M1(b) disc surface respectively.(c) & (d) profilometry profile of worn cast iron disc of M2 at different temperatures.

Figure 8.3.10: Cross section of worn pin surfaces of two friction materials M2 (part-I) and M1(part-II) at different temperatures.

Figure 8.3.11: Average elemental composition of wear debris on M2 cross section surfaces.

Figure 8.3.12: Comparison of XRD spectra acquired on samples M1-155°C, M1-200°C, M1-250°C and M1-300°C.

Figure 8.3.13: Maud Rietveld fit relative to sample M1 – 250°C with the identification of the most relevant phases.

Figure 8.3.14: Comparison of Raman spectroscopy at secondary plateaus of a worn brake pad pin surface under different working temperature.

Figure 8.3.15: Wear mechanism involved in dry sliding of friction material (M2) at higher temperatures.

Figure 8.3.16: Wear mechanism involved in dry sliding of friction material (M1) at higher temperatures.

Figure 8.4.1. a) Martensitic microstructure of heat treated disc, b) The decarburized surface of the heat treated disc.

Figure 8.4.2: Evolution of the friction coefficient (a) and of the average contact temperature (b) during wear tests.

Figure 8.4.3: Surface profile across the wear track of heat treated disc.

Figure 8.4.4: Comparison of specific wear coefficient, K_w of the M2 pin and different discs.

Figure 8.4.5: SEM micrographs of the wear tracks on the pin surface after sliding against the untreated (a), the heat-treated (b) and the heat treated and grinded disc (c).

Figure 8.4.6: SEM planar view of the wear surface of the untreated cast iron disc. The picture shows a region where the graphite lamellae emerge (region 1) at the surface and there is an accumulation of wear fragments from the friction material (region 2).

Figure 8.4.7: Cross sectional SEM micrographs of the friction layer on the pin after sliding against the untreated disc. Low (S_x) and higher (D_x) magnification.

Figure 8.4.8: Cross sectional view of the pins against a) Heat treated, b) Heat treated and ground.

Figure 9.1.1: Reliable combination of characterization tools for particulate matters.

Figure 9.1.2: Flow chart describing major findings of each one of the tribological Cases.

Contents

Abstract [i]
Acknowledgments [iii]
List of Tables [iv]
List of Figures [v]

I Introduction

1. Introduction [1]

- 1.1. Introduction [1]
- 1.2. Brake-disc system and wear particle emission: Background [1]
- 1.3. Motivation [5]
- 1.4. Research goals [6]
- 1.5. Organization of the thesis [7]
- 1.6. Major contributions of the thesis [10]

2. Characteristics of Braking Systems [11]

- 2.1. Introduction [11]
- 2.2. Disc brake system [12]

3. Braking Pad Materials (General Features of Friction Material Ingredients) [17]

- 3.1 Introduction [17]
- 3.2 Dry friction materials [17]
- 3.3 Future trends in frictional materials [20]

4. Wear Mechanisms in Pad-Disc Braking Systems [21]

- 4.1. Introduction [21]
- 4.2. wear models [21]
- 4.3. Basic Wear Mechanism [22]
- 4.4. Wear Mechanism in Pad-Disc Braking Systems [27]

5. Particulate Matter: Hazard and Risk [32]

- 5.1. Introduction [32]
- 5.2. Effect of particulate matters on human health [33]

II Aim of the work

6. Defining Problems [36]

- 6.1. Tribological behavior of two low steel friction materials (M1 & M2) at room temperature [37]
- 6.2. Characterization of wear particles from M1 friction material [38]
- 6.3. Role of friction layer in the high temperature pin-on-disc study of M1 & M2 friction materials [39]
- 6.4. Role of the heat-treatment of the cast iron disc in dry sliding wear of the brake pad-disc system [40]

III Experimental methods and materials

7. Experimental Procedures and Characterization Tools [41]

7.1. Frictional Materials - M1 & M2 [41]

7.2. Cast iron disc counterpart [43]

7.3. Pin-on-Disc (PoD) tribometer [44]

7.4. Characterization tools [56]

IV Results and Discussions

8. Results and Discussions [65]

8.1. Tribological behavior of two low steel frictional materials (M1 & M2) at room temperature [65]

8.1.1 Friction and wear behavior [65]

8.1.2 Analysis of worn surfaces of M1 & M2 (SEM-EDXS) [67]

8.1.3 Analysis of wear debris (TEM-SAED and XRD) [69]

8.1.4 Wear mechanisms at room temperature [72]

8.2. Characterization of wear particles from M1 frictional material [75]

8.2.1 X-ray diffraction results [75]

8.2.2 Scanning Electron Microscopy -Energy Dispersive X-ray Spectroscopy [80]

8.2.3 Transmission Electron Microscopy - Energy Dispersive X-ray Spectroscopy
- Selected Area Electron Diffraction [83]

8.2.4 Discussion on the characterization methodology [86]

8.3. Role of friction layer in the high temperature pin-on-disc study of M1 & M2 friction materials [91]

8.3.1 Thermal behaviour of M1 & M2 friction materials [91]

8.3.2 Friction and wear behaviour of M1 & M2 friction materials [92]

8.3.3 SEM observations of high temperature worn surfaces of M1 & M2 friction materials pins [97]

8.3.4 Raman spectroscopy of black spot at higher temperatures [103]

8.3.5 SEM observation of high temperature worn surfaces of M1 & M2 cast iron discs [105]

8.3.6 SEM of cross-sections of M1 & M2 pins - evolution of frictional layer with temperature [109]

8.3.7 Additional information of M1 pin at higher temperatures [112]

8.3.8 Wear mechanisms at high temperature [116]

8.4. Role of the heat-treatment of the cast iron disc in dry sliding wear of the brake pad-disc system [120]

8.4.1 Friction and wear behaviour of heat-treated cast iron disc [120]

8.4.2 SEM observation of the wear tracks on heat-treated cast iron disc [123]

V Conclusions

9. Concluding Remarks [128]

9.1 Conclusions [128]

9.2 Future developments [134]

VI Appendices

Appendix A: Abbreviations and definitions [135]

Appendix B: List of scientific publications [136]

Appendix C: Participation to conferences, schools and workshops [142]

Appendix D: Research internships [146]

References [148]

Chapter 1

Introduction

1.1 Introduction

These days, modern automobiles have disc brakes systems on the front wheels and brake drums on the rear wheels but there is a growing trend to have disc brake system on the rear wheels as well. The main purpose of a disc brake is to slow down a vehicle by transform the kinetic energy of the vehicle into thermal energy by friction between pad materials and metal, usually cast iron, disc [Straffelini et al.,2015]. Brakes dissipate energy by converting rotational motion into heat. Disc brakes slow the rotational motion of automobile wheels with friction caused by a brake pad pushing against a brake disc. Heat is then dissipated through exchange mainly with the outer environment, although during braking, temperature may rise tremendously in the contact regions. During this operation, both brake pad and counterface disc wear out, releasing huge amount of wear debris or particulate matters in the surrounding atmosphere. Particulate matter also known as particle pollution or PM, is a complex mixture of extremely small particles and liquid droplets in a range of micron to nano level. Particle pollution is made up of a number of components such as, organic chemicals, metals, and soil or dust particles. This chapter discusses the major contributions of the different researcher in the field of brake pad-disc system. The importance of addressing the potential health effects of the PM particles has been introduced. This chapter also includes the motivation for the work reported in this thesis, research goals, the major contributions of this thesis and synopsis of all the chapters of this thesis.

1.2 Brake-disc system and wear particle emission: Background

Brake pads are an important part of braking systems for all types of vehicles that are equipped with disc brakes. The real development of the braking system dating from the early nineteenth century, with the advancement of the railways, it passes from a brake system of wood against the steel rail. With the birth of the automobile, the birth of the drum brake and brake pad friction materials took place.

With new advanced technology in manufacturing of brake pad friction materials, we have many advantages and choices in the market today i.e., non-asbestos organic (NAO), semi-metallic, and low metallic. According to Sanders et al.,2003, non-asbestos organic brake pads exhibit relatively low brake noise and wear rates, but lose tribological properties at high temperature. Semi-metallic brake pads have a high steel fiber and iron powder content and low wear, but are noisier. High abrasive content in low-metallic brake pads which makes high friction and good braking capacity at high temperatures.

The performance of the brake is mainly controlled by the composition and microstructure of the pad material. Industrial pads usually contain a large number of different constituents like ceramic particles and fibers, minerals, metallic chips, solid lubricants and elastomers, all bound by, for instance, phenolic resin [Osterle et al.,2001]. Infact brake material should maintain a relatively high, stable and reliable friction coefficient at a wide range of braking conditions, temperature, and humidity. But during braking or extreme forced deceleration, the highest concentration of brake wear particles emitted into the atmosphere. Due to "open" design of automotive disc brake, environmental factors have access to the tribological friction zone. During braking operation, both brake pad and counterface disc wear out, releasing huge amount of wear debris in the surrounding atmosphere. P. Filip et al.,2010, conducted a dynobench test and compared the commercial low-metallic brake pad with other modified NAO brake pad having natural fibers, potassium titanate and alumina, without having copper and other potentially hazardous materials and got very promising results in terms of friction and wear behavior which open the door of possibilities to replace the ingredients of commercial brake pads with natural fibers, although further research needed in this direction. Another researcher, Osterle et al., 2010, has shown that macro-particles of copper have the capability to support the contact site (plateaus) in a same way as the reinforcing fibres do and at higher temperatures copper inclusions takes places in the friction layer and copper particles with certain concentration in the friction layer improves the wear behavior.

Following the work of P. Filip et al.,2010, Vlastimil Matejka et al.,2013, developed two eco friendly friction materials containing jute fibres and combination of jute fibres with hazelnuts shells, when properly combined, shown significantly improvement in the friction and wear behaviour of the prepared friction materials, although they were having low thermal stability. P.Filip et al.,2013, has studied the friction and wear behavior of Cu-free and Sb-free environmentally friendly automotive brake friction materials and found Cu-free and Sb-free friction materials exhibit excellent brake fade property at higher temperature but has a higher wear rate when compared to the baseline material which has fully developed and stable friction layer.

The main factor responsible for particle production is the generation of shear forces by the relative movement of surfaces, when brakes are employed to decelerate the vehicle. A secondary mechanism involves the evaporation of organic compounds of the pads and disc at the high temperatures developed during contact. Mechanical abrasion generates particles of larger sizes, whereas brake pad materials contribute to the smaller particle size fractions by volatilisation and condensation.

Garg et al.,2000, found out that mechanically generated particles are generally relatively large but a surprisingly high proportion of the emitted particles had an aerodynamic diameter $< 0.1 \mu\text{m}$. This might be due to the high temperature produced during the brake process. It is possible that the heat enables brake pad and lining materials to volatilize during the braking event, which followed by condensation in the air stream, results in small particles. The results also revealed that the number of particles emitted in the brake process increases with temperature. These hazardous wear debris need to be addressed in order to reduce their potentially hazardous effects on human health and, in general, on the environmental conditions. Similar finding has been illustrated by Osterle et al.,2007, in which he mentioned that fragmented oxide layer of the friction material remains on the pad and the disc, whereas the rest wear debris released into the atmosphere. Another researcher J. Wahlstrom et al,2008, has found the measured mean particle

number and mass diameters of airborne particles were $0.39\mu\text{m}$ and $1.5\mu\text{m}$, respectively when conducted a field test in urban traffic area of Stockholm using low metallic brake pad and gray cast iron rotor as a counterpart.

P. Filip et al., 2008, demonstrated a research work in that different varieties of particles were released during the wear of friction materials and nanoparticles were also associated with the wear debris generated during friction process. S. Abbasi et al., 2012, demonstrated the wear test of organic brake pad material using pin-on-disc and identified three particle size regimes i.e., ultrafine particle region (dia. 70-120nm), fine particle region (dia. 500-600nm) and coarse particle region (dia. 3-6 μm).

J. Kukutschova et al., 2009, have shown the environmental and biological threat of wear debris emitted from tribological process. According to her study, wear debris were toxic in nature, killing bacteria cells and changing DNA of the bacterial cells after metabolic activation. The authors have also shown wear debris has similar chemistry as friction layer on the worn brake lining. Since wear debris produced during friction represents potential hazard to environment. Therefore it is very important to characterize the wear debris released during friction operations.

An important and better understanding of wear phenomenon during tribological operation can be achieved by modeling and simulation methodology of the brake pad-disc system. In this context's, G.P. Ostermeyer et al., 2003, 2006, 2007, with the help of cellular automata model, demonstrated better understanding of friction dynamics and surface topography in three dimensions in brake-disc system. J. Wahlstrom et al., 2009, 2010, 2011, has shown that pin-on-disc machine can be used to measure the concentration and size distribution of airborne wear particles generated from disc brake materials and further shown the ability to rank different pad-disc combinations with respect to the concentration of airborne wear particles and these wear particles were rich in metals like iron, copper and tin. He also proposed, with the help of finite element software, a simulation methodology that numerically determines the size distribution and concentration of wear debris generated from pin-on-disc machine. U. Olofsson et al., 2009, presented a new model for the number of wear particles generated by the sliding contact. The model proposes three different particle coefficients that associated with three particle regimes (ultra fine particles, fine particles and coarse particles) with distinct number peaks. Therefore, all these studies cooperates to the better understanding of the different phenomenon occurring in brake system.

Another aspect of the wear debris, if we see it from the angle of wear behavior of brake pad-disc system, is the entrapment of wear debris in between the sliding surfaces i.e., brake pad and counterpart disc [Wirth et al., 1994, Jiang et al., 1995, 1997, 1998, Straffelini et al., 2001] which helps in the formation of the so-called friction layer, friction film or third layer, that is paramount in determining the friction behavior of the brake pad-disc mating surfaces in sliding contact [Filip et al., 2002, Osterle et al., 2004].

Jacko et al., 1987 concluded that “when stable friction films, commonly called friction layers, are readily formed for a given friction couple, a stable friction level and low wear rates can be maintained at various temperatures, as long as the friction film is not destroyed”. The wear processes that occur at the pad and disc interface, display several steps, including the formation of the primary plateaus, formed by tough metallic fibers and large, hard particles and secondary plateaus, that build up for the compaction of the wear debris blocked by the primary plateaus. The wear behavior of brake systems is thus influenced by the formation of the friction layer

[Anderson et al.,1987], its transformation related to its compactness and thickness, and finally, by its possible detachment with consequent release of fragments and wear debris [Osterle et al.,2004, Bode et al.,2014]

Eriksson et al.,1999, investigated the connection between brake pad surface topography. The results showed the presence of contact plateaus flat areas rising a few micron over the rough surrounding after the sliding action of the pads against the cast iron disc. In 2000, Eriksson and co-workers have shown the comprehensive study of the formation, mechanical properties and composition of the tribological surfaces of an organic brake pad against a grey cast iron disc. It was shown that the primary plateaus are the nucleation sites for the secondary plateaus which are formed by compaction of wear debris near the primary plateaus. It was also shown that the contact plateaus are continuously worn or fragmented and rebuilt. This rebuilding of plateaus is due to the particles flowing through the narrow channels formed between the contact plateaus. In his observation he showed that the formation of plateaus is more near the reinforcing fibres and abrasive particles. In the same context, Osterle et al., 2006, has shown that there is existence of the friction layer at the friction material and counterpart disc and comprises of a nanocrystalline microstructure which helps further in investigating the wear behavior. He also mentioned that the tribological oxidation plays a major role in debris production and third layer formation. A nanocrystalline oxide layer (friction layer) is necessary to have stable tribological behavior.

One of the critical factor which promote the wear rate and hence the particulate matters in the atmosphere is the working 'Temperature' of the brake pad-disc system. Wear behavior of a brake pad materials at elevated temperatures resulting from the braking conditions, is highly dependent on the ingredients of the friction materials. These are to be selected in order to guarantee suitable braking conditions, high temperature stability and, consequently, reduced wear rates. However, at high temperatures, the degradation of friction material is a major issue, mostly associated to the thermal decomposition of phenolic resins (thermoset polymer). These thermosetting resins are widely used as binders for friction materials [Jacko et al.,1984, Anderson et al.,1987, Tayeb et al.,2006,]. They embed the ingredients effectively over most of the operational regimes, thanks to a good combination of mechanical properties, such as high hardness, compressive strength, creep resistance, and very good wetting capability with respect to most of the ingredients of the friction material. However, these resins are sensitive to heat and humidity, which cause serious threat to friction, wear behaviour at elevated temperatures, notwithstanding the common practice to add to the formulation suitable, carbon-based stabilisers, like graphite, coal or coal coke [Seong et al.,2001, Gurunath et al.,2007]. Therefore, binder decomposition is blamed for various brake operational problems, with specific studies displaying the importance of the heat resistance and mechanical strength of the binder in the wear behaviour of brake materials. Thermal decomposition of the phenolic resins involves several reactions, depending on the actual formulation and thermal history of the material. Temperatures falling in the 250°C - 475°C interval are reported for the onset of the main transformations involved with the resin decomposition [Ramousse et al.,2001, Bode et al.,2014]. P.Filip et al.,2004, and co-authors have demonstrated that in addition to temperature another key role in the phenolic resin degradation at higher temperature in friction process is the elimination of formaldehyde by metals particles and their oxides (note that formaldehyde serve as a important curing agent for resin). G.P. Ostermeyer et al.,2014, modeled the effect of temperature field in organic friction materials and made calculation on the basis of finite difference method shown that flow of energy between the brake pad and disc was not constant over time, although disc contributes most of the energy

sharing. The results shows that under severe braking, decomposition of the brake pad component can occur only at the pad surface, although oxidation of coke has been noticed away from the contact zone. The results highlighted that thermal degradation of phenolic resin was a slow occurring process.

Other researcher J.R. Laguna et al.,2015, conducted a reciprocating tests on the surface of the friction material and shown that the major wear mechanism was delamination of filler particles from the organic binder, supported by local degradation of the phenolic resin during high temperature test.

The optimal performances of the pad-disc braking system depend on the properties of the friction material and also the counterface disc [Anderson et al.,1992]. S. Abbasi et al., 2012, has shown that the emission rate of ultrafine particles from cast iron disc is far more than the organic brake friction material, using pin-on-disc machine. During braking, the kinetic energy of the moving vehicle is converted into thermal energy. The disc provides a correct friction coefficient during sliding against the friction pad. Moreover, it ensures an important contribution to the cooling of the system, since the largest fraction of the frictional heat abandons the system through the disc [Day et al.,2014].

Nevertheless, the counterface pearlitic cast iron disc greatly contributes to the overall wear of the braking system [Anderson et al.,1992, Staffelini et al.,2013], and recent investigations have actually shown that the wear of the discs contributes to a major extent to the emissions in the environment of particulate matter [Sanders et al.,2003]. This was confirmed by a number of research projects, reporting large amount of particle release, mostly originating from the wear of the cast iron rotors and concerning specifically particles with an average size below 20 μm [Sanders et al.,2003].

So far, we have seen most experimental investigations on the reduction of the wear in pad-disc braking system have been focused on the optimization of the friction pad material, by selecting suitable ingredients and relevant concentrations. Thornton et al.,2011, have recently shown that a deep cryogenic treatment may increase the wear resistance of pearlitic cast iron when sliding against a bearing steel counterface. Also, conventional heat-treatments have reported to increase its dry sliding wear resistance against a steel counterface [Haseeb et al.,2000]. These treatments include the usual quenching plus tempering treatment and the austempering treatment, typically carried out to obtain a ductile cast iron material [Hirasata et al.,2007, Staffelini et al.,2011]. The experimental results are quite promising and provide solid indications that an excellent wear performance can be achieved by adopting a treatment inducing the formation of hard phase in the alloy matrix, which creates the conditions for a mild tribo-oxidative wear and shifts to highest loads the occurrence of a severe adhesive wear [Staffelini et al.,2015].

1.3 Motivation

The motivation behind the present work was the realization of the hazardous wear debris, generated during tribological test of brake pad-disc system, which need to be addressed and characterized in order to reduce their potentially hazardous effects on human health and, in general, on the environmental conditions. In contexts to this, Garg et al.,2000, performed dynamometer experiments on the most common brakes used in the US and concluded that 86% of the emitted particles were PM_{10} , 63% was $\text{PM}_{2.5}$ and 33% was $\text{PM}_{0.1}$, also were reported mass

median diameters in an average of 1.49 μm and Sanders et al.,2003, found that variations in particle size distributions between brake lining materials of different type were small but the mass of particulate matter emitted during braking was highly dependent on the lining material used. PM_{10} accounted for 80% of the mass of emitted particles, with only 2% present as PM_1 . For this reason, one of the main guidelines for the development of new friction materials for disc brake systems for road vehicles is the reduction of wear and wear debris release. In this respect, the study of wear products from real brake assemblies is providing not only paramount information to understand the main active wear mechanisms, but also data on potential health and environmental threats that brake contribution to atmospheric PM may have [Riediker et al.,2004, Denier et al., 2013]. According to Osterle et al.,2007, the analysis and assessment of wear debris from brake pad-disc system will be a great challenge for future research in respect to environmental and health issues. J. Kukutschova et al.,2010, performed a dynobench test on semi-metallic friction material and shown that wear debris collected displayed a wide spectrum of coarse-nano particle size. The authors also recommended for refinement of combined analytical techniques for wear debris generating from friction tests. Thus, a need for analysis and assessment of wear debris gave us motivation to establish an experimental protocol suitable for characterizing particles coming from laboratory pin-on-disc wear tests, involving brake disc materials, which includes the refined combination of several analytical techniques which give us fast, reliable and streamline characterization of wear particles and airborne.

1.4 Research goal

During my PhD research project, I have been working on a topic, which has a goal to understand the wear mechanisms in the disc-pad braking system with the aim of reducing the particulate matters emissions

To do so, pin-on-disc tests has been conducted at low and high temperatures. We also developed a multi-analytical characterization approach of the wear debris and worn surfaces, in order to provide reliable, effective and meaningful results. The aim of this study was to establish an experimental protocol suitable for characterizing particles coming from laboratory pin-on-disc wear tests, involving brake disc materials, collected on different substrates. The formation mechanism of the primary and secondary plateaus have to be elucidated and also the wear behavior of the friction materials pins at different temperatures along with different heat treated cast iron disc at normal temperature were investigated.

X-ray diffraction measurements were carried out on powder specimens and worn pin surface. Collected data were then analyzed with MAUD software using a full pattern fitting procedure based on the Rietveld method. Scanning electron microscope (SEM) equipped with energy-dispersive X-ray spectrometer (EDXS) was used to reveal morphology and to identify the different constituents of the wear debris and worn surface topography of the friction materials pins. Transmission electron microscopy (TEM) combined with selected area electron diffraction (SAED) and EDXS was employed to investigate the microstructure, crystallographic phases and composition of wear particles, involved in the study required specific sample preparation procedures.

1.5 Organization of the thesis

A brief synopsis of each of the chapters of this thesis is included here below:

Chapter 1 deals with the introduction of the thesis with goal, motivation and contributions of this thesis work in detail. It also includes a discussion on the particulate matters emission, their side effects and importance of brake pad materials revision, in particular the need of lowering down the brake pad-disc wear debris emissions, by cooperating the research and development in the brake field. *Chapter 2* deals with the characteristics of real automobile braking systems. This chapter will help to understand how brake system actually work. *Chapter 3* discusses the material ingredient used in the manufacturing of brake pad friction materials. This chapter includes a detailed discussion on the general features of friction materials ingredients. *Chapter 4* provides general information on the wear mechanisms during dry sliding. This chapter also brings out the importance of understanding wear mechanism as they are directly linked to the size and shape of the released particulate matters of friction materials. *Chapter 5* presents the over view of environmental impact of released particulate matters, their different sources and their effect on human health, in particular the hazard and health risk associated with the different size and shape of the particulate matters (wear debris). *Chapter 6* discusses the main research work encounter in this thesis. We have tried to develop a characterization protocol for the particulate matters specially wear debris originating from automobile brake pad system to understand wear mechanism and further to improve in particular, the brake pad system for lesser side particulate emission. In this chapter we have addressed four critical aspect in which how a brake pad-disc system release rate can minimize.

Figure 1.5.1 is a flowchart showing the main steps of the experimental work. In *Case I*, an experimental work has been done to compare and investigate the tribological properties of two commercial brake pad friction materials named M1 and M2. The Pin-on-disc rig has been used for tribological testing and evaluation. A gray cast iron rotating disc has been used in all friction (pin-on-disc) testing. The working condition for both the friction materials, M1 and M2 was effect of constant contact pressure load (2MPa) and a constant sliding speed of 3.14 m/s up to 50 minutes of run at room temperature.

In the second case, named *Case II*, we have discussed the reliable characterization protocol to study wear products involved in disc brake materials. The goal was to optimized way, based on the kinds of available samples, instrumentation and related methodologies in order to get comparatively fast responses useful to identify wear mechanisms and, thereby, improve materials properties from the functional and environmental point of view. The particulate matters generated here were in normal conditions i.e., frictional heating, low load. We want to understand the wear mechanism in brake pad-disc system at higher temperature, which results in the ambitious high temperature experiment work named *Case III*.

In the third case, *Case III*, of the thesis is dedicated towards the wear mechanism of friction materials (M1 & M2) at elevated temperatures, in particular the role of binder at high temperature and wear mechanism at elevated temperature, which directly help in understanding of wear at high temperature during extreme braking condition and the role of friction layer were also investigated.

The fourth part, *Case IV*, is devoted to the heat treatment of the counterpart i.e., cast iron disc and investigation of dry sliding wear behaviour of heat treated cast iron disc. This investigation

has been restricted to material M2, i.e., the material that displayed the lowest wear rate in the tests at room temperature (Case I).

Chapter 7 present the general elemental composition of the friction materials used in this thesis to investigate the dry sliding wear behavior of the friction materials and also focus on the different type of characterization tools used for all above mentioned conditions. *Chapter 8* provides the results and discussion on the main important finding of this whole investigation (*Case I, II, III and IV*). *Chapter 9* gives the conclusion detailing the overall implications of the methodologies introduced in this thesis and recommendations for future work are also presented in this chapter.

In the appendices, abbreviations and definitions and a list of the paper published by myself and co-authors during my PhD course are provided in the last appendix.

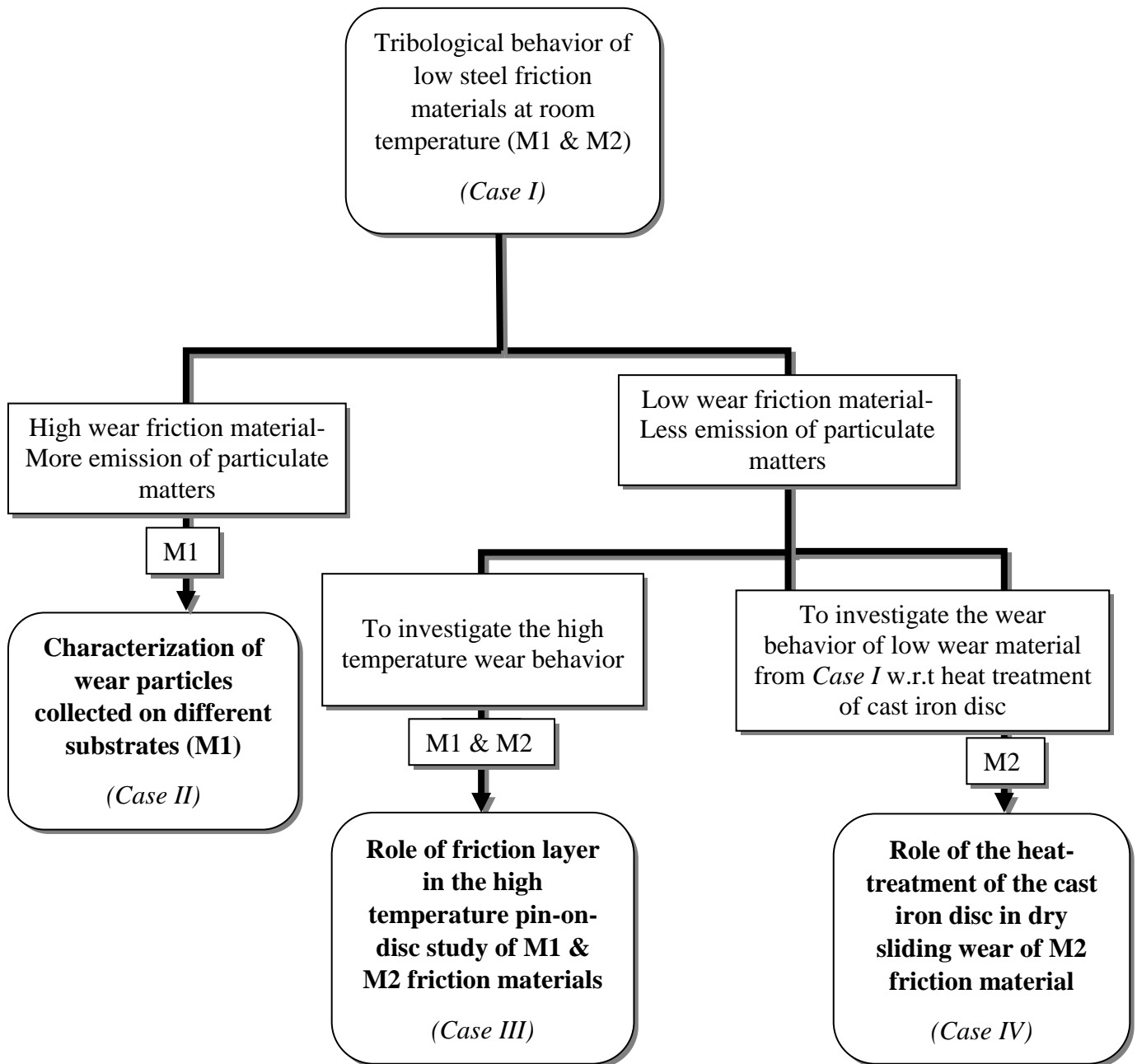


Figure 1.5.1: layout of the main goals of the thesis.

1.6 Major contributions of this thesis

This thesis contributes various scientific information regarding dry sliding of friction materials for the effective enhancement and friction materials development for the brake community. The thesis also incorporates many experimental basis for improvement in performance of friction materials and reduction in wear, which results lowering of particulates matter emissions from disc brake system.

Some of the major contribution that this thesis work will going to present is:

- A characterization protocol has been developed for effective, reliable and comparatively fast responses useful to identify wear mechanism and, thereby, improve materials properties from the functional and environmental point of view.
- Investigated compositional and dimensional range of wear debris.
- Wear and frictional behavior of friction materials pin at higher temperature.
- Role of friction layer in dry sliding of friction materials at higher temperature.
- Role of heat-treatment of a cast iron disc in dry sliding against a low-metallic friction material.
- Understanding of wear debris mechanism at high temperature by characterization of friction layer.
- Wear mechanism of friction materials at elevated temperatures.

Chapter 2

Characteristics of Braking Systems

2.1 Introduction

The presence of a braking system is an essential part in any automobile. It has four basic functions:

- It must slow a moving vehicle.
- It must bring a vehicle to a stop.
- It must hold a vehicle stationary when stopped.
- It allows directional control during maximum braking.

If the brake system does not operate properly, the driver and passengers could be injured or killed in an accident. The main important phenomenon occurring during braking is the friction between the brake pad and counterpart cast iron disc. Friction expresses the resistance to motion during sliding and experienced when one solid body moves tangentially over another solid body (tribological coupling). The resistive tangential force, which acts opposite to the direction of motion, is called the friction force. As illustrated in Fig. 2.1.1, a tangential force ' F_T ' is required to move the solid body over the stationary counterface at a given sliding speed. The ratio between the tangential force (friction force) and the normal load ' F_N ' is known as the *coefficient of friction*, generally represented by ' μ ':

$$\mu = F_T / F_N \dots\dots\dots(2.1)$$

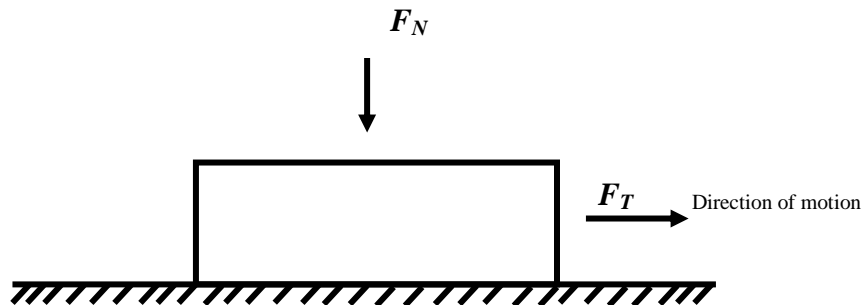


Figure 2.1.1: A simple solid body sliding on a surface [Source: Introduction to Tribology Bhushan et al.,2002].

Thus, in braking operation, friction dissipates the kinetic energy, which is proportional to the square of the speed, into heat. This heat goes mostly to increase the internal energy of the bodies

in contact, thereby causing a temperature rise. The work of friction that can be absorbed in unit time, can be defined as a parameter characterizing the braking system, the work of friction (W_t) can be expressed as the product between the friction force (F_t), his arm action along the diameter (D) and the number of rotations during braking (N_t).

$$W_t = F_t \cdot \pi \cdot D \cdot N_t \dots \dots \dots (2.2)$$

2.2 Disc Brake system

Figure 2.2.1 shows a schematic picture of a pad-disc brake system. The main components are the Brake Pads, Rotor, Caliper and Caliper Support.

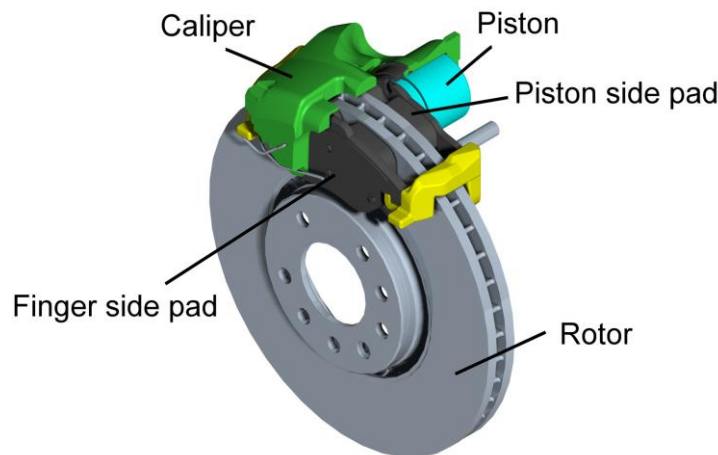


Figure 2.2.1: Schematic diagram of disc brake system. [Source: Jens wahlstrom et al, 2009].

The brake discs are fixed to the frame of the vehicle and must meet some basic requirements such as:

- **Wear resistance:** The brake pad and disc should have less in wear as little as possible.
- **Compression strength:** It must have high compressive strength and resist the pressure exerted by the pads during braking.
- **High thermal capacity:** It must be able to dissipate heat well, in fact about 90 % of the heat is dissipated by the estimated complex designed disc.
- **High coefficient of friction:** It must ensure the safe braking when coupled to the friction material.
- **Light weight:** The weight should be as low as possible, in conjunction with the other parameters.

- **Cost:** It depends on the application. For use in advanced sectors such as Formula1 or trolleys airplanes, cost is important but not essential as it is in the automobile sector.

- **Brake Pads**

The brake pads are among the most complex ever produced composite materials, as they contain the three main different types of materials, i.e., metals, ceramics and polymers. This chemical diversity and chemical-physical, makes it very difficult to find the right composition and mixing [Eriksson et al.,2000, Chan et al.,2004].



Figure 2.2.2: *A commercial brake pad friction material.*

In general, the friction materials have to withstand conditions of high pressures and temperatures throughout their use, certainly these materials should be of durability, comfort, affordability and above all ensure safety at all times that they can perform their function braking efficiently. In particular, the properties that are required to friction materials are:

- Resistance to wear.
- Resistance to thermal fatigue.
- Resistance to shear and compression that are generated during braking.
- Low sensitivity to environmental conditions such as water, oils and corrosive salts.
- Thermal stability and oxidation.
- Workability and ease of production.
- No or very little vibration and noise during operation.
- Ensure a stable friction coefficient under different conditions and time.

Two other very important features, which however are specifically addressed and described is the 'fade' and 'recovery'. The 'fade' is a temporary loss of braking efficiency due to the increase of heat that brings down the friction between disc and pad, to ensure the efficiency and safety under

braking, the resistance to this phenomenon is to be maximized. The 'recovery' instead is the ability to recover the capacity (coefficient) of friction after the original cooling pad, in doing so, even if it takes unwanted phenomena of 'fade', it can have a complete recovery of braking efficiency [Mukesh et al., 2014].

In general, there are three category of brake friction materials or brake pads are available in the market today. They are Non-asbestos organic (NAO) brake pad, semi-metallic brake pad and ceramic brake pad friction materials.

Non-asbestos organic (NAO) brake pads consist of organic fibers that are used to reinforcement of the friction materials and provide strength to the brake pad. NAO friction materials contains less steel by weight. Whereas, a *semi-metallic brake pads* consists of steel wool instead of non-asbestos organic (NAO) material as a reinforcing fiber. Most semi-metallic friction materials contain at least 60% steel by weight. The steel fibers are act as a framework to lock the friction ingredients together. Semi-metallic pads provide better high temperature performance and wear characteristics than conventional non-asbestos friction materials.

Table 2.1.1: *Generally classification of brake pads based on metal content and coefficient of friction [A. Mattia et al.,2015].*

| Disc material family | Coefficient of friction | | | | | | | | Metal Content |
|-----------------------------------|-------------------------|--|--|--|------|--|--|--|---|
| | Low | | | | High | | | | |
| Semi-Metallic | | | | | | | | | $\%Fe+Cu \geq 50\%$ |
| Low Steel | | | | | | | | | $\%Fe+Cu = 10-50\%$ |
| Very Low Steel | | | | | | | | | Derived from NAO with improved efficiency (Metal content can be higher that 10%) |
| Non-Asbestos Organic (NAO) | | | | | | | | | $\%Fe+Cu < 10\%$ |

Ceramic brake pads are rich in ceramic compound and copper fibers in place of semi-metallic pad's steel fibers, which give the ceramic pads an excellent ability to handle high brake temperatures with minimum heat fade and generate less wear debris during tribological operation. Ceramic pads have following primary advantages such as very stable under a wide range of temperatures, providing more consistent performance and have minimize harmonic pad vibration, thus reduce brake noise. Ceramic brake pads are less abrasive, which minimizes brake rotor wear, a primary cause of wear. Thus it is used specially in aircraft and high-speed trains, where high thermal stability and large amount of energy to be dissipated with high tribological loads [Bijwe et al.,1997].

• **Cast iron disc**

The cast iron mostly used in the brake discs is the pearlitic gray cast iron alloy. It contains graphite flakes in a pearlitic matrix. Gray cast iron has high thermal conductivity which is due to a greater amount of graphite present in the microstructure, allowing lower temperatures in the region under friction, which contributes to an increase in life of the component [W. Keiner et al.,1990,J.R. Laguna-Camacho et al.,2015].

Graphite flakes are interconnected and disposed in the form of plates, constituting an easy path for fast heat dissipation, whereas, in ductile iron, spherical graphite particles are isolated from one another therefore the contribution for the thermal conductivity being very small but unique microstructure allows ductile iron to have the excellent strength and wear resistance comparable to other cast irons [C.H. Hsu et al.,2011].

Compact graphite iron (CGI) has a vermicular graphite (modification in graphite shape, flakes become shorter and thicker) resulting in intermediate mechanical and thermal properties between gray and ductile iron. With the addition of alloying elements, such as Mn or Ce, the nodular cast iron can be formed, with the formation of graphite nodules instead of slats. The presence of nodules or lamellae changes the tribological behavior of gray cast iron, in fact, the lamellar cast iron has better thermal conductivity and high coefficient of friction but has greater wear than the ductile iron [W.L. Guessser et al.,2001].

A review of cast iron disc used today by the automotive industry shows that there are three distinct classes of brake pad-disc material (low, medium and high carbon-iron disc) and their parameter characteristic is depend on the carbon equivalent (C.E.), which is defined as the empirical value in weight percentage, relating the combined effects of different alloying elements used in the making of carbon-iron disc material to an equivalent amount of carbon. This value can be calculated using a mathematical equation shown in equation 2.3.

$$\text{Carbon Equivalent} = [\%C + \%Mn/6 + \%(\text{Cr}+\text{Mo}+\text{V})/5 + \%(\text{Ni}+\text{Cu})/15] \dots\dots\dots(2.3)$$

Table 2.1.2: General chemical analysis of different forms of disc materials [Malcolm et al.,1998].

| Disc Material Category | C | Si | Mn | S | P | Fe |
|--|---------|---------|---------|----------|----------|------|
| Low Carbon | 3.0-3.4 | 1.9-2.2 | 0.5-0.8 | 0.10 max | 0.10 max | rest |
| Medium Carbon | 3.3-3.5 | 1.9-2.2 | 0.5-0.8 | 0.10 max | 0.10 max | rest |
| High Carbon | 3.6-3.9 | 1.8-2.1 | 0.5-0.8 | 0.10 max | 0.10 max | rest |
| Alloys - Molybdenum = 0.3 - 0.5%, Chromium = 0.2 - 0.4%, Nickel = 0.1 - 0.3%, Copper = 0.5 - 0.8% , Titanium = 0.02 - 0.04% | | | | | | |

Low carbon cast iron have high strengths, are relatively hard and are therefore used where resistance to wear, thermal cracking are considered. The medium carbon cast iron has increased

carbon content offer improved castability and higher thermal conductivity. Medium carbon cast iron can be easily machined, having excellent standard of surface finish and have good wear resistance. The high carbon disc have good thermal conductivity and good resistance to distortion and thermal cracks [Keiner et al.,1996]. The carbon equivalent control the properties of cast iron as the elastic modulus, which increases with decreasing carbon equivalent and the thermal conductivity that decreases with decreasing in carbon equivalent. When it is required a high energy load, elasticity and thermal conductivity using high carbon equivalent, as in the brakes for trucks. Where, instead, it is necessary mechanical strength and ease of processing, such as in automobiles, using low carbon equivalent.

Chapter 3

Braking Pad Materials (General Features of Friction Material Ingredients)

3.1 Introduction

The brake pads materials are among the most complex ever produced composite materials, as they contain the three main different types of materials i.e., metals, ceramics and polymers, this chemical diversity and chemical-physical makes it very difficult to find the right composition and mixing. In general the friction materials have to withstand conditions of high pressures and temperatures throughout their use certainly these materials should be of durability, comfort, affordability and above all ensure safety at all times that they can perform their braking function efficiently. An automotive brake functions by converting the vehicle's kinetic energy into heat energy. During braking, the heat energy is first borne by the two contact surfaces of the brake system, namely the brake disc and the brake pad (or drum and shoe in the case of drum brakes), and is then transferred to the contacting components of the brake such as the calipers of the brake, as well as the surroundings. [Eriksson et al.,1999]

3.2 Dry friction materials

The main components of a brake pad, namely the reinforcing fibers, binders, fillers and frictional additives. It is important to note that certain substances perform multiple functions and may be placed in more than one classification. Table 3.1.1 shows the general features of M1 and M2 friction materials ingredients used in this thesis work. It also shows the major category of the ingredient which a frictional materials should possess. The details of the M1 and M2 friction materials can be find in chapter 7 under sub heading friction materials.

Table 3.1.1: *General features of friction materials ingredients.*

| Category | M1 Materials | M2 Materials |
|-------------------|------------------------------------|---|
| Reinforcing Fiber | Steel Fiber | Aramid fiber, Rockwool fiber, Potassium titanium oxide |
| Binder | Phenolic resin cross linked | Phenolic resin cross linked, Cashew resin cross linked |
| Filler | Vermiculite | Barium sulfate, Mica |
| Abrasives | Magnesium oxide, Aluminum oxide | Zirconium silicate, Zirconium oxide & Aluminum oxide |
| Lubricant | Tin sulfide | Graphite, Tin sulfide |
| Metal | Zinc, Copper | Zinc, Copper, Iron |

Let's have a brief general introduction of the major ingredient of the friction materials used in the brake pad-disc systems. The main categories are:

- **Reinforcing fibers**
- **Binders**
- **Fillers**
- **Frictional additives**

• **Reinforcing fibers**

The reinforcing fibers are the main components as regards the maintenance of the mechanical strength, the friction properties and the thermal stability of the friction materials. Eriksson et al.,2002, have shown that the braking load is actually carried by tiny plateaus that rise above the surrounding lowlands on the friction materials. Friction materials typically use a mixture of different types of reinforcing fibers with complementing properties including mineral fibres, metal fibres and artificial polymer fibres such as glass fibres, Al₂O₃ fibres, carbon fibres, steel fibres, aramid fibres, etc. [S. Narayanan et al., 1999, S.K. Rhee et al,1974 and X. Xin et al., 2005].

• **Binders**

Binder is consider as the heart of the brake's ingredient system, which usually bind the all ingredient tightly so that they can perform their functions properly. The binders are mainly made from organic polymers such as thermosetting resins: Phenolic resin, polyimide resin, cyanate ester resin and polyurethane rubber [D chan et al.,2004]. Their primary function is to ensure the mechanical strength and integrity of the pad during its production and in working conditions. Another function of the binder is to dampen the vibration and improve comfort during braking and for this, the binder should possess high thermal stability, oxidation resistance at higher temperature and high wear resistance.

Phenolic resin is now a days the most common resin binder used in brake friction materials due to good mechanical properties such as comparatively high hardness, compressive strength, creep resistance and good wetting capability with most of ingredients and it is cheap to produce [Jayashree et al.,2013]. It has ability of crosslinking, since the number of intermolecular bonds formed by the material frictionals the desired characteristics [Critchley et al.,1983]. In high-energy braking applications, the temperature induced can be high enough to decompose the phenolic resin by means of high-temperature oxidation. Phenolic resins carbonize at approximately 450°C [Yesnik et al.,1996]; at temperatures beyond this, it decomposes by charring and evaporation. This process decreases the density of the brake friction material at the wear surface and also increases its porosity, thereby losing its structural integrity [Lampert et al.,1998].

- **Fillers**

Fillers are used to improve the thermal conductivity, porosity, resistance to wear and reduction to noise. They are low cost materials, also used to reduce the total cost of the pad, without deterioration of the properties; these components are typically calcium carbonate (CaCO_3), barium sulfate (BaSO_4), clays, mica, cashew dust and vermiculites. Vermiculites are plane netlike structure, which is porous in nature and having wear resistance property as well as suppress noises generated during braking. Fillers in a brake pad are present for the purpose of improving its manufacturability as well as to reduce the overall cost of the brake pad [Eriksson et al.,2002].

- **Frictional additives**

The frictional additives are special materials that modify the interaction between the brake pad and disc during braking. Frictional additives are components added to brake friction materials in order to modify the friction coefficients as well as the wear rates. They are divided into two main categories: lubricants, which decrease the friction coefficients and wear rates, and abrasives, which increase friction coefficients and wear rates.

The main purpose of a lubricant is to stabilize the developed friction coefficient during braking. Graphite and various metal sulphides are commonly used as lubricants. Graphite has the ability to form a lubricant layer on the opposing counter friction material rapidly [Taylor et al.,1998] and widely used in brake pad. A stable friction coefficient is achieved with the self-sustaining lubricating layer. Metal sulphides such as antimony sulphide are very popular in friction materials now a days as they are able to provide good lubrication but metal sulphides have quite lower conductivities than graphite [Taylor et al.,1998].

The abrasives are mainly oxide powders of various metals and their function is to create a high and stable level of friction during braking and are also needed to prevent the formation of deposits of dirt, rust or friction materials on the same brake disc surface or to ensure their removal [Eriksson et al.,1999]. The abrasives in a friction materials increases the friction coefficient and also increasing the rate of wear of the counter face material (cast iron disc). Abrasives remove iron oxides from the counter friction materials as well as other frictional surface films formed during braking. A few examples of the commonly used abrasives include magnesium oxide, zirconium oxide, zirconium silicate, aluminum oxide and chromium oxide [Kobayashi et al.,2002].

Typical examples of abrasives in ascending order of Mohr's hardness value:

| Abrasives | Mohr's hardness value |
|---|------------------------------|
| Barite (BaSO₄) | 3.0 |
| Zinc oxide (ZnO) | 4.5 |
| Magnetite (Fe₃O₄) | 5.5-6.5 |
| Hematite (Fe₂O₃) | 5.5-6.5 |
| Magnesium oxide (MgO) | 6.0-6.5 |
| Zirconium silicate (ZrSiO₄) | 6.5-7.5 |
| Quartz (SiO₂) | 7.0 |
| Zirconium oxide (ZrO₂) | 8.0 |
| Chromium oxide (Cr₂O₃) | 8.5 |
| Aluminum oxide (Al₂O₃) | 9.0 |

3.3 Future trends in frictional materials

The future trends in frictional materials mimic the current trends and more emphasis on cars will be on lower emissions and higher fuel efficiency as environmental regulations become more stringent [Chan et al.,2003].

The main focus will be on vehicle fuel efficiency and lower emissions that mean brakes will have to be lighter, more efficient in terms of less wearing during braking and not release any toxic particulate matter into the atmosphere during use. This means that the choice of brake friction materials will need to be more environmentally friendly and not include toxic substances.

Chapter 4

Wear Mechanisms in Pad-Disc Braking System

4.1 Introduction

Wear is a dynamic process which quite often involves progressive dimensional losses from the surface of a solid body due to mechanical interaction between two or more bodies in sliding contact [Abu Bakar et al.,2008]. Wear is a material removal by physical separation due to microfracture, by chemical dissolution, or by melting at the contact interface. Furthermore, there are several types of wear: adhesive, abrasive, fatigue, and oxidative. The dominant wear mode may change from one to another for reasons that include changes in surface material properties and dynamic surface responses caused by frictional heating, chemical film formation, and wear. Wear mechanisms are described by considering complex changes during the tribological interaction. In general, wear does not take place through a single wear mechanism, so understanding each wear mechanism in each mode of wear becomes important.

4.2 Wear Models

Wear phenomena are heavily influenced by the fact that most engineering surfaces are rough (and hence surfaces come in contact at single asperities and the real area of contact is usually much smaller than the nominal contact area). Furthermore, wear behavior is also influenced by the presence of adsorbed species or surface layers. Wear phenomena are intimately linked to frictional processes. Recall that friction forces are generally the result of two main physical processes: shearing and ploughing. If solid surfaces in relative motion are not separated in some way, wear can be expected.

Research on wear mechanism prediction and modeling has been carried out for over 50 years [P.J. Blau et al.,1997].

Early researcher named Archard who developed a linear wear model for metals, his model talked about the wear volume per sliding distance was in terms of wear coefficients [J.F. Archard et al.,1953]. Archard's linear wear model represented by equation (4.1).

$$V = [\mu \cdot (F_N \cdot S)/H] = (K_a \cdot F_N \cdot S) \dots \dots \dots (4.1)$$

where ' μ ' is the wear coefficient, wear volume ' V ', ' K_a ' is the specific wear coefficient, ' F_N ' is the applied load, ' S ' is the sliding distance and ' H ' is the hardness of the material that is worn. Archard refined the theory behind the wear model by assuming the following [J.F. Archard et al.,1953]:

- The wear rate is proportional to the load.
- The wear rate is independent of the apparent area of contact.
- For metals, the asperity deformation is plastic.
- A single asperity contact is circular.
- The system is isothermal.

S.K. Rhee et al.,1970, proposed a nonlinear wear model for the friction materials in a disc brake system. Rhee developed a nonlinear wear equation at given temperature for specific application such as brake systems under which the frictional force (F) is directly related to normal load (P) and the sliding speed (V). Rhee's nonlinear wear model represented by equation (4.2).

$$F = (\mu \cdot P^a \cdot V^b) \text{ at given temperature } (T_i) \dots \dots \dots (4.2)$$

where ' F ' is the frictional force, ' P ' is the normal load, ' V ' is the sliding speed, ' μ ' is the friction coefficient, which is constant regardless of the load and speed. ' a ' and ' b ' are the set of parameters that are specific to the friction material and depend on the temperature only [S.K. Rhee et al.,1974].

However, Soderberg et al., 2009 and Abubakar et al.,2008 proposed a new interpretations of the law of Archard for wear by inserting the exponents derived from experimental data and give importance to the modeling of the pressure applied, as characteristic parameter. However, the pattern at the base of the analysis remains the law of Archard.

4.3 Basic Wear Mechanism

In upcoming paragraphs, there will be a brief introduction of different wear theories and general wear mechanisms associated with the contact between the friction materials and counterpart disc, the wear mechanisms underlying the process of dry sliding wear of the braking system are adhesion, abrasion, surface fatigue and tribo-oxidation, in the presence of hard particles.

- Adhesive Wear (plus Fretting Wear) - Encountered in 23-45 % of cases - Scuffing or galling areas, holes, plastic shearing, material transfer.
- Abrasive Wear (plus Erosive Wear) - Encountered in 36-58 % of cases - Scratches, groove , ripples.
- Surface Fatigue Wear - Encountered in 14-15 % of cases - Cracks, pitting.
- Oxidative Wear - Encountered in 4-5 % of cases - Reaction products (layers, particles).

• **Adhesive wear**

The adhesive wear resulting from the contact and from phenomena of adhesion between two surfaces in contact. In general, to understand the adhesive wear is necessary to introduce the concepts that relate to the adhesion and the interactions between these bodies in contact. If the contact interface between two surfaces under plastic contact has enough adhesive bonding strength to resist relative sliding, large plastic deformation caused by dislocation is introduced in the contact region under compression and shearing. As a result a crack is initiated and is propagated in the combined fracture mode of tensile and shearing. When the crack reaches the contact interface, a wear particle is formed and adhesive transfer is completed. This type of wear, which occurs when there is enough adhesive bonding at the contact interface, is called adhesive wear.

A first simple model of adhesive wear stated by Archard et al.,1980, he examined the contact mechanics of multiple asperity contacts with respect to their elastic and plastic deformations. He proposed that adhesive welding of the contact generates a worn particles from the weaker material of volume ' δV ', the volume of worn material removed ' δV ' as a result of a tribological interaction is directly proportional to the load ' P ' and also to the total sliding distance ' L '. However, since less wear is observed when the hardness of the softer member of the tribological couple increases, ' δV ' can also be regarded as inversely proportional to the hardness ' H ' of the material being worn away. Therefore ' $\delta V = 2\pi a^3/3$ ' for sliding distance of ' $\delta L = 2a$ ' and $\delta V/ \delta L = \pi a^2/3 = \delta A_t/3 = \delta P/3H$ In symbols, the above is represented as:

$$(V/L) = \Sigma(\delta V/ \delta L) = (K/3) \cdot \Sigma(\delta A_t) = (K \cdot P)/H.....(4.3)$$

where ' K ' is the previously introduced wear coefficient, ' δA_t ' is a circular contact area of maximum radius ' a '.

Adhesive wear behaviour of pure metals could be related to their ability to form solid solution, i.e., counterface materials will have higher adhesive wear if they are mutually inter-soluble [E. Rabinowicz et al.,1961]. Dyson et al.,1980, described the mechanism of initial mild adhesion, more severe adhesion, pitting and finally mild abrasive wear from loose and adhered debris, with corresponding increases in friction and temperature.

Although adhesive wear is the predominant mechanism with high friction, dry contact wear such as pin-on-disc testing, under such conditions, as contact loads are steadily increased, wear rates can be subject to sudden changes. These effects are due to thermal and tribo-chemical effects, rather than any alteration in the adhesion mechanism.

• **Abrasive Wear**

Abrasive wear occurs when any solid object is sliding against a solid material and have difference in hardness, usually a hardness difference between the interacting solid should be greater than 30% is required to have abrasive interaction. In such case of plastic contact between hard and sharp material and relatively soft material, the harder material penetrates to the softer one. When the fracture is supposed to be brought about in the manner of micro-cutting by the

indented material, the resultant wear is called abrasive wear. In abrasive wear the hard asperities can be the counterface material (2 body wear) or hard debris particles (3 body wear). These micro-plough the soft surfaces pushing a wedge of material ahead and displacing material to each side.

Archard et al.,1986 used a simplified model to analyze abrasion. He proposed that the hardness of the two couples must have wide differences and there must be pure cutting of material rather than plastic flow (ploughing). According to him volume removed per sliding distance has a linear variables.

$$(\delta V/\delta L) = K_a (2\cot\phi/\pi) \cdot (\delta P/H) \text{ or } V/L = K_a (2\cot\phi_{av}/\pi) \cdot (P/H) = K \cdot (P/H) \dots \dots \dots (4.4)$$

Where ' K_a ' is a constant of proportionality and ' $\cot\phi_{av}$ ' is a average value for all the abrasive particles and ' K ' is highly dependent upon asperity shape.

M. Khruschov et al.,1974, developed some principles of abrasive wear through the study of fixed ceramic grains abrading against pure metals, heat-treated steels, wear resistant metals and ceramics. Khruschov explained that the abrasive action, on a micro scale, works the materials to its maximum hardening level, more than can be achieved via cold working. Another researcher Moore et al.,1980, explained the different mechanism of abrasion i.e., ploughing deformation and micro cutting. According to Moore, micro cutting could be related to the material's fracture toughness, rather than its resistance to plastic deformation. He observed that the abrasive work was offset by energy dissipation due to plastic deformation within the material.

Kato et al.,1992 has carried out a pin-on-disc test to study the micro mechanism of abrasive wear between materials of similar hardness. He noted that the disc wear was highly sensitive to small changes in the angle of leading edge of the pin with three distinct mechanisms, cutting, wedge formation and ploughing. His work demonstrated that there was a transition from cutting, to wedge, to 'shear tongue' formation (side extrusion and adhesive transfer) and finally to ploughing; latter marked by a lower steady state wear rate and an increase in friction.

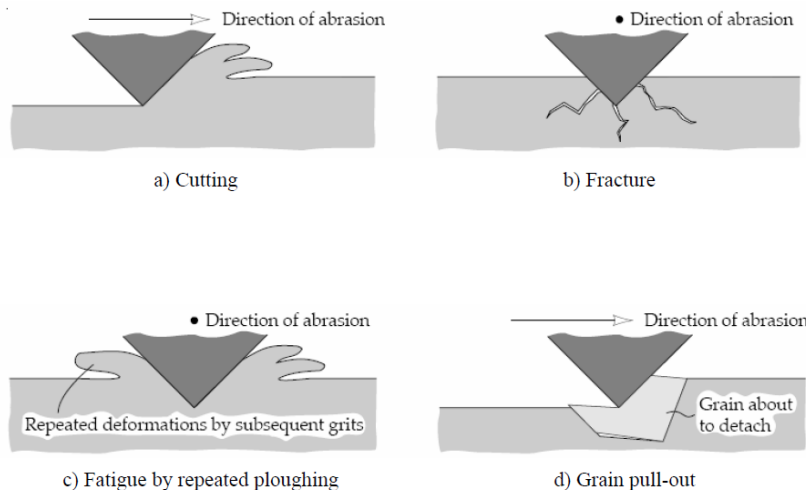


Figure 4.3.1: Mechanisms of abrasive wear: microcutting, fracture, fatigue and grain pull-out [Source: Pooley et al.,1972].

The nature of abrasive wear can be 'two body' abrasive wear or 'three body' abrasive wear. Two body abrasive wear is like action of sand paper on a material surface. Hard asperities or rigidly held grits pass over the surface like a cutting tool. In three body abrasive wear the grits are free to roll as well as slide over the surface, since they are not held rigidly. Fig. 4.3.2 shows the two body and three body modes of abrasive wear.

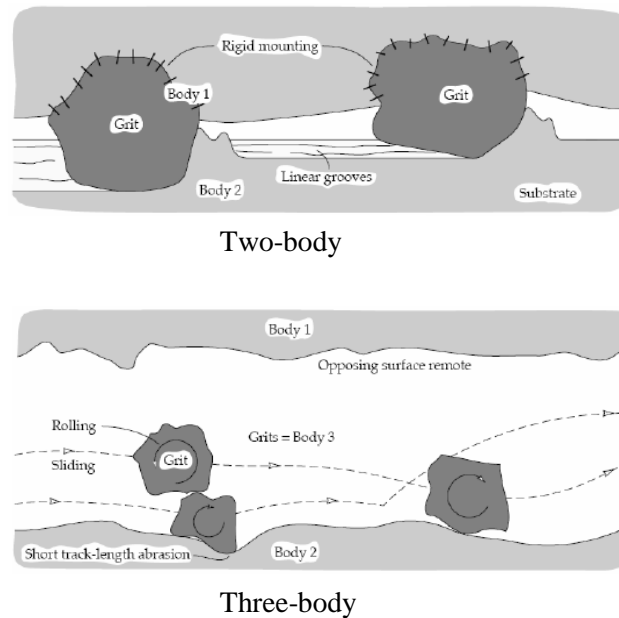


Figure 4.3.2: Two and three-body modes of abrasive wear [Source: Blanchett et al., 1989].

It was found that three-body abrasive wear is ten times slower than two-body abrasive wear since it has to compete with other mechanism such as adhesive wear [N.S. Eiss et al., 1979]. Two-body abrasive wear corresponds closely to the 'cutting tool' model of material removal whereas slower mechanisms of material removal can be seen in three-body abrasive wear [Warren et al., 1978].

• Surface Fatigue Wear

Fatigue in wear can be observed at two levels firstly, rolling contact fatigue spalling of the contacted surfaces with surface or sub-surface crack initiation and secondly, at microscopic level, the fatigue and fracture of deformed surface asperities to form wear debris. Subsurface cracks may also form in more ductile materials by fatigue processes associated with cyclic loading. While less wear may be observed prior to fatigue events extensive pitting may be observed once fatigue sets in. Consider again a tribological system formed by a large number of microscopic contacts. Each individual asperity experiences multiple contact interactions with asperities of the counterface.

For the micro-fatigue wear mechanism, Archard et al., 1980, re-described wear coefficient 'K' in equation 4.3 i.e., $[V/L = K.(P/H)]$, Since K can be interpreted as the proportion of contacts that

contribute to wear debris by failing, the number of stress cycles to failure N_f is simply $N_f = 1/K_{fatigue}$.

When fatigue failure takes place at a particular asperity contact, the volume of material removed can be expected to be proportional to a^3 where 'a' is the contact radius. Moreover, the sliding distance over a particular contact is '2a'. An expression for the worn volume per unit sliding distance for the system can then be obtained by adding the contributions from all contacting asperities where fatigue has occurred, i.e.

$$(V / L) = K_{fatigue} \Sigma(\delta A_t) = K_{fatigue} \cdot (P / H) \dots \dots \dots (4.5)$$

• Oxidative Wear

In oxidative wear the contact surfaces (wear couple) are oxidized on contact with the oxidizing atmosphere, typically air; fragments of wear resulting from it are mainly metal oxides formed on the surface of the materials and removed from the motion between the surfaces. The fragments are usually very small, below one micron, although larger particles form agglomerates. Frictional heat of the wear test can generate such processes as oxidation, steel decarburization and near surface hydrogen embrittlement. For most of the metallic surfaces which contact in air, oxidation is the most significant reaction. The oxide themselves, adhered or separate, are a wear product resulting in metal loss. Air humidity is also a factor in the oxidation wear process.

Archard et al.,1980, developed his wear relationship, to account for oxidative wear. It was based on the multiple asperity contact developed for equation 4.3 (maximum asperity contact area πa^2). His proposed oxidative wear rate equation is:

$$V/L = K_b \cdot \lambda/2a \cdot \Sigma(\delta A_t) = (K_b \cdot \lambda/2a) \cdot A_t = K \cdot (P/H) \dots \dots \dots (4.6)$$

Where 'K_b' is the proportionality constant for all tribo-chemical process which produce wear debris and it will increase with temperature (exponentially), chemical reactivity of the environment and chemical reactivity of the wear couple for a given environment. 'λ' critical thickness of a protective and undamaged film developed during asperity contact.

Quinn et al.,1984, have studied the oxidative wear of a low alloy steel using pin-on-disc wear test. They observed that for oxidative wear load and frictional heat were correlated with the type of iron oxide that formed, below 400°C the formation of α-Fe₂O₃, between 400°C and 600°C, Fe₃O₄ and above 600°C the formation of FeO. Quinn observed that oxidative wear rates and general surface temperature (T_s) were proportional to applied load. Wear rate transitions were associated with sudden changes in surface temperature and with a change in the balance of oxide type found in the wear debris.

The oxidative wear mechanism can be represented, in the case of metals:

- On the surface it has a metal contact that creates joints with plastic mechanism of accession; small fragments that come out of the tribological system, to break the junctions, can be oxidized.
- The chemical reaction of the surface with the environment reduces the metallic contact between the parts, thus creating a layer of protective oxide.

- The breakage of the protective layer to increase the local pressure or surface fatigue produces non-metallic fragments.
- The fragments of metal and non-metal act as abrasive surface not in contact, leading to a pointed shape the contours, which mean that the phenomenon is spreading.

4.4 Wear Mechanism in Pad-Disc Braking Systems

Wear of the friction materials is mainly due to adhesion and abrasion, and it usually proceeds through the formation and detachment of a *friction layer*, which bears the contact load and also influences the frictional behavior [Eriksson et al.,1999]. The friction layer is made of two contact plateaus: the primary and secondary plateaus [Eriksson et al.,2002].

During the contact between the brake pad and the disc, the hardest parts of the pad are in contact with the disc which creates micro-grooves in the disc itself as confirmed by the studies of Eriksson et al., 2000, Filip et al., 2002 and Osterle et al., 2006, in which the fragments of wear flowing in a continuous way. A combination of temperature, pressure and tangential force makes fragments to compressed and piled against the existing plateau and ensure that the compaction of the fragments is heterogeneous at the same time the smaller fragments come out of during this operation and are released as wear debris into the atmosphere. Wear initially induces the detachment of particles from the phenolic matrix close to large and hard constituents, which thus form protruding primary plateaus. The formation of the plateau is not a stationary process but a dynamic evolving process as confirmed by Eriksson et al.,2000 and Roubicek et al., 2008.

The components that form such plateaus was found to be generally larger than 100 μm , and their hardness values are in excess of the disc material hardness: steel fibers and highly strain-hardened copper or brass particles, are usually involved in the formation of these primary plateaus. Subsequently, micrometric and sub micrometric wear particles tend to accumulate close to such plateaus, where they are also compacted to some extent, depending on the contact pressure and sliding shear stresses. In this way, the secondary plateaus will form, made of small compacted particles coming from wear of the pad as well as of the disc. In this regard, it is distinguished between "primary contact plateau", i.e., the part of material more resistant to wear on the surface of the pad and the "secondary contact plateau", which is more resistant to wear.

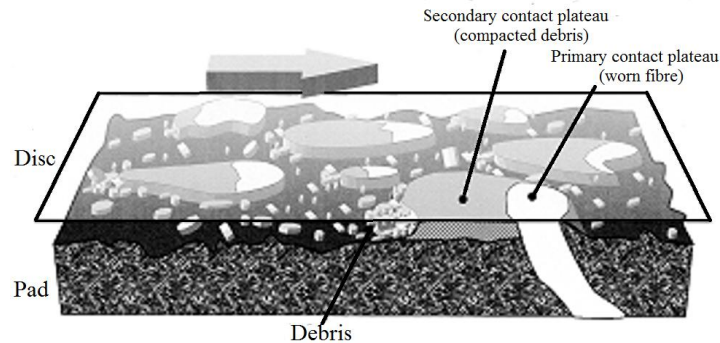


Figure 4.4.1: Schematic of the contact situation between an organic friction material and a brake disc and formation of compacted plateaus [source: Filip et al.,2002].

The compacted plateaus with typical sizes ranging from 50 to 500 μm of a width of a few microns thick and is formed from the body softer of the two bodies in contact [Gwidon et al.,2006]. Iron oxide particles, produced by tribo-oxidative mild wear of the cast iron disc, are typically present in the friction layer and often constitute the main part of it. Wear particles are mainly formed by the disruption of the friction layer, and a contribution also derives from the wear of the so-called low-land regions (in between the friction layers), even if the damaging mechanisms have not been fully elucidated as yet. As seen, also the counterface of cast iron disc takes part into the wear process and undergoes a tribo-oxidative wear with a wear rate 20-50% of that of the friction pad.

Due to intense pressure and tangential force, the contact plateaus get damaged and form wear debris especially from the secondary plateau. The damage occurs due to the loss of support from the fiber that detached to wear, irregularities or impurities on the disc, the three body abrasion and adhesion. This type of damage can lead to the breakdown of secondary plateau even though the primary platform is not ejected from the frictional material and when the pressure is reduced the secondary plateau detaches in the form of flakes forming of large fragments of compact wear [Eriksson et al.,2000]. The damage of the friction layer is the main cause of formation of fragments of wear and wear particles that are released into the atmosphere.

In the brake pad system, wear occurred during normal braking and heavy braking. It termed as mild wear and severe wear respectively, which are the function of applied load for deceleration and contact temperature rise during braking. These wear phenomena are discussed below:

- **Mild Wear (Normal Braking Condition)**

In this case the contact temperature and braking pressure is low and the plateaus are enriched in iron oxide because of the transfer (by adhesion and abrasion) from the cast iron disc. The emission of airborne fragments is mainly due to the fragmentation of the contact plateaus. The airborne particles are thus mainly primary in nature.

• Severe wear (Heavy Braking Condition)

In this case the contact temperature is high and the chemical composition of the contact plateaus (and thus of the wear fragments) is strongly influenced by contact temperature. Friction and wear strongly depends on contact temperature, it is reported that the transition temperature (above which friction coefficient starts to decrease because of fading, and wear rate starts to exponentially increase because of thermal decomposition of the phenolic resin) [J. Bijwe et al.,2007] may be expressed by the average contact temperature, (T). As shown in Fig. 4.4.2, K_a exponentially increases with contact temperature, T. The contact temperature is determined by sliding conditions (contact pressure 'p', sliding speed 'v') and system geometry. During heavy braking the following reactions have been recognized:

- **Oxidation** of Cu and Fe and other, with the formation of different kind of oxides.
- **Thermal degradation** of the metal sulphides and organic constituents like binder (phenolic resins often revealed by the formation of water vapor and black carbon char) [J. Bijwe et al.,2007].

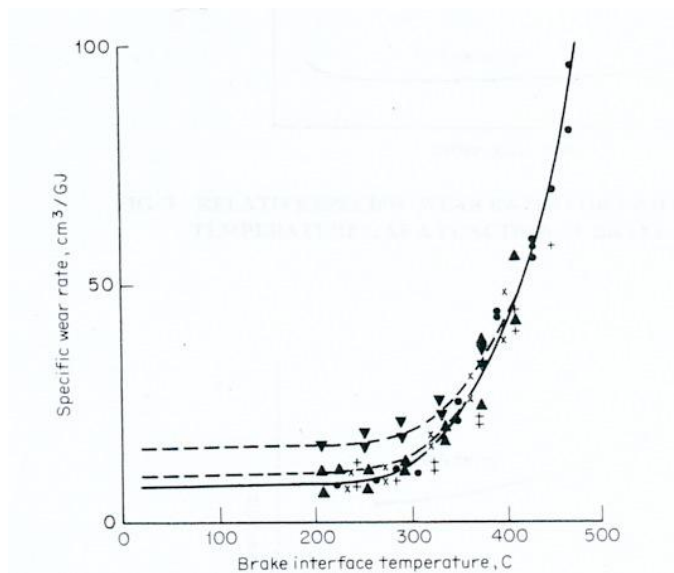


Figure 4.4.2: Influence of contact temperature on the wear rate of a friction material [Source: A.E. Anderson et al.,1992, wear control handbook].

The two braking conditions therefore depend on the applied pressure and the contact temperature achieved i.e., normal braking when the contact temperature remains below a critical temperature of about 300°C, while if it exceeds this temperature it comes to braking heavy. In fact, many authors found that 300°C is a kind of transition temperature, beyond which it has the degradation of the polymer matrix [J. Bijwe et al.,2007] with the release of ultrafine nanoparticles in the

atmosphere, with possible serious damage to people's health. Table 4.1.1 summarized the above two brake wear conditions.

Table 4.1.1: *Different type of braking condition in disc brake system.*

| Braking conditions | Braking pressure (pa, MPa) | Deceleration rates (m/s ²) | Average contact temperature | Brake wear, Ka (m ² /N) |
|-----------------------|----------------------------|--|-----------------------------|---|
| Normal Braking | 0.2 - 1 | < 2 | < 300°C | $5 \times 10^{-15} - 4 \times 10^{-14}$ |
| Heavy braking | 1.1 - 4 | > 5 | > 300°C | Increases with Temperature |

In addition to temperature and pressure, the tribological behavior of the system is also governed by sliding speed, even with lower applied loads it has been expected to have moderate wear with temperatures below the critical one, Heussaff et al., 2012 noted that for high sliding speed, there is severe wear.

In Fig. 4.4.3, a schematic of the influence of p and v on braking conditions is shown.

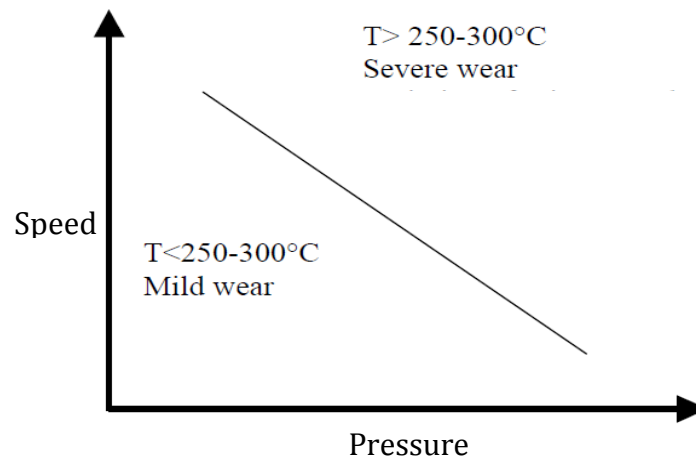


Figure 4.4.3: *Schematization of the influence of sliding parameters on the braking conditions.*

So, here in this chapter, we have tried to understand the basic wear mechanism, in general and the wear mechanism in pad-disc braking system. Fig. 4.4.4, is demonstrate the summary of the basic wear mechanism in pad-disc braking system.

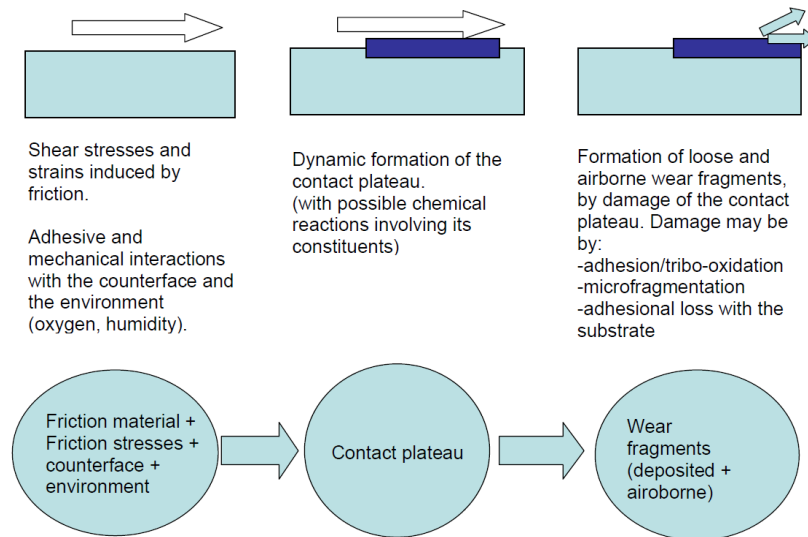


Figure 4.4.4: Summary of the basic wear mechanisms in braking systems.

In the next chapter we will going to see the consequences and health hazard due to the release of wear debris in atmosphere, which is produced during the tribological operation of pad and disc together. It is interesting to know that these nano particles have a greater health damage for human being. In chapter-5, we will going to see how these nano-particles would affect our environment eco systems.

Chapter 5

Particulate Matter: Hazard and Risk

5.1. Introduction

The wear mechanisms occurring at the pad-disc interface are responsible for the particulate matter emission and the airborne particles area fraction of the total wear particles. Generally speaking, in case of pad-disc braking system the wear particles are mainly formed by the disruption of the friction layer, and possibly by the wear of the low-land regions. The characteristics of the airborne particles depend on the characteristics of the friction layer and, in turn, to those of the friction materials (their ingredients and their role in the wear process). The high contact temperature may induce several chemical reactions in the contact spots, including thermal degradation of the organic constituents (phenolic resin, rubbers); direct oxidation of Fe and Cu, with the formation of different kinds of oxides; thermal decomposition of sulphides; dehydration of vermiculite. Airborne particles are thus either primary and secondary in nature. Secondary particles are small in size (with diameter lower than about $0.1\mu\text{m}$) and they may form in the atmosphere by volatilization and condensation, and by collisions among the emitted precursors [Thorpe et al.,2008]. Secondary particles may also form under normal braking conditions because of the high flash temperature achieved during sliding at the contact spots.

The wear particles as airborne released into the atmosphere and deposited away from the roadside and non-airborne particles deposited on vehicle, retained on the wheel, brake and steering/suspension equipment or on road surfaces. Materials deposited on road surface can be re suspended by tyre shear, turbulences and wind, having a temporally and spatially dynamics [Barlow T.J. et al.,2007], or the emitted particles may be washed into the storm drains and end into creeks, rivers and marine waters. Brake wear generates particles across a wide range of diameters from a few hundred nanometres (nm) to a few tens of a micrometer (μm). Whilst brake wear emissions are predominantly the result of a mechanical process and thus expected to release particles in the coarse size fraction, it appears that a significant proportion of brake debris may be emitted in the fine size mode [Wahlin et al.,2006, Iijima et al.,2007].

The particle size is an important parameter of atmospheric PM. Particle size controls the dynamic behavior of particles as well as their chemical and physical impacts on the environment. It is also certainly an important parameter for the health consequences of the respective human exposure as particle size determines:

- The deposition of particles within human respiratory system;
- The amount of surface area that can contact tissues;
- The rate of particle clearance from lungs [Oberdorster et al.,2005].

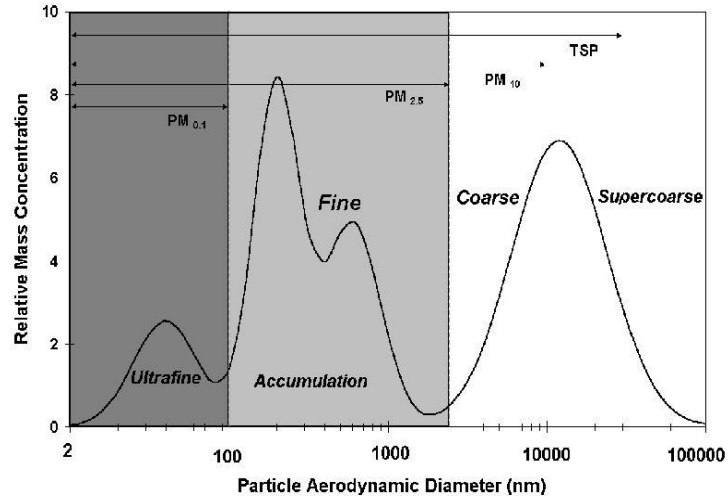


Figure 5.1.1: Schematic representation of the size distribution of atmospheric particles [Source: <http://dx.doi.org/10.5772/54775>; Slezakova et al., 2013].

Fine mode is composed of particles with aerodynamic diameter smaller than 2500 nm. Typically, these particles are generated by anthropogenic (caused or influenced by humans) sources. The small sizes of the particles make them less susceptible to the gravitational settling resulting in atmospheric lifetimes in range of days up to weeks and the ability to travel over very long distances in the atmosphere [Anastasio et al., 2001].

In order to protect human health and the environment EU standards were established for exposure limits to several air pollutants. National laws and regulations are targeted more at reducing the exhaust emissions, both gaseous and particulate matter, from engines of road vehicles, traditionally regarded as most responsible for air pollution from vehicular traffic. Nevertheless, PM from non-exhaust sources provides a further significant contribution to airborne matter. Brake and tyre wear are an important source of trace metals in the urban environment, and at locations influenced by traffic can be more important than industrial emissions.

5.2. Effect of particulate matters on human health

PM is a heterogeneous pollutant, particles are different in size, mass and chemical composition, in such a way determining the health effects should take into account emission sources. Since early '90s researchers revealed a link between air pollution and human health effects among populations in cities throughout the world. An increasing number of studies and research efforts were made since then, so adding further evidences that a number of respiratory and cardiovascular system dysfunctions are caused by the ambient particulate matter. Exposure to particulate matter in ambient air is associated with various impacts on health:

- Increase in lower respiratory symptoms;
- Reduction in lung function;
- Increase in chronic obstructive pulmonary disease;

- Reduction in life expectancy, mainly due to cardiopulmonary mortality and probably to lung cancer.

The diagram shown in the Fig. 5.2.1 represents the correlation between the proportion of affected population and severity of human health risk associated to exposure to atmospheric particulate matter.

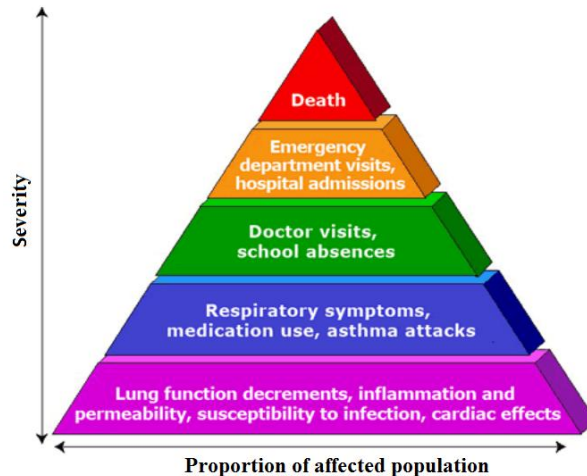


Figure 5.2.1: *The correlation between the proportion of affected population and severity of human health risk associated to exposure to atmospheric particulate matter [Source: <https://fortress.wa.gov>].*

Nano-sized airborne particles and their effect on human health were studied by Oberdörster et al.,2005, revealing that due to their increased surface area and higher reactivity with biomolecules and tissues they can be easily inhaled into the respiratory tract, posing hazards related to potential oxidative stress. Several studies proved that the nano-sized particles may become blood-borne and translocated to other target tissues like liver, kidneys, and brain. Furthermore, due to small size of nano-sized particles their sedimentation is very slow and when released to air, these particles may be transported over thousands of kilometres from a source [Oberdörster et al.,2005]. Particles less than 2.5 microns in diameter, categorized as “fine” particles or PM_{2.5}, penetrate into the small airways and air exchange regions of the lungs. Fine particles are of concern because exposure to PM_{2.5} can cause short-term health effects, such as eye, nose and lung irritations, or long-term health effects, such as chronic bronchitis, reduced lung function and increased mortality. The nano particles enter human body through the skin, lung and gastrointestinal tract [Nel et al.,2006]. Because of their very small size, nanoparticles can penetrate deeper into the lungs and enter the pulmonary interstitium and vascular space to be absorbed directly into the blood stream [Terzano et al.,2010]. Nano particles have a large surface area and that makes them more reactive and toxic leading to detrimental health effects such as oxidation stress, pulmonary inflammation and cardiovascular events [Buseck et al.,2008, Nel et al.,2006]. They may also translocate within the body to the central nervous system, the brain, into the systemic circulation and to organs like the liver [Helland et al.,2007]. Though these nano particles appear in smaller concentrations than other atmospheric nano particles they may pose much larger health risks [Oberdörster et al.,2005]. Ultrafine particles possess a higher mutagenic and toxic potential than larger particles, which might be partially explained by the enhanced

ability of translocation from the respiratory tract to extra pulmonary sites, together with their high number concentration and large surface area [Schlesinger et al.,2006, Spurny et al.,1998, McClellan et al.,2002]. Studies have shown that ultrafine particles have a high capacity to absorb organic molecules and possess the ability to penetrate cellular targets in the lung and systemic circulation [Sehlstedt et al.,2012]. Agglomeration of particles may differ in effects as compared with single particles of the same size and there are indications that the physical surface and crystalline structure can account for some of the reactive potential. The biological response is often correlated with the exposure dose; smaller particles can reach deeper in the tissues, while particles larger than 10 μm are filtered in the upper airways. Particles between approximately 5-8 μm are most likely deposited in the tracheobronchial tree while those between 1-5 μm often are deposited in the respiratory bronchioles and the alveoli [Squadrito et al.,2001].

Metals that are components of ambient air particulate matter (including copper particles generated from brake pad wear), and especially some of those that are within the fine PM fraction, have the ability to generate reactive oxygen species (ROS) in biological tissues. Oxidative stress may be one of the major mechanisms causing the adverse health effects and copper is among the metals capable of inducing such oxidative stress. Gasser et al.,2009, evaluated potential toxicological effects of human epithelial lung cells exposed to freshly generated brake wear particles. Metals on brake wear particles damage tight junctions with a mechanism involving oxidative stress, also increase pro-inflammatory responses. One of the most commonly reported adverse health effect of copper is gastrointestinal distress. Copper is also irritating to the respiratory tract. The liver and kidney are also sensitive targets of toxicity.

Table 5.1.1. *Brake wear PM and human health effects – summary table.*

| Brake wear PM | Effects | Reference |
|--|--|------------------|
| PM ₁₀ | Cardiovascular and respiratory diseases, lung cancer | AQEG |
| PM _{2.5} | Heart rate variability | USEPA |
| <PM _{2.5} | Blood born particles translocated in liver, kidneys and brain | Oberdorster |
| | Oxidation stress, pulmonary inflammation, cardiovascular events | Buseck; Nel |
| PM ₁₀ ; PM _{2.5} | Increased heart rhythm, elicits pro-inflammatory and pro-thrombotic | Riediker |
| Brake wear debris rich in copper and iron oxides | Inflammatory reactions in bronchial branch | Kukutschova |
| Iron | Oxidative stress, inflammatory response, Iron may cause conjunctivitis, and retinitis if it contacts and remains in the tissues. | Ghio |
| Nickel | Allergic reaction, several Ni compounds are carcinogenic, causing cancers of the lung, nose, larynx or prostate | EEA report |
| Copper | Gastrointestinal distress, irritation of the respiratory tract, liver injury and kidney failure, eye irritation. | Geiger |

Chapter 6

Defining Problems

In this thesis a set of four main issues for the friction materials has been identified and addressed in order to find optimal solution for novel brake systems. In the following paragraphs, each one of these problems has been introduced and discussed with the test highlight and study code-names listed in table 6.1.1:

Table 6.1.1: List of problem defined in the thesis and test highlight.

| Problem Defining | Test highlight | Tribometer Used | Frictional material | Code name |
|--|---|------------------------------------|----------------------------|------------------|
| <ul style="list-style-type: none">• Tribological behavior of two low steel friction materials (M1 & M2) at room temperature. | Pin-on-disc test | Pin-on-disc | M1 & M2 | <i>Case I</i> |
| <ul style="list-style-type: none">• Characterization of wear particles from M1 friction material. | Particles collected on Polycarbonate filter & Aluminium Foil | Pin-on-disc | M1 | <i>Case II</i> |
| <ul style="list-style-type: none">• High temperature wear behavior of M1 and M2 friction materials: Role of the friction layer in the high-temperature pin-on-disc study. | External high temperature (>300°C) heating Test & Frictional heating Test | High Temperature Pin-on-disc Setup | M1 & M2 | <i>Case III</i> |
| <ul style="list-style-type: none">• Role of the heat-treatment of the cast iron disc. | Heat treated cast iron disc | Pin-on-disc | M2 | <i>Case IV</i> |

6.1 Tribological behavior of two low steel friction materials (M1 & M2) at room temperature - (Case I)

The performance of the brake is mainly controlled by the composition and microstructure of the friction materials. Industrial pads usually contain a large number of different constituents like ceramic particles and fibers, minerals, metallic chips, solid lubricants and elastomers, all bound by phenolic resins. In fact, brake materials should retain a relatively high, stable and reliable friction coefficient over a wide range of braking conditions, temperature and humidity. Metals, such as copper, steel and brass have been used in order to affect the frictional characteristics and wear of friction materials by their type, morphology and hardness. The ceramic powders, like zirconium silicate (ZrSiO_4), zirconium oxide (ZrO_2), calcium carbonate (CaCO_3), iron oxide (Fe_2O_3 or Fe_3O_4) etc., are present in friction materials to create a high and stable level of friction during braking.

This experimental work aims at comparing and investigating the tribological properties of two commercial friction materials, codenamed M1 and M2. A pin-on-disc instrument has been used for tribological testing and evaluation. A gray cast iron rotating disc has been used in all friction materials (pin-on-disc) testing. The working conditions for both M1 and M2 friction materials, resulted from a constant contact pressure load (2MPa) and a constant sliding speed of 3.14 m/s, up to 50 minutes of run at room temperature (25°C).

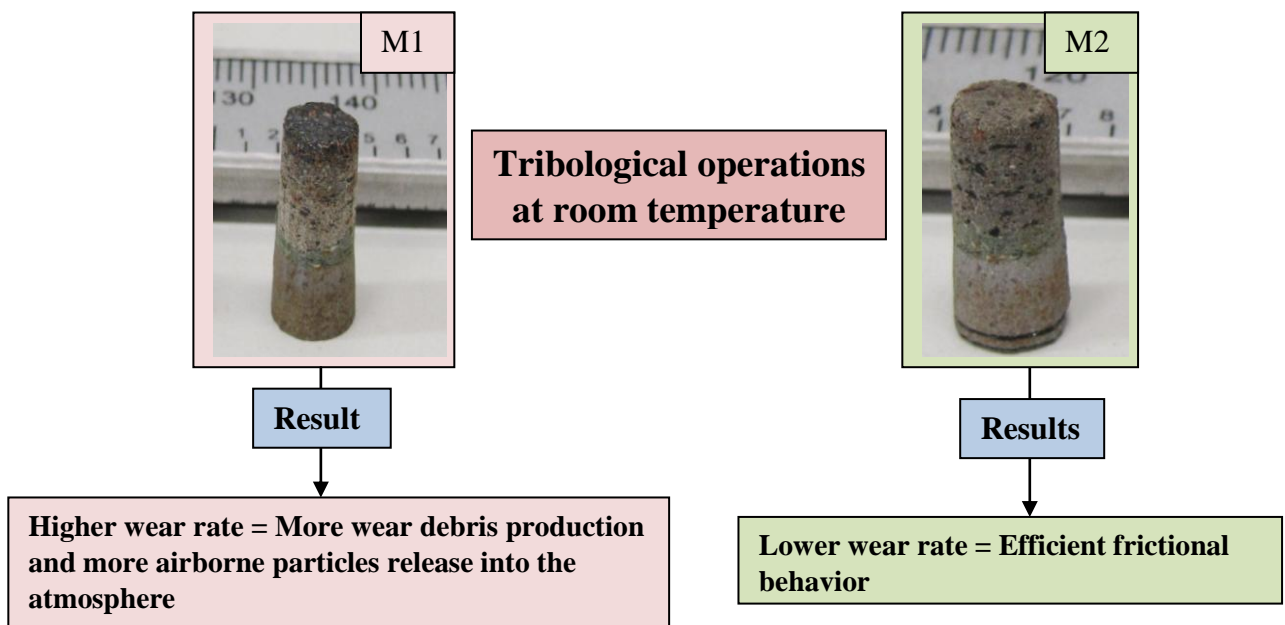


Figure 6.1.1: The flow-chart of tribological results of M1 & M2 friction materials.

6.2 Characterization of wear particles from M1 friction material - (Case II)

The aim of this part of study was to establish an experimental protocol suitable for characterizing particles coming from laboratory pin-on-disc wear tests, collected on different substrates, of M1 friction material. From *Case I*, we have the information about the tribological properties of both friction materials. Characterization of wear debris produced during tribological testing is an important piece of work and characterization results can have a leading role in the development of novel friction materials. To develop the protocol for materials characterization, techniques like, X-ray diffraction, Scanning electron microscopy (SEM) equipped with energy-dispersive X-ray spectroscopy (EDXS), Transmission electron microscopy (TEM) were employed. The experimental study required specific sample preparation procedures, that are important parts of the streamline characterization procedure implemented and optimized in view of its systematic application also to PM collected in other environmental monitoring contexts.

In Fig.6.2.1 the main finding and aspects of the overall methodology are summarized.

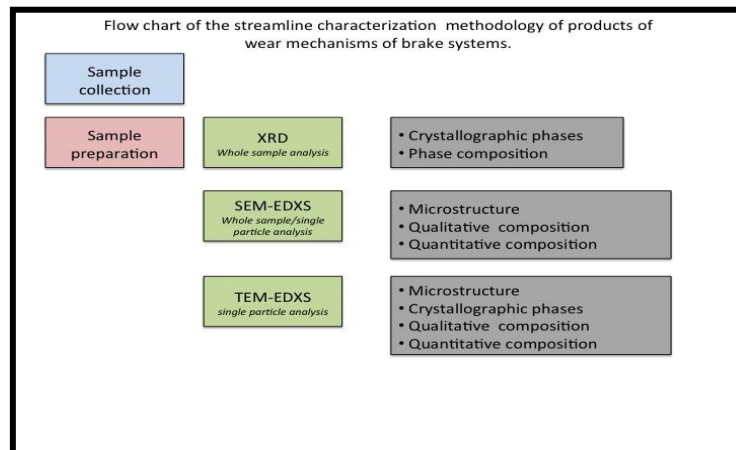


Figure 6.2.1: *The flow-chart of the characterization methodology.*

6.3 High temperature wear behavior of M1 and M2 friction materials: Role of the friction layer in the high-temperature pin-on-disc study - (Case III)

The major findings of *Case I*, motivated us to know further more what exactly happens when friction materials (M1 and M2) are subjected to high temperature working conditions. As continuation of the *Case I*, concerning research work on dry sliding (frictional heating) test, an attempt has been made to investigate the friction and wear behavior of commercial low-steel M1 & M2 friction materials at different high temperatures and to understand the mechanisms of mild to severe wear transition during dry continuous sliding conditions (pin-on-disc), starting from a mild regime (1.31m/s and 2MPa). Furthermore, the work aimed at gaining some understanding on the formation and function of the friction layer forming at the mating surfaces. A heating attachment for the pin-on-disc rig was developed (see Fig. 6.3.1) to conduct the friction tests from room temperature up to elevated temperatures, i.e., 170°C, 200°C, 250°C, 300°C and 350°C.

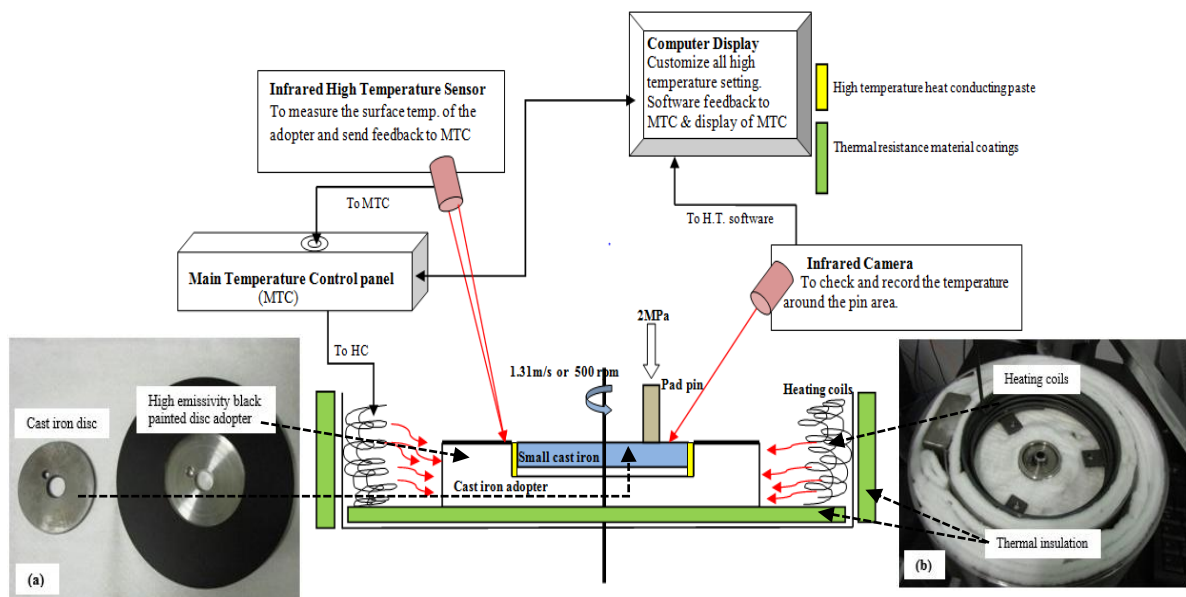


Figure 6.3.1: High temperature wear test rig.

6.4 Role of the heat-treatment of the cast iron disc - (Case IV)

It is confirmed that, irrespective of the braking conditions, the counterface cast iron disc plays an important role in the wear process and in the formation of airborne particles. Therefore, an increase in the wear resistance of the braking disc could produce a decrease in wear and emission. A possible way to achieve this goal is through suitable heat-treatments, avoiding though excessive embrittlement of the disc. As the major findings of *Case II*, shows that iron oxide has a major weight percentage contribution to the wear debris and airborne particles. This major weight percentage of iron oxide reflects that the counterpart i.e., cast iron disc, wearing at high rate during tribological operations, which directly affect the braking efficiency, maintenance cost and life expectancy of the braking systems.

Therefore, in this section of study we had modified the mechanical and physical properties of the tribo-counterpart i.e., cast iron disc, the role of a conventional heat-treatment on the dry sliding behavior of a cast iron material, commonly employed in the production of braking discs, with M2 friction material (having lower wear rate, as confirmed from *Case I*), is investigated. The wear tests were carried out again in a pin-on-disc configuration, and the pins were made of the same commercial low-steel friction material as in the previous cases. The aim of the work is to provide preliminary information on the feasibility of the disc modification process that of course has to be possibly optimized to address all the engineering requirements of a real braking system.

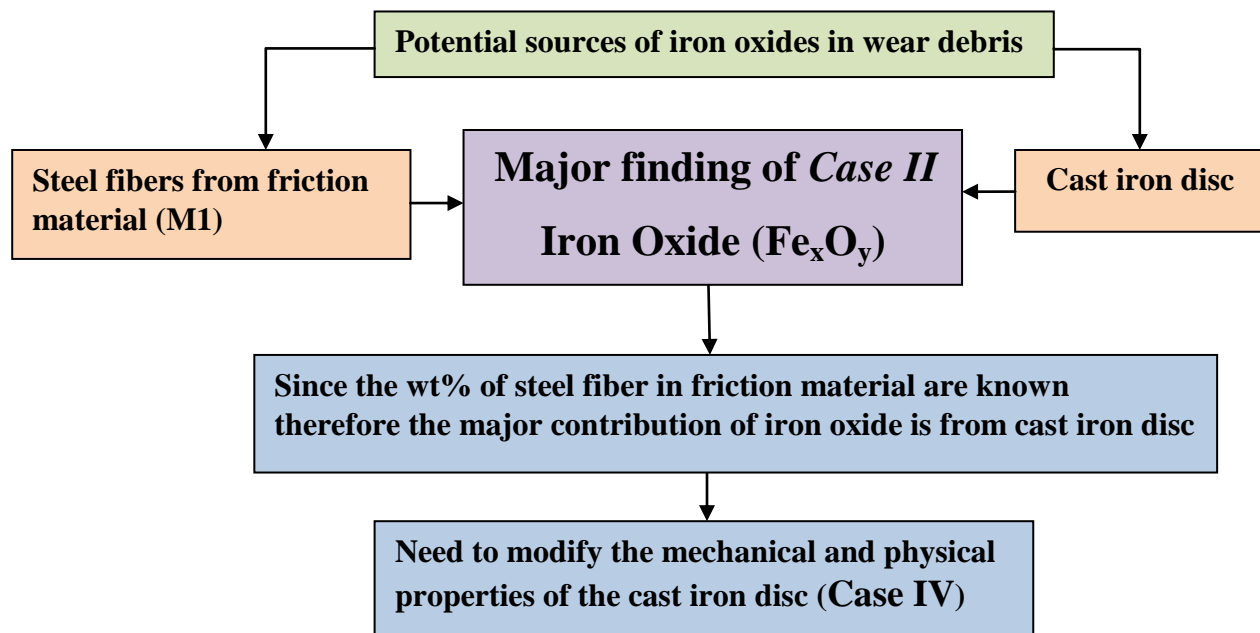


Figure 6.4.1: Highlighting the reason for the heat treatment of the cast iron disc.

Chapter 7

Experimental Procedures and Characterization Tools

7.1 Friction Materials - M1 & M2

The tribological wear tests were carried out on commercial low steel friction materials M1 & M2 pins, ($\text{Ø } 5.5 \text{ mm} \times 7.7 \pm 0.3 \text{ mm}$ long), dry sliding against a cast iron disc lamellar pearlite. After carrying out the test, debris were collected and analyzed, with different techniques, together with traces of wear of the disc and of the pins and the cross sections of the pins. The friction materials (M1 & M2), whose XRF composition is displayed in table 7.1.1, used in the tribological pin-on-disc tests have distinct features, as concerns structure and compositions, as you can see from table 7.1.2.

In all tribological testing, the pins were cut from real brake pads with the help of conventional mechanical machining. The friction material M1 is based on phenolic resin, featuring reinforcing fibers, such as copper and iron whereas M2 is rich in zirconium and featuring potassium titanate as reinforcing fiber. In addition to these components, there is a large quantity of other elements in both the friction materials, which influence the wear behavior during braking.

The percentages by weight of the components, evaluated from data XRF and according to the stoichiometries of the various compounds for M1 & M2 friction materials are listed in table 7.1.2.



Figure 7.1.1: Brake pad pins from the two different friction materials, M1 & M2.

Chapter 7: Experimental Procedures and Characterization Tools

Table 7.1.1: *Experimental composition measured by X-ray fluorescence spectroscopy (XRF) for M1 & M2 friction materials.*

| Elements | Mg | Al | S | K | Ca | Ti | Fe | Cu | Zn | Zr | Sn | Si | Cr | Ba |
|----------------------|------|-----|-----|-----|-----|-----|-----|-----|------|------|-----|-----|-----|-----|
| M1 XRF (wt %) | 10.4 | 9.1 | 5.2 | 0.6 | 5.0 | 0.2 | 7.1 | 5.4 | 12.5 | 0.1 | 8.7 | 5.8 | 3.6 | ND |
| M2 XRF (wt %) | 1.3 | 3.5 | 2.7 | 3.7 | 3.6 | 9.7 | 4.2 | 5.9 | 3.5 | 24.7 | 2.2 | 3.0 | ND | 3.9 |

Table 7.1.2: *Stoichiometries of the various compounds present in M1 & M2 friction materials.*

| M1 Components | M1 wt % | M2 Components | M2 wt % |
|---|----------|---|----------|
| Magnesium oxide (MgO) | 14.1 | Zirconium Oxide (ZrO ₂) | 31.0 |
| Tin Sulfide (SnS) | 9.3 | Silicate of Al and Mg | 9.5 |
| Aluminium oxide(Al ₂ O ₃) | 5.7 | Iron (Fe) | 8.0 |
| Vermiculite (Mg ₃ Al ₄ S ₄) | 13.6 | Copper (Cu) | 7.5 |
| Zinc Oxide (ZnO) | 13.8 | Vermiculite (Mg ₃ Al ₄ S ₄) | 6.0 |
| Copper (Cu) | 2.8 | Barite (BaSO ₄) | 5.0 |
| Iron Sulfide (FeS) | 9.4 | Potassium titanate (K ₂ O ₃ Ti) | 5.0 |
| Organic resin, graphite fibers and carbon-based | Balanced | Aluminum oxide (Al ₂ O ₃) | 3.0 |
| | | Calcium carbonate (CaCO ₃) | 2.5 |
| | | Tin sulfide (SnS) | 2.5 |
| | | Zinc (Zn) | 2.0 |
| | | Bismuth (Bi) | 0.6 |
| | | Iron sulfide (FeS) | 0.5 |
| | | Organic resin, graphite fibers and carbon-based | Balanced |

Table 7.1.1 shows an average X-ray fluorescence (XRF) probe as complementary elemental techniques was used to identify the main constituent elements present in the two different friction materials. Frictional additives, which is a mixture of lubricants and abrasives and which shows the characteristic properties of a friction material has higher value in M2 and it is zirconium silicate, zirconium oxide, aluminum oxide, graphite and tin sulfide. In addition to these components, however, there may be a large quantity of other elements, which influence the behavior during braking and to wear.

In Fig.7.1.2 shows the microstructure of the virgin M1 & M2 friction materials. It is showing in the figure that the fiber of potassium titanate (yellow outline) (refer Fig.7.1.2b) can be seen in M2 (Fig.7.1.2b) while absent for M1 (Fig.7.1.2a). While in Fig.7.1.2a the distribution of magnesium oxide (dark black phases) is clearly visible. In addition the distribution of tin and sulphur rich area (small shiny phases) of M1 can also be seen in Fig.7.1.2a.

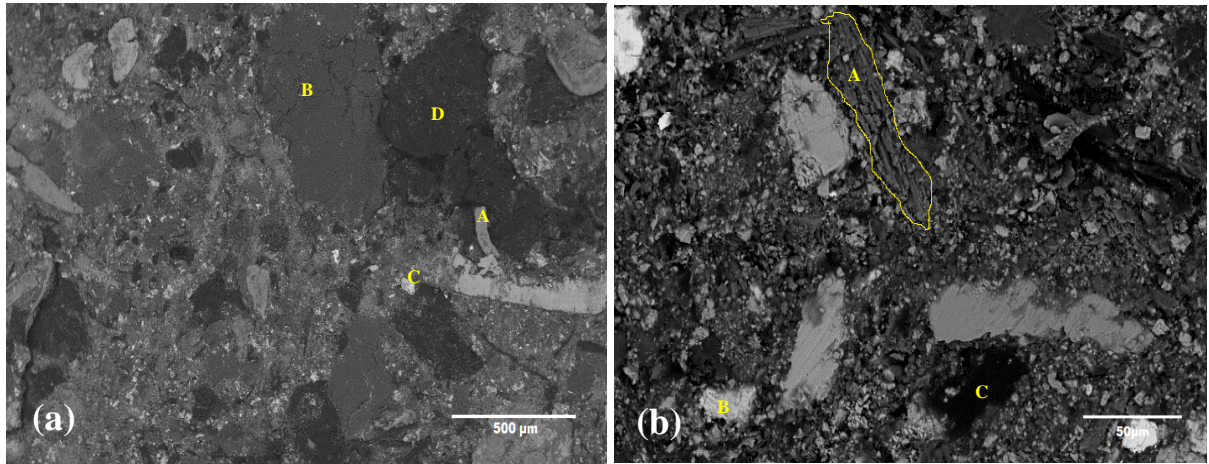


Figure 7.1.2: Microstructure of virgin friction materials (a) M1 friction material in which **A:** Steel fiber, **B:** Magnesium oxide, **C:** Tin sulfide and **D:** Area rich in Fe, Mg, Ca and Zn. (b) M2 friction material where **A:** Potassium titanate fibre, **B:** Tin sulfide and **C:** Resin binder.

7.2 Cast iron disc counterpart

The counterface discs used for the tribological tests, were made of a gray cast iron. It is a common lamellar pearlitic cast iron with a hardness of 287 ± 37 HV 0.05. Two size of cast iron disc were used, small cast iron disc (dia. 63.0 mm) was used in *Cases III & IV* and large cast iron disc (dia. 140 mm) was used in *Case I & II* (Fig.7.2.1).

The physical properties of the lamellar pearlitic gray cast iron are given in the following :

- Density: 7.0 g/cm^3
- Thermal conductivity (at 100°C): $49 \text{ W/m} \cdot \text{K}$
- Specific heat (T = $20\text{-}200^\circ\text{C}$): $461 \text{ J/kg} \cdot \text{K}$
- Thermal diffusivity (T = $20\text{-}100^\circ\text{C}$): $2.45 \times 10^{-5} \text{ m}^2/\text{sec}$
- Coefficient of thermal expansion (at 100°C): $9\text{-}12 \times 10^{-6}/\text{meter} \cdot \text{K}$

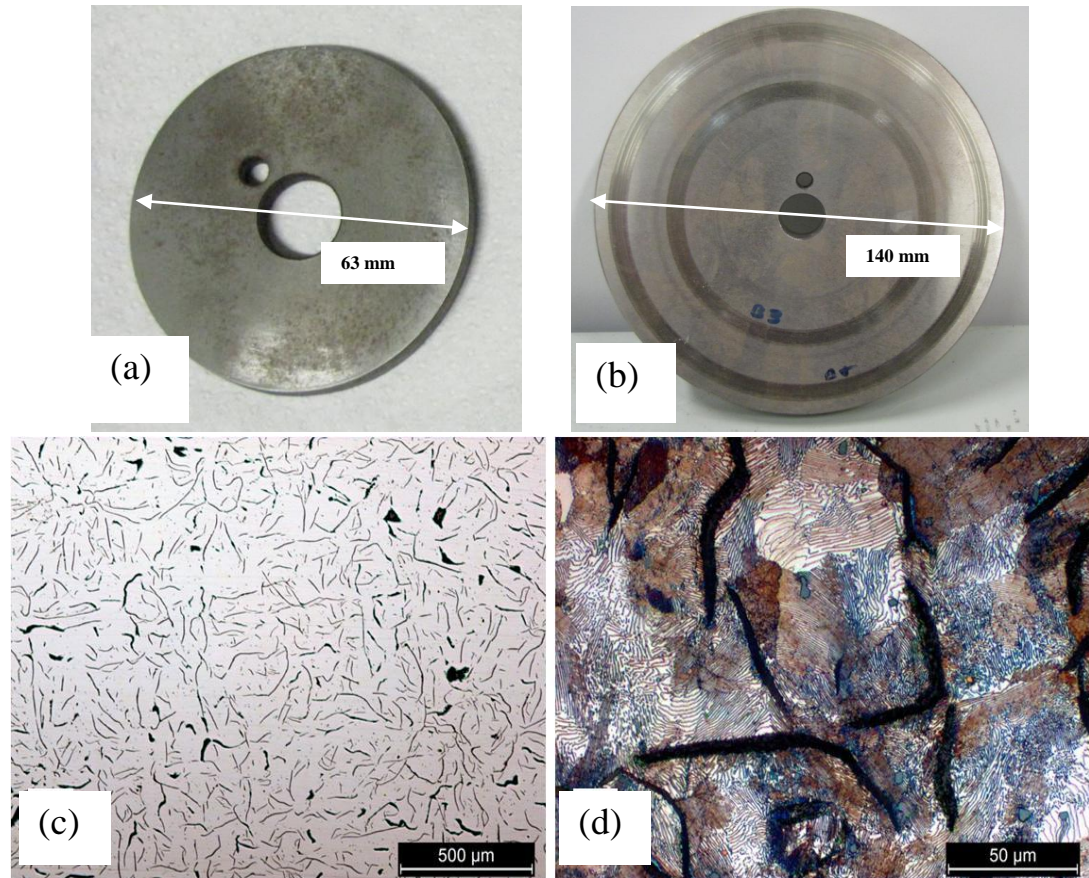


Figure 7.2.1: a) Optical image of the small cast iron disc, used in case III & IV b) Optical image of the big cast iron disc, used in case I & II, c) Microstructure of the grey cast iron, d) microstructure after etching with 2% Nital + 2% Picral (50-50 vol%).

7.3 Pin-on-Disc (PoD) tribometer

The pin-on-disc test is primarily used to study the wear process of friction materials. Through this test it is possible to simulate the mechanisms of adhesive and abrasive wear. In pin-on-disc machine a pin is forced by an applied load to remain in contact with the surface of the disc and the disc is put in rotation by a motor, which provides a constant rotation speed. The pin-on-disc tests have allowed us to obtain information on the wear mechanisms occurring in the pads and disc, as well as being able to measure the losses in weight and height to calculate the volume of wear. In this way, once obtained the parameters of wear, we have been able to correlate these results to supplement the analysis of fragments of wear and to obtain information on the mechanisms of wear.

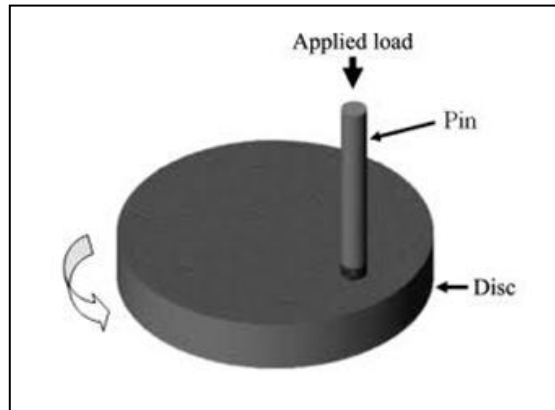


Figure7.3.1: Simple pin-on-disc machine fundamentals.

7.3.1 Pin-on-disc used in *Case II* for wear debris collection (polycarbonate filter)

The pin-on-disc wear test is a robust method for studying wear mechanisms. In the thesis, this test is used to study some tribological aspects of the brake action to be comparatively investigated with the outcome of field tests [S. Abbasi et al.,2011]. Tests were performed using a pin-on-disc machine with a horizontal rotating disc and a deadweight-loaded pin. A climate chamber was used as a closed box with control of the cleanness of the incoming air. As shown in Fig.7.3.2, the fan (B) takes the air from the room (A) into the box (G) via a flow measurement system (C), a filter (D) and the air inlet opening (F). The connections between fan and measurement system, between measurement system and filter, and between filter and chamber were flexible tubes (E). The air in the box was well mixed due to the complex volume of the pin-on-disc machine (H) and the high air change rate. This mixing was verified by the smooth concentrations measured during the tests. The air in the box transported the generated particles to the air outlet (J), where sampling points for particle measurement were situated. The fan had a variable speed and was set at a flow rate of 7.2 m³/h; this corresponds to an air change rate during the tests of 72 l/h. The inlet air was verified particle-free by measuring the particle concentrations in the inlet and the outlet of the box before the tests started and after the tests were finished. In both cases the measured particle concentrations were zero. During the measurements one particle counter (P-Track) continuously monitored the inlet concentration. Inside the box a small pneumatic tube was attached to the pin-on-disc machine to direct high velocity air (>10 m/s) at the contact point in order to minimize the number of particles sticking to the test materials. The pressurized air was filtered to remove all particles from this source. The working conditions for the this test were:

- Linear speed = 13.0 m/s (corresponding to 500 rpm)
- Applied load = 1.39 MPa.
- Actual sliding distance = 14000 metres.
- Cast iron disc diameter = 63.0 mm.
- Test time = 180 minutes.

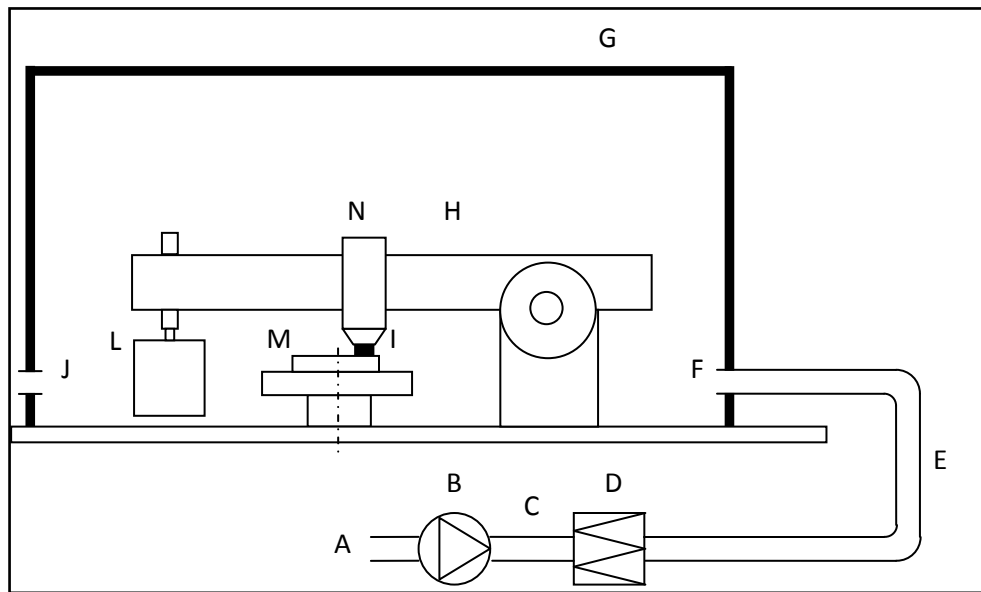


Figure 7.3.2: Schematic of the test equipment [Olofsson et al.,2009]. A: Room air; B: Fan; C: Flow rate measurement; D: Filter; E: Flexible tube; F: Inlet for clean air, measurement point; G: Closed box (Chamber); H: Pin-on-disc machine; N: Air inside box, well mixed; J: Air outlet, measurement points; L: Dead weight; M: Rotating disc sample; I: Pin Sample.

Table 7.3.1. Characteristic features of Polycarbonate filter.

| Filter | Poly carbonate filter membranes |
|----------------|---------------------------------|
| Material | White |
| Diameter (mm) | 24.8 |
| Thickness (mm) | 0.02 |
| Grease applied | High vacuum |

7.3.2 Electrically Low Pressure Impactor (ELPI+) - A particles collector instrument

The main particles-collecting instrument for *Case II* on polycarbonate filters was an ELPI+ impactor. The collection of wear debris made through an active sampler capable to capture fine particles from the working atmosphere. These samples are provided with polycarbonate (PC) filters on which a spray of vacuum grease is applied to improve their particle trapping capability. ELPI+ is a new, improved version of the widely used system, with collection plate diameter of 25 mm, which enables real-time measurements of particle size distribution and concentration over a size range of 6nm–10µm with 10Hz sampling frequency and 10 litre/min flow rate.

The ELPI+ operating principle can be divided into three main steps: particle charging, size classification in a cascade impactor and electrical detection with sensitive electrometers. Particles are first charged to a known charge level in the so-called corona charger. After charging, the particles enter a cascade low-pressure impactor with 14 electrically insulated collection stages, on which they get selectively stack according to their aerodynamic diameter (D_i).

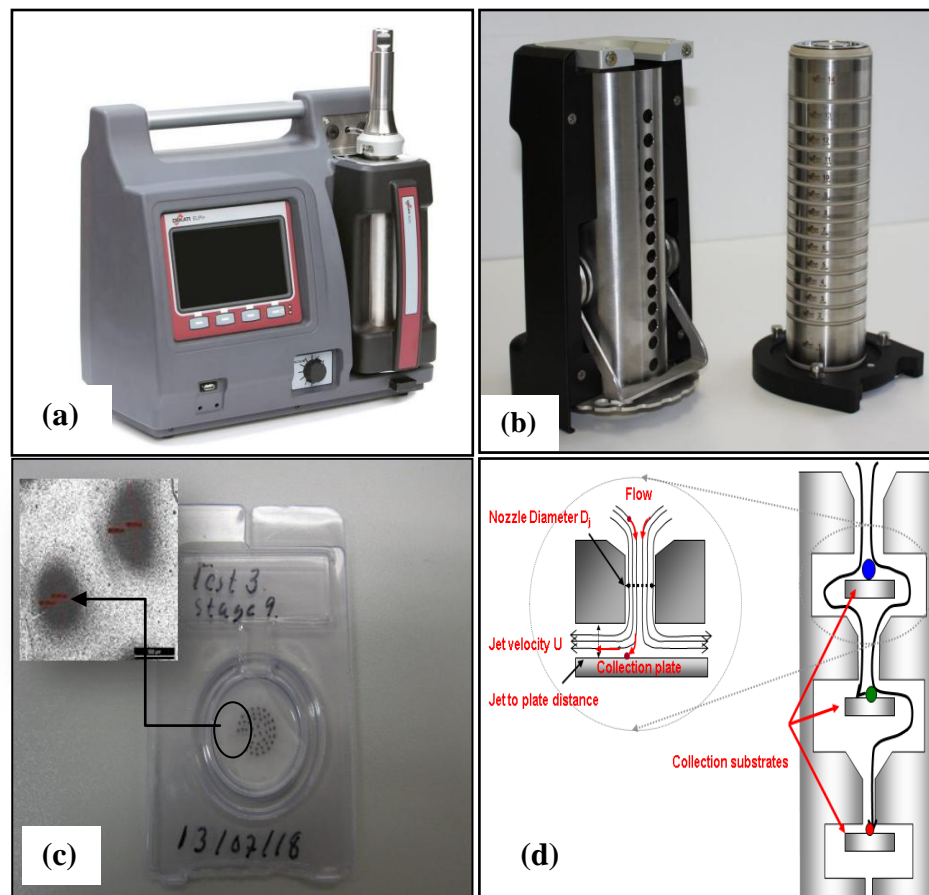


Figure 7.3.3: ELPI+ particle collection instrument (a) and (b). Polycarbonate filters with collected particles, (c). Scheme of working principles, (d).

Particles number and concentration are evaluated through the real time measure of the electric charge deposited by particles onto each impactor stage using high sensitivity electrometers [ELPI+, Dekati,2014]. These samples are provided with polycarbonate (PC) filters on which a sprayed film of vacuum grease is applied to improve their particle trapping capability [Olofsson et al.,2009 , Abbasi et al.,2012]. The impactor provides a set of 14 PC filters. Eight (stage 2, 3, 4, 7, 8, 9, 12 and 15 shown in Table 7.3.2) of these have been selected for methodological study as representative of the different particle size range interesting for our research.

Table 7.3.2: List of different stages of ELPI+ with total particle number and total mass (Case II, PC filters-1.39MPa, 13.0m/s).

| Stages | Di [μm] | Total Particles Number [1/cm ³] | Total Particle Mass [g/m ³] |
|--------|----------------------|---|---|
| 15 | 10.0 | - | - |
| 14 | 6.8 | 0.25 million | 69.6 |
| 13 | 4.4 | 0.44 million | 31.1 |
| 12 | 2.5 | 0.86 million | 13.1 |
| 11 | 1.6 | 2.2 million | 8.5 |
| 10 | 1.0 | 2.9 million | 2.8 |
| 9 | 0.64 | 3.5 million | 0.81 |
| 8 | 0.4 | 11.7 million | 0.68 |
| 7 | 0.26 | 18.4 million | 0.29 |
| 6 | 0.17 | 59.5 million | 0.24 |
| 5 | 0.108 | 253.8 million | 0.22 |
| 4 | 0.06 | 1.9 billion | 0.36 |
| 3 | 0.03 | 7.9 billion | 0.24 |
| 2 | 0.017 | 26.0 billion | 0.13 |

7.3.3 Pin-on-disc used in Case II for wear debris collection (aluminium foil) and also used in Case I & IV

A simple pin-on-disc tribometer is shown in fig. 7.3.4. It was used for the *Case I, II and IV* with maximum disc rotation capacity is 500 rpm. The tribometer installed with specific software that can detect and acquire the main parameter of the pin-on-disc test i.e., coefficient of friction, temperature of the tangential surface of the pin and measured point was 4mm & 6mm above the real contact surfaces and change in elevation can be measured with the help of transducer which is properly calibrated for every wear test.

With this dry sliding pin-on-disc tribometer another approach for collecting wear debris particles was adopted by using an aluminium foil placed at the bottom part of the tribometer, beneath the rotating disc. Tests were carried out at room temperature under controlled environmental humidity. The working conditions for the test were:

- Linear speed 3.14 m/s (corresponding to 500 rpm) for *case I* (big cast iron disc 140 mm dia.) and 1.31 m/s for *case III & IV* which is due to smaller size of counterpart disc of 63.0 mm in dia.
- Applied load = 2 MPa.
- Actual sliding distance = 4000 metres.
- Cast iron disc diameter = 140.0 mm (*case I*) and 63.0 mm (*case III & IV*)

The experimental time duration of the every wear test was 50 minutes.

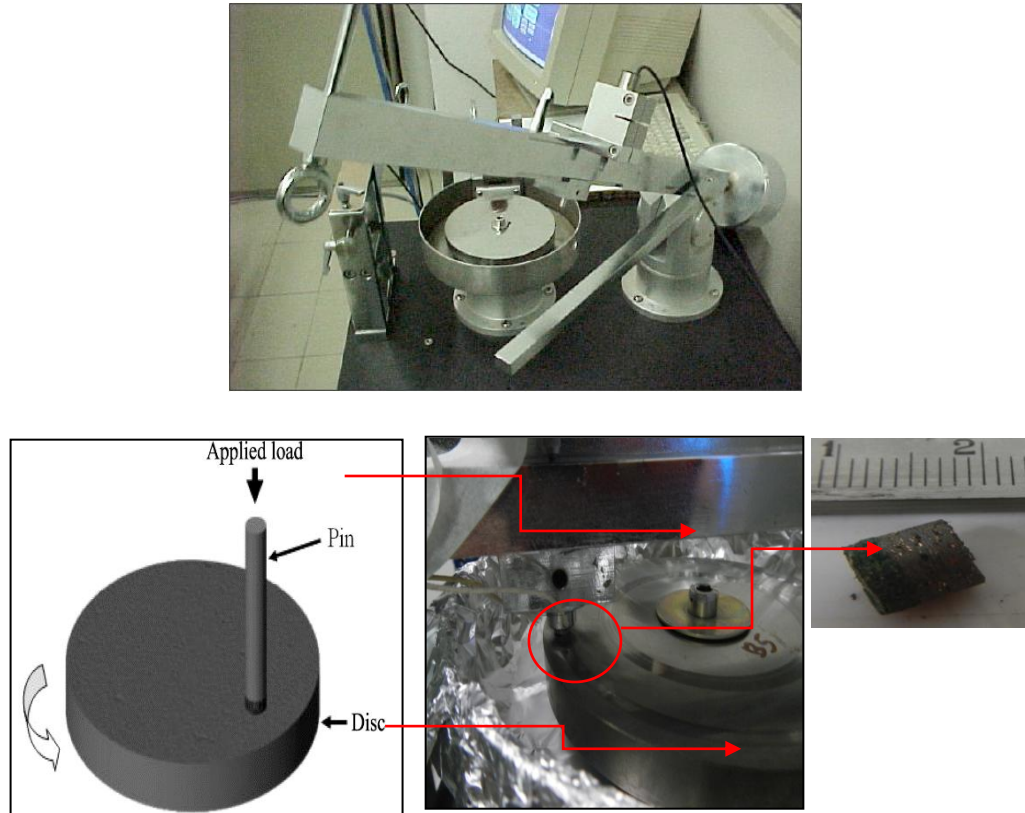


Figure 7.3.4: Pin-on-disc equipment with aluminum foil for collecting of wear debris.

7.3.4 Pin-on-disc used in *Case III* (high temperature PoD or external heating test)

A modified version of the pin-on-disc tribometer used for high temperature is recalled in the following as high temperature pin-on-disc (H.T. PoD). The experimental studies were carried out in a laboratory made high temperature pin-on-disc wear test rigs. The tests were performed at controlled temperatures, in which the temperature of the disc for a given test at elevated temperature remain constant throughout the test. The high temperature wear tests were conducted at different temperatures with a view to studying the influence of temperature on friction and wear behaviour of commercial M1 & M2 friction materials were referred as, temperature of the pin-on-disc system at room temperature (25°C) and at 170°C, 200°C, 250°C, 300°C and 350°C. The working conditions of the test were: linear speed of 1.31 m/s (corresponding to 500 rpm), applied load of 2MPa and actual sliding distance of approx. 4000 meters, for a total duration of 50 min. per test. At the beginning of each test, a 10 minutes running in period was conducted to obtain a good and a stable contact during the subsequent test. This wear test condition were referred for every test at room and elevated temperatures. The pin-on-disc wear test machine was equipped with an external heater, which enable the test at a temperature up to 1000°C.

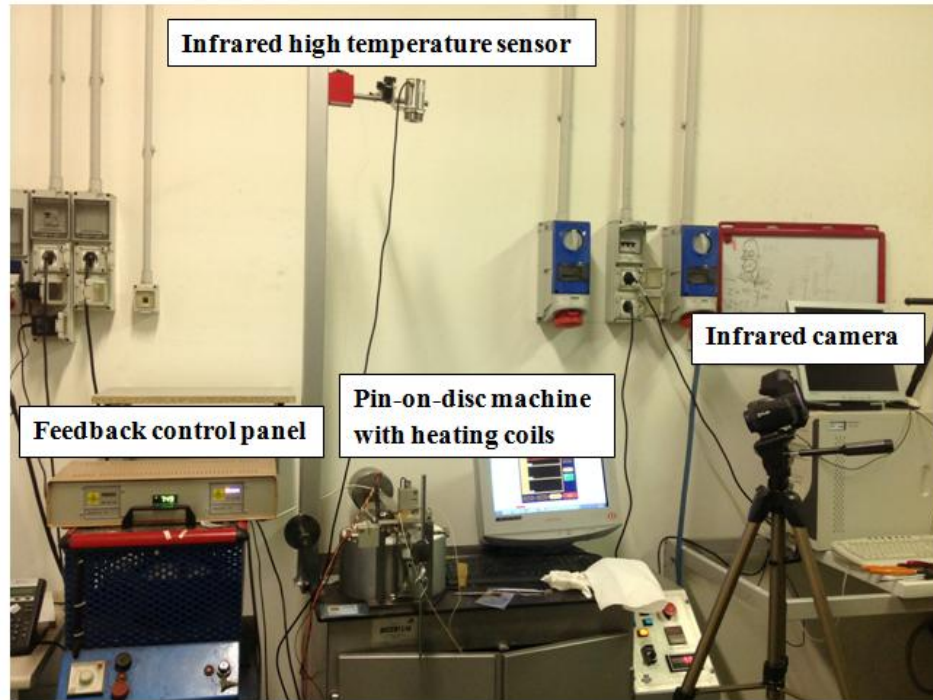


Figure 7.3.5: *Real time and schematic closed loop feedback high temperature wear test setup.*

A computerised feedback control system enables accurate control on the heater in order to have a constant and fixed disc temperature during the entire test. The data acquisition system records coefficient of friction, temperature of the pin and manually recording the weight loss of the pin.

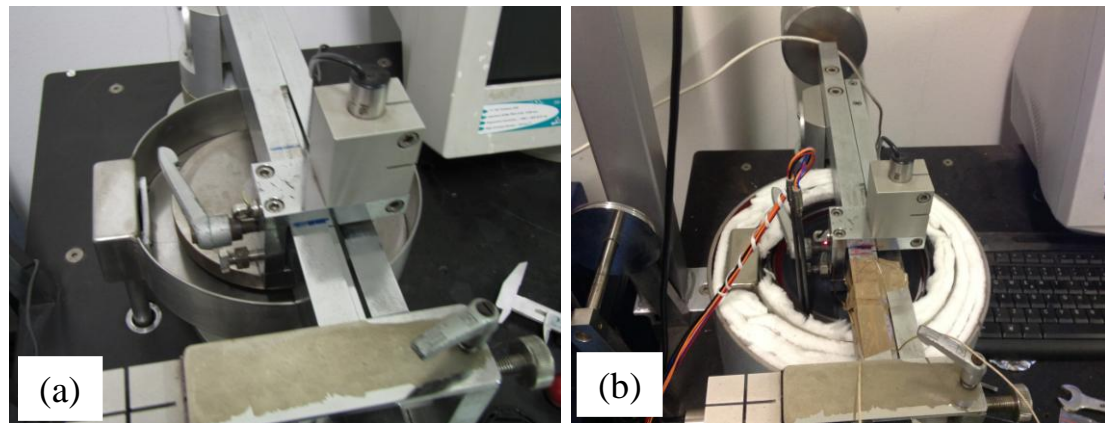


Figure 7.3.6: *a) Low temperature Pin-on-disc: Frictional heating system with 140mm diameter cast iron disc used in Case I. b) High Temperature Pin-on-disc: External heating system with 63.0 mm diameter cast iron disc used in Case III.*

Fig.7.3.5 shows schematic view of high temperature wear test arrangement which is a closed loop feedback system, in which the temperature of the cast iron disc were constantly maintain by the *Heating coils* (HC) (Fig.7.3.6b) which is govern by the *Main Temperature Control panel* (MTC) through infrared high temperature sensor and infrared camera (Fig.7.3.7).

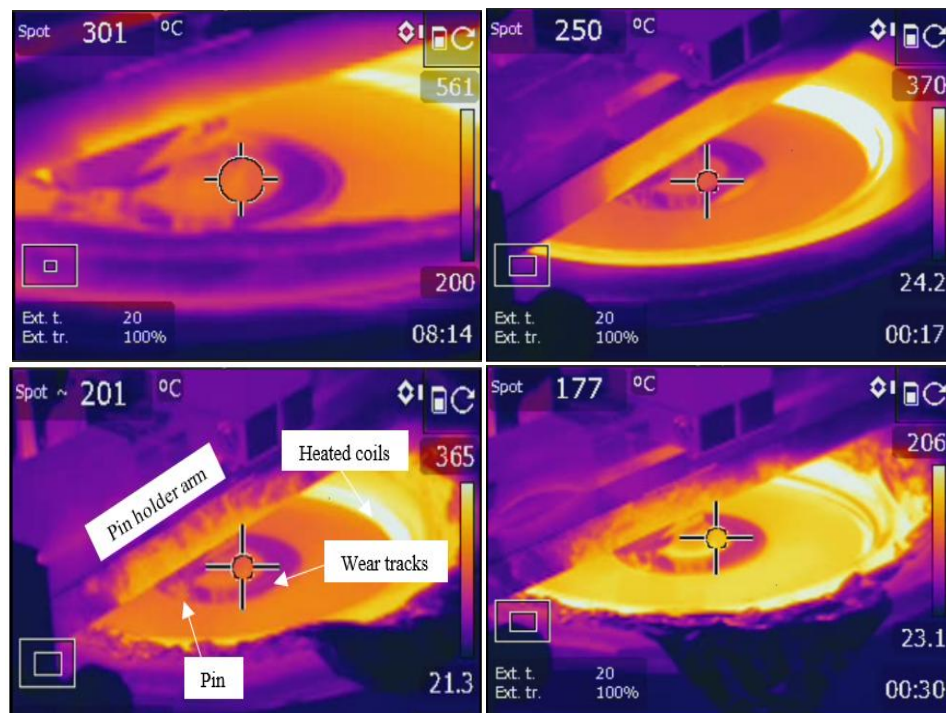


Figure 7.3.7: Infrared camera images of high temperature pin-on-disc at different temperature.

In this high temperature work, the testing counterpart, cast iron disc of diameter 63.0 mm was fitted into the groove of another cast iron adapter (dia. 140.0 mm) (Fig.7.3.6a). The upper surface of the adapter was coated with high emissivity black paint in order to eliminate the reflection of infrared rays from the shiny metal surface, which otherwise infrared camera and high temperature sensor would usually measure as an error in reading the disc surface temperature. The clearance between the adapter and cast iron disc was filled with high temperature conductive paste, which insures the correct and spontaneous heat flow without any important drop. The high temperature pin-on-disc test rig was wrapped (Fig.7.3.6b) into an alumina refractory sheet, providing thermal insulation, in order to minimize any damage to friction test rig and surrounding, caused by heat leakage.

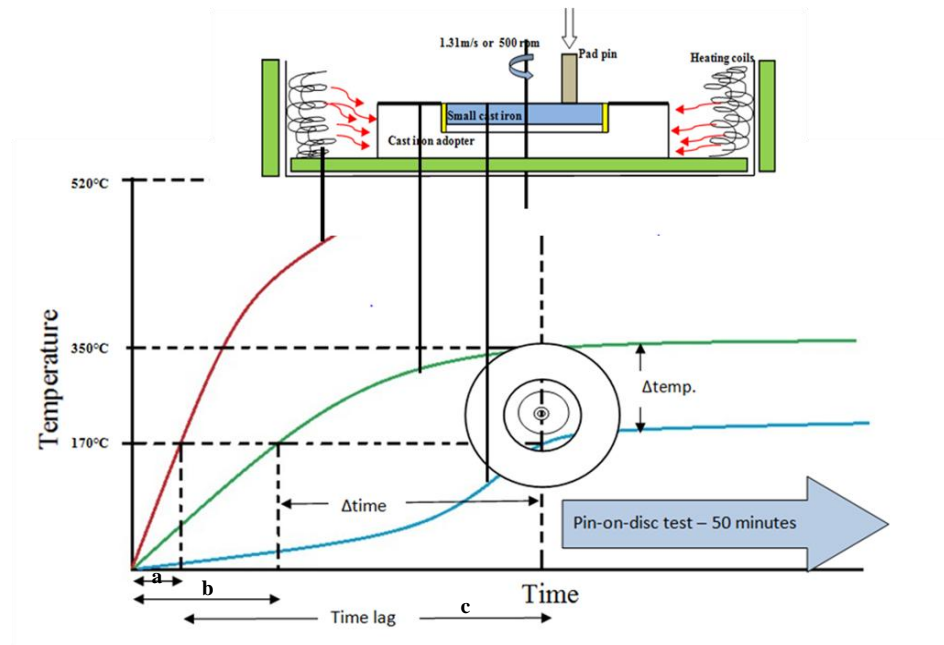


Figure 7.3.8: Shows time lag of heating between the heating coils, adapter and cast iron disc.

Before starting of the high temperature wear test, there was a time delay between heating of heater to the desired cast iron heating (Fig.7.3.8). Heating coils reached rapidly to the set temperatures, whereas couple of minutes was required for the adapter and cast iron disc to heat up to the desired temperature. For low temperature heating, let say 170°C, when in the main control panel shows the temperature of the heating coils reached 170°C at that moment the adapter temperature is far behind of the desired temperature goal. At this temperature the time taken by the adapter to match up with the heating coils temperature was nearly 30 minutes. This was due to the higher mass and, therefore, thermal inertia of the adapter-disc and to the thermal coupling between them and the heating coils. In fact that there is some air gap between the heating coils and adapter and little clearance between adapter and cast iron.

At high temperature the tribo-oxidation of the cast iron occurred and with different high temperature different colour of the cast iron achieved at the last of every wear test. Figure 7.3.9 shows worn cast iron disc at different temperatures.

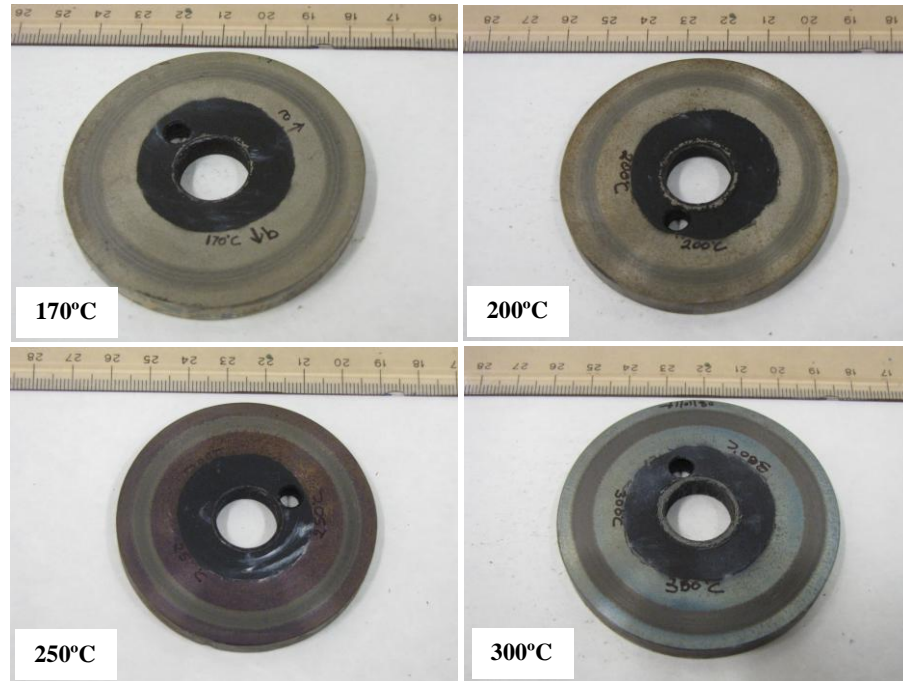


Figure 7.3.9: Tribo-oxidation of cast iron at different high temperature test.

Note:- In this thesis work, dry sliding (*frictional heating tests*) and high temperature wear (*external heating tests*) tests were carried out using the pin-on-disc testing rig described in figure 7.3.5. The M1 & M2 pins were abraded on the bottom side with SiC 800 grit abrasive paper in order to render this surface as more planar as possible in order to have a stable contact with the pin-holder and a conformal contact with the disc. Pin wear was measured by checking its weight, W , before and after each test using an analytical balance with a precision of 10^{-4} g. Data were then converted into wear volumes using a measured density of the pad materials equal to 2.2 g/cm^3 for M1 and 2.9 g/cm^3 for M2 frictional materials. It was calculated by using the following relation:

$$W = [(W_1 - W_2) / \rho \cdot d] \dots \dots \dots (7.1)$$

where W_1 and W_2 are the weight of the pin before and after the test, ' ρ ' is the density of the friction material and ' d ' is the sliding distance. From ' W ', the specific wear coefficient, ' K_a ', was determined, by using the following relation:

$$K_a = W / F \dots \dots \dots (7.2)$$

where ' F ' is the applied load. Disc wear was measured with a profilometer, used to evaluate the cross section of the wear trace. During each test, the friction coefficient was continuously recorded with the evolution of high contact temperature. For this purpose, two chromel-alumel-type thermocouples were placed in two holes drilled in the pin holder at a distance of 4 and 6

mm from the contact surface of the pin with the disc. The measurement of the temperature by the thermocouple is a continuous contact with the pin and the data were recorded by the computer. In the figure 2.3.10, two thermocouple was used and inserted into the hole 1 and 2 for temperature measurement of the pin, at a distance from the surface of the pin equal to the height of 6.0 mm and 4.0 mm respectively.

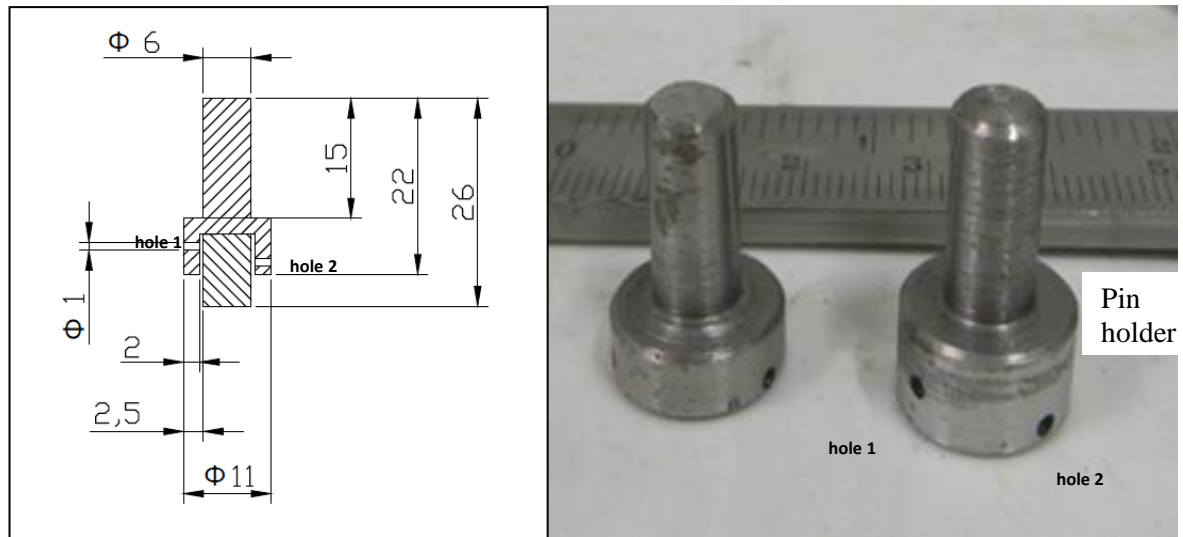


Figure 7.3.10: Pin holder with two holes for chromel-alumel-type thermocouples.

The temperatures involved with frictional pin-on-disc test rig are:

- T_{sup} is the surface temperature of the pin unknown that we need to calculate
- T_1 is the temperature recorded by the thermocouple in the hole 1
- T_2 is the temperature recorded by the thermocouple in the hole 2

From the diagram 7.3.11 we can derive the ' T_{sup} ' as:

$$T_{sup \text{ pin}} = T_1 + \frac{h_{pin}}{h_{pin} - (h_{pin} - 3.5)} * (T_2 - T_1) = T_1 + \frac{h_{pin}}{3.5} * (T_2 - T_1) \dots \dots \dots (7.3)$$

where ' h_{pin} ' is the initial height of the pin used in the wear test. The other equation used to calculate different wear parameters are the following:

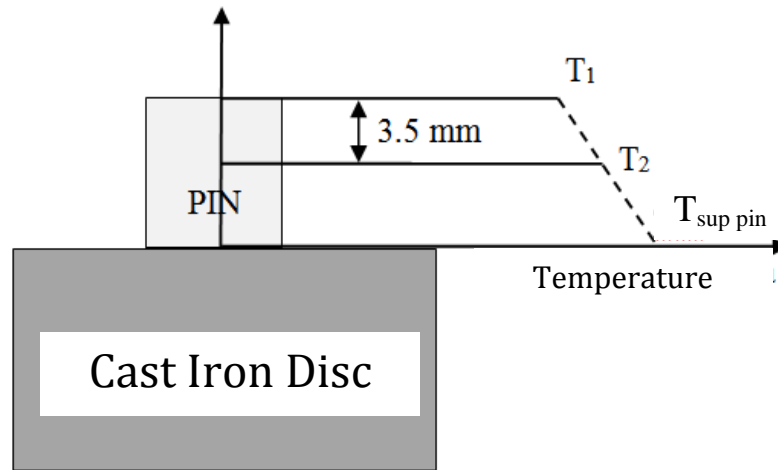


Figure 7.3.11: Diagram showing T_{sup} which is resultant linear gradient of $T1$ and $T2$.

- Wear rate (W) is calculated from the volume of wear, according to:

$$W = \frac{V_{\text{wear volume}}}{v * t * 60000} \text{ [mm}^3\text{/mm]} \dots \dots \dots (7.4)$$

where ' v ' is the speed of the test expressed in m/s and ' t ' is the test time in minutes.

- Specific wear coefficient (K_a) is calculated from the wear rate, according to:

$$K_a = \frac{W * 10^{-6}}{P * A_{\text{pin}}} \text{ [m}^2\text{/N]} \dots \dots \dots (7.5)$$

where ' P ' is the pressure, expressed in MPa and ' A_{pin} ' is the area of the cylindrical pin, expressed in mm^2 . The measures of weight loss and loss of height were made both before and after the run-in, and for the calculation of the wear rate and the coefficient of specific wear have been used.

7.4 Characterization tools

For characterization of wear debris the leading idea was to combine together experimental tools operating on large number of particles, so to provide average compositions, with techniques suitable for a limited number of particles, even single particles, in order to obtain information on microscopic scale. In this process two main selection criteria for the experimental methodologies were adopted: the availability of material specimen and the dimensional resolution required by the actual average size of the analyzed particles. Of course, crucial aspects of the proposed approach are: first, the matching and compatibility of the results moving from large down to small scale; second, the statistical significance of the experimental data.

7.4.1 X-ray diffractometer (XRD)

For identifying the crystalline phases of the wear debris powders collected on aluminum foil and polycarbonate filters and to check the information on their crystalline phases and relevant micro structural parameters, X-ray diffraction measurements were carried out on a IPD 3000 Diffractometer (compact 3K5 X-ray generator), using $\text{CuK}\alpha$ ($\lambda = 1.5406 \text{ \AA}$) radiation with Ni-filter. The X-ray generator settings were 40 kV and 30 mA (Fig.7.4.1).



Figure 7.4.1: *IPD 3000 Diffractometer.*

Wear debris or airborne particles from pin-on-disc tests were either spread on the original ELPI+ polycarbonate filters substrate or inserted into capillary glass tubes. Several reflection and transmission geometries have been considered in order to optimize the diffraction geometry for any specific sample. After these exploratory tests it has been concluded (Table 7.4.1) that the transmission mode geometry can give better X-ray diffraction patterns and peaks of wear debris collected on polycarbonate filters (Fig.7.4.3c).

The main problems with the reflection mode with these specimens were:

- In limited amount.

- In reflection mode it was particularly critical to place the powder with sample holder exactly in the path of X-ray beam, due to constraints in the geometry of the reflection mode, limitations which were not there in transmission mode.

Fig.7.4.2 shows the X-ray diffraction setup for the wear debris on polycarbonate and for a 0.5mm diameter capillary glass tube in transmission mode which shows higher degree of setup flexibility as compared to the reflection mode (Fig.7.4.4).

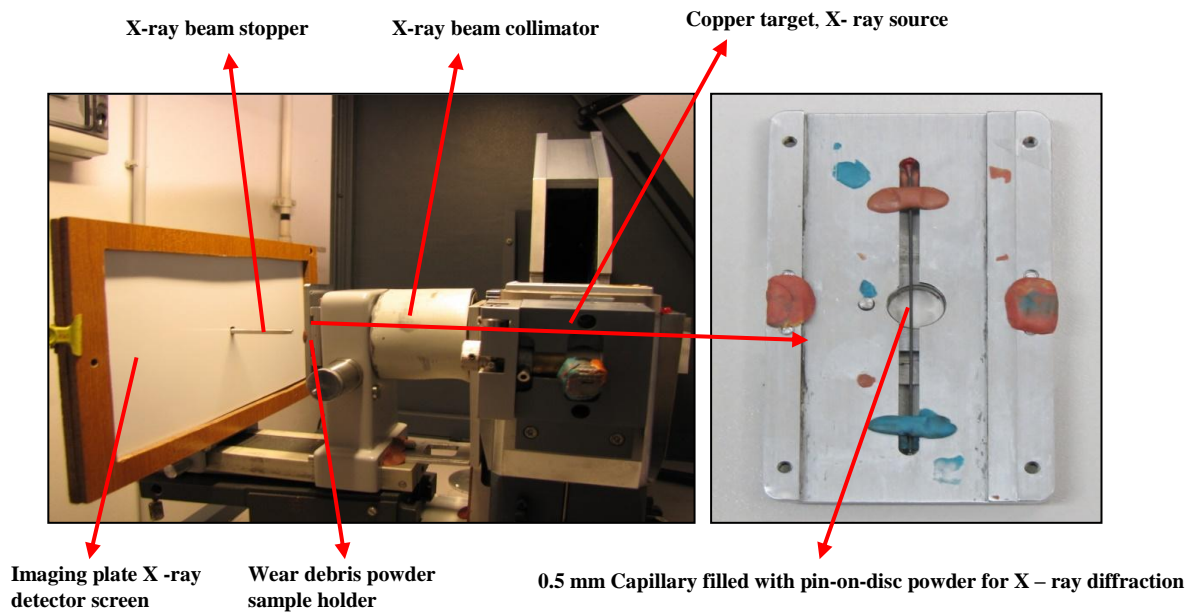


Figure 7.4.2: *IPD 3000 Diffractometer: transmission mode configuration.*

In reflection mode, some precautions have to be taken in order to avoid or limit as much as possible the incoming beam from impinging the sample holder outside the sample area. Images in Fig.7.4.4 show the imaging plate X-ray screen detector with the diffraction pattern of a standard silicon powder in both transmission mode and reflection mode.

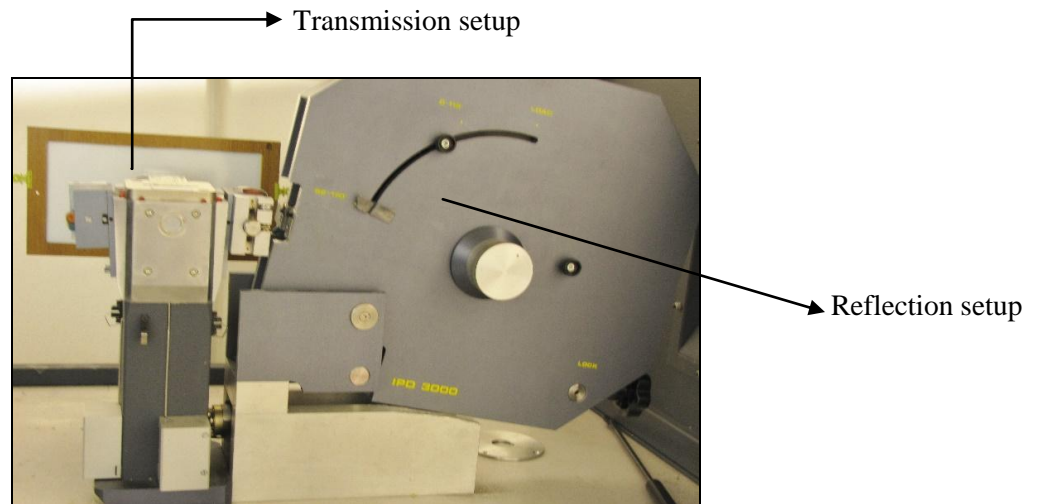


Figure 7.4.3: Two different configurations of operation for XRD analyses.

Here it has to be noted that in both modes i.e., transmission and reflection, the amount of silicon powder is definitely enough to intercept all incoming X-rays. The purpose of making the diffraction pattern of the silicon powder was to calibrate the X-ray diffraction system in both transmission mode and reflection mode.

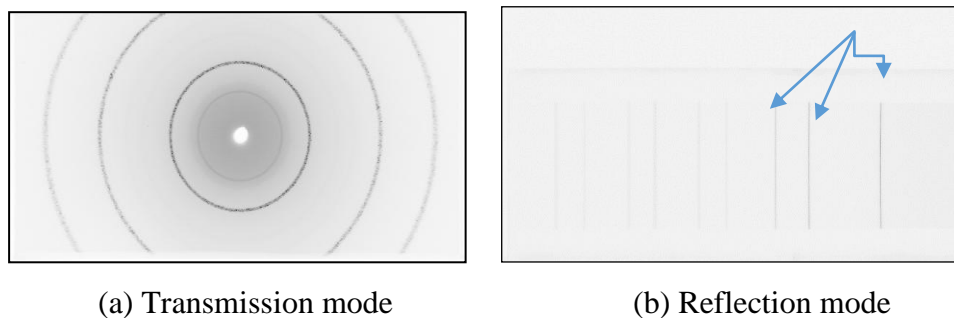
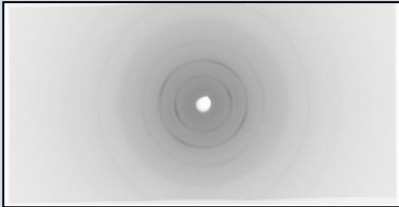


Figure 7.4.4: Imaging plate X-ray screen detector / Diffraction pattern of Si standard powder.

The plane rectangular sample holder (Fig.7.4.2) with small hole in the center was used for the diffraction of powder. The filter containing small powder spots of diameter ($400\mu\text{m}$ - $700\mu\text{m}$) of wear debris was placed exactly in the center of the hole of the sample holder in order to have good alignment with the X-ray beam.

Table 7.4.1: Comparison of two different mode of XRD operation.

| Flat Image Transmission mode | Flat image reflection mode |
|---|--|
| Good X- ray diffraction geometry for small amounts of powder, like ELPI+ (0.4 mm – 0.7mm diameter). | Unsuitable X- ray diffraction geometry for small amount of powder. |
| Small quantity of powder is required to be mounted in a capillary glass tube of 1mm or 0.5mm. | Large amount of powder is required for diffraction. (1 cm ³ approx.) |
| Powders spots on filters can be easily align centrally and perfectly X- ray beam can be focussed on the powder with high degree of flexibility. | In case of little powder it is difficult to focus X- ray beam on the powder spot. |
|  |  |
| Wear debris powder diffraction of M1 on polycarbonate filter, ring pattern in transmission mode. | Wear debris powder diffraction of M1 on polycarbonate filter, ring pattern in reflection mode. |

Depending on the size of the wear debris spot (Fig.7.4.3c) on the polycarbonate filters, several different sizes of X-ray collimator (Fig.7.4.5) have been used in order to have good diffracted intensity and, on the other hand, still a good X-ray focus on the wear debris spot, which has a diameter varying from 400 μm to 700μm.



Figure 7.4.5: Different size of incoming X-Ray beam collimators.

The diffracted X-ray beam was collected on an imaging plate (Fig.7.4.2) of flat rectangular shape, which was just placed beyond the wear debris powder sample, in transmission mode (Fig.7.4.2). The diffraction pattern of wear debris on polycarbonate filter and wear debris powder in capillary glass tube was recorded in the form of concentric circles, showing the polycrystalline nature of the wear debris.

In our experimental set up, using Cu K-alpha radiation, the reach of diffraction angle (2θ) was limited to 60° with relevant consequences on the range of the recorded diffraction patterns. This is to be compared with nearly 180° (2θ) accessible to semi circular imaging plate used in reflection mode.

Table 7.4.2: *Diffraction instrument calibration setup used in MAUD software.*

| Intensity calibration | None Cal |
|------------------------------|-------------------------|
| Angular calibration | Flat image Transmission |
| Geometry | Image 2D |
| Measurement | 2Theta |
| Source | X-Ray tube |
| Detector | Scintillation |
| Instrument Broadening | Caglioti PV |

Using the *Materials Analysis Using Diffraction* (MAUD) software [Lutterotti et al.,1999, Lutterotti et al.,2010] the following steps were implemented to analyze the XRD data:

- Rings were transformed into intensity vs diffraction angle patterns.
- Identification of the diffraction peaks and assignment to crystalline phases (peak search-search match).
- Fitting of the experimental data to the modeled spectrum.
- Refinement of the fitting through the least square procedure working on phase composition and microstructural parameters.

The procedure requires an accurate calibration of the diffractometer, in order to take into account the instrumental effects. Table 7.4.2 is showing calibration setup used in analysis of experimental diffracted rings of wear debris on polycarbonate filters and in capillary glass tube. For reflection geometry specific calibration parameters are available in the instrument and control program.

Due to limitation in sample placing in IPD 3000 Diffractometer, another X-ray diffractometer (D8) using $\text{CuK}\alpha$ ($\lambda = 1.5406 \text{ \AA}$) radiation to have better count statistic, has been used for characterization of friction layer on the worn surfaces of the M1 pin at high temperatures wear test. The X-ray generator settings were 40 kV and 40 mA and the sample were exposed to the X-ray at a scan speed of 3sec/step with an increment of 0.05 and 10° to 90° was the 2θ range of observation.

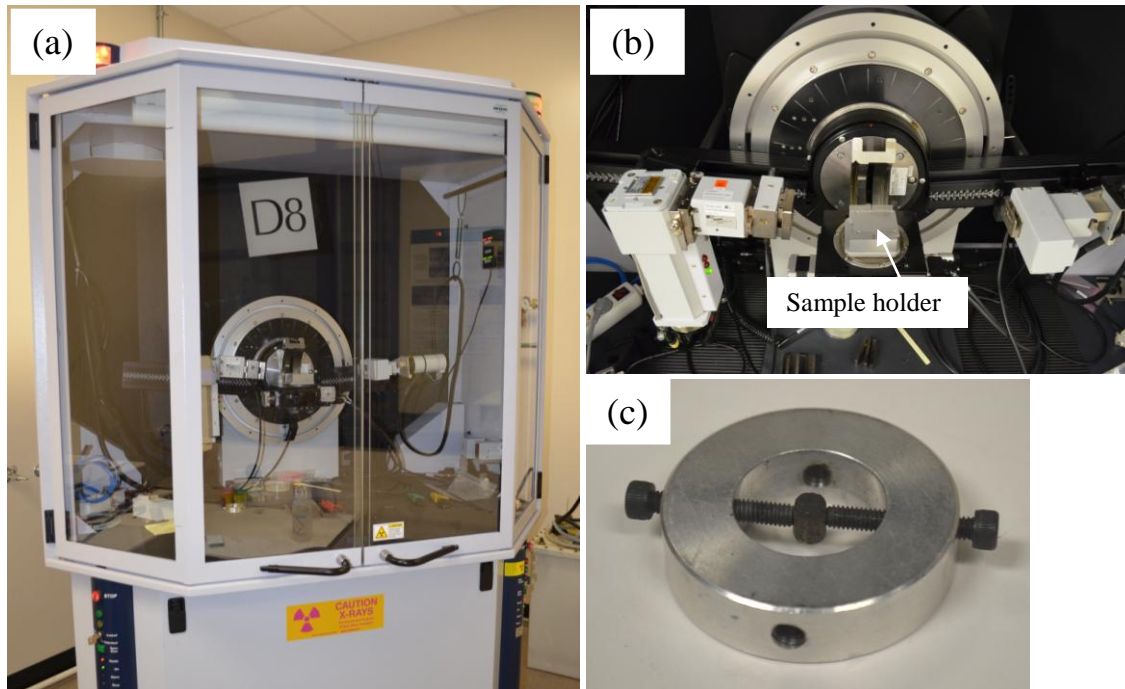


Figure 7.4.6: a) D8 diffractometer, b) position of sample holder, c) Sample holder with M1 pin.

7.4.2 Scanning Electron Microscopy - Energy Dispersive X-ray Spectroscopy (SEM-EDXS)

In order to characterize the wear debris for microstructure and chemical composition, observations were carried out using two SEMs: one that could be operated in the conventional high vacuum mode only, the other also in low-vacuum mode. The SEM images were acquired with an XL30 ESEM equipment, using Back Scattered Electrons (BSE) mainly, since backscattered electrons allow us to distinguish areas with different atomic weights and thanks to the fact that with increasing atomic weight, increases the scattering cross section. Therefore, lighter areas correspond to higher atomic number, while the darker areas correspond to lower atomic weights. Both microscopes were equipped with EDXS systems sensitive to energy ranging from carbon to uranium. In case of high vacuum instrument, to prevent charging effects because PC and nylon substrates are not conductive and tend to degrade under the effect of electron bombardment, observations required the preliminary deposition of a thin carbon film on the surface of the specimens [Suzuki et al.,2002]. In Fig.7.4.7 the equipment used for carbon coating is displayed.

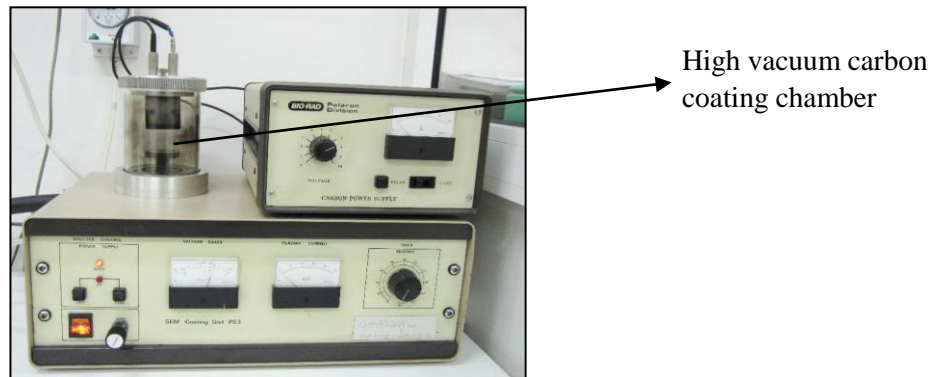


Figure 7.4.7: Carbon coating apparatus.

The wear debris collected on polycarbonate filters have been observed just cutting tiny pieces (few millimetres) of filters with the help of cutter and sticking them on aluminium SEM stubs (Fig.7.4.8), with a carbon two sided adhesive tape.

The same sample preparation processes for SEM observation were applied to the wear debris powder produced during tribological operation and collected on aluminium foil.



Figure 7.4.8: Carbon sputtered samples for SEM observation. In this case, a graphite disc substrate was also present on each SEM stub.

Non-conducting specimens may be imaged uncoated using low-vacuum SEM (LVSEM) operation [H. Policarp et al.,2005]. Carbon coating was not necessary in case the LVSEM, as the partial pressure of residual gas in the microscope chamber can be profitably used to eliminate any surface charging effect. In LVSEM instruments (Fig.7.4.9) specimens are kept in a relatively high-pressure chamber where the working distance is short and the electron optical column is differentially pumped to keep vacuum adequately low in the electron-optical column. The high-pressure region around the sample in the LVSEM neutralizes charge and provides even an amplification of the secondary electron signal if gaseous secondary electron detector is available (GSE). Backscattered electron (BSE) images can be also acquired and are not particularly affected by the pressure conditions.

The main advantages of LVSEM are:

- No risk to damage nylon and PC filters during carbon coating;
- No extra line, enhancement, or carbon K line in the EDX spectra of the specimens.

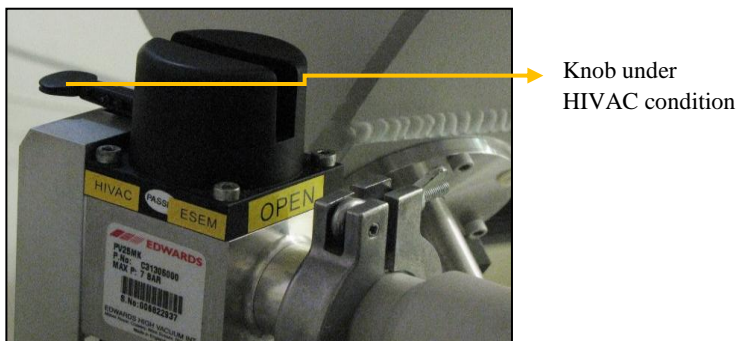


Figure 7.4.9: Switching valve for high vacuum (HV) or low vacuum (LV=ESEM) SEM operational modes.

7.4.3 Transmission Electron Microscopy and Energy Dispersive X-ray Spectroscopy (TEM-EDXS)

For identifying the single particle crystallographic phases and quantitative composition a transmission electron microscopy (TEM-SAED) analytical instrument was used for single particle analysis, acquiring bright field (BF) and dark field (DF) images, selected area electron diffraction (SAED) pattern and EDXS spectra.

TEM samples were prepared by removing the particulate matter from the polycarbonate filters or nylon substrates. This was achieved by putting a small fragment of nylon filter in ethanol and ultrasonic bath for about 15 min. Then a single drop of ethanol suspension containing wear debris was deposited onto TEM gold grids, which were coated with a thin carbon support film. Since the film is amorphous and very thin and has a relatively low electron density, it provides a uniform substrate for imaging wear debris samples. Gold was chosen for grid material, as it is not providing X-ray lines interfering with most of the line of the elements present in the analysed samples.



Figure 7.4.10: a) Ultrasonic bath. Beaker containing ethanol and small piece of filter. b) TEM instrument with EDXS.

For polycarbonate filters, due to the high vacuum grease applied on it for trapping the particles, warm ethanol (about 50°C-70°C for approx. 7min.-10 min.) and then ultrasonic bath for about 15 min was needed to remove and clean the debris (Fig.7.4.10a). A suitable quantity of ethanol has to be critically selected not to dilute too much wear debris.

A similar approach was adopted for the wear debris powder collected on the aluminium foil. The wear debris powder suspended in ethanol with, so that the agglomerated wear particles can be separated from each other and to have a good number of single particles on the grid.

7.4.4 Raman Spectroscopy

The Raman spectrometer used for the study was a Thermo scientific DXR spectrometer using diode pumped solid-state type laser as a source of illumination. The collection system was used in back scattered configuration. The samples were analyzed without any sample preparation by visualizing the sample using 10x microscope objective lens. To record the Raman spectra a solid-state laser was used with a frequency of 532nm with maximum power output of 10mW. It was necessary to use low laser power to avoid excessive sample heating. For this study a laser power of 10mW was used. The laser spot diameter was 2 micron with 25 mm slit size, for the fully focused laser beam. The spectral resolution was 5cm^{-1} at 532nm with wavelength range from 50cm^{-1} to 3500cm^{-1} .

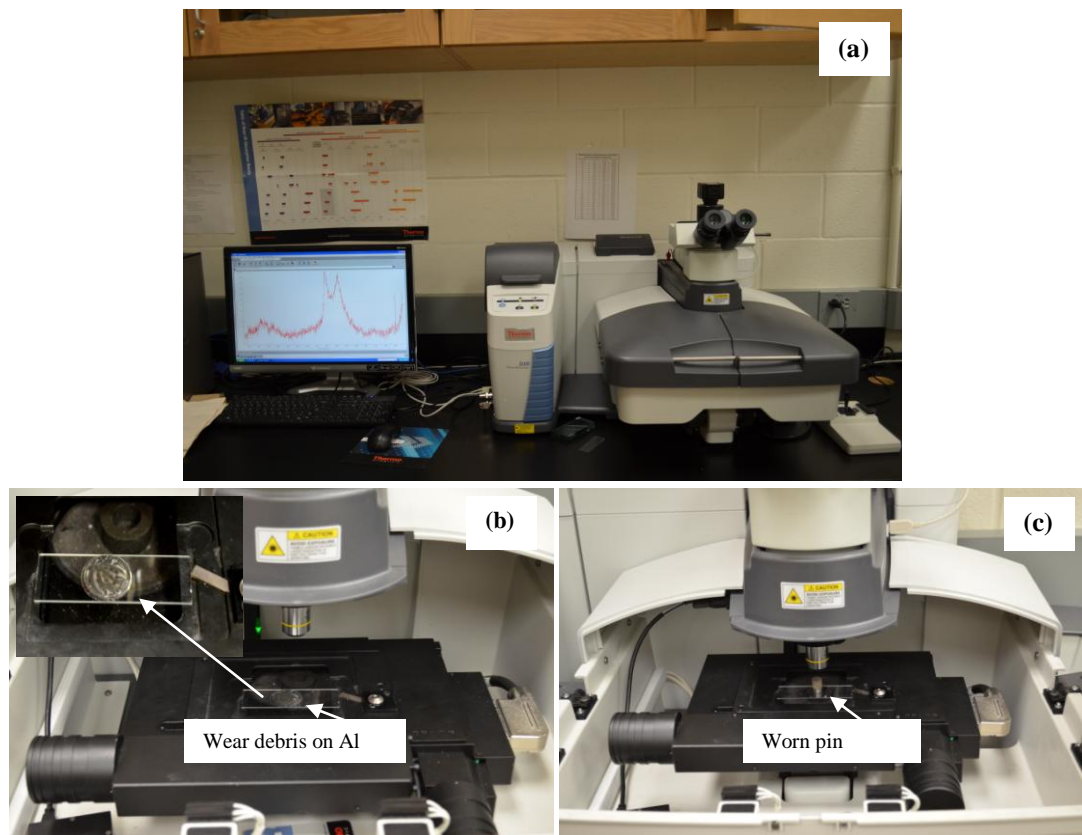


Figure 7.4.11: a) A thermo scientific DXR Raman spectrometer, b) wear debris Raman analysis, c) worn pin surface Raman analysis.

Chapter 8

Results & Discussions

In this chapter the results obtained from the characterization of wear products obtained from pin-on-disc tribometer are presented. In particular, in this chapter, one by one we will going to analysis the results obtained for every case i.e., case I, II, III and IV.

8.1 Tribological behavior of two low steel frictional materials (M1 & M2) at room temperature - (Case I)

8.1.1 Friction and wear behavior

Fig.8.1.1 shows the evolution with sliding distance of coefficient of friction of the two friction materials, M1 & M2, subjected to a constant speed of 3.14 m/s and constant normal loading of 2MPa at room temperature (25°C) and humidity. Fig.8.1.1, is clearly showing an initial continuous increase in the coefficient of friction for both the friction materials. However, at some stage, M2 shows a stable coefficient of friction behavior and less fluctuations up to the end of the experiment than M1.

The initial value of the coefficient of friction at the time of commencement of the test for M1 pin at 25°C was ~ 0.45 and for M2 pin at 25°C was ~ 0.38. An increasing trend was observed for as the test progressed and increasing again towards the end of the test to a value of ~ 0.7 for M1 and 0.4 for M2.

Under the same operating condition i.e., normal load (2MPa) and speed (3.14m/s) the M1 shows the larger amount of height and weight loss of the pins as compared to M2 (Fig.8.1.2). From the data in table 8.1.1, it can be concluded that wear rate of M1 is higher as compared to the wear rate of M2.

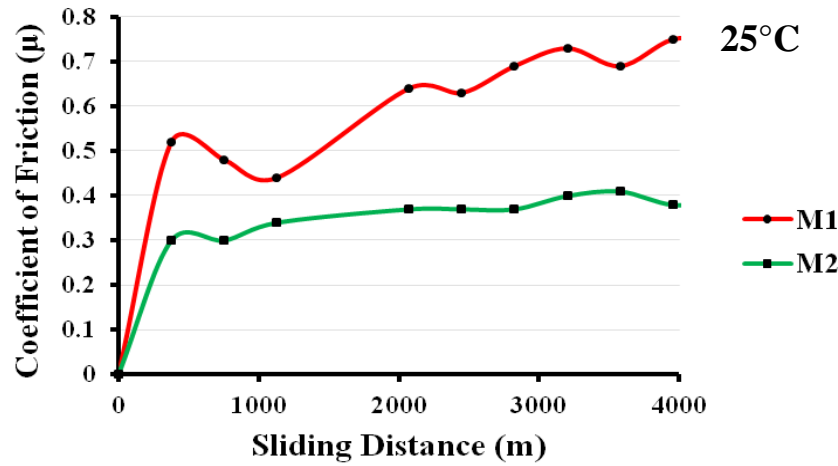


Figure 8.1.1: Coefficient of friction vs sliding distance of M1 & M2 at 25°C temperature.

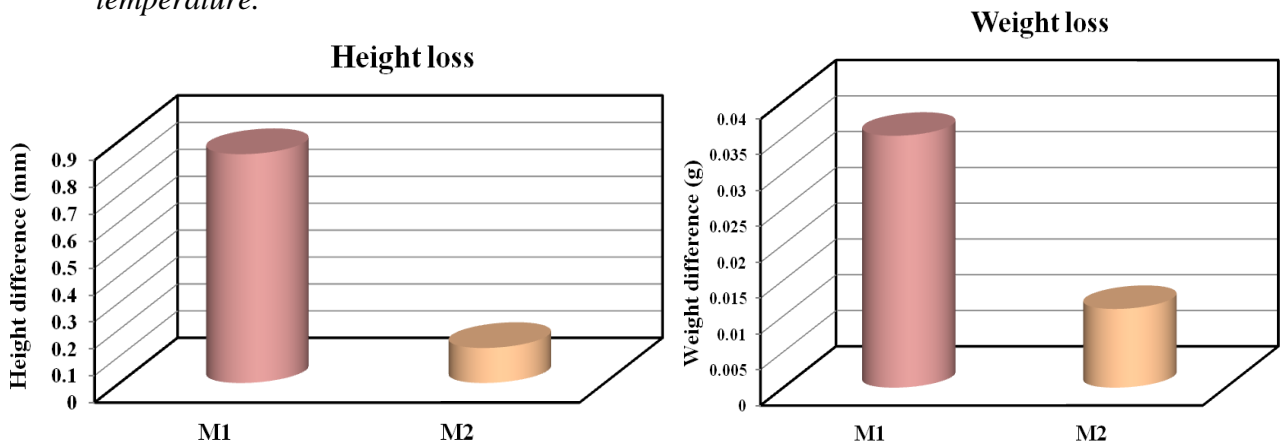


Figure 8.1.2 : Shows the height loss difference and weight loss difference between the two friction materials: M1 & M2.

Table 8.1.1: Friction and wear data of M1 & M2 friction materials.

| 2.0 MPa and 3.14 m/s | M1 | M2 |
|---|------------------------|-----------------------|
| Friction Limit (μ) | 0.4 - 0.8 | 0.4 - 0.5 |
| Loss in weight (g) | 0.084 g | 0.011g |
| Wear rate W (mm^3/mm) | 13.5×10^{-7} | 4.63×10^{-7} |
| Specific wear rate Ka (m^2/N) | 26.5×10^{-15} | 9.6×10^{-15} |
| Height loss (mm) | 1.65 mm | 0.13 mm |
| Pin temperature T_{max} ($^{\circ}\text{C}$) | 49.0 | 31.0 |

8.1.2 Analysis of worn surfaces of M1 & M2 (SEM-EDXS)

The fragments of wear released by a tribological system, like a pin-on-disc apparatus, are important to know what happens at the interface between disc and pad, because the morphology and chemical composition of the wear debris let us to understand the origin of these fragments and the possible causes that have led them to form. The analyses were carried out using main techniques, such as SEM-EDXS.

The SEM images (fig.8.1.3) it has been observed a different wear behavior for the M1 pin. It has been noted that large amount of wear debris were scattered on the worn surface of M1 which is associated with the fact that secondary plateaus were delaminated and flakes were formed and large amount of micro crack is noticed (fig. 8.1.3a).

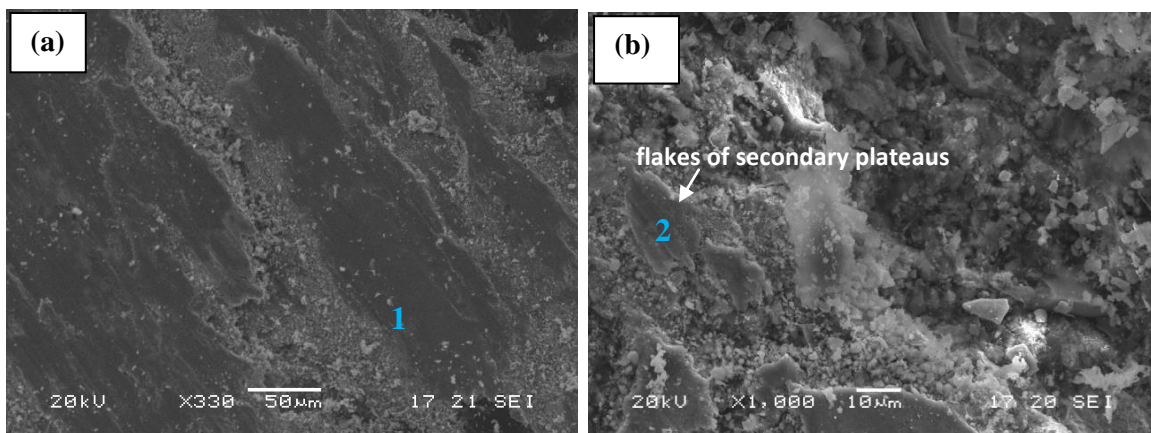


Figure 8.1.3: SEM images of the M1 pin worn surfaces rubbed against cast iron rotating disc.

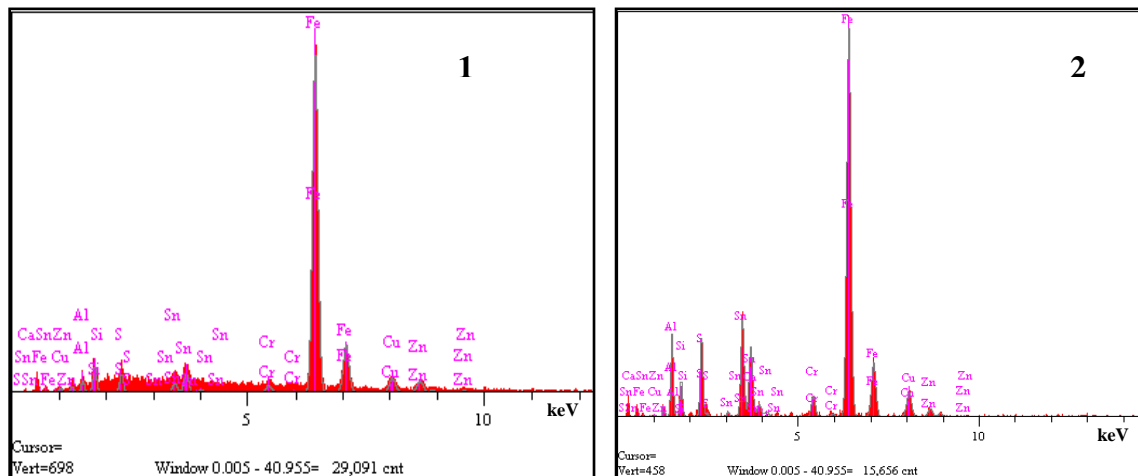


Figure 8.1.4: Energy dispersive X-ray spectroscopy analysis of the third layer formed on the worn surface of M1 pin when tested against rotating cast iron disc at different location named 1 & 2 (see figures 8.1.5, a) and b)).

In fig. 8.1.3 the friction layer is not continuous and uniform and it is severely torn apart. This might be due to the abrasive hard particles (MgO, ZnO etc), which could not compacted under the given load of 2MPa and thus enhanced large amount of material removal which results high amount of wear debris generated. The evidenced shown in the fig 8.1.3 can justify the wear and friction data presented in fig. 8.1.2.

Fig. 8.1.5a shows SEM image for the M2. On the pin surface well secondary plateaus developed near the primary plateaus. The wear debris that generated during sliding, formed a sort of protecting layer (friction layer) on the sliding surface of the pin, which results in major decrement in the material removal process during the entire test run (fig. 8.1.1).

The formation of the friction layer is so extended once again due to the load applied. Indeed, with a load of 2 MPa the fragments, once produced, are trapped and then compacted. Actually two different modes of compaction of the fragments of wear have been identified: poor compaction and high compaction, as shown by the SEM micrograph in figure 8.1.5b).

The chemical composition of the friction layer, obtained by means of EDXS analysis, appears to be mainly iron oxide and zirconium oxide, with the presence of copper. The presence of iron, in the form of oxides, in M1 & M2, is coherent with the tribo-oxidation of the counterface disc and debris transfer onto the pin surfaces and friction plateaus.

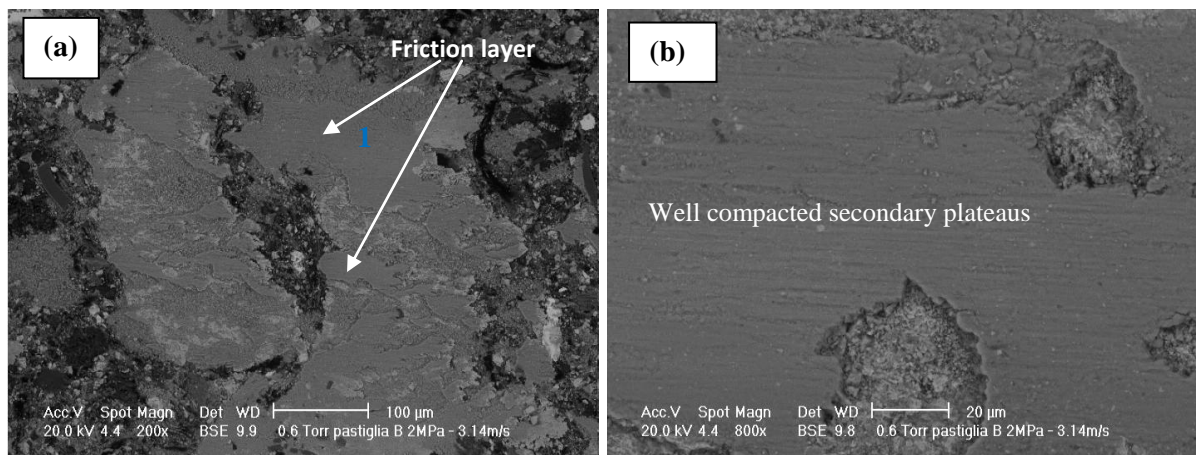


Figure 8.1.5: SEM images of the M2 pin worn surfaces rubbed against cast iron rotating disc.

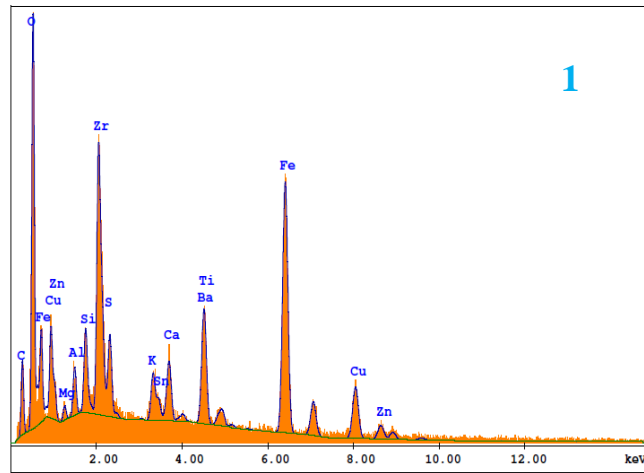


Figure 8.1.6: (a) Energy dispersive X-ray spectroscopy analysis of the third layer formed on the worn surface of M2 pin when tested against rotating cast iron disc.

8.1.3 Analysis of wear debris (TEM-SAED and XRD)

The study of the wear debris produced during tribological tests are critical to interpret the phenomena occurring at the interface between disc and pad. The chemical and Phase compositions of the wear debris make us to understand the origin of these fragments and the possible causes to their formation.

The TEM-EDXS analysis was integrated with SAED analysis with data processing using the Process Diffraction software [Ruth Hinrichs et al., 2011]. TEM-SAED analyzes were conducted on the number of fragments of wear with sizes below 500 nm.

In fig. 8.1.7 and fig. 8.1.9 show the single nano particle of M1 & M2 respectively. The fig. 8.1.7 a) and fig. 8.1.9 a) show the agglomerated particles of M1 & M2 respectively, The analysis of SAED in fig. 8.1.7 b) represents the peaks of mixed phases of iron, zinc, magnesium and oxygen for M1 whereas the SAED analysis in fig.8.1.9 b) reveals the strong presence of iron oxide and zirconium oxide in the nano particle of M2 (fig. 8.1.9 a). The presence of large amount of iron oxide, in both M1 & M2 wear debris, is mostly from the oxidation of cast iron disc. Fig. 8.1.7 c) confirm the EDX analysis of M1 which represent the presence of mostly iron, magnesium, zinc and tin respectively The single particle EDX analysis fig. 8.1.9 c) indicates the presence of mostly iron, zirconium, copper and oxygen. Fig. 8.1.7 d) of M1 pin shows diffraction rings corresponding to mixed phases of iron, zinc, magnesium and oxygen. The SAED analysis fig. 8.1.9 d) of M2 gives the diffraction rings corresponding to Fe_2O_3 , Fe_3O_4 and ZrO_2 as the main phases present in the nano particle (fig. 8.1.9 a). Thus the TEM analysis of single particle of M1 shows iron oxide and other metal (Zinc, Tin) oxide where as for M2 gives the strong presence of iron oxide and zirconium oxide.

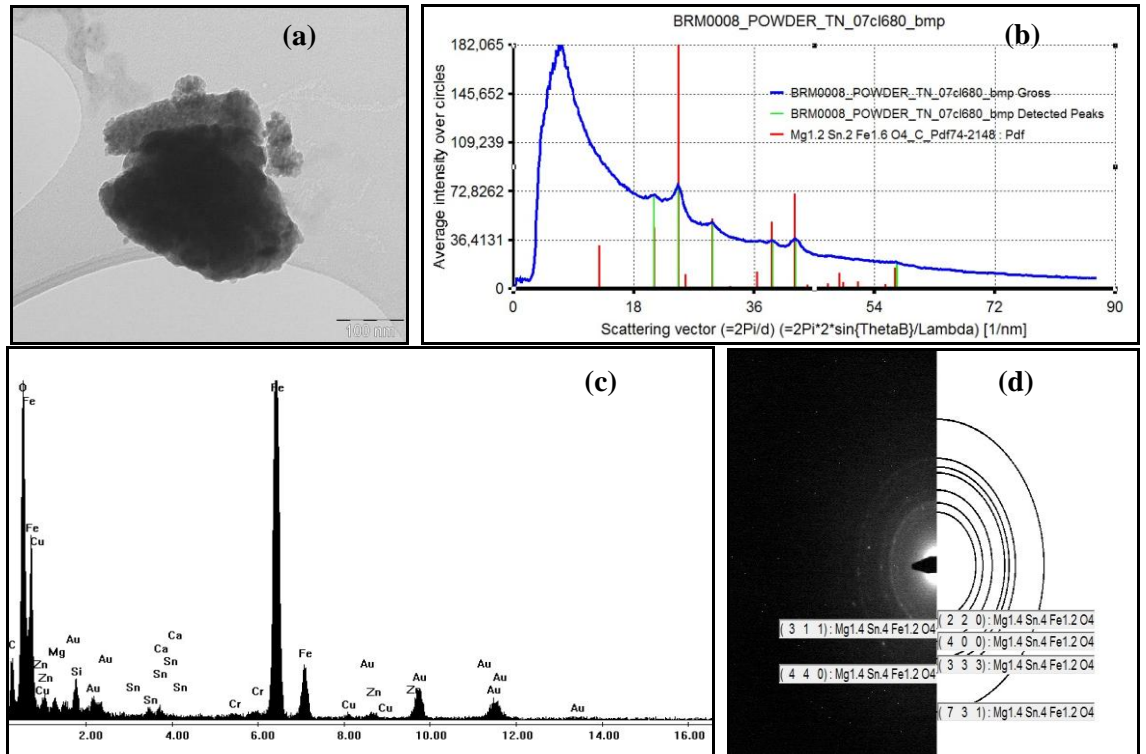


Figure 8.1.7: (a) Nano wear debris paricle of M1 brake material. (b) Process diffraction-identification of mixed phase of magnesium oxide, tin oxide and iron oxide as a major phases present in fig. 8.1.8a. (c) EDX analysis of fig. 8.1.8a M1 friction material wear debris. (d) Electron diffraction patterns (SAED) corresponding to nanocrystalline wear debris fig. 8.1.8a. The diffraction pattern shows concentric rings corresponding to Fe_3O_4 , SnO_2 and MgO .

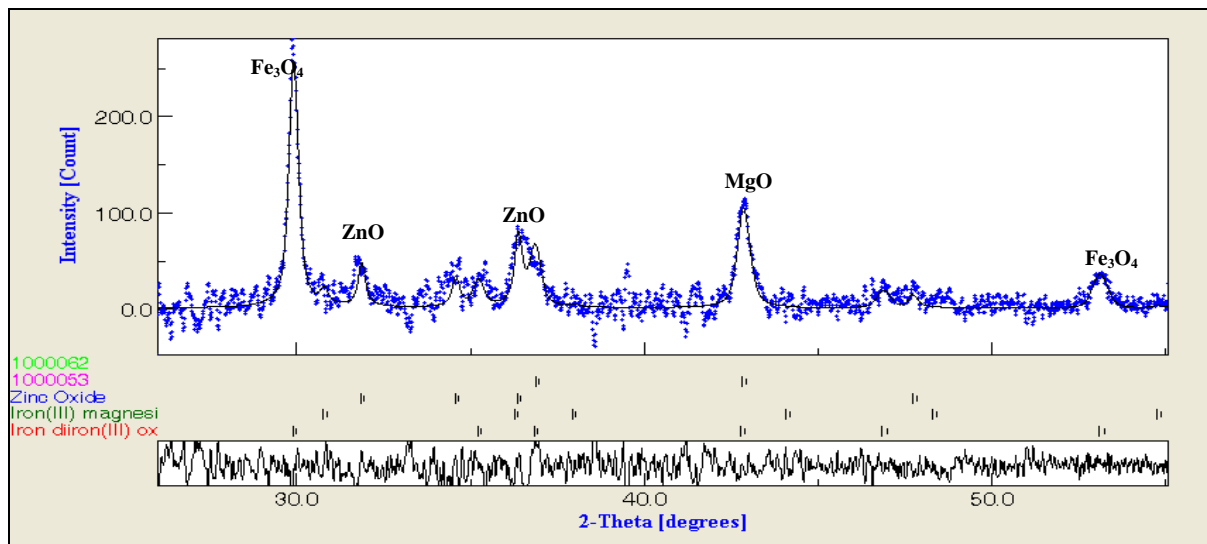


Figure 8.1.8: X-ray diffraction of M1 wear debris powder (bulk) placed in a 0.5 mm capillary tube diffracted in transmission mode.

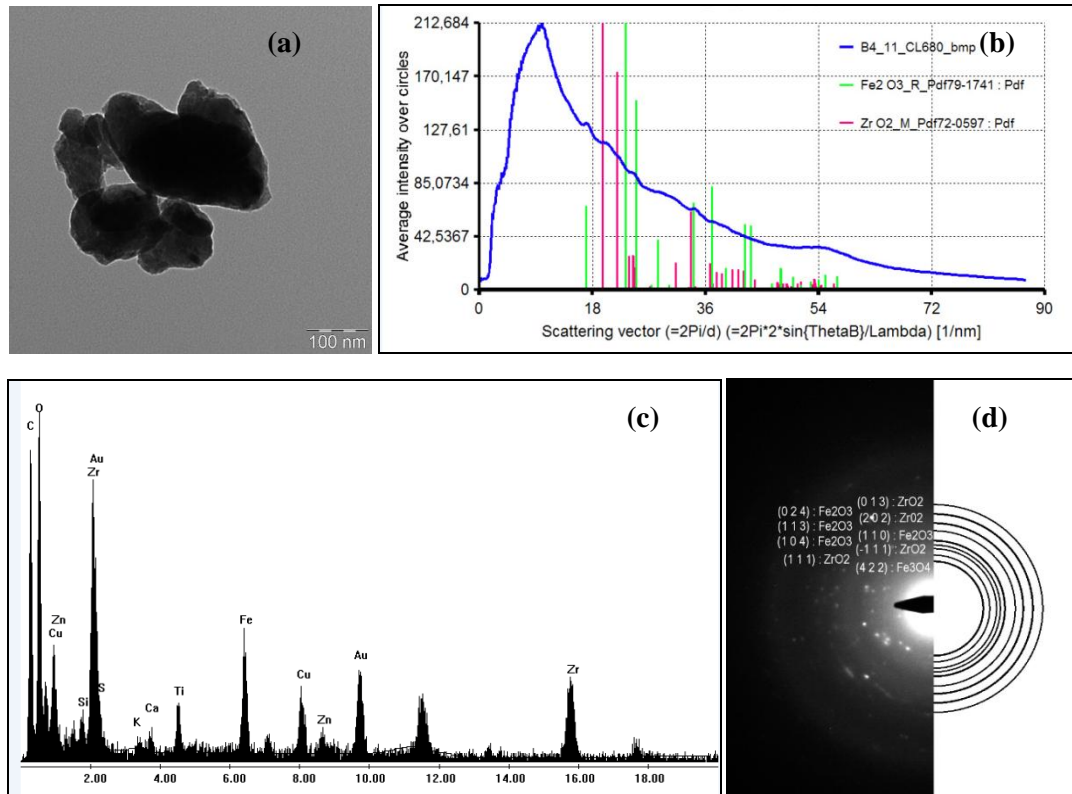


Figure 8.1.9: (a) Nano wear debris particle of M2 brake material. (b) Process diffraction – identification of iron oxide and zirconium oxide as a major phases present in fig. 8.1.6a. (c) EDX analysis of fig.8.1.6a M2 friction material wear debris. (d) Electron diffraction patterns (SAED) corresponding to nanocrystalline wear debris fig.8.1.6a. The diffraction pattern shows concentric rings corresponding to Fe₂O₃, Fe₃O₄ and ZrO₂.

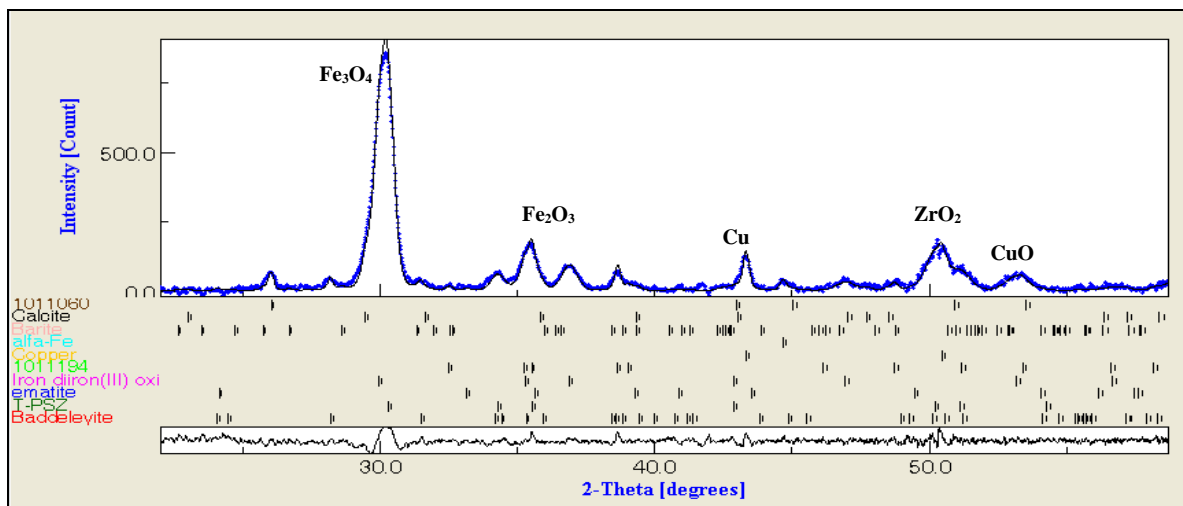


Figure 8.1.10: X-ray diffraction of M2 wear debris powder (bulk) placed in a 0.5 mm capillary tube diffracted in transmitted mode.

Fig. 8.1.8 is showing the X-ray diffraction of M1 wear debris. Comparing with TEM analysis shows strong presence of major peaks of magnetite-(36 wt%), zinc oxide-(13 wt%) and magnesium oxide (48 wt%) respectively. However the presence oxidized iron may come from both the pad and from the rotating cast iron disc.

The X-ray diffraction on wear debris (Fig. 8.1.10) of M2, shows a strong presence of zirconium oxide and magnetite, with the presence of copper oxide, copper and hematite; also there is the appearance of graphite in the fragments of wear. The X-ray diffraction spectrum analysis for M2 wear debris powder is shown in fig.8.1.10. In particular the major peaks are Magnetite- (38 wt%), tetragonal zirconium oxide-(35 wt%), copper oxide-(8 wt%), copper-(5 wt%), graphite-(11 wt%) and Hematite-(2 wt%).

As it is seen from fig. 8.1.7b and fig. 8.1.9b, the presence of iron oxides, such as magnetite, hematite and ZrO_2 is confirmed by both the technique X-ray and electron diffraction for M1 and for M2. However, the XRD analysis were performed by inserting only those steps that are considered significant by the integration of the information obtained from the analysis of the spectra and by EDXS, TEM-SAED analysis. The presence of additional phases could be the subject of study for future development.

8.1.4 Wear mechanisms at room temperature

The data obtained from the characterization of the wear products, presented in the previous paragraphs, the relevant wear mechanisms were identified. In particular, the wear debris generated during the tribological tests, presented the wear modes caused due to the constant sliding and abrasion actions that affect considerably the constituents used to formulate M1 and M2 friction materials.

For the analysis of wear mechanisms that underlie the pad-disc brake, I started from the analysis of surface of the pin, in particular by SEM-EDXS, from these analyzes it became very clear that for the two friction materials, M1 & M2, there is a distinctly different wear behavior. In general, the worn surfaces of the M1 & M2 pins have smeared wear debris on the surfaces that was caused by the deformation of the metallic particles, fiber (more in M1) and abrasive particles (fig.8.1.3 b). The wear debris has compaction process to form a friction layer. The composition of the friction layer is mainly from the wear fragments of the pins surfaces and oxide particles from the disc. The detachment of the fragments were governed by tribo-oxidation of the disc and the rolling and sliding abrasive (fig.8.1.11) action caused by the abrasive particles in contact with the counter cast iron disc. The friction layer is important as it maintains the stable and consistent friction coefficient between pin and disc. It seems that M1 does not have uniform friction layer and it is because of abrasion action of more abrasive particles (MgO, ZnO etc.) and steel fibers chips, the friction layer is removed and new pin surface are exposed as the wear damage continues (Fig.8.1.2). Steel fibers might cause excessive wear of the brake disc if they are present in large proportions. Steel fibers have also been shown to increase friction coefficient fluctuations [H. Jang et al.,2001]. This occurs since they abrade the friction layer, which is responsible for friction coefficient stabilization. On the other side, M2 pins have relatively lower content of the steel fiber (see table 7.1.1) and have higher weight percentage of potassium titanate. This compound is present as fibers, prepared from highly refined single crystals have high melting point (1250–1310 °C) [S.Kim et al.,2001], which give higher stability and shearing

strength to the secondary plateaus. Presence of zirconium oxide, copper and potassium titanate lower the friction coefficient and magnesium oxide increases the friction coefficient [M.H. Cho et al.,2005].

From SEM-EDX of pins surface, we have large amount of iron oxides (mainly from counter disc) as it formed by tribo-oxidation caused by the sliding wear of pin and disc surfaces. The abrasive particles in the M1 friction pin has a positive impact on the friction behavior (higher than M2) but at the same time it has a more wear behavior. From the TEM-EDXS and XRD analysis, the wear fragments have revealed the presence magnetite, zinc oxide and magnesium oxide for M1 and zirconium oxide and iron oxides primarily in the form of magnetite for M2. The result is pretty obvious given that the major constituents of the M2 friction material is analyzed as zirconium oxide and for M1 it is magnesium oxide and zinc oxide (table 7.1.1). The most of the iron oxide is coming from tribo-oxidation of the cast iron disc. In the wear fragments of the friction layer other elements also reported but in a much lesser extent which is due to the absence of other elements in the field view of the TEM/XRD analysis.

| Wear mechanisms | Characterization tools | Observations |
|------------------------|-------------------------------|--|
| Tribo-oxidation | XRD results + SAED | Iron oxide, MgO, ZnO |
| Abrasive action | SEM-EDX | Wear debris analysis, worn pin & disc surfaces |

Thus, wear mechanisms identified in the wear testing of M1 and M2 friction materials at room temperature were tribo-oxidation and three-body abrasive wear.

Wear behavior at room temperature

Wear rate: M1>M2

Wear Mechanism at room temperature

Tribo-oxidation & Three-body abrasive wear

Wear mechanism of M1 & M2 pin at room temperatures

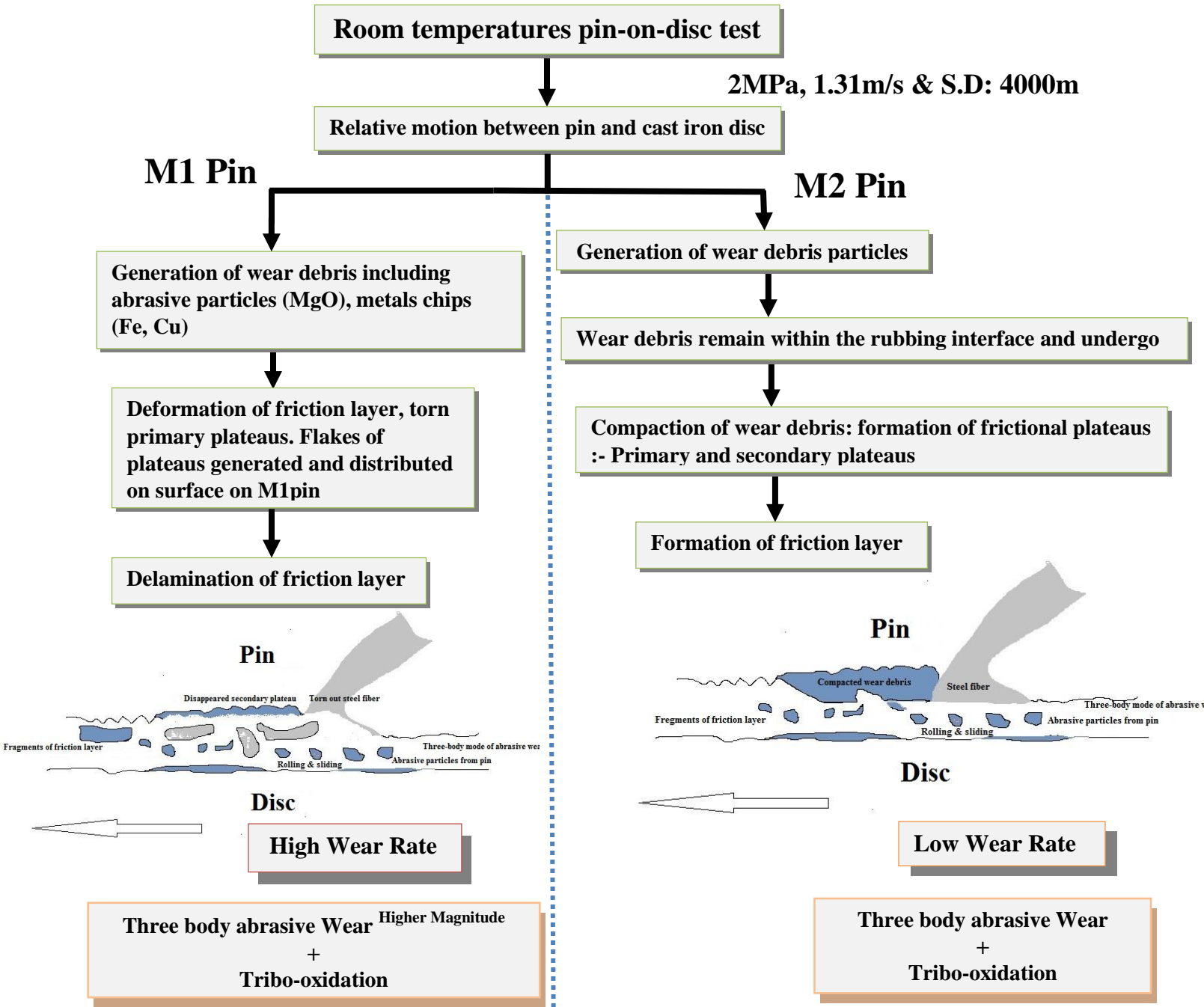


Figure 8.1.11: Wear mechanism involved in dry sliding of friction materials (M1 & M2) at room temperatures.

8.2 Characterization of wear particles from M1 frictional material - Case II

In this section, a streamline characterization protocol for wear debris emitted under different wear testing conditions by material (M1) used for disc brake assemblies is presented. An important aspect of the experimental test methodology concerns the powder collection methodology on different substrates: aluminum foil, for a gravitational integral collection, and polycarbonate filters of an ELPI+ impactor equipment, on which particles are selectively trapped, according to their average size. The deliberate aim of the study was to identify suitable selection parameters, like specimen availability and average particle size, for an effective and smart application of the mentioned experimental techniques so to optimize testing times and obtain statistical reliable results.

Table 8.2.1: *Impactor stage specification. For each stage, corresponding to different aerodynamic diameters (D_i), the total number of collected particles and the relevant mass density is measured.*

| Stages | D_i [μm] | Total Particles Number [1/cm ³] | Total Particle Mass [g/m ³] |
|--------|----------------------------|--|--|
| 15 | 10 | - | - |
| 14 | 6.8 | 0.25 million | 69.6 |
| 13 | 4.4 | 0.44 million | 31.1 |
| 12 | 2.5 | 0.86 million | 13.1 |
| 11 | 1.6 | 2.2 million | 8.5 |
| 10 | 1.0 | 2.9 million | 2.8 |
| 9 | 0.64 | 3.5 million | 0.81 |
| 8 | 0.4 | 11.7 million | 0.68 |
| 7 | 0.26 | 18.4 million | 0.29 |
| 6 | 0.17 | 59.5 million | 0.24 |
| 5 | 0.108 | 253.8 million | 0.22 |
| 4 | 0.06 | 1.9 billion | 0.36 |
| 3 | 0.03 | 7.9 billion | 0.24 |
| 2 | 0.017 | 26.0 billion | 0.13 |

8.2.1 X-ray diffraction results

8.2.1a) Pin-on-disc wear debris powder of M1 frictional material collected on aluminum foil (AF-M1)

Fig. 8.2.1 and Fig. 8.2.2 is the experimental X-ray diffraction pattern of the debris from test carried out at a load of 2MPa and speed of 3.14 m/s respectively for M1. Fig.8.2.1 shows the XRD rings obtained on image plate detector. The experimental peaks of the intensity v/s diffraction angle plot are compared and modelled to match different phases, which have been identified on the basis of the diffraction peaks present in the spectrum (Fig.8.2.2). From the

fitting of the modelled spectrum patterns to the experimental data the oxide phases and relevant composition listed in Table 8.2.2 were found. The XRD analysis thus confirms the presence of Fe_3O_4 , MgO and ZnO .

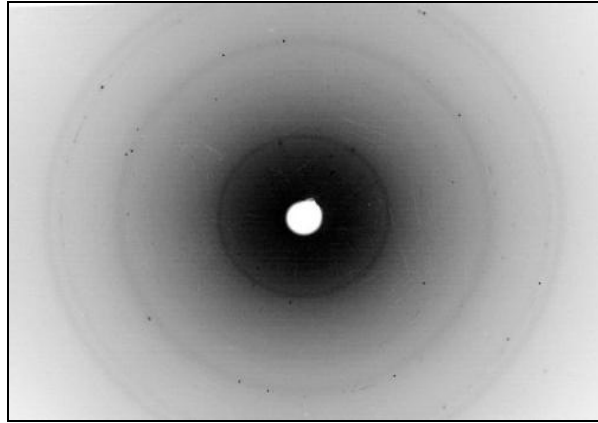


Figure 8.2.1: *Experimental imaging plate XRD ring pattern of AF-M1 sample.*

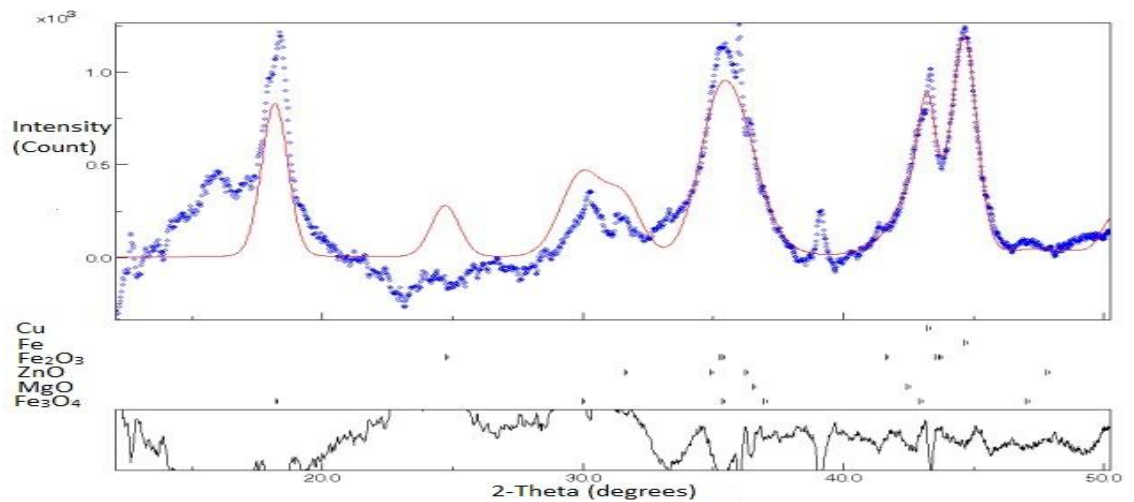


Figure 8.2.2: *Experimental (blue dots) and modelled (continuous black line) XRD spectrum patterns of AF-M1 sample. Main diffraction peaks of identified phases are marked in the graph.*

8.2.1b) XRD of different stages of M1 frictional material collected on polycarbonate filters

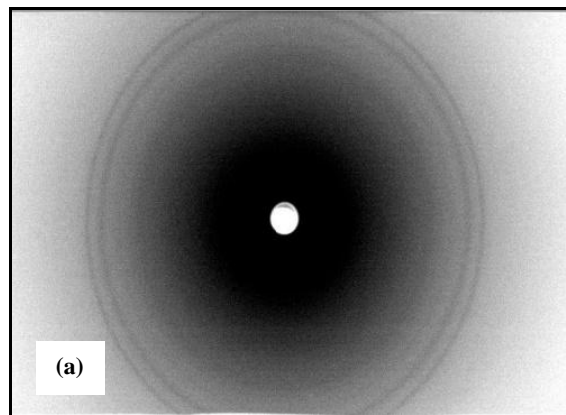
Several stages of wear debris on polycarbonate filter, namely from stage_02 to stage_15 have been considered and every stage has different concentration of wear debris on it. The concentration of wear debris depends upon several factors such as:

- Nozzle diameter (D_i) of ELPI+ particle collection instrument,
- Jet velocity of the air flow (U) which contains wear debris particle.
- Jet to plate (filters) distance and pore size of polycarbonate filters within the ELPI+ particle collection instrument.

The stage_12 filter was placed just below the nozzle of the ELPI+ whereas the stage_02 filter was placed at the bottom of the filter plate container of ELPI+ particle collection instrument. Therefore, the mass density of the wear debris on filter varies from top to bottom. Table 8.2.1 shows the concentration of wear debris on those stages that have been selected as more representative of the whole lot, to set up the experimental procedure. Stage_12 displays the higher value of total particle mass and lowest value of total particle numbers, which means large (coarser) particle size roughly in range ($800\text{nm} < \text{PM} < 10\text{micron}$) were entrapped on the polycarbonate filter. On the other hand stage_02 shows least value of total particle mass and highest value of total particles number, among all the stages, having ultra-fine particle range ($200\text{nm} < \text{PM} < 1000\text{ nm}$).

It turns out that XRD patterns obtained from stage_02 to stage_09, i.e., upper stages, are too weak to provide reliable data. This is in agreement not uniformly distributed and scarce present of wear debris, mostly clustered in a comparatively few large agglomerates Fig.8.2.8a, on the PC filters, as resulted from SEM observations. Therefore the overall amount of debris was not enough to produce a good quality XRD spectrum.

From stage_10 to stage_15 the powder on the filter was uniformly distributed and at the center of wear debris spot it has layers of wear debris powder which provide enough quantity of powder to have a good XRD spectrum to obtain, as shown in Fig. 8.2.8e. The major peaks were (Fig.8.1.3) hematite and wustite for stage_12 of polycarbonate filter having wt% as shown in Table 8.2.2. Fig.8.2.4 shows the diffraction pattern of stage_15 of polycarbonate filter having major phases shown in Table 8.2.2.



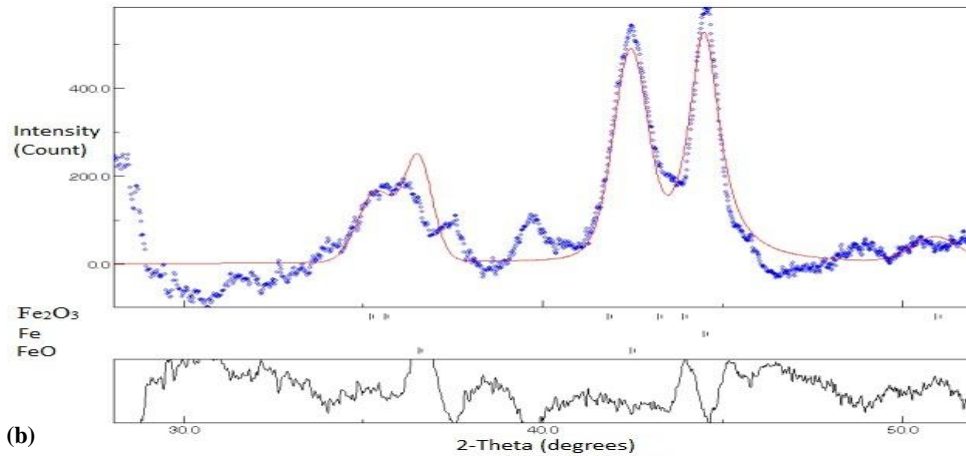


Figure 8.2.3: (a) Experimental imaging plate XRD ring pattern of stage_12 of PC-M1. (b) Experimental (blue dots) and modelled (continuous black line) XRD spectrum patterns of stage_12 of PC-M1. Main diffraction peaks of identified phases are marked in the graph.

Table 8.2.2: List of different phases present in MI-AF and different stages of polycarbonate filter.

| Phases | MI-AF | MI- stage_9 | MI- stage_12 | MI- stage_15 |
|--------------------------------|-------|-------------|--------------|--------------|
| ZnO | 13 | - | - | - |
| MgO | 49 | - | - | - |
| Fe ₃ O ₄ | 36 | - | - | - |
| Fe ₂ O ₃ | - | - | 25 | - |
| FeO | - | 75 | 44 | 66 |
| Fe | - | 25 | 31 | 34 |

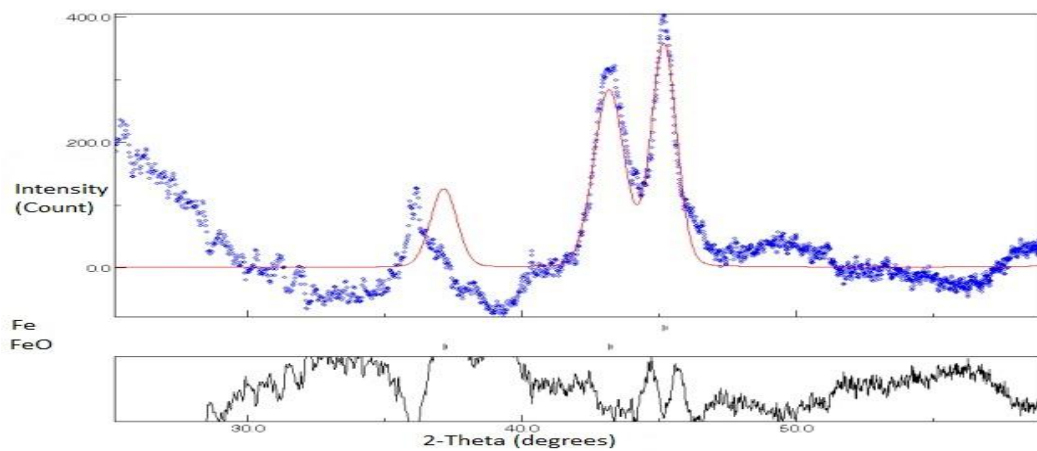


Figure 8.2.4: Experimental (blue dots) and modelled (continuous black line) XRD spectrum patterns of stage_15 of PC-M1 sample. Main diffraction peaks of identified phases are marked in the graph.

It can be concluded that from Stage_09 to stages_15 the relevant XRD patterns are very clear and detectable and also a good match between experimental and modelled XRD spectrum patterns has been obtained by using MAUD software. From stage_02 to stage_08 the sensitive range of the imaging plate is appropriate to detect the diffraction cones and indeed dark rings have been detected. However these dark diffracted rings were from PC filter, whereas the diffracted rings of the stage_02 was very weak, as coming from a too little number of agglomerated particles scattered on the PC filter substrate. From the other ELPI+ stages XRD observation it has been concluded that stages below 9 has a poor sensitivity for the X-ray diffraction and this is because the stages below 9 does not have sufficient amount of wear debris powder in a single debris spot. It has been calculated that a critical mass is required to perform a successful X-ray diffraction, powder mass than 30 mg will not be sufficient for diffraction. In figure 6 shows the X-ray diffraction detectability range of different ELPI+ stages. Stages 9 and 10 has a high detectability of diffracted X-rays which is due to the higher single wear particle spot mass than the stages 8 to 2.

In Table 8.2.1 an example of number and weight of the particles collected on each stage are indicated. The finer the average particle size the larger is the number of collected particles. A generally decreasing trend can be noticed in the total weight of collected particle with their average size (Fig. 8.2.5). This weight reduction introduces a limitation in the applicability of the XRD approach, since below a certain mass of the available specimen, the diffracted signal becomes too weak to provide statistically meaningful results.

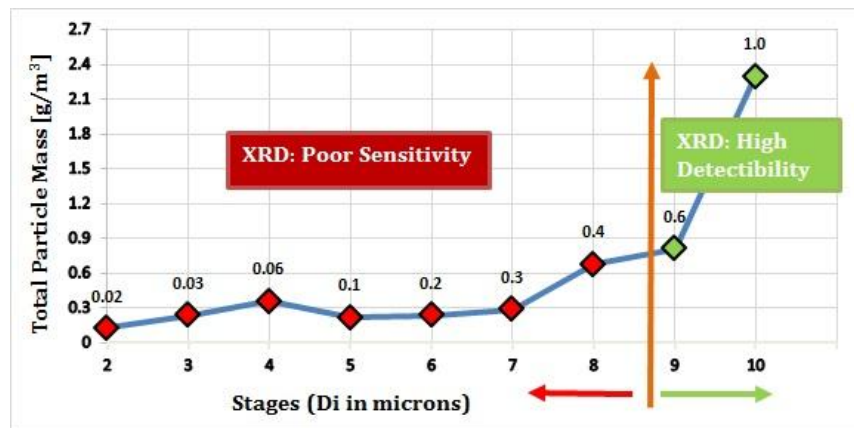


Figure 8.2.5: X-ray diffraction spectrum of powders collected on polycarbonate filters.

8.2.2 Scanning Electron Microscopy -Energy Dispersive X-ray Spectroscopy

8.2.2a) SEM of pin-on-disc wear debris of M1 frictional material collected on aluminum foil (AF-M1)

The SEM images (Fig.8.2.6) are wear debris of M1 friction material from pin-on-disc tests (AF-M1). In Fig.8.2.6b the cluster of many ultrafine particles (agglomerated) can be seen. These agglomerations are typical of nanoparticle and are due to their high surface energy. SEM images also reveal that the pin-on-disc produce ultrafine size (Fig.8.2.6b) and also coarser size wear debris particle (Fig.8.2.6d). EDXS spectrum of sample AF-M1 of fig.8.2.7a shows the peaks of oxygen, in association with those of iron, magnesium, aluminum, zinc etc, confirms the presence of different metal oxide.

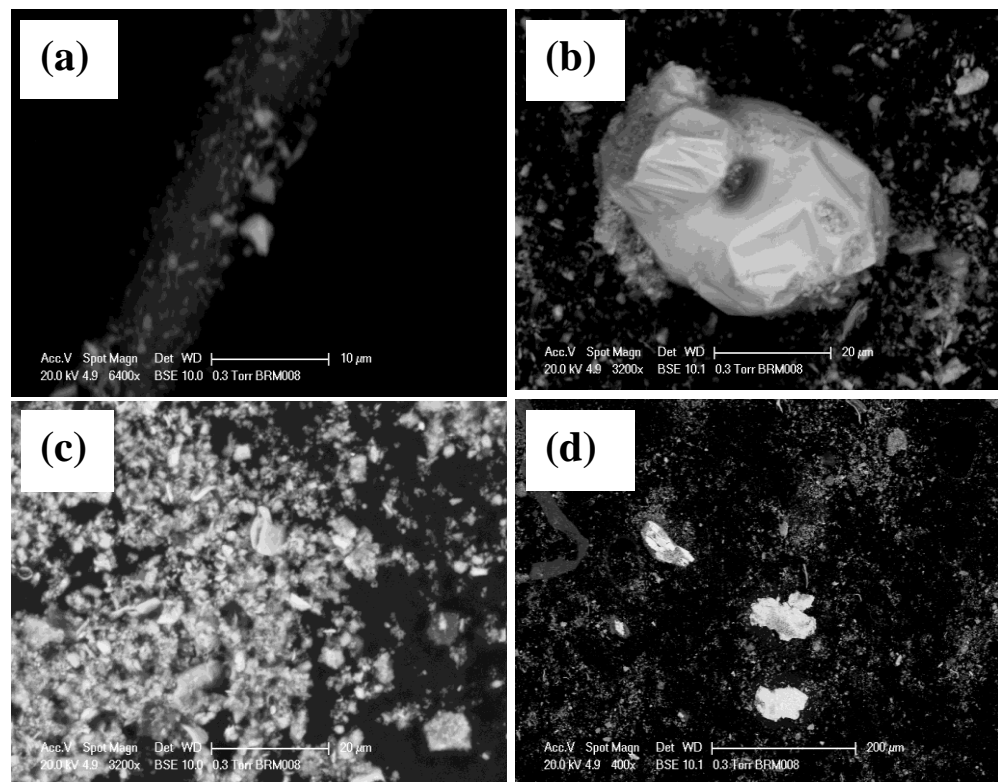


Figure 8.2.6: SEM images of pin-on-disc wear debris of AF-8.

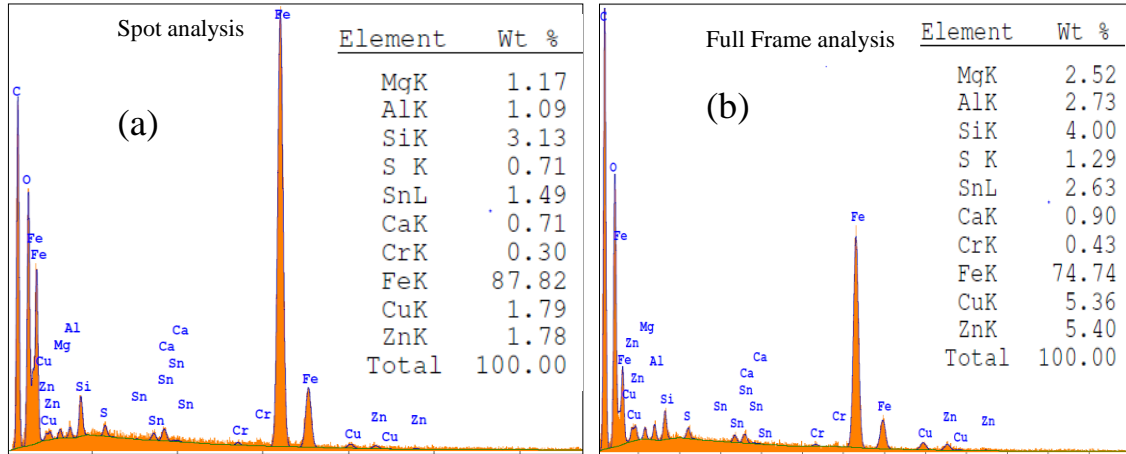
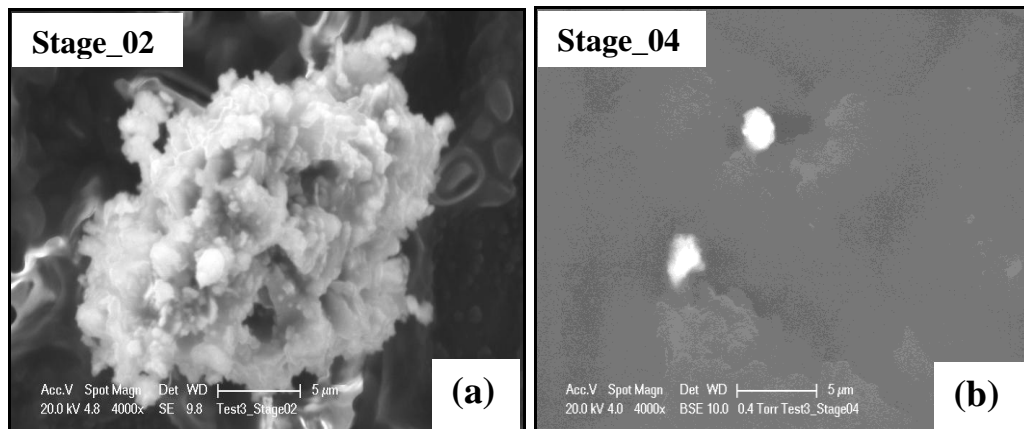


Figure 8.2.7: EDAX spectrum (a) ultrafine particle of fig.8.2.6a, (b) full frame of coarser particles of fig.8.2.6c.

8.2.2b) SEM of pin-on-disc wear debris of M1 frictional material collected on polycarbonate filters (PC-M1)

From the SEM images of PC filter it has been observed that the ultra fine particle range (200nm < PM < 1000nm) are, as expected, at the upper stages, i.e., stages_2, stage_4 and stage_7 respectively and coarser size particle range (800nm < PM < 10micron) and uniform distribution is at the lower stages i.e., stages_9, stage_12 and stage_15 respectively. In Fig.8.2.8a ultra fine particles are agglomerated to form bigger particles. This tendency can be seen up to stage_7, although to lesser extent. In Fig.8.2.8d to Fig.8.2.8f the coarser particles can be seen having uniform distribution on filter which helps with EDXS analyses.



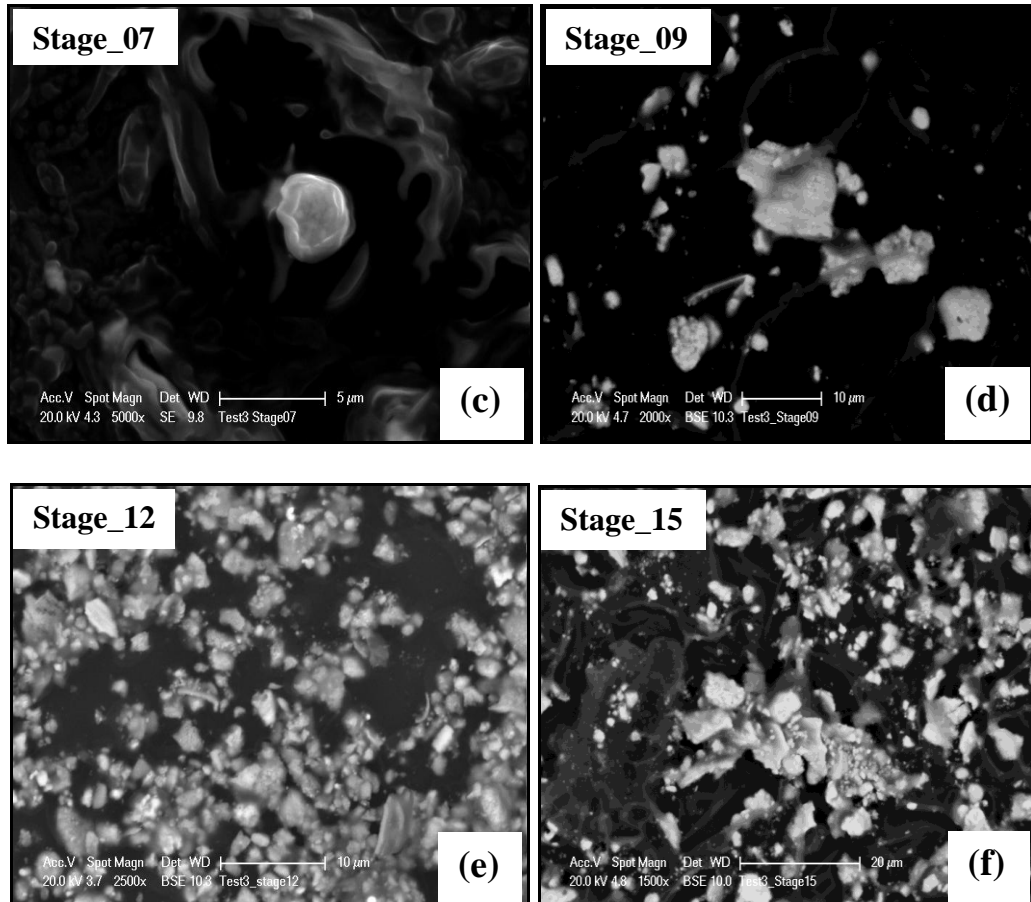


Figure 8.2.8: SEM Images showing different stages of PC-8.

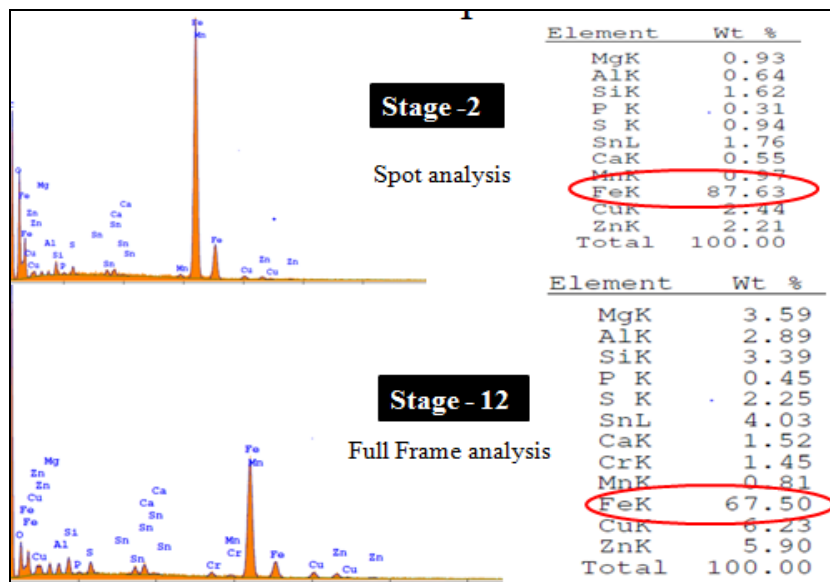


Figure 8.2.9: EDAX spectrum (a) agglomerated particles of fig.8.2.8a, (b) full frame of coarser particles of fig.8.2.8e.

In Fig.8.2.10 shows the average wt% of main elements present in the different stages of polycarbonate filters and aluminum foil substrates (bright red dots). Fig.8.2.10b showing average wt % distribution of iron along the different stages of polycarbonate filters and aluminum foil. This shows that iron is a main constitution of wear debris which is coming from M1 pin and as well as counterpart cast iron.

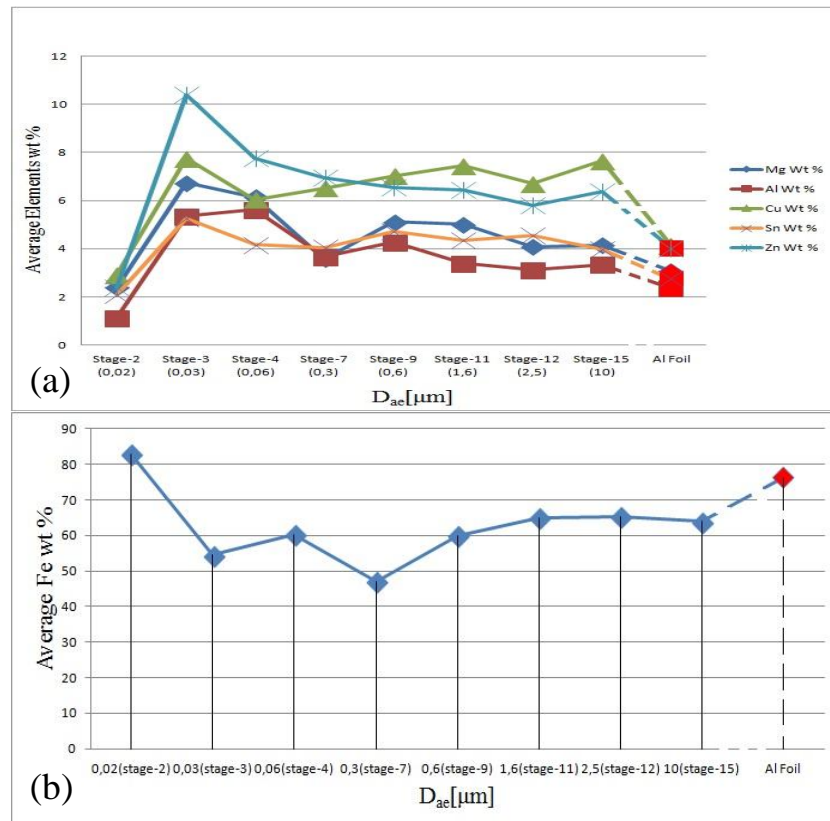


Figure 8.2.10: Average elemental wt % of different stages of polycarbonate filters and aluminum foil.

8.2.3 Transmission Electron Microscopy - Energy Dispersive X-ray Spectroscopy - Selected Area Electron Diffraction

TEM-EDXS analyzes were conducted on the wear fragments collected on aluminum foil and specific stages for polycarbonate filters, for the determination of the phases and compounds present in them, we have used electron diffraction. The SAED patterns are analyzed with the package Process Diffraction [Labar et al.,2005, 2008]. SAED is referred to as "selected" because the user can easily choose from which part of the specimen to obtain the diffraction pattern.

8.2.3 a) TEM – EDXS - SAED of wear debris of M1 frictional material collected on aluminum foil

An ultra fine particle (200 nm) is visible in bright contrast surrounded by an agglomerate of fine particles (Fig.8.2.11a). Some of the fine particles appear in dark diffraction contrast [Osterle et al.,2009], thus contributing to the ring pattern shown in Fig.8.2.11b. The rings can be attributed to the magnetite and magnesium oxide though not unambiguously, because their intensity is very weak and not all diffraction rings are clearly visible. The EDX spectrum of the iron rich nano particle mostly reveals a mixed composition. The main constituent is always iron oxide followed by silicon, Sn, Cu, Zn and Mg corresponding to the major pad constituents. Furthermore, small amounts of elements from the pad constituents like Cr and Ca are also visible.

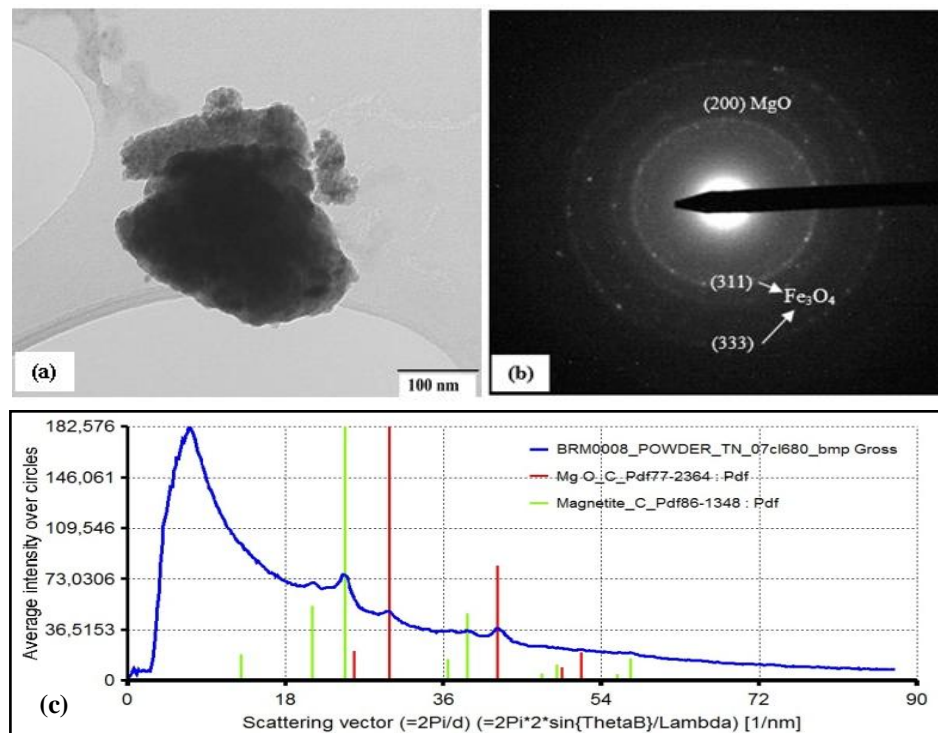
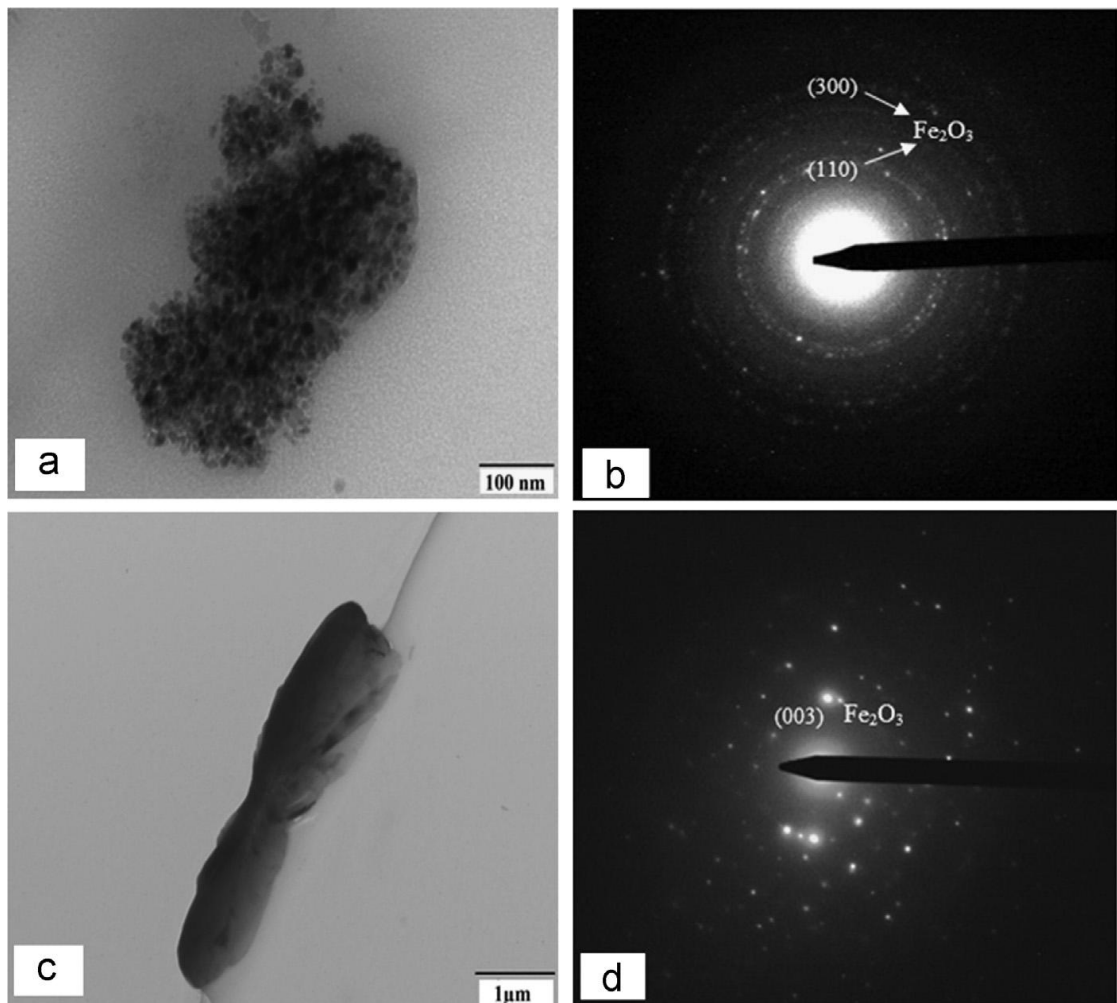


Figure 8.2.11: TEM image (a) and relevant SAED of sample AF-M1. (c) Process Diffraction analysis of the same SAED pattern showing the imaged particles contain iron (red) and magnesium (green) oxides.

8.2.3b) TEM-EDXS-SAED of airborne particles of *Stage_03* & *Stage_12* of M1 frictional material collected on polycarbonate filters

The TEM analysis of the particles shows a strong presence iron oxide. In Fig.8.2.12b Process Diffraction of airborne particle, spectrum can be indexed according to iron oxide (Fe_2O_3). Process Diffraction of airborne particle informed us the presence of iron oxide phase. Fig.8.2.11c shows the nanoparticle wear debris of stage_12 of PC-M1 sample. From the Process Diffraction the phase identified was Fe_2O_3 .



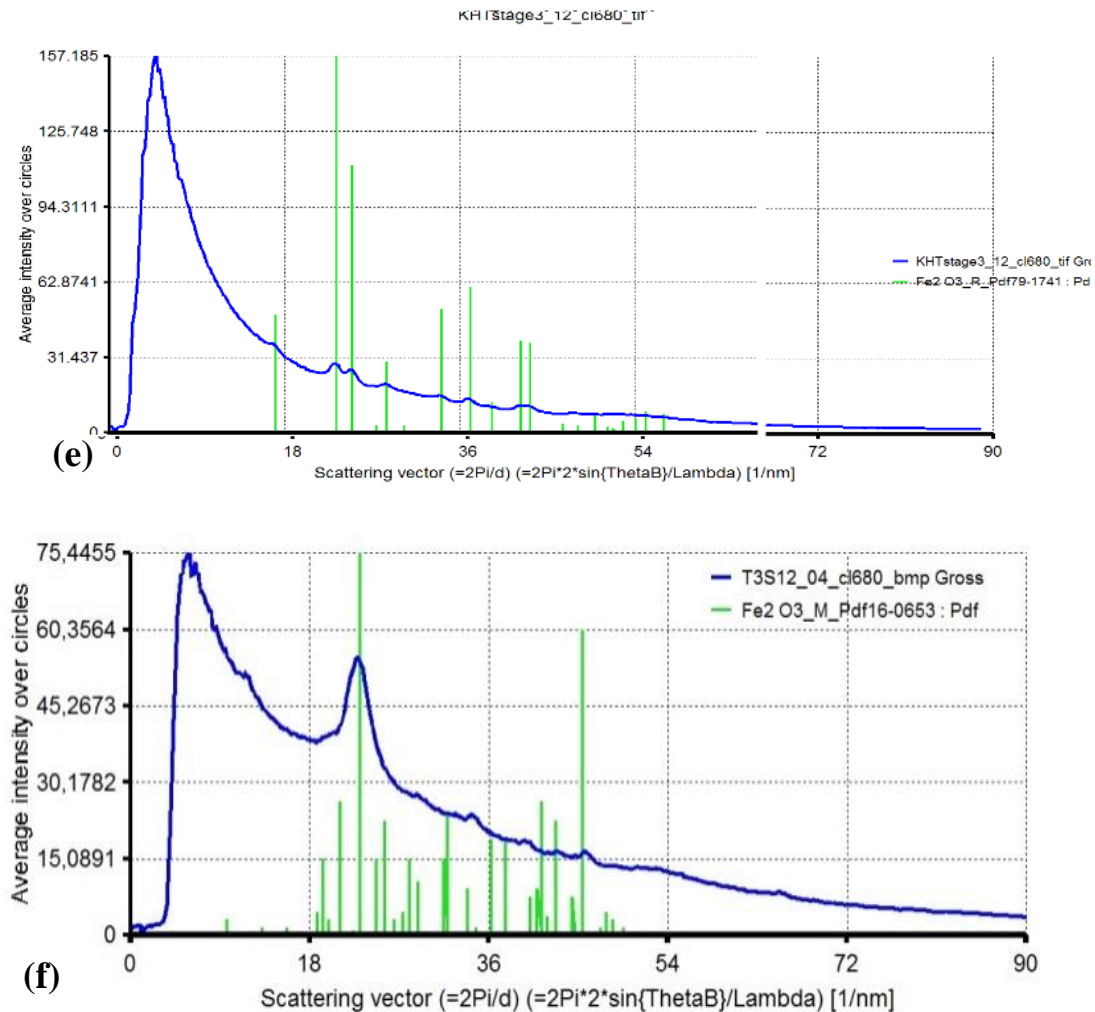


Figure 8.2.12: (a) TEM image of stage_03 of PC-M1. SAED of the same field of view as fig.8.2.12(a). (e) Process Diffraction of the airborne particle of stage_03 of PC-M1 showing Fe_2O_3 phase. (c) TEM image of stage_12 of PC-M1. SAED of the same field of view as fig. 8.2.12 (c). (f) Process Diffraction of the airborne particle of stage_12 of PC-M1 showing Fe_2O_3 phase.

8.2.4 Discussion on the characterization methodology

In the chapter 8, section 8.2 the results of the different characterization techniques have been presented, i.e., XRD, SEM-EDXS and TEM-SAED-EDXS. In this section of 8.2.4, we show how suitable combinations of the above techniques may be adopted for a better and more effective characterization of the samples, even in case only limited amount of powder is available, so that not a complete set of analyses can be carried out. This aspect can be particularly interesting when a set of filters from ELPI+ is considered with very different quantities of collected particles. As an example we show how to deal with a specimen featuring an amount of particles sufficient to perform all the analyzes mentioned in the report, like sample PC-M1 stage_12

As concerns crystallographic data, SAED and XRD patterns of debris M1-stage 12 confirmed the presence of iron oxides (Fig. 8.2.13). In the SAED, the Fe_2O_3 phase only is explicitly indicated, in apparent discrepancy with the corresponding XRD pattern, where FeO and Fe reflections are also visible.

Actually, additional phases are probably present in the electron diffraction pattern too, although to a too lower concentration to be undisputably detected, this is due to the field of view of the TEM Image analysis. The presence of minority phases can be inferred from a number of characteristic X-ray lines in the TEM-EDXS spectrum in Fig. 8.2.15.

The results obtained from TEM-EDXS are coherent with those of SEM-EDXS (Fig. 8.2.15) and relevant quantifications displayed in table 8.2.3. These finds assign a central role to scanning and transmission electron microscopy in association with X-ray spectroscopy in this sort of investigations, since they may straightforwardly validate single particle analyses and crystallographic data obtained through SAED. Moreover, no limitations to the applicability of these techniques come from the more or less large quantity of specimen.

8.2.4 a) TEM-SAED_(single particle analysis) v/s XRD_(bulk analysis) of M1 friction material collected on polycarbonate filters

From both characterization tools (SAED and XRD) it has been confirmed the presence of different iron oxides. Other phases are present in the SAED but the relevant lines are too weak to be reliably indexed. We can summarize the above results with the intersection diagram in Fig. 8.2.14. Clearly the situation might be improved when a sufficiently large number of particles is considered, even on the basis of EDXS analyses both in SEM and TEM (see next section). Both set of techniques can be profitably used to characterize the wear debris of PC-M1 stage_12 sample.

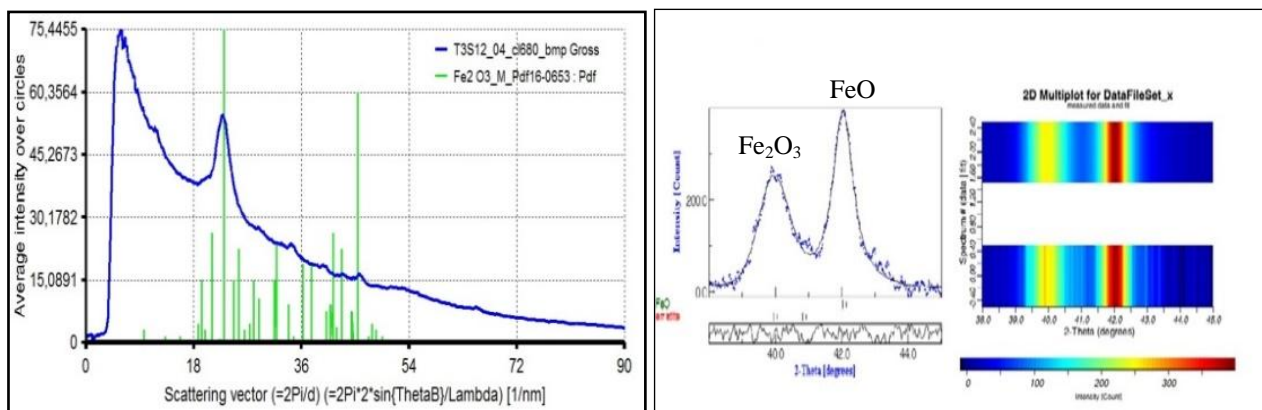


Figure 8.2.13: SAED (left) and XRD (right) patterns for PC-M1 stage_12 sample. In the SAED in green reference lines for Fe_2O_3 . As concerns the XRD pattern, the main diffraction peaks of identified phases are marked.

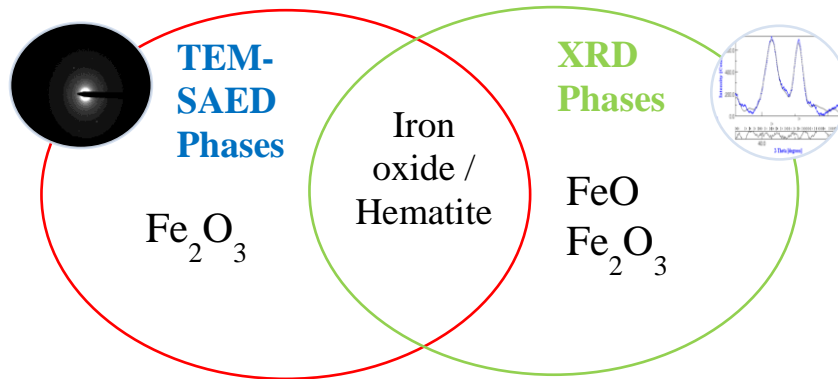


Figure 8.2.14: Intersection diagram for SAED and XRD results of sample PC-M1 stage_12 sample.

8.2.4 b) TEM-EDXS v/s SEM-EDXS of M1 friction material collected on polycarbonate filters

The qualitative and quantitative EDXS data provide useful indications to guide and complete even other analyses, such as the already mentioned SAED and XRD. As expected, data in Table 8.3.1 confirm iron oxides to be the main phases in sample PC-M1 stage_12. On the other hand, other elements are present, although present to a lower extent, so that could not be reliably detected in the XRD spectra of this sample. Nonetheless, the information provided by TEM, SEM and EDXS are efficiently completing, with XRD, the characterization of the examined sample.

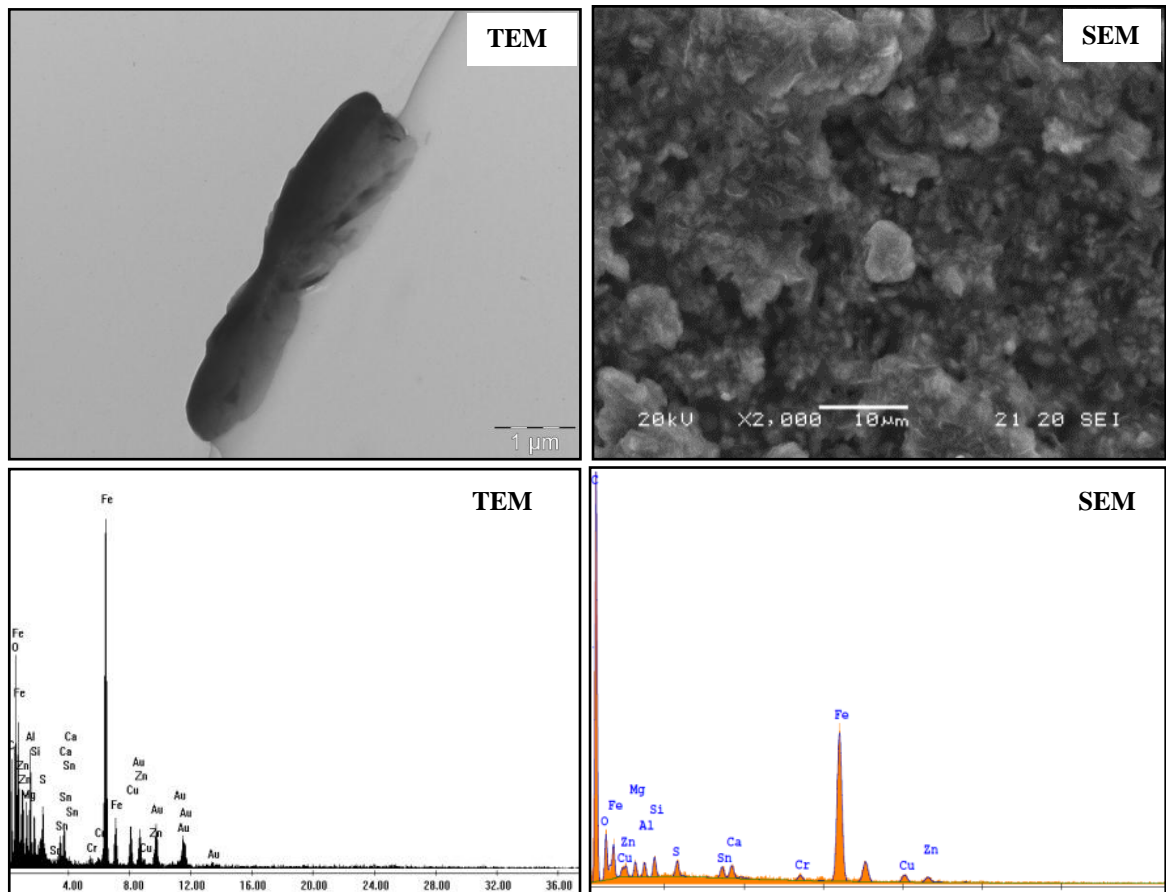


Figure 8.2.15: PC-8 stage_12 sample TEM (left) and SEM (right) wear debris and relevant EDX spectra. In both spectra the main detected elements are indicated. Gold lines in EDX-TEM spectrum are due to carbon coated gold grid used for TEM sample preparation.

Table 8.2.3: PC-8 stage_12 sample. Quantitative analyzes of the EDXS data taken from the spectra in Fig.8.2.15.

| (TEM-SAED) | Wt % | (SEM-EDXS) | Wt % |
|--------------------------------|------|--------------------------------|------|
| MgO | 3.3 | MgO | 4.1 |
| Al ₂ O ₃ | 7.1 | Al ₂ O ₃ | 3.7 |
| SiO ₂ | 3.9 | SiO ₂ | 4.3 |
| SO ₃ | 5.7 | SO ₃ | 3.6 |
| SnO ₂ | 8.1 | SnO ₂ | 4.3 |
| CaO | 2.3 | CaO | 1.4 |
| Fe ₂ O ₃ | 55.4 | Fe ₂ O ₃ | 66.8 |
| CuO | 6.8 | CuO | 5.3 |
| ZnO | 6.4 | ZnO | 5.1 |

We conclude the discussion part with Table 8.2.4, which indirectly provides selection rules for the experimental techniques to be used with powder samples coming from wear tests. It turns out that a critical aspect is the amount of available material. Our approach is providing a tool for getting anyway reliable results in the characterization of the powders so that relevant wear mechanisms may be effectively investigated.

These observations are summarized in table 8.2.4, that provides a synthetic view of the outcomes of the present methodological study. The effectiveness of electron microscopy is determined by the generally little amount of required powder specimens. Still with regard to Table 8.2.4, two more points can be made. The first one concerns the limit in using XRD when a sufficient amount of sample is not available, that indeed, in the present study, cannot be used for ELPI+ stages below stage 9. As concern TEM observations, its effective application to particle imaging is basically associated to an excessive average thickness of the wear particles and consequent lack of electron transparency.

Table 8.2.4: Summary indications about the experimental protocol for wear debris characterization emerging from the present study. ✓ : indicates that the technique can be profitably employed; ✗ : unsuitable techniques; ? : TEM observations can be conducted in principle, although imaging may result quite problematic owing to the excessive average thickness of the particles.

| Wear debris on PC filter | Diameter (µm) | Total particle mass (g/m ³) | XRD | SEM | SEM-EDXS | TEM-SAED | TEM | TEM-EDXS |
|----------------------------------|---------------|---|-----|-----|----------|----------|-----|----------|
| Stage-02 | 0.017 | 0.131 | ✗ | ✓ | ✓ | ✓ | ✓ | ✓ |
| Stage-03 | 0.03 | 0.238 | ✗ | ✓ | ✓ | ✓ | ✓ | ✓ |
| Stage-04 | 0.06 | 0.355 | ✗ | ✓ | ✓ | ✓ | ✓ | ✓ |
| Stage-07 | 0.26 | 0.296 | ✗ | ✓ | ✓ | ✓ | ✓ | ✓ |
| Stage-08 | 0.4 | 0.680 | ✗ | ✓ | ✓ | ✓ | ✓ | ✓ |
| Stage-09 | 0.64 | 0.813 | ✓ | ✓ | ✓ | ✓ | ? | ✓ |
| Stage-12 | 2.5 | 13.10 | ✓ | ✓ | ✓ | ✓ | ? | ✓ |
| Stage-15 | 10 | - | ✓ | ✓ | ✓ | ✓ | ? | ✓ |
| Wear debris collected on Al foil | | | ✓ | ✓ | ✓ | ✓ | ✓ | ✓ |

8.3 Role of the friction layer in the high-temperature pin-on-disc study of M1 & M2 friction materials - Case III

This section of work is the extension of work that has been done in *Case I*, in which frictional behavior of a M1 & M2 friction materials dry sliding against a cast iron disc at room temperature are considered. In the low wear behaviour friction material, the formation of primary and secondary plateaus was observed. Two main kinds of secondary plateaus were identified: well compacted plateaus rich in copper, zirconium and iron oxide particles, forming quite large plate like fragments; less compacted plateaus, featuring a lower copper content, that tend to form comparatively smaller degradation fragments, whereas in M1 (higher wear behavior) friction material, the friction layer coverage is limited and destroyed by the abrasive particles and metal chips. In this section an attempt is made herewith to investigate the friction and wear behaviour of the above low-steel friction pad materials at different disc temperatures.

The degradation mechanisms observed in the friction material induced a transition from mild to severe wear during continuous dry sliding conditions. Through this study, it was possible to gain further information on the main wear mechanisms and in this way identify critical parameters to develop better friction materials, as concerns performances, lifetimes and pollutant emissions.

8.3.1 Thermal behaviour of M1 & M2 friction materials

The TGA curves shown in Fig.8.3.1 shows the thermal decomposition pathway of phenolic resins in M1 & M2 friction materials, in air at a heating rate of 10 K/min. In TGA curve, the red line represent the thermal behaviour of M1 friction material and green for M2 friction material. It is clearly noticed that M1 friction material has more mass reduction when compared to M2 at any given temperatures. The inset image (fig.8.3.1) shows details on the thermal behaviour of M2 friction material.

In both pin materials, there is a two mass-loss step representing partial decomposition. A first minor mass reduction appears at 150°C and major decomposition starts in between 230°C-350°C with a maximum decomposition rate (Fig.8.3.1) which can be attributed to a process decomposition of the phenolic resin, which is used as a binder in the friction materials, that proceeds by forming a char [Eriksson et al., 2001]. Similar effect has been observed by G.M. Ingo et al.,2004, reporting on the thermal decomposition of a organic friction materials has broad exothermic drift in the temperature range from 200°C to 375°C with an associated weight loss of 3-5wt%, which is due to the oxidation or evaporation of organic compounds. Different authors reported the thermal degradation of phenolic resin at elevated temperature [Patel et al.,2012]. The main components evolving during the decomposition of the phenolic resin at 230°C-450°C are H₂O and CO₂, which mainly correspond to the decomposition of binder and combustion of carbon [Seong et al.,2000]. Bijwe et al.,2005, have investigated similar effects of deterioration of resin in brake pads during operation at 300°C - 400°C. Huong et al.,2009, have investigated wear of three friction materials, featuring three different types of phenolic resin. They observed that up to 200°C the wear process was due to breaking of hydrogen bonding, and at temperature higher than 300°C the phenolic resin undergoes a random scission of polymeric chains, oxidation and carbonisation.

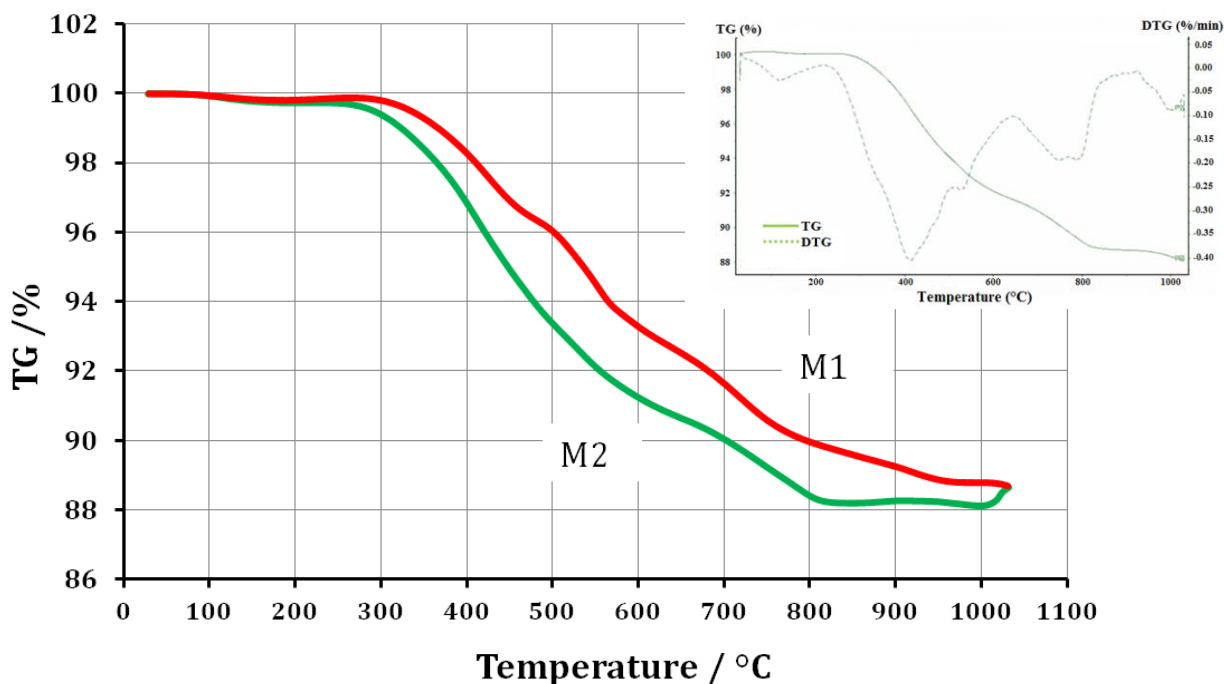


Figure 8.3.1: TGA curves of friction materials M1 & M2 in air. DTG curve of M2 in inset.

8.3.2 Friction and wear behaviour of M1 & M2 friction materials

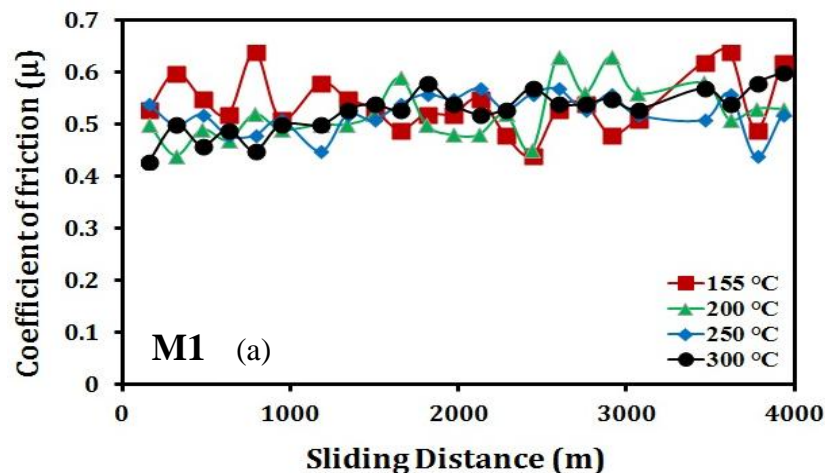
Fig. 8.3.2(a, b) shows the frictional characteristics results obtained from different temperature tests (155°C/170°C - 300°C) with M1 & M2 friction materials sliding against cast iron disc. The friction behaviour of M1 & M2 pins at room temperature (25°C) was already discussed in *Case I*, the reader is referred to previous paragraph. The friction behaviour at higher temperatures i.e., 155°C/170°C for M1 & M2 is described herewith. The frictional behavior as a function of temperature of friction materials is shown in table 8.3.1. As the working temperature is increased an increase in the coefficient of friction is observed (fig.8.3.2).

The initial coefficient of friction value at the time of commencement of the test for M1 pin at 155°C was relatively higher than the M2 (table 8.3.1), which might be due to the surface abrasion by the hard particles entrapped in the surface interface during test. For M1 pin, at higher temperature >200°C, there was decomposition of phenolic resin and the decomposed resin product i.e., carbon widespread on the plateaus (mainly primary plateaus) which act as a lubricant in the sliding friction (as shown by XRD of friction layer of M1, Section 8.3.7) and thus maintain the stable coefficient of friction at higher temperatures, in the range of 0.4-0.6.

The friction results from the test at 170°C for M2, have shown different frictional behaviour as compared to other higher temperatures tests. The friction coefficient is almost constant which is due to the formation of friction layers, reducing frictional coefficient and wear rate. The frictional coefficient is almost smooth and attains a steady state value as the test progressed, which reflects in lower wear rate and better frictional behaviour. It is clear from the Table 8.3.1 that at 170°C the frictional coefficient varies over narrow band as compare to other high temperature tests. Frictional behaviour of brake pin at 200°C is shown in Fig.8.3.2b). The initial

frictional coefficients at the commencement of the test were ~ 0.51 and then decrease trend was observed as the test progressed, to the final value of ~ 0.39 , which is due to the compaction (sintering process) of wear product at high temperature. At high temperature, the frictional behaviour at 250°C and 300°C increases with increase of temperature. Both the friction curve shows the same trend up to 2500 meters and afterward, there is slight drop in frictional behaviour of 250°C curve, which is believed to have some compaction of wear debris on the frictional surfaces. At 300°C high temperature the coefficient of friction increases with increase of temperature which is due to the fact that at this range of temperature corresponds to degradation of phenolic resin of friction material (Table 8.3.1).

Fig.8.3.2(c, d) shows the extrapolated temperature as a function of sliding distance which is a representative temperature of friction materials (M1 & M2) measured by two chromel-alumel type thermocouples at 6mm (T_1) and 4mm (T_2) from the contact surface of the pin with the disc. As a matter of fact, a sharp temperature gradient should be present at the surface since the pin temperature must strongly increase to the contact (disc) temperature. This also shows that the thickness of (pin) material subjected to very high temperature (the disc temperature) is quite small. Increase trend of temperature at $155^\circ\text{C}/170^\circ\text{C}$ test and other high temperatures for both the friction materials were shown as the test progressed. At $155^\circ\text{C}/170^\circ\text{C}$, frictional heating between two sliding surfaces caused the increase in temperature. As far as temperature of pin at elevated temperature is concerned, a major part came from external source heating (heating coils) and less from frictional heating.



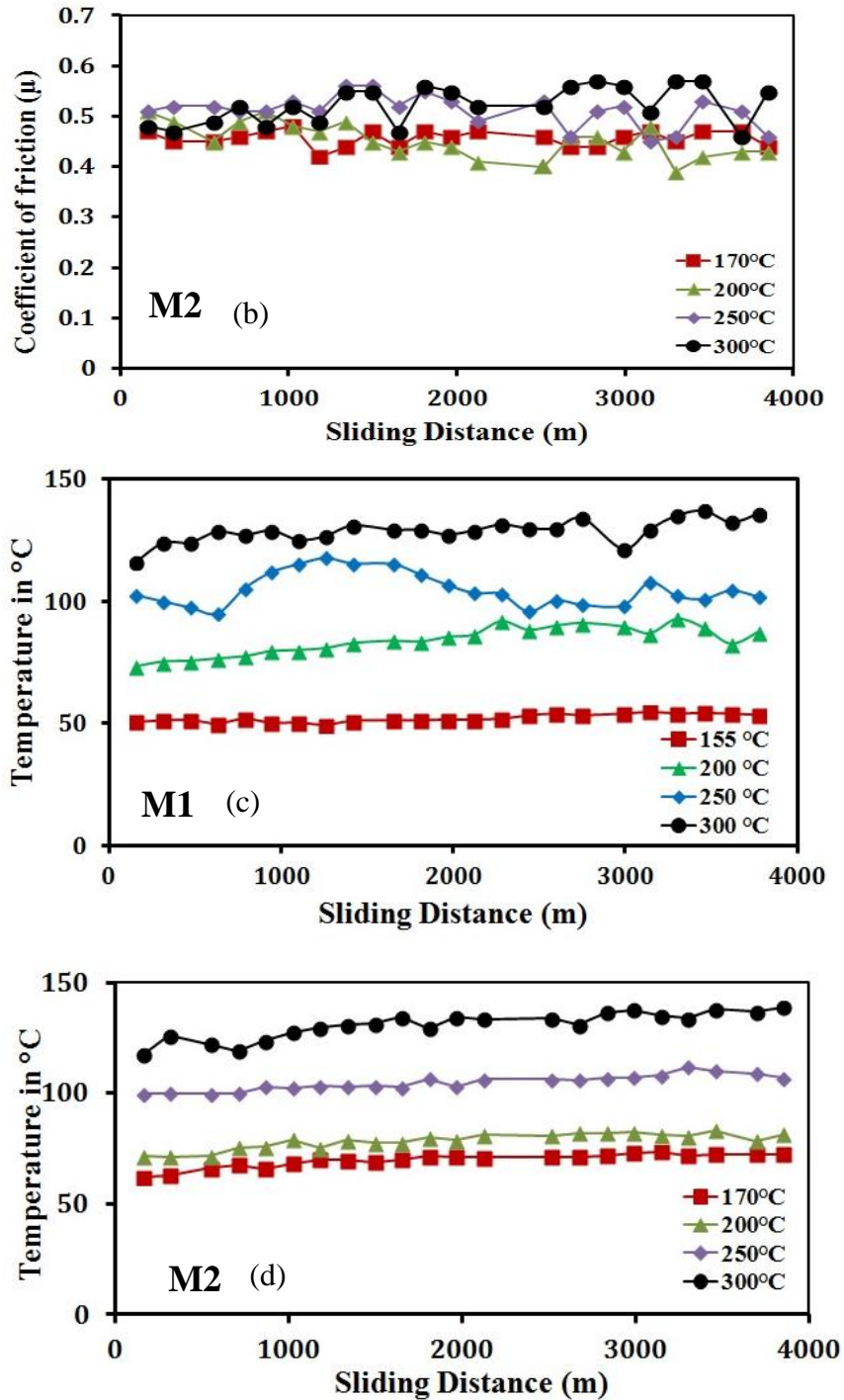


Figure 8.3.2: Evolution of the friction coefficient of M1 & M2 friction materials (a & b) and (c & d) extrapolated contact temperature of pins measured by thermocouple at 6mm and at 4mm.

Table 8.3.1: Wear rates, Average pin temperature and friction coefficient of the M1 & M2 pins at different temperatures.

| Temperature of the cast iron disc | Wear Rate [mm ³ /mm]*10 ⁻⁷ | | Specific Wear Coefficient [m ² /N] *10 ⁻¹⁵ | | Pin temperature T _{max} (°C) | | Coefficient of friction (μ) | |
|-----------------------------------|--|------|--|------|---------------------------------------|-------|-----------------------------|-----------|
| | M1 | M2 | M1 | M2 | M1 | M2 | M1 | M2 |
| 170 °C M2/ 155 °C M1 | 30.7 | 4.1 | 61.2 | 8.5 | 55.0 | 73.0 | 0.4 - 0.6 | 0.4 - 0.5 |
| 200 °C | 43.2 | 6.1 | 86.1 | 12.6 | 88.0 | 83.0 | 0.4 - 0.6 | 0.4 - 0.5 |
| 250 °C | 65.0 | 8.7 | 130.4 | 18.0 | 97.0 | 112.0 | 0.5 - 0.6 | 0.5 - 0.6 |
| 300 °C | 102.5 | 27.7 | 204.6 | 57.5 | 135.0 | 138.0 | 0.4 - 0.6 | 0.5 - 0.6 |

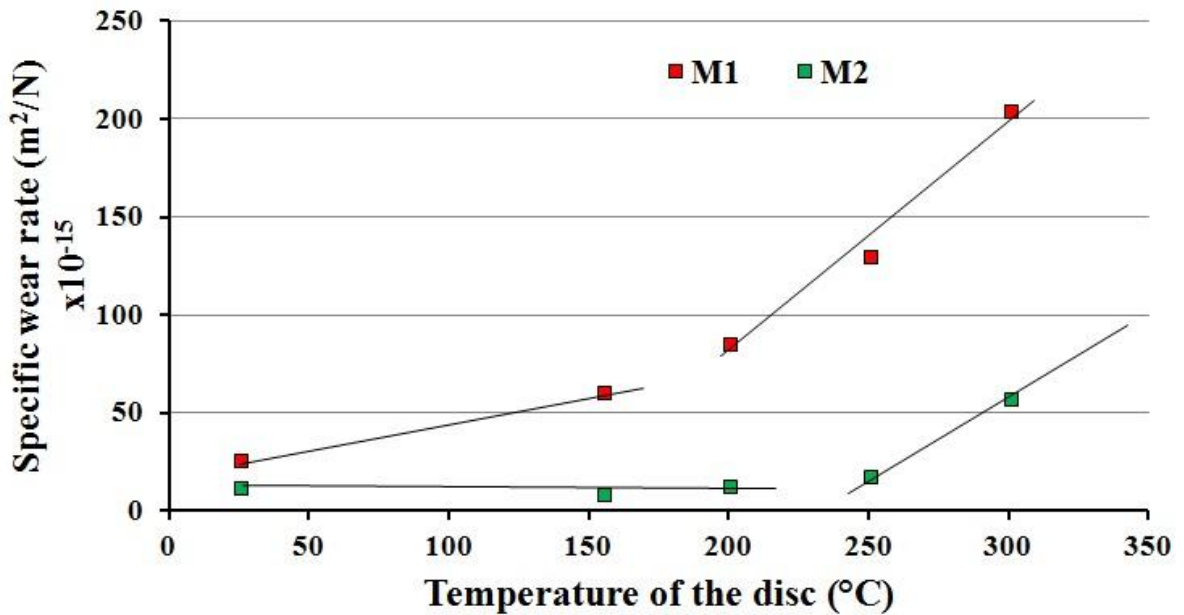


Figure 8.3.3: Specific wear behaviour of M1 & M2 friction materials pin at different temperatures.

Here, in wear comparison section, I have considered the wear behavior at room temperature (25°C) in order to have a better plotting and wear understanding as a working temperatures increases and also in the upcoming results and discussions sections, I have considered the SEM microstructure at (25°C) to better understand the evolution of friction plateaus with respect to the temperature rise.

The wear trend was same for the two friction materials i.e., exponentially increased w.r.t temperature and from the figure 8.3.3 it has been clear that M1 has more wear rate than M2 at higher temperature. The lower friction and wear of material M2 with respect to material M1 (Fig. 8.3.3) can be attributed to the formation a quite uniform friction layer, due to the presence of ingredients, such as zirconium oxides, able to form small particles during sliding that are compacted and held together by the presence of metallic ingredients, such as copper. The absence of zirconium oxides in the formulation of M1 and the presence, in their place, of hard and abrasive Mg and Zn oxides, reduced the formation of friction layer. Such oxides favored the abrasion of the counterface disc and formed friction layer, as confirmed from the XRD of M1 wear debris from *Case II*, thus increasing the coefficient of friction and wear rate (Table 8.3.1). Table 8.3.1 summarizes the results of the frictional and wear tests for materials M1 & M2.

Figure 8.3.3, shows the experimental wear coefficients as a function of the disc temperature for materials M1 & M2. As expected, the wear coefficient is initially constant up to a working temperature, that is in the range 150-200°C for M2 material, which indicated that, the wear characteristics curve has an exponential trend after 170°C-200°C and before this temperature it is linear, which indicates wear rates are very less. The same phenomenon for M1 pin but have one degree higher magnitude of wear (table 8.3.1).

For M2 pin, at 25°C, when the mating surfaces sliding under given load conditions, there were formation of compacted layers of oxide and other alloy oxide particle from the friction material on the sliding surfaces. These layers further developed by agglomeration and compaction of the wear debris produced during sliding operation. The wear debris undergo deformation, fragmentation and breaking down in to smaller debris. As the sliding continues these compacted layers made by, agglomerated clusters of particles were subjected to thermos-elastic stresses, which act as load-bearing regions or friction layers helps in protecting further wearing of the sliding surfaces. At 170°C the value of specific wear rate slightly goes down as it is observed that rise in temperature and constant load could leads to the occurrence of sintering process in which the fine particles are sintered together to form more stable compacted layers. Rise in temperature increase the sintering rate which further increase the development of very solid smoothly surface i.e., friction layers, these layers helps in minimising the wear rate. Thus, Mild wear region existed between temperatures 170°C to ~200 °C with the oxide sintering to form a stable comprehensive friction layers; hence reduction in the specific wear rate. As the temperature increased the nature of the oxide deposit changed. The loose wear particles undergo agglomeration and sintering at around 170°C with the result in formation of friction layers. The extent of friction layers formation increased with temperature (under mild wear region). Ones the friction layers is formed the wear of the friction material substantially reduced, but for M1, at 155°C, the delamination of plateaus acquired (fig.8.1.3b) by the three body abrasive mechanism, thus higher wear.

The wear characteristics of both friction materials at 300°C have shown higher wear as compare to 250°C, which shows temperature play an important role in wear and the main reason was degradation of the phenolic resins at higher temperatures. As higher temperature both pin materials losses their density, porosity increased, since M1 has a potassium titanate as a fibres,

these fibres are prepared from highly refined, single crystals, which have a high melting points, always hold the material ingredients firmly. The absence of such fibres in M1 leads to more wear than M2.

8.3.3 SEM observations of high temperature worn surfaces of M1 & M2 friction materials pins

Fig.8.3.4 (a) and (b) shows SEM images of the worn surfaces of the friction materials M1 & M2 pins at different temperatures respectively. For M1 pin (fig. 8.3.4 a) at 25°C, the deterioration of secondary plateaus can be observed which is due to abrasion action by the abrasive particles such as MgO. More wear debris and flakes can be seen on the surface of the pin. The EDX analysis on less compacted plateaus indicates that higher content of Fe rich particles followed by Zn, Sn and Cu. At temperature 155°C, 200°C and 300°C, few area of the pin were spotted to have secondary plateaus, only torn primary plateaus can be seen in the micrographs. At high temperature ~300°C, the deterioration of phenolic resins is at higher extend, this will be shown in the next paragraph, in the Raman spectrum as formation of disordered graphite lattice which is a temperature dependent phenomenon. The EDX analysis at 155°C, 200°C and 300°C on the less compacted secondary plateaus indicates the higher presence of Fe, which is mostly coming from cast iron disc and torn out steel fibers and other elements like Al, Sn, Zn and Cu. Cu is next most finding in EDX at higher temperatures for M1, as from XRD of friction film of M1 at different temperatures also confirm higher wt% of copper. The presence of copper is from brake M1 pin and at high temperature it might be possible to see more copper rich primary plateaus than iron, as copper has more ductility as compare to the steel fibers which get torn out during the high temperature tribological operation.

A severe wear regime persisted at 200°C and 300°C, high-temperature oxidation in which phenolic resins decomposes by charring and evaporation. This process decreases the density of the brake friction material at the wear surface and increases its porosity, thereby losing its structural integrity thus promoting the large size flattened debris generated by adhesion and delamination wear was unable to remain at the sliding interface that led to further adhesion between wear surfaces and continued high wear rate. The failure of wear debris to undergo the level of sintering required for the formation of the low residence time of the debris between the wear interfaces as a large amount of debris was ejected at higher temperature, thus reducing the contact times between the particles. Agglomeration and sintering require the particle to maintain their shape and integrity. The deformed particle failed to satisfy this condition thus between 200°C to 300°C, a severe wear mechanism dominated in M1 friction material. Although increasing temperature clearly increases the rate of oxidation, no friction layers formation occurred mainly due to the low debris retention and low residence time of the debris on the friction material surface. Which results almost no friction layers at the interface, as it is found in cross section of the M1 pin, high rate of thickness loss and wear rate is noted. In the absence of friction layers, under the high temperature condition, higher friction coefficient has been observed. As the temperature increases the, the main phenomenon start with in the brake system materials:

- The phenolic resin starts decomposing and the structural integrity of the pin is degraded and a large amount of debris was ejected (Fig.8.3.4-350°C). Hence higher wear rate of the friction material pin at higher temperature.

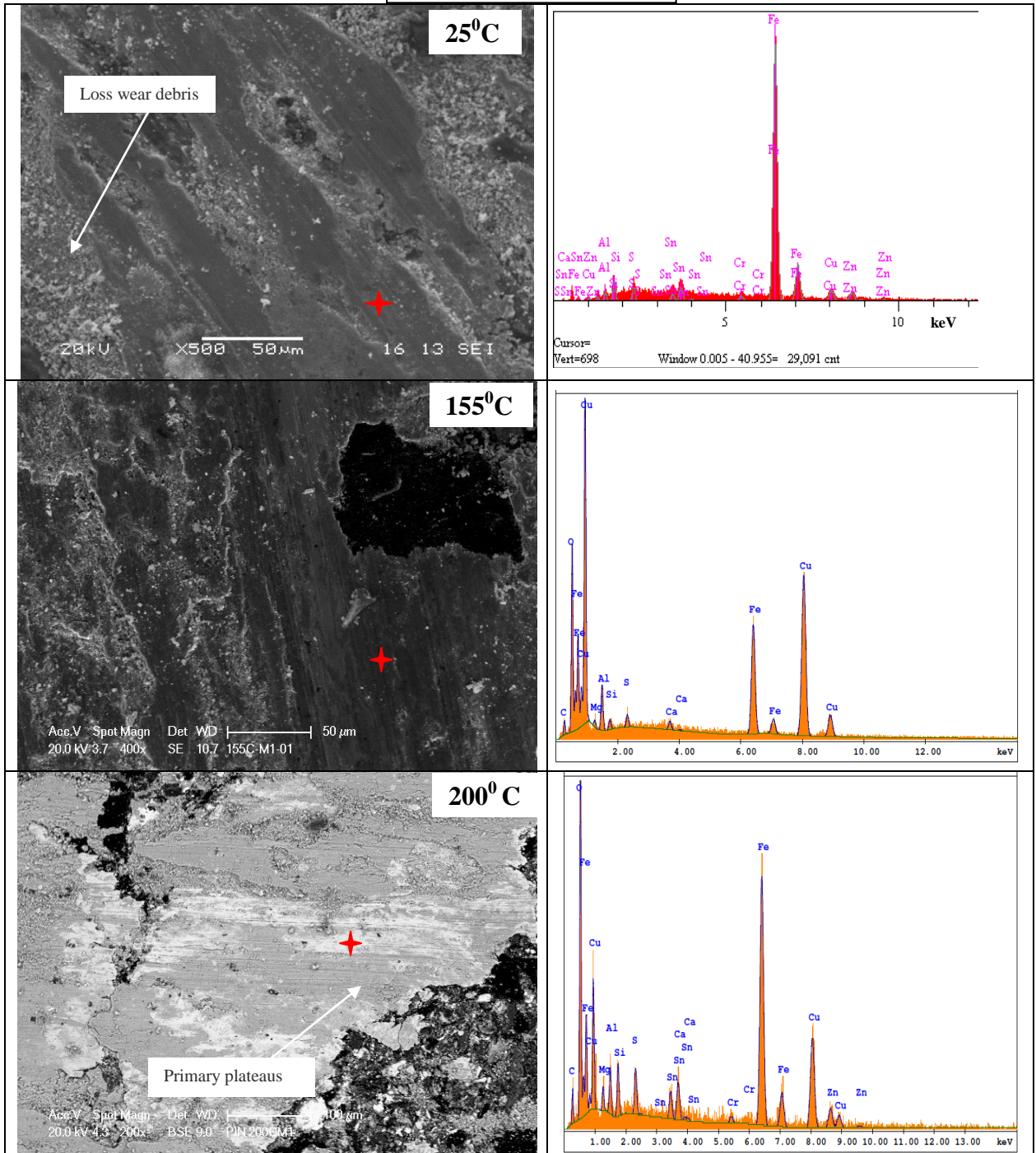
In fig. 8.3.4 b) for M2 pin at 25°C, show the formation of different contact plateaus. Contact plateaus consist of two parts - primary plateaus and secondary plateaus. The primary plateaus first form due to the lower removal rate of the mechanically stable and wear resistant ingredients of the pad: hard particles-fibers, protruding to the surface and making the barrier against which the small wear particles accumulate and are compacted. In a second stage, these protruding hard phases may form nucleation sites for the growth of secondary plateaus [Osterle et al.,2004]. These secondary plateaus, made by the compaction of wear particles (including the oxides from the counter face) were less compacted plateaus and very well compacted plateaus. The wear debris undergone a compaction process to form friction layers. The formation of the friction layers extended due to the applied load that the fragments that are produced, are compacted more effectively, thus reducing wear.

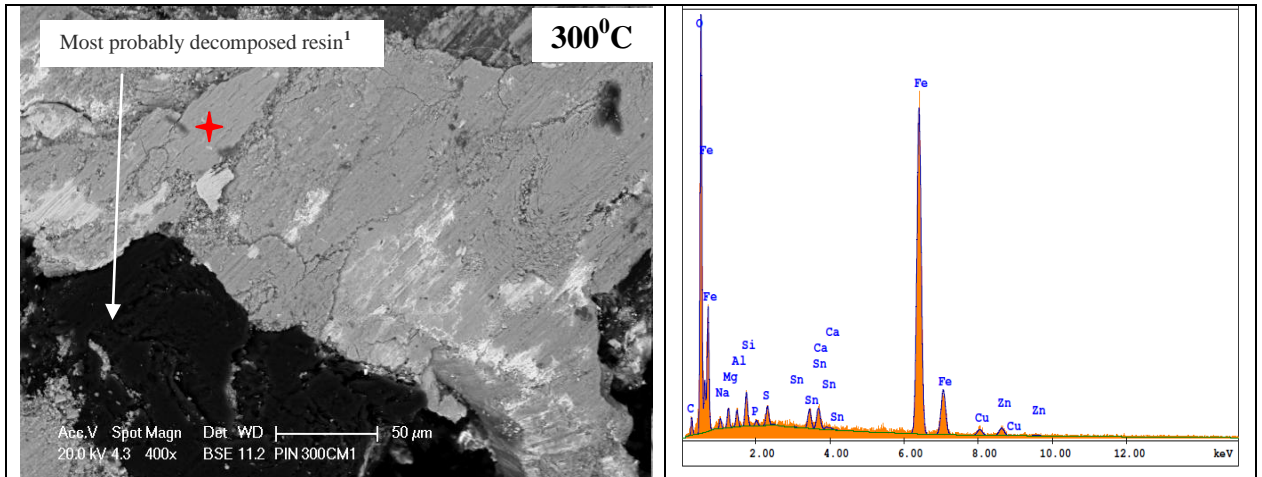
The chemical composition of the friction layers formed, obtained by means of EDXS analysis appears to be mainly iron, zirconium and oxygen, with the presence of copper. There are also barium, silicon, aluminum, magnesium, zinc, carbon, titanium and potassium, although in smaller quantities. The presence of iron in large quantity indicates a possible transfer of the disc material.

The primary plateaus derive from a lower removal rate of the mechanically stable and wear resistant ingredients of the pin material: hard particles and fibers, protruding from the surface of the pins when they start to wear out. The primary plateaus act as barriers to the movement of the finer wear particles, that therefore tend to stop and to accumulate at the interface with such barriers. If these particles start to stick together, this promotes the formation of the secondary plateaus. The friction layer displays a progressive reduction at increasing temperatures i.e., 170 °C. At 170°C the formation of a secondary plateaus was observed and the loose particles were agglomerated and sintered to form a wear protective layers. The formation of secondary plateaus was examined by other researchers previously like Osterle, W. et al.,2006 and Eriksson, M. et al.,2000.

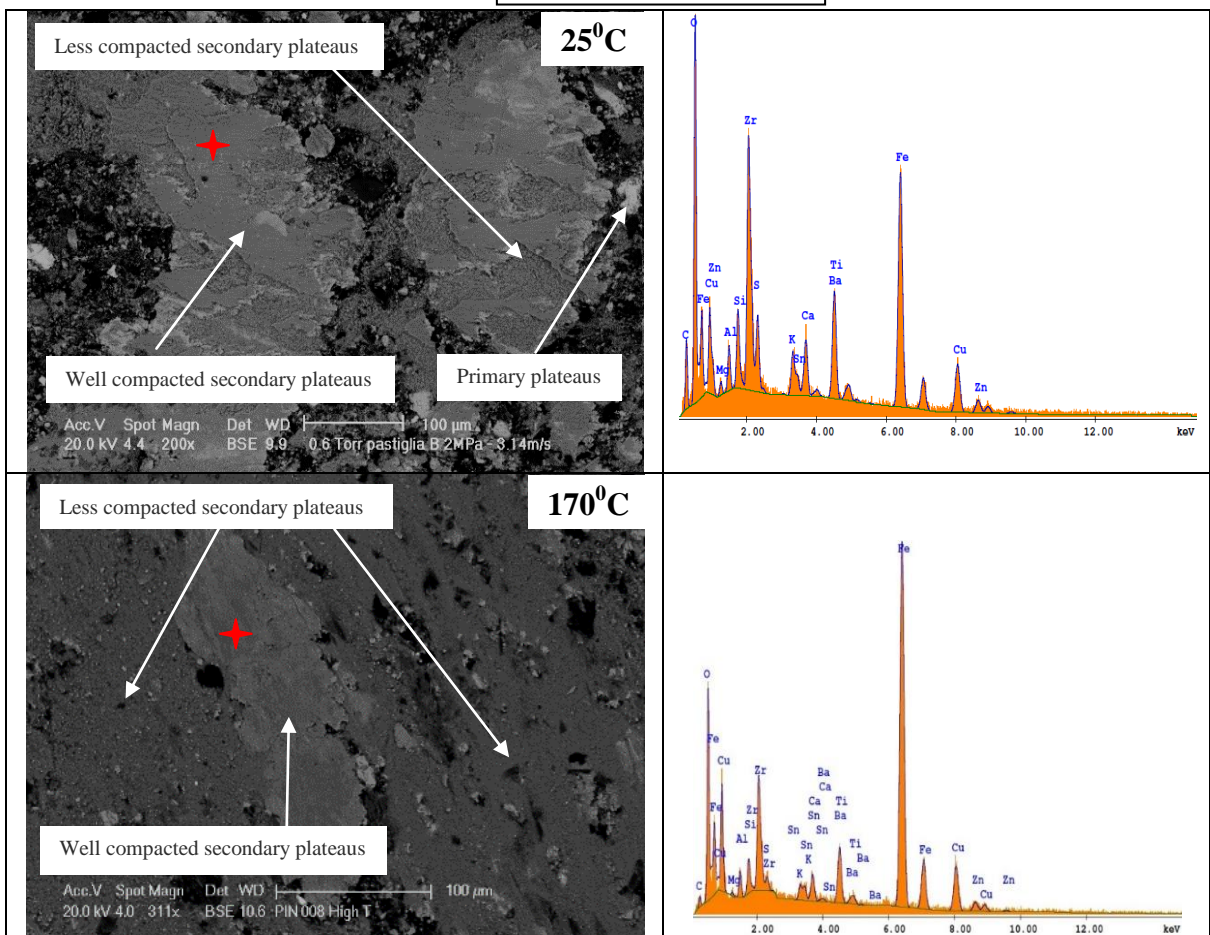
Note here:- In the EDX analysis of wear protective layers shows the main wt% is of Iron as it was come from both disc and friction material, zirconium and copper from friction material. At 200°C, less compacted secondary plateaus observed with few black patches. These black patches are the decomposed phenolic resin carbonaceous product. The EDX analysis on less compacted plateaus indicates that higher content of Zr abrasive particles followed by Fe, Ti and Cu. Primary plateaus are also observed on a smaller area, their chemical composition also contain Zr, but the Cu and Fe content is much higher, Fe increased amount may indicate the particles transferred from the disc surface, in view of lower Ti concentration. The EDX analysis at 250°C and 300°C on the less compacted secondary plateaus indicates the higher presence of Zr, as an abrasive particles originating from the pin; other elements are present too such as Ti, Cu, Al and less Fe which is mostly coming from friction material and less from disc. Still the area covered by the friction layers is smaller, probably due to the higher wear rate at high temperature caused by breaking of weak bonding between pin ingredients and polymeric matrix.

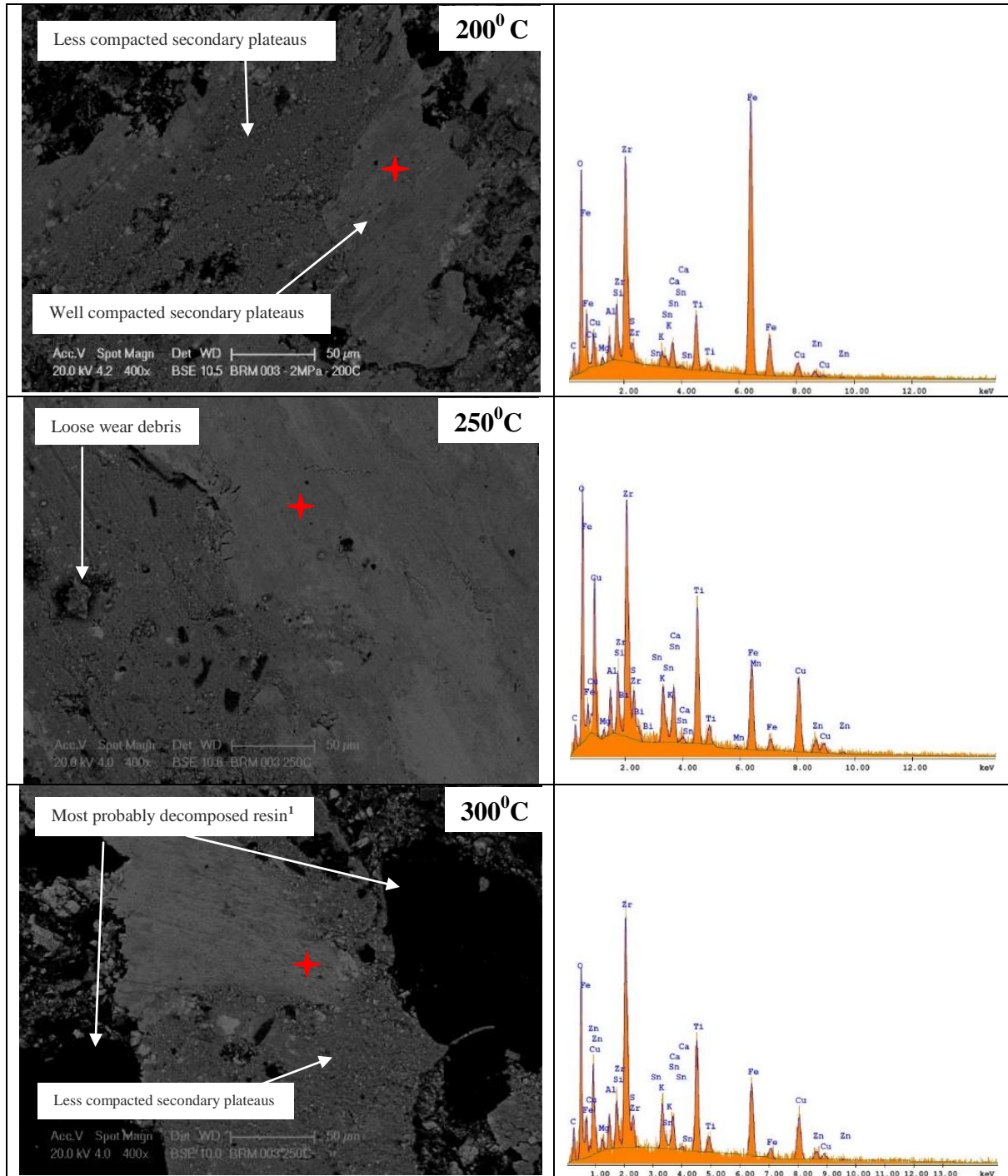
M1 Pin (a)





M2 Pin (b)





¹ Most probably decomposed phenolic resin in the form of disordered carbonaceous product at elevated temperature.

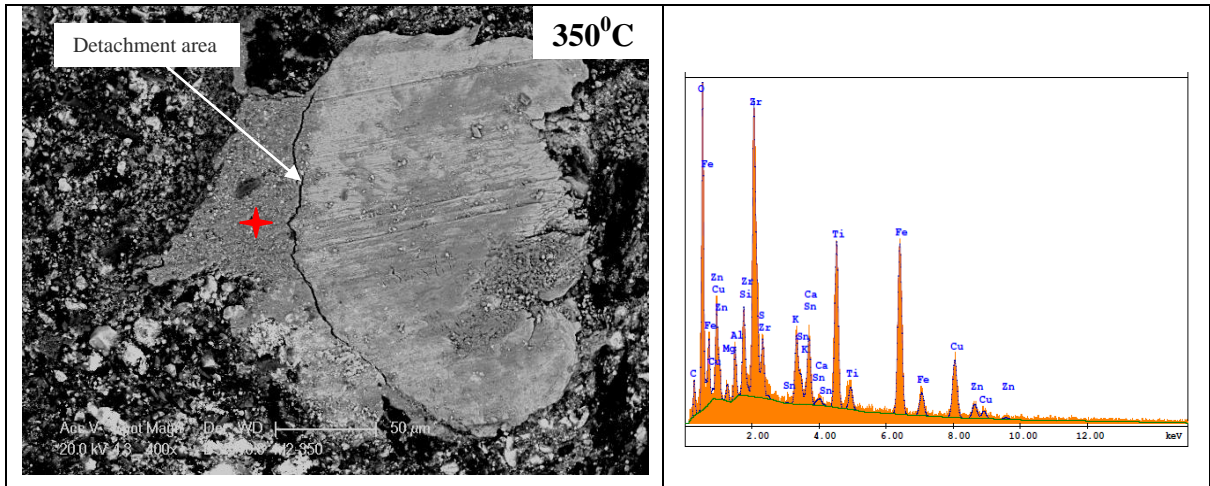


Figure 8.3.4: SEM of worn surfaces of M1 (a) & M2 (b) friction materials pins at different elevated temperature.

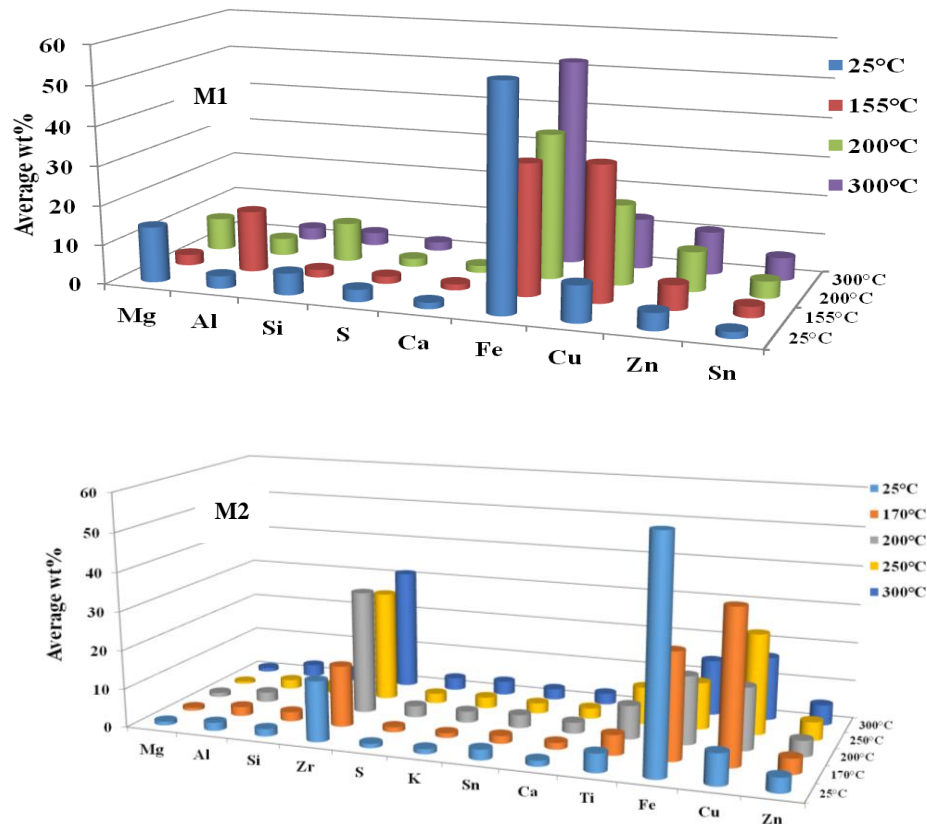


Figure 8.3.5: Average elemental composition of friction layer on M1 & M2 worn pin surface-planar view.

8.3.4 Raman spectroscopy of black spot at higher temperatures

[Please note that in the below paragraphs the following alphabets represent: G = Ideal graphitic lattice. D1 = Disordered graphitic lattice. D3 = Amorphous carbon. D4 = Disordered graphitic lattice, ionic impurities.]

Fig.8.3.6 shows the typical Raman spectra observed for black carbonaceous product, which evolved during different temperature frictional test, with a laser having a $\lambda = 532$ nm in the range of $50 - 3300\text{cm}^{-1}$. The spectra exhibit two broad and strongly overlapping peak at intensity maxima $\sim 1360\text{cm}^{-1}$ and at $\sim 1590\text{cm}^{-1}$ for 250°C and 300°C . Previous studies [Fatima et al.,2015] revealed that the intensity maxima at 1590cm^{-1} (known as G band) is similar to the ideal graphitic vibration mode and other peak intensity maxima at $\sim 1360\text{cm}^{-1}$ corresponds to disordered graphite structure. This peak is known as D1 peak (Defect bands). The high signal intensity between the two peak maxima can be attributed to another band at $\sim 1500\text{cm}^{-1}$, designated as D3 band which originates from the amorphous carbon fraction of decomposed resin (organic molecules, fragments or functional groups) and/or amorphous sp^2 bonded forms of carbon. sp^2 bonded carbon in planar sheets in which the bond energy of the sp^2 bonds is high. The higher energy of the sp^2 bonds in graphite pushes the vibrational frequency of the bonds and hence the higher frequency of the band in the Raman spectrum. W. Osterle et al.,2004 showed in Raman spectroscopy that the binder during oxidation produces amorphous carbonaceous product, which is also termed as “highly disordered graphite”. Raman spectra recorded with $\lambda = 532$ nm also exhibit second order spectra in the range of about 2300cm^{-1} to 3300cm^{-1} . For the given studies only first order spectra have been considered for further analysis.

Fig.8.3.7 shows the analysis and determination of spectral parameters by curve fittings various line shapes were evaluated. In this study we have used the Lorentzian peak fit for all three peaks of high temperature black carbonaceous product as it offers the best fit. At 250°C and 300°C , Raman spectra of black product exhibit a broad band at about $\sim 1500\text{cm}^{-1}$. The band at 1500cm^{-1} is associated with amorphous sp^2 bonded carbon. Fig. 8.3.7(b, c) shows that the best fit was invariably achieved by either combination of line shape for G, D1 and D3 peaks and a fourth peak (D4), which was introduced in the fitting to take into account for the disordered graphitic lattice due to ionic impurities. At 25°C , the polycrystalline graphite exhibits a sharp peaks at 1590cm^{-1} and mild peak at 1360cm^{-1} that correspond to the G and D1 peak, respectively and also peak of D3 at $\sim 1500\text{cm}^{-1}$ (Fig. 8.3.7a), which showed that the formation of distorted graphite layers started at this temperature (at 25°C , temperature of the cast iron disc after frictional test was measured about 115°C). The graphite with just the D1, D3 and G peak was fitted with three Lorentzian curve fits. This fitting of the spectrum is in good agreement with recent studies [Fatima et al.,2015, Georges et al.,1967]. The curve fitted spectra of black carbonaceous product of high temperature frictional test are shown in Fig. 8.3.7[(a)–(c)], respectively.

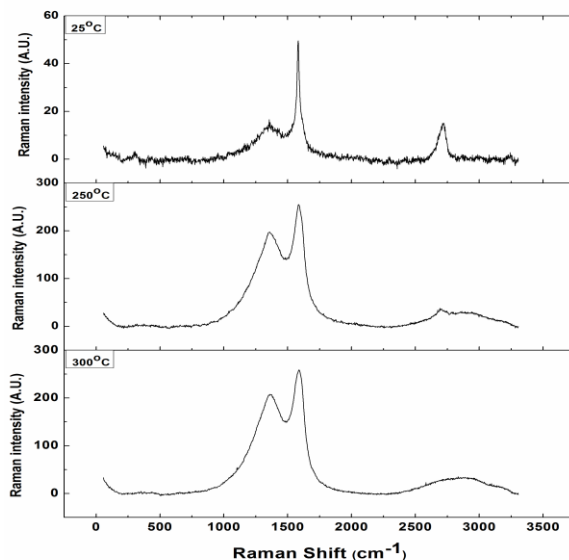


Figure 8.3.6: Raman spectra of decomposed phenolic resin at different temperatures.

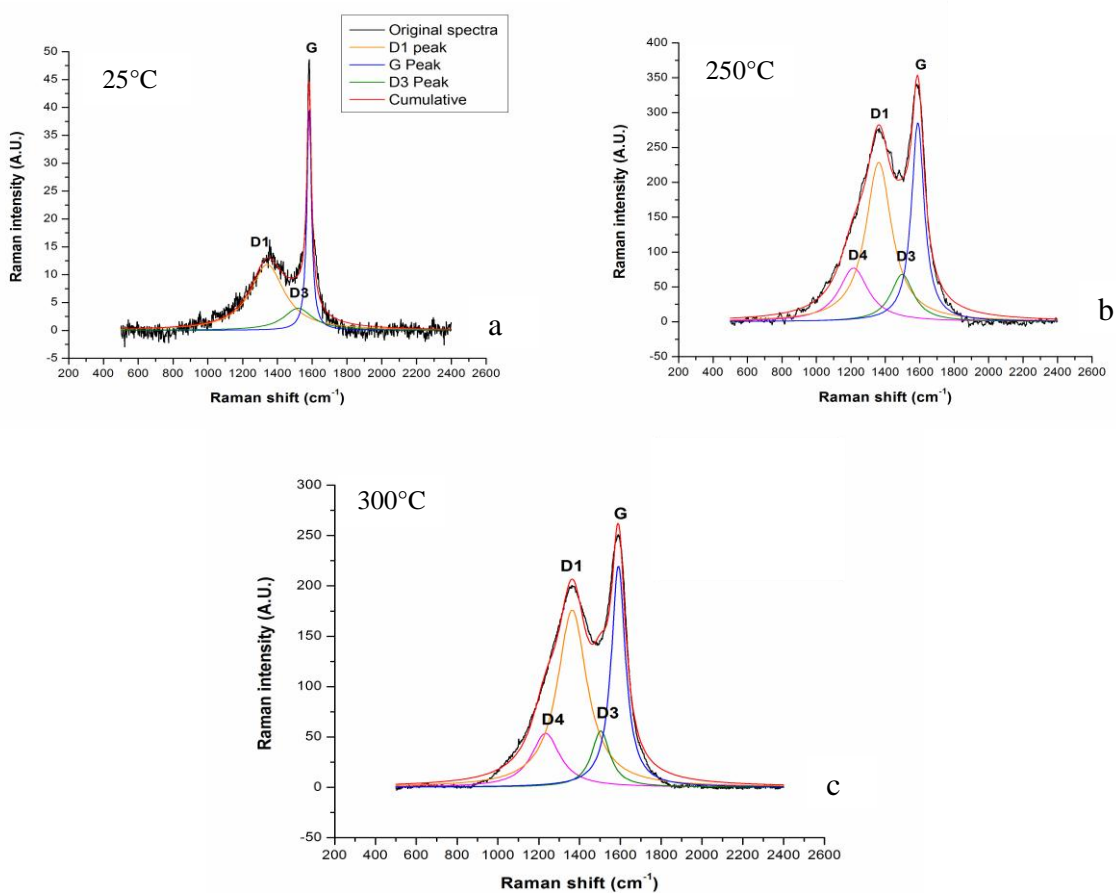


Figure 8.3.7:(a) Lorentzian curve fit for the deconvoluted Raman spectra of black carbonaceous product of high temperature frictional test at 25°C, (b) 250°C and (c) 300°C.

8.3.5 SEM observation of high temperature worn surfaces of M1 & M2 cast iron discs

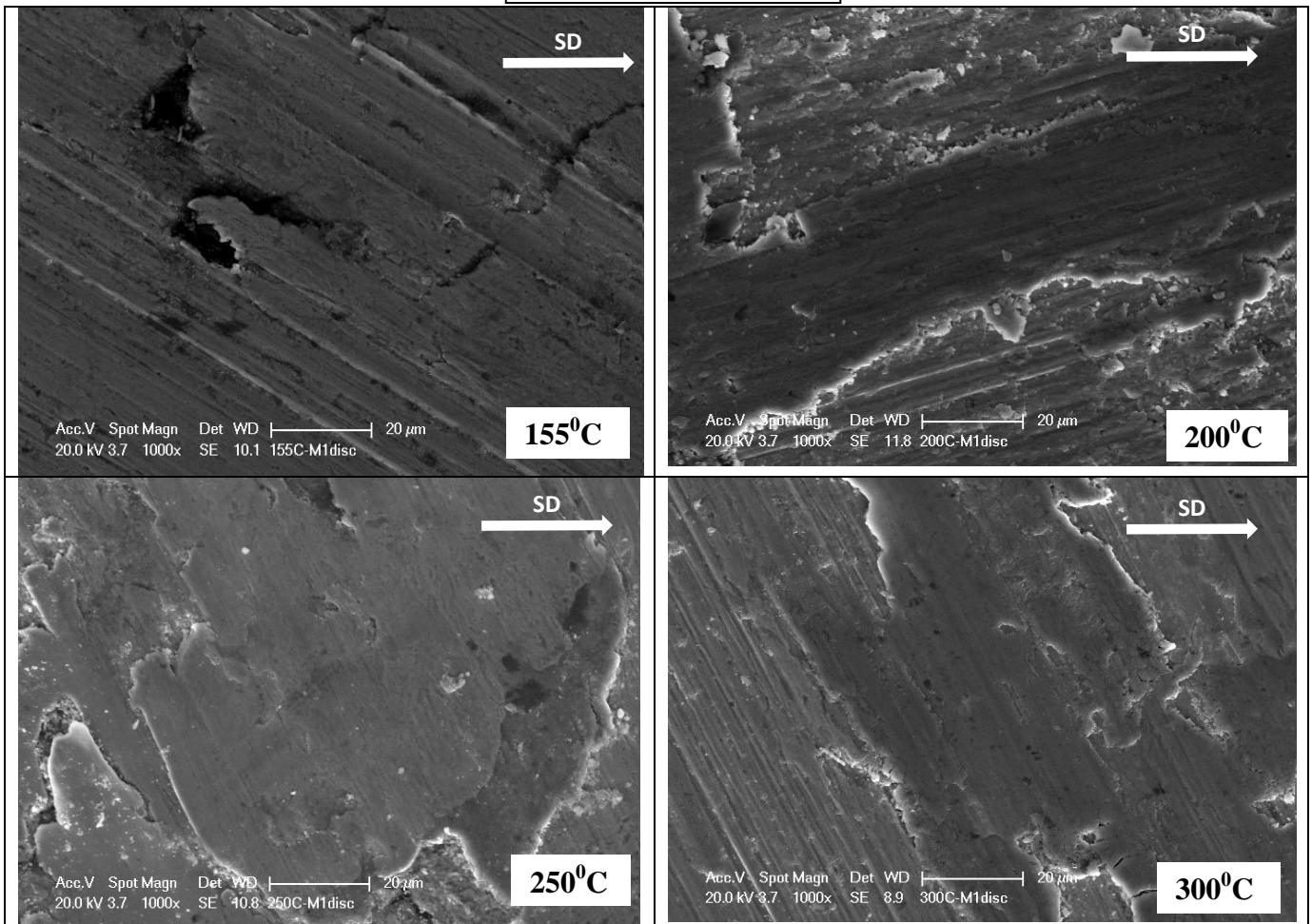
The SEM micrographs of the worn surfaces of cast iron disc of M1 (a) & M2 (b) observed at different temperature are shown in Fig.8.3.8. In a mild wear friction test, friction layer play an important role since it maintains a stable and consistent friction coefficient between the friction material and cast iron disc.

For M1 disc, fig.8.3.8 a), at lower temperature i.e., 155°C, grooves were identified but at higher temperatures ($\geq 200^\circ\text{C}$) the detached friction layer can be seen on the surface of the cast iron disc. At higher temperature an interesting observation on the M1 cast iron disc surface is the attachment of the detached flakes of friction layer to the surface of disc, which is likely to be caused by the adhesion, which might be acquired due to the damaged to the secondary plateaus and consequently to friction layer caused by the hard abrasive particles and metal chips during the tribological operations. For this reason the friction layer is not favourably remained in the SEM cross section of the M1 pins (section:8.3.6). Such deformation in the friction layer is always carried by initiation of crack and is propagated in the combined fracture mode of tensile and shearing. When the crack reaches the contact interface, a detachment of friction layer acquired and adhesive transfer on the disc surface occurs due to enough adhesive bonding at the contact interface. EDX analysis (fig. 8.3.9 a) on flakes surfaces revealed the compositions as majority of Fe, Al, Sn, Zn and Cu on the high temperature disc surfaces. Although these compositions are of friction layer which was found on the M1 friction pin at similar temperature range.

An interesting observation of M1 pin at higher temperature is the size nature of wear debris, which are mostly released from the degrading resin, do not suffer too intense grinding associated with the relative sliding against the cast iron disc. The microstructure of these debris, particularly those of the discs tested at 300 °C and 350°C appear coarse grained. The increasing coverage of the disc surface with wear debris is in agreement with the slight reduction in the wear coefficient that the discs. However, the surface of the wear tracks on the cast iron discs becomes increasingly covered with wear debris, whose composition qualitatively resembles the outer layer on the pin worn out surface, particularly as concerns the presence of iron oxide and copper, that of course are coming from the M1 pin material.

The formation of friction layers on pin surface also depends upon the cast iron grooves. For M2 disc, fig.8.3.8 b), when the cast iron counterpart at high temperature (300°C), shallow grooves were formed (Fig. 8.3.9 d)). The shallow grooves could not able to retain oxide wear debris to support the friction layers, whereas at low temperature (170°C), deep grooves were formed on the cast iron disc surface (Fig. 8.3.9 c)), these deep grooves potentially capable to hold and retain the oxide wear debris, which helpful in the formation of wear protective layers or friction layers on pin surface. At 300°C the larger area of disc surface is covered by particles transferred from the pin surface. EDX analysis (fig.8.3.9 b) revealed the compositions as Zr, Al, Ti, Fe and Cu. The large amount of particles discovered on the disc surface covering large area of the counterface may be explained by the previous observations on pin friction layers, as at 300°C the friction layers on the pin is detected in small spots obviously detached from the surface, while the presence of particles on the disc surface increases.

M1 Pin (a)



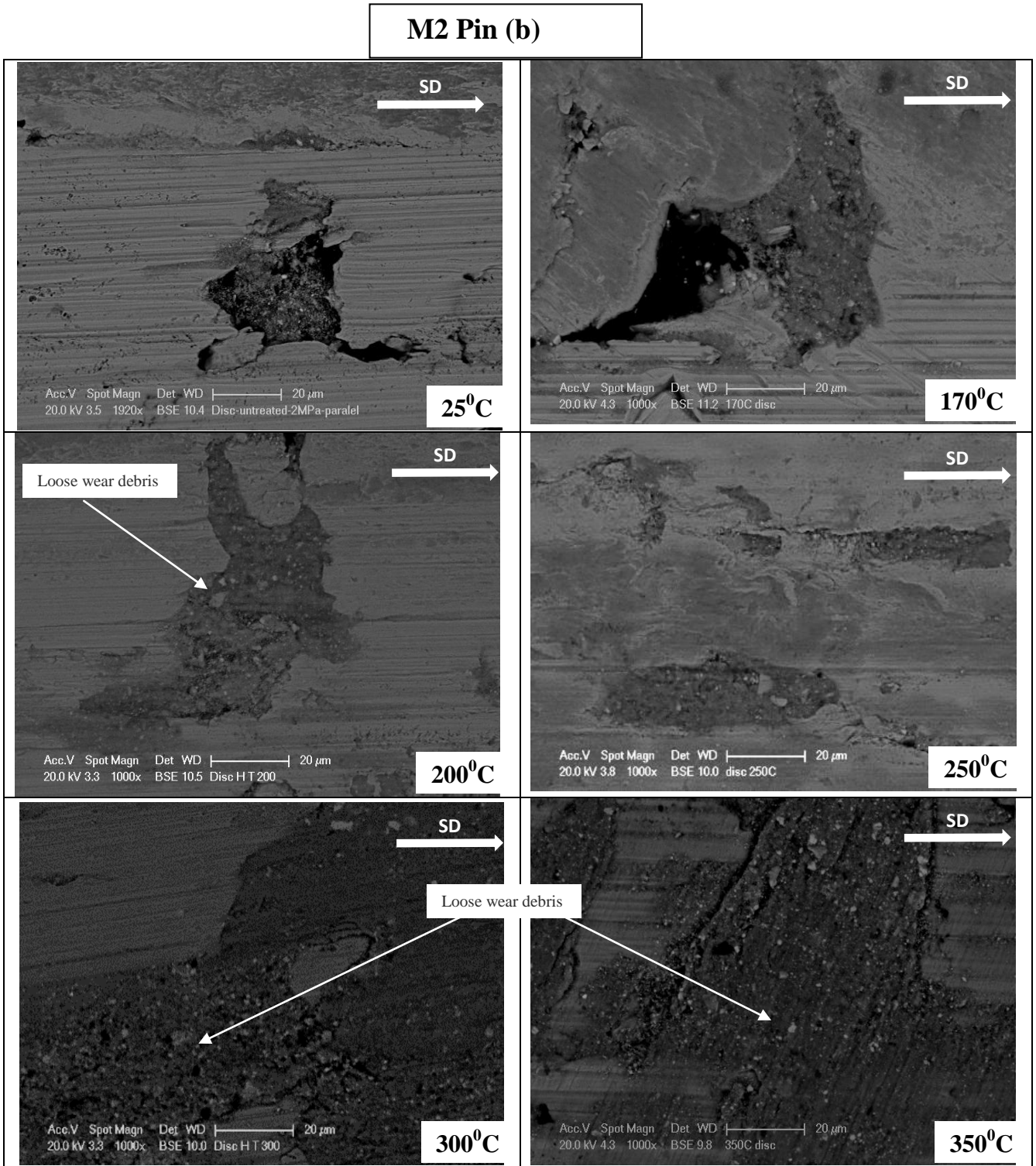
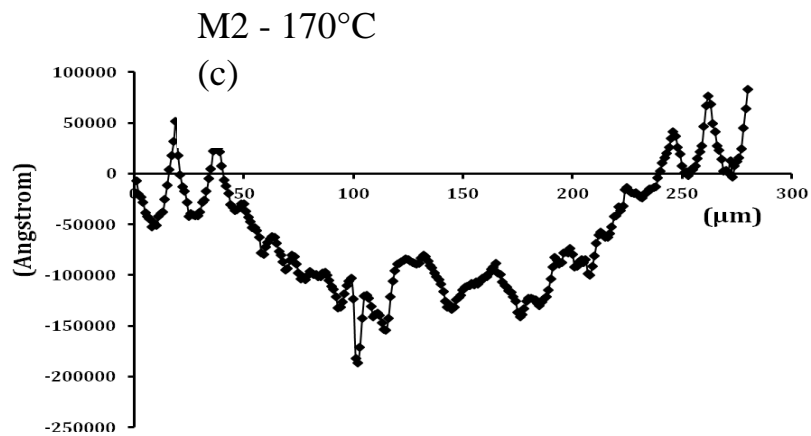
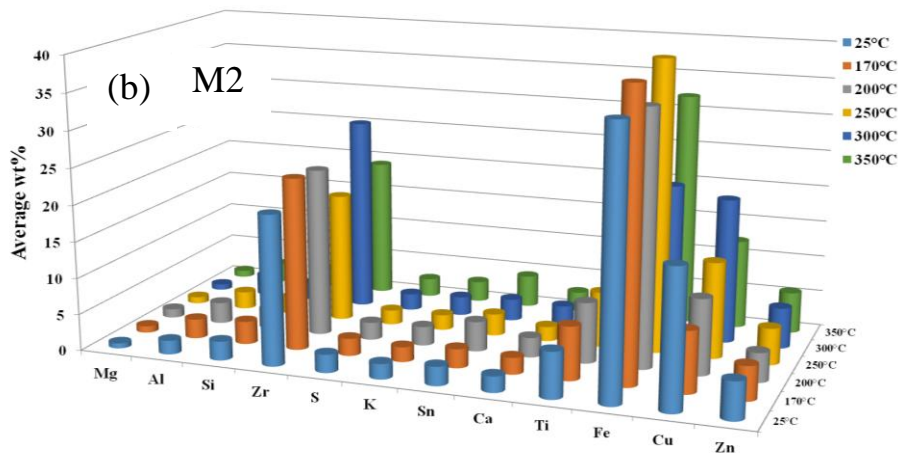
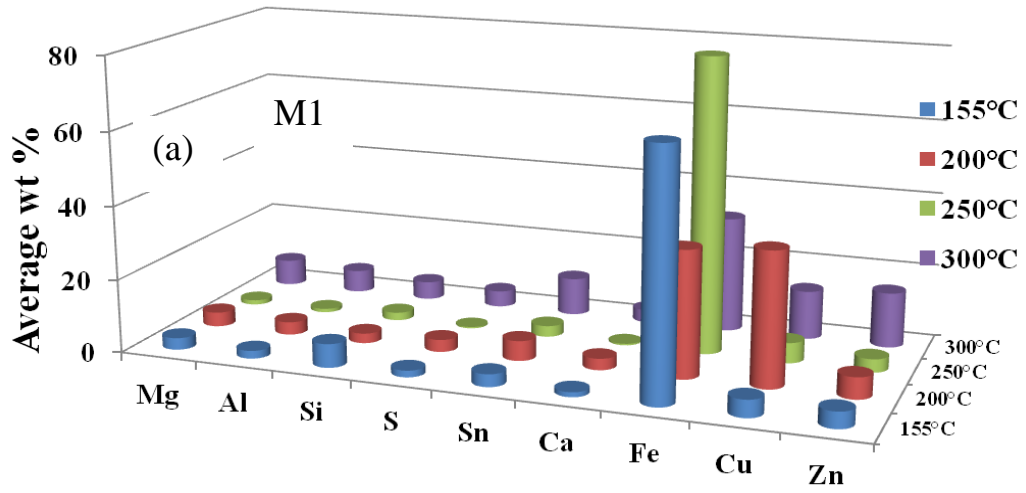


Figure 8.3.8: SEM observation of disc surface of M1 (a) and M2(b) at different temperatures.



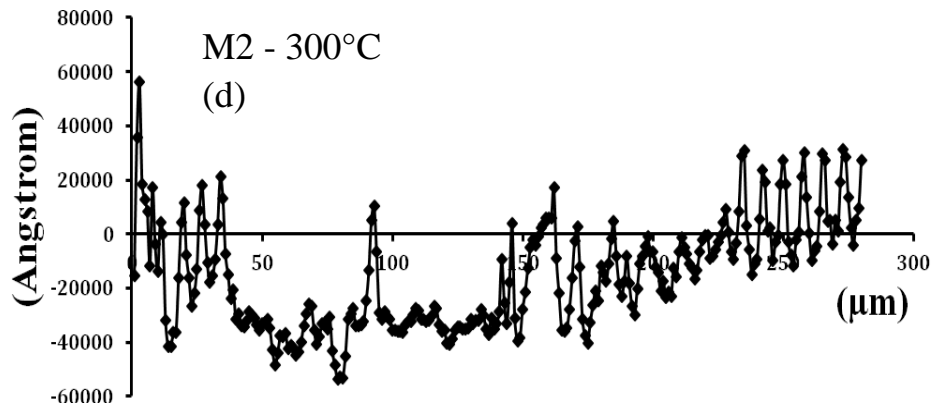


Figure 8.3.9: Average elemental composition of wear debris on M1(a) & M2(b) disc surface respectively.(c) & (d) profilometry profile of worn cast iron disc of M2 at different temperatures.

8.3.6 SEM of cross-sections of M1 & M2 pins - evolution of frictional layer with temperature

The SEM micrographs of the pin cross sections M1(a) & M2(b) at different temperatures are shown in Fig.8.3.10.

Cross sectional views of M1 pin surfaces, after the wear tests carried out at higher temperatures (25°C, 155°C, 200°C and 300°C) (fig.8.3.10 a), shows there is no any sign for friction layers, only plateaus flakes and torn metal fibers has been observed at some places. Low magnification observation indicate that at 155°C the pin surface displays a poor coverage by the friction layers and also observed torn primary plateaus (mainly metals fibers) caused by abrasive particles. The primary plateaus derive from a lower removal rate of the mechanically stable and wear resistant ingredients of the pin material: hard particles and fibers, protruding from the surface of the pins when they start to wear out. The primary plateaus act as barriers to the movement of the finer wear particles, that therefore tend to stop and to accumulate at the interface with such barriers. If these particles start to stick together due to load and working conditions i.e., temperature, this promotes the formation of the secondary plateaus, which further developed, when well compacted and sintered, a friction layer which is the primary cause of reduction in wear behavior. The cross sectional view of M1 pin at higher temperatures (155°C, 200°C and 300°C) confirms that the secondary plateaus are nearly absent and the pin surface would rather display typical components of the torn flakes of plateaus and abrasive particles. The EDX revealed the presence of Fe along with Al, Cu, Zn and Mg.

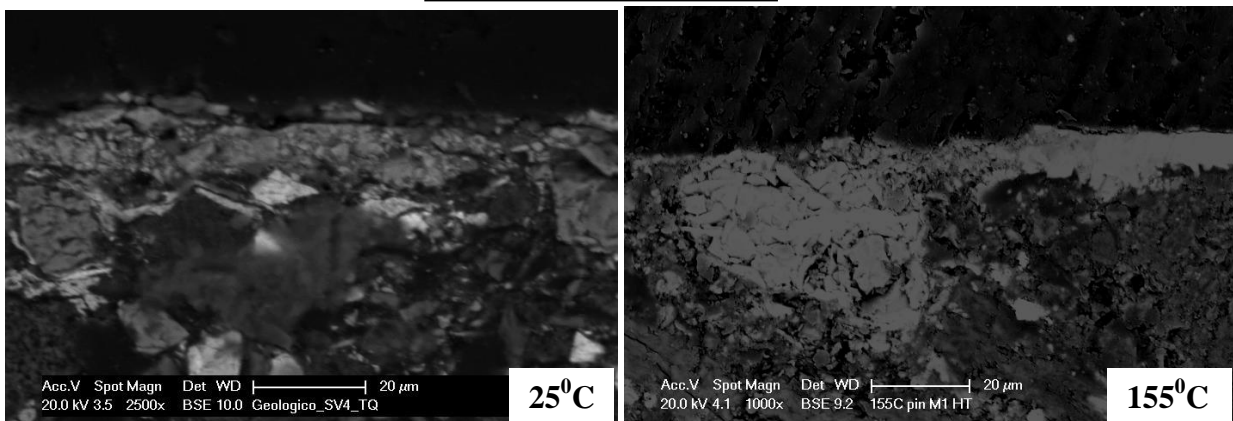
For M2 friction material (fig.8.3.10 b), the vertical extent of the friction layers at 25°C, with high applied load, it is noted that the fragments are better compacted. At 170°C, cross-sectional observations indicated the same less compacted structure, but the higher thickness. The degree of

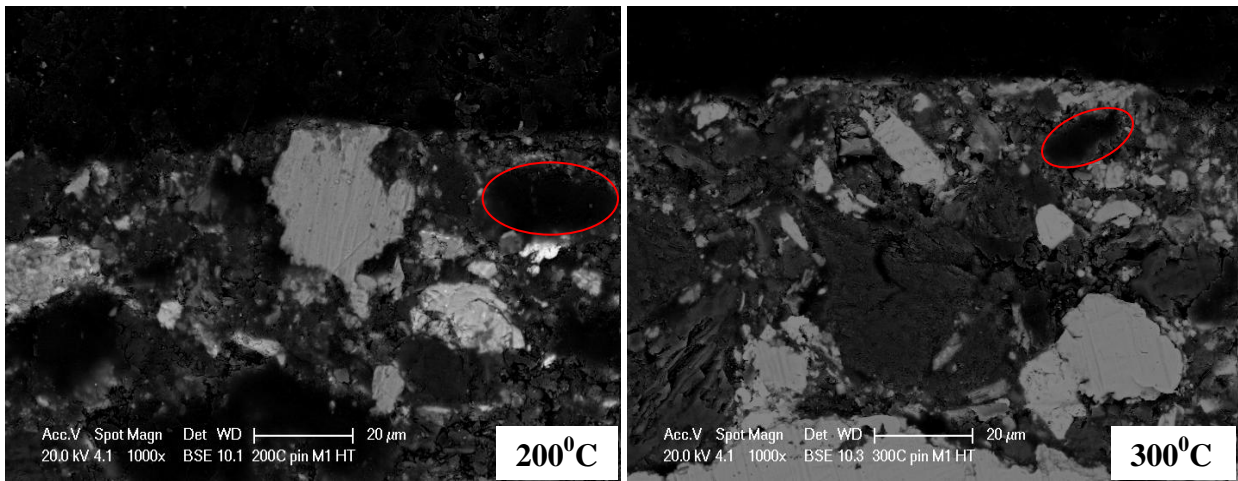
coverage of pin surface is still ununiformed, friction layers is composed by particles detached from the pin matrix and also from the disc predominating elements which are Fe, Zr, Cu, Ti. As the temperature increases 200⁰C to 250⁰C there is decrement in the formation of the wear protective layers and at 300⁰C, the layers is almost vanished, only small spots of friction layer are covering randomly the pin surface, which is due to the inclusion of more and more zirconium oxide particle in the friction layer at higher temperature, which breakdown the wear protective layers. The area covered by the friction layer is smaller, probably due to the higher wear rate at high temperature caused by breaking of weak bonding between pin ingredients and polymeric matrix. Cross section of 350⁰C indicates primary plateau, formed by zirconium particles as a base for the new friction layer formation.

As a general trend for friction layer evolution: by moving from 25⁰C to 350⁰C the area covered by friction layer is smaller and thinner, from the planer view it may be noticed that small spots of friction layer increase and cover larger surfaces and primary and secondary plateaus are distinguished up to 250⁰C, after this temperature friction layer is more compacted and decrease in thickness, ending at 350⁰C as small spots covering randomly the pin surface. As concern elemental composition Zr amount is bigger in less compacted friction layer, Cu and Fe wt% is bigger for more compacted friction layer as a general trend, but at 350⁰C was observed that white edges of friction layer are reach in Cu while the rest of friction layer is composed more from Fe. Due to the fact that thickness of friction layer is decreasing when testing temperature increase, and it became more compacted, also the surface area covered are evaluating into small spots.

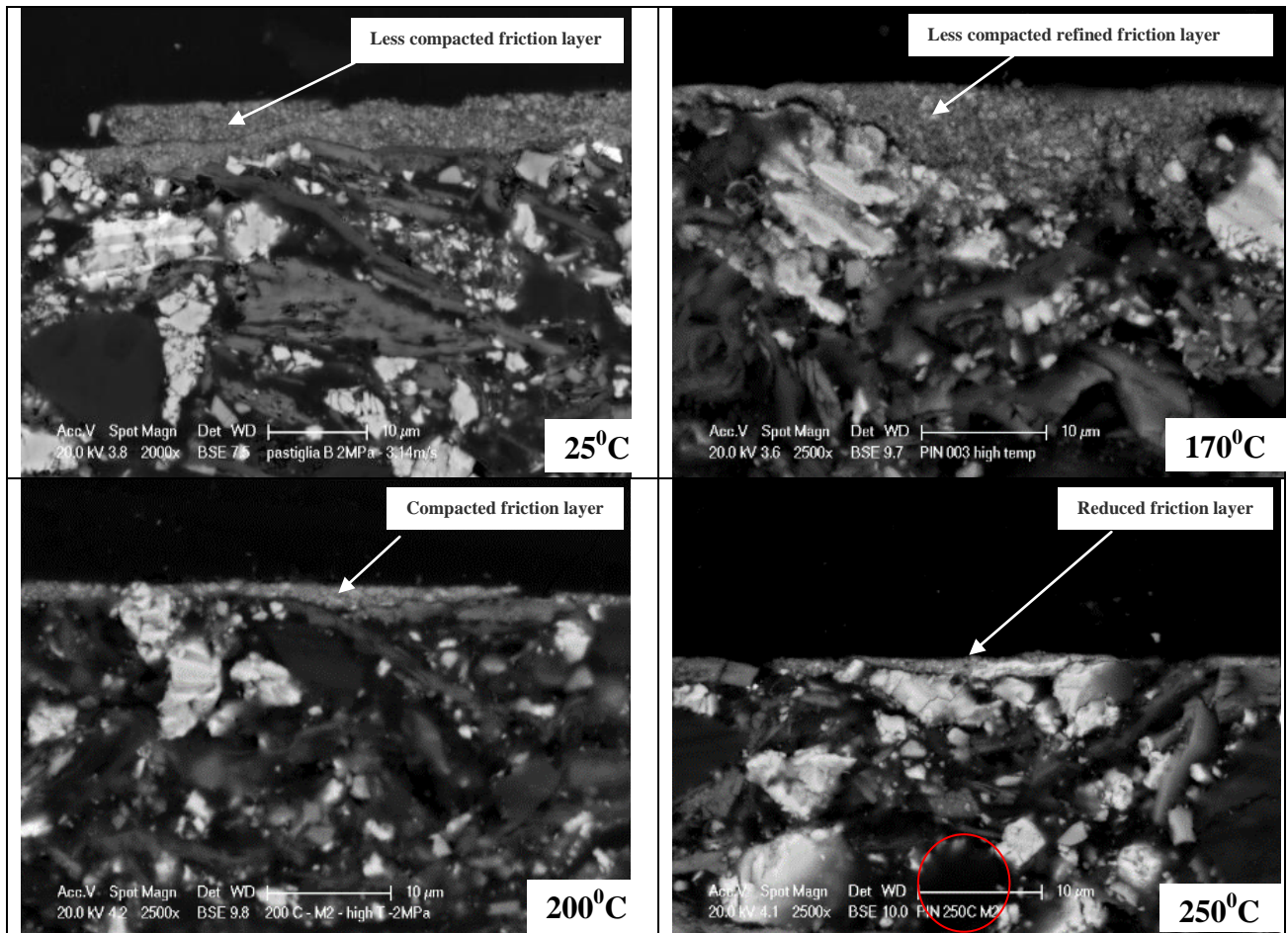
The interesting observation can be drawn from figure 8.3.10 (a, b), at temperature >200⁰C, area enclosed in a red circle on both M1 & M2, the presence of void in the form of gas bubble within the vicinity of plateaus, These gas bubble (CO₂) or voids might be formed due to the byproduct of decomposition of phenolic resin (binder) at elevated temperatures and their occurrence is higher at high temperatures [Patel et al.,2012]. This finding needs further investigation for better representation of black spots in friction materials at elevated temperature. In this case, the presence of void might lower down the density of the friction materials and enhancing the porosity within the material structure. The consequence of this phenomenon shows structure (friction plateaus) collapse or not supporting the plateaus firmly at elevated temperatures, which causes higher rate of wear debris generation and thus higher wear rate of the friction materials at elevated temperature (table 8.3.1).

M1 Pin (a)





M2 Pin (b)



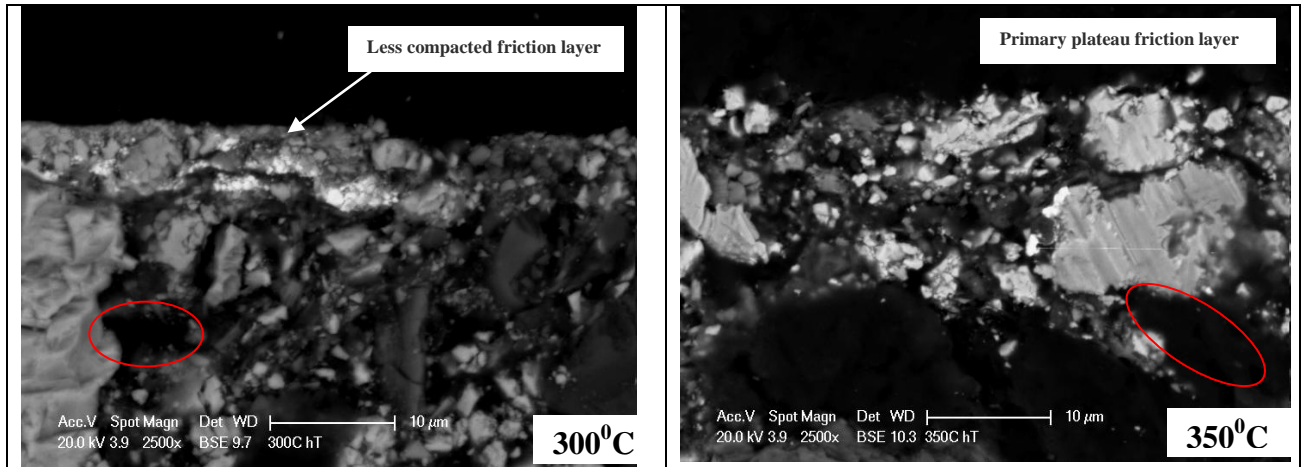


Figure 8.3.10: Cross section of worn pin surfaces of two friction materials M1 (a) & M2(b) at different temperatures.

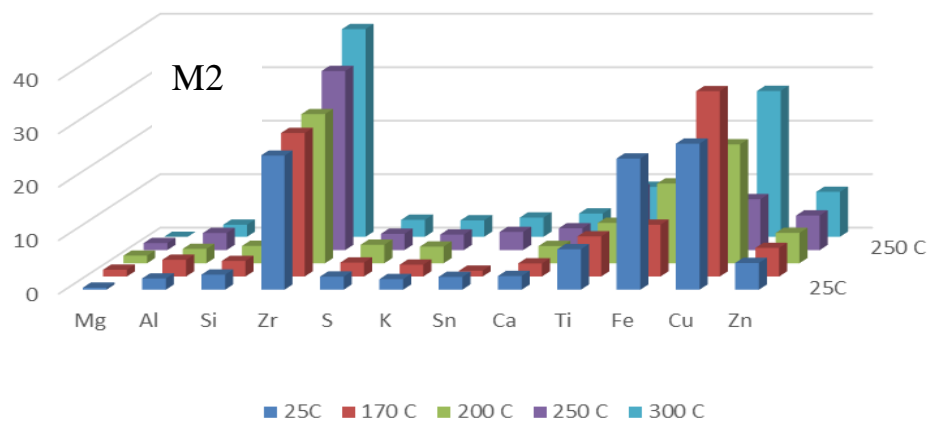


Figure 8.3.11: Average elemental composition of friction layer on M2 cross section surfaces.

8.3.7 Additional information of M1 pin at higher temperatures

- **X-ray diffraction of the friction layer at higher temperature**

X-ray diffraction of the frictional layer of M1 pin at elevated temperature is shown in fig. 8.3.12. All the M1 pin samples were measured in reflection geometry, with fixed incident beam ($\omega=10^\circ$), to ensure a constant penetration depth of the beam in the friction layer and avoid collecting an excessive amount of signal from the substrate.

Raw experimental data collected on samples M1-155°C, M1-200°C, M1-250°C and M1-300°C are reported in Fig.8.3.12 respectively.

Qualitative analysis was performed on the basis of the available information about the chemical composition. In particular, the search-match procedure was focused on Fe, Cu, Zn, Mg and C bearing phases (both pure elements and oxides).

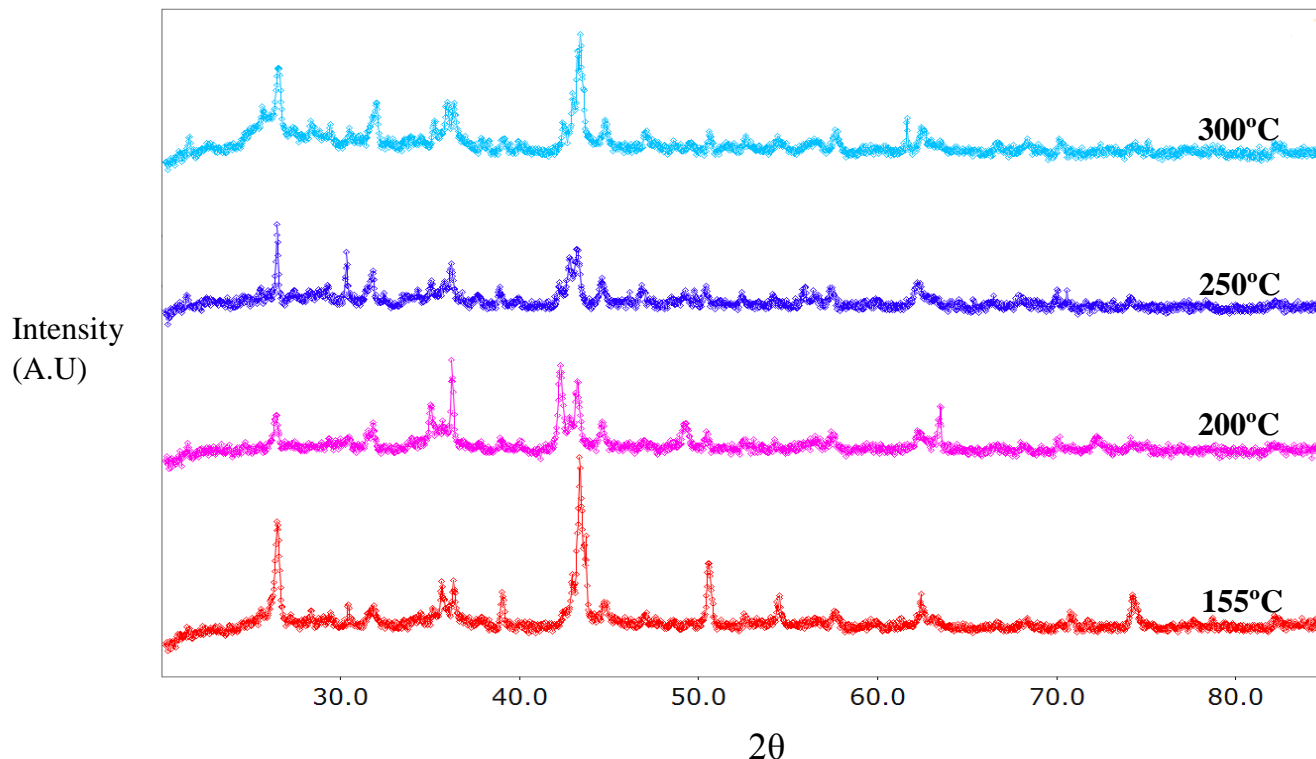


Figure 8.3.12: Comparison of XRD spectra acquired on samples MI-155°C, MI-200°C, MI-250°C and MI-300°C.

Based on the qualitative results, quantitative analysis was performed using a full-profile Rietveld approach using the Maud software [Lutterotti et al.,1999, Lutterotti et al.,2010]. Example fits relative to samples M1-250°C are reported in Fig.8.3.13 respectively.

XRD analyses were conducted in order to identify the phases present in the wear fragments as well as friction plateaus present on the surface of pin and to evaluate their concentrations. In Table 8.3.2 the results of the quantitative evaluation of the phase compositions are listed. In any case the majority phase is graphite, mostly coming from the decomposition of the resin binder at high temperature. All other detected phases were already in the pad material from which they were removed by the wear process. Copper is found in the friction layer as a pure metal. The detailed quantitative analysis for all the samples is reported in Table 8.3.2.

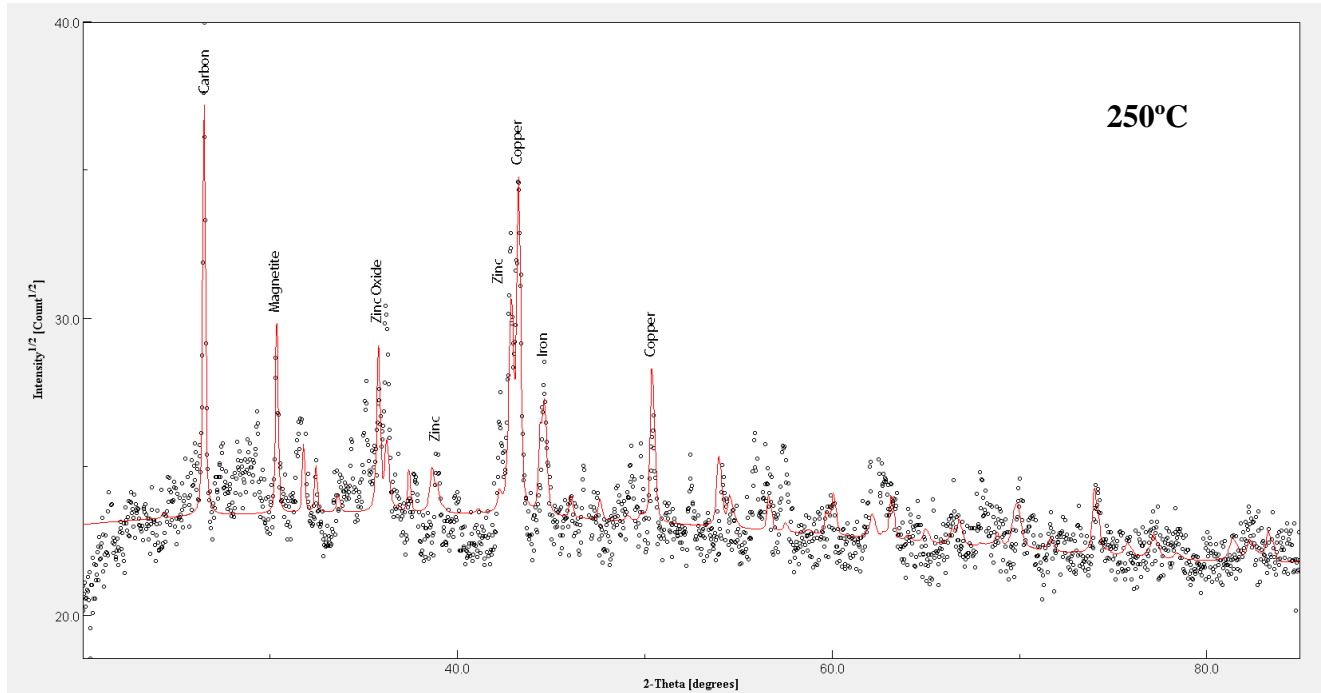


Figure 8.3.13: Maud Rietveld fit relative to sample M1- 250°C with the identification of the most relevant phases.

Table 8.3.2: Quantitative crystallographic analysis results obtained for M1 pin.

| Phase W% / Sample | 155°C | 200°C | 250°C | 300°C |
|--|-------|-------|-------|-------|
| Graphite (C) | 20.46 | 18.22 | 23.39 | 23.19 |
| Alfa-Fe (Fe) | 0.17 | 0.84 | 0.81 | 0.41 |
| Ematite (Fe₂O₃) | 0.23 | 0.78 | 0.21 | 0.13 |
| Magnetite (Fe₃O₄) | 2.63 | 3.10 | 4.79 | 4.48 |
| Zincite (ZnO) | 0.32 | 3.03 | 2.53 | 1.13 |
| Periclase (MgO) | 3.06 | 6.30 | 11.54 | 5.68 |
| Copper (Cu) | 50.03 | 31.79 | 42.11 | 48.67 |
| Zinc (Zn) | 22.18 | 35.57 | 13.41 | 15.92 |
| Tenorite (CuO) | 0.92 | 0.37 | 1.21 | 0.39 |

Table 8.3.2 demonstrated the different phases present on the friction plateaus at different temperatures. The presence of copper phase in large amount at different temperatures indicate that the copper is present in a form of primary plateaus, as displayed by SEM microstructures and EDX analysis of pin surface, which is present in the initial brake pin as a metal fibers. At elevated temperatures the presence of disordered graphite (black carbonaceous byproduct) is higher, which is due to the decomposition of the phenolic resins. The lesser amount of Fe, might

be due to the removal of iron plateaus by the hard particles (MgO). The results obtained from XRD helps in determining the prominent thermal tribo-oxidation wear behavior of M1 pin at high temperature.

• Raman spectroscopy of friction plateaus at higher temperature

Fig.8.3.14 shows the comparison of Raman spectroscopy at secondary plateaus of a M1 worn pin surface under different working temperature i.e., 155°C, 200°C, 250°C and 300°C respectively. The result is very interesting when it comes to the presence of carbon black (characteristic lines at 1360 cm^{-1} & 1590 cm^{-1}) on the secondary plateaus. The spectrum with high frequency line at about 1590 cm^{-1} is attributed to crystal phase graphite and Raman spectra for disordered graphite structure corresponds to the peak intensity at 1360 cm^{-1} . The carbon black is spotted by Raman at every high temperature wear test and the evolution of disordered graphite lattice is higher at 300°C temperature wear test than 155°C. One more thing to be considered here is due to higher temperature and shearing force, the resin binder get decomposed and decomposition product carbon black disperse in every direction i.e., on the plateaus from the source of origin, thus providing a mixed carbonaceous friction layer, which is also verified by the XRD results carried on friction layer of high temperature pins. In addition to the carbon black spectra at 1360 cm^{-1} and 1590 cm^{-1} , there are other spectra for copper sulfides corresponds to the peak intensity at 967 cm^{-1} , SnO_2 at 774 cm^{-1} and Mg_2SiO_4 at 794 cm^{-1} .

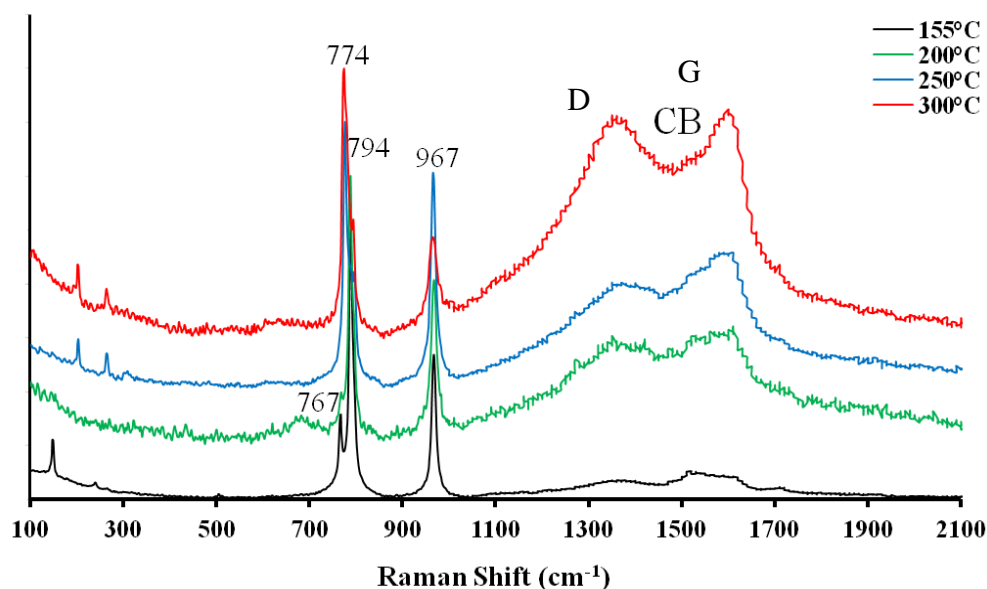


Figure 8.3.14: Comparison of Raman spectroscopy at secondary plateaus of a worn pin surface under different working temperature.

The interesting observation can be drawn from figure 8.3.14, the presence of carbon on friction plateaus, due to tangential shearing force the decomposed product of phenolic resin i.e., carbon, spread in every direction on the friction plateaus, degree of occurrence of this phenomenon is totally depend on the working temperature. The black spectrum in fig.8.3.14 at 155°C, shows

that, when the temperature is low, the carbon released is not so intense as compared to relatively red spectrum which is at 300°C. The presence of carbon on friction plateaus might provide some sort of lubrication during the tribological testing at higher temperatures, for this reason, the coefficient of friction of M1 friction pin at higher temperature i.e., 300°C (fig.8.3.2), has a uniform and more stable friction behavior than the others lower temperatures tests.

8.3.8 Wear mechanisms at high temperature

Wear mechanism of the two friction materials M1 & M2, tested under dry sliding conditions against a cast iron disc with a modified pin-on-disc heating apparatus (see paragraph 7.3.4), is discussed below. Tests were conducted at increasing temperatures of the disc i.e.,

| Friction Materials → | M1 | M2 |
|-------------------------------|-------|-------|
| Elevated working temperatures | 155°C | 170°C |
| | 200°C | 200°C |
| | 250°C | 250°C |
| | 300°C | 300°C |
| | ----- | 350°C |

The results showed a clear evolution of frictional parameters with temperature.

For M1 pins, at all temperatures there was progressive reduction of friction layer coverage. The order of wear for M1 pins was one degree higher in magnitude when compared to M2 Pin wear. The complimentary XRD and Raman analysis of friction layer of M1 pin at different temperatures shows presence copper which is in the form of deformed primary plateaus and presences of carbon in a form of graphite, is due to the thermal decomposition of phenolic resin which was accomplished with the Raman results of carbon spectra.

Wear tracks on the discs form from the piling up of wear fragments produced both by the tribo-oxidation of the disc itself and from the wearing out of the pin materials (M1 & M2). This accumulation of wear debris on the disc surface nearly compensate for the weight loss associated with disc wear. The analyses of the cross sections showed that temperature exert major appreciable influence on the characteristics of the friction layers. These results support the idea that the in the severe wear regime the wear mechanisms are entirely different to those observed in the mild regime with the only difference given by the degradation of the binder that reduces the cohesion of the ingredients in the friction materials, thus increasing the wear rate.

The observed tribological behaviour at higher temperature for both friction materials is very much influenced by the thermal degradation of the phenolic binder of the friction material. The thermal decomposition kinetics was confirmed by thermogravimetric analyses, conducted on purpose on the pin material (fig. 8.3.1), and by Raman spectroscopy results (fig. 8.3.7), that confirmed the presence of carbonaceous products on the worn out pin surface. Although referring to rather extreme conditions and simplified sliding conditions, the results obtained in Raman study provide useful indications on the role that the thermal stability of the organic component may have in determining wear rate in brake systems in which the temperature rise may be induced by actual operational conditions. During high temperature tests, the breakdown of phenolic resin takes place and its constituent element expose to high heat and high mechanical

stress, which leads to the formation of disordered graphite lattice and amorphous carbon at higher extend. The complimentary tools like Raman Spectroscopy and TGA have a coherency in results which justify the severe wear loss of frictional material at higher temperature.

For M2 pin, above 170°C a transition from mild to severe wear was observed (fig. 8.3.3). This transition can be ascribed to the drastic changes occurring in the friction layers, in particular, the secondary plateaus, which develop on the pins and disc surface during sliding, as proved by electron microscopy observations and X-ray spectroscopy analyses (see fig.8.3.4 and fig. 8.3.5). At 170°C, the friction layer consists of primary and well compacted secondary plateaus. At 200°C and above, a progressive reduction of the pin surface coverage by the secondary component of the friction layer and a corresponding thinning of this component are observed. Secondary plateaus are barely present on the samples tested at 350°C. The evolution of the compacted plateaus formed and decomposed phenolic resin at the pin surfaces as the wear particles are mainly dislocated from the friction materials at higher temperature.

Therefore, considering all above mentioned observations and results, the wear mechanism for M1 pin, at 155°C, higher order of abrasive wear mechanism with the participation of hard particles and metals chip, caused delamination of the friction plateaus. For M2 pin, at 170°C, is based on primarily three-body abrasive wear, agglomeration and compaction of wear debris caused by sintering effect and adhesive wear. While the wear mechanism at 300°C for M1 & M2 pin, is based on thermal decomposition of phenolic resin, higher wear rate and large friction layer detached from the pin surface and adhere to the counter disc under given compressive load, highlighting the adhesive wear, tribo-oxidation and abrasive wear mechanisms.

| Wear mechanisms | Characterization tools | Observations |
|-----------------|--------------------------------------|--|
| Tribo-oxidation | XRD results, TEM-SAED and Raman data | Iron oxide, graphite, MgO, ZnO |
| Abrasive action | SEM-EDX | Wear debris analysis, worn pin & disc surfaces |
| Adhesive action | SEM-EDX | Worn pin & disc surfaces, transferred friction plateaus on the disc surface. |

Thus, wear mechanisms identified in the wear testing of M1 & M2 friction materials at higher temperature is adhesive wear, tribo-oxidation and three-body abrasive wear.

| |
|---|
| Wear behavior at higher temperatures |
| M1(one degree of magnitude higher) > M2 |
| Wear Mechanism at higher temperatures |
| Three-body abrasive wear + thermal tribo-oxidation + Adhesive wear |

Wear mechanism of M1 pin at high temperatures pin-on-disc test

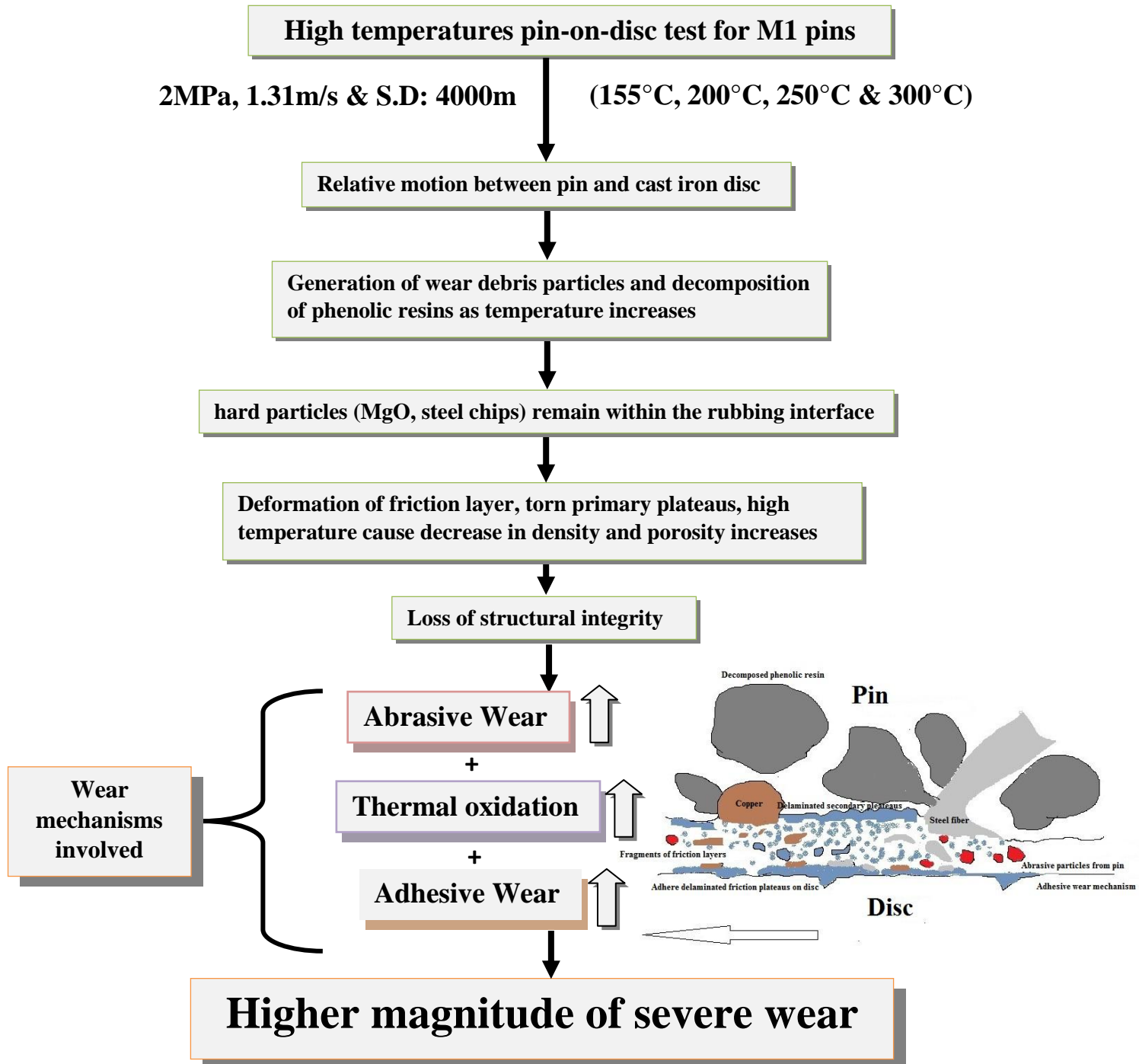


Figure 8.3.16: Wear mechanisms involved in dry sliding of M1 friction material at higher temperatures.

Wear mechanism of M2 pin at high temperatures pin-on-disc test

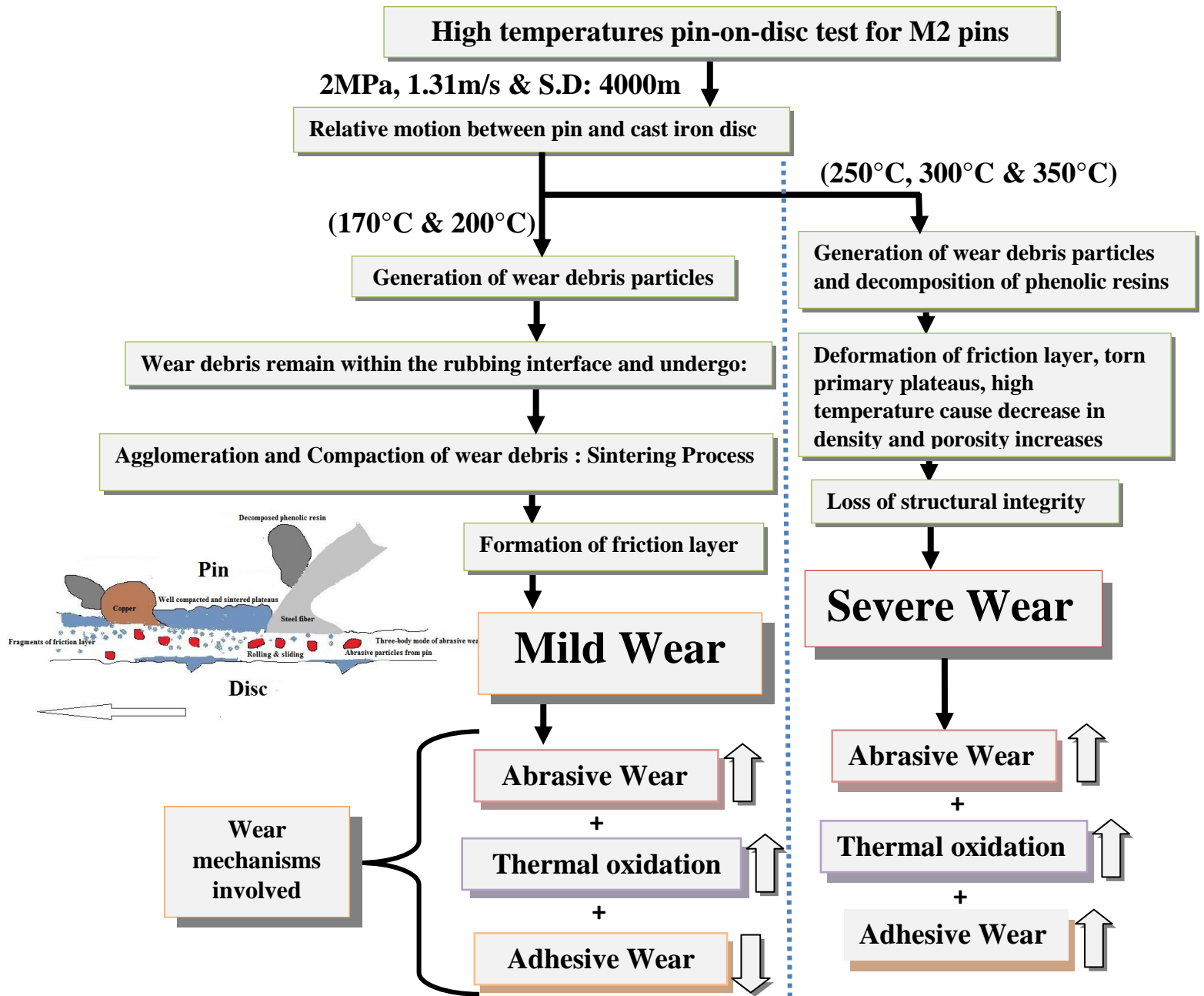


Figure 8.3.15: Wear mechanisms involved in dry sliding of M2 friction material at higher temperatures.

8.4 Role of the heat-treatment of the cast iron disc - Case IV

This section will illustrate the role of conventional heat-treatments of the disc on the friction and wear behavior. The heat treatment has been carried out in an industrial plant by “Trattamenti Termici Ferioli & Gianotti SpA”, Rivoli-Torino following a typical treatment cycle of austenitization at 850°C in controlled atmosphere for 2 hours, oil quenching followed by tempering at 180°C for 1 hr to exploit its elevated hardness.

The cast iron disc counterface was investigated in three conditions:

1. Untreated (reference condition)
2. Heat-treated
3. Heat-treated and ground

The microstructure of the base untreated disc is comprises a fine pearlitic matrix and graphitic lamellae. The microstructure of heated treated disc is shown in fig. 8.4.1 a) (please refer fig.7.2.1 c & d for microstructure of untreated disc). In the core, a uniform martensitic matrix was obtained but at the surface some decarburization was observed as it can be seen in fig. 8.4.1 b). It has been induced by the treatment cycle which is a usual case in this treatment of cast irons. Some heat treated sample were mechanical grinded in order to remove the decarburized layer characterize by lower hardness. Roughness of discs were measured and the surface roughness of the untreated and heat-treated disc was about $R_a=2\mu\text{m}$ because of the presence of the machining grooves/asperities. The ground disc had a surface roughness of $R_a=0.58\mu\text{m}$.

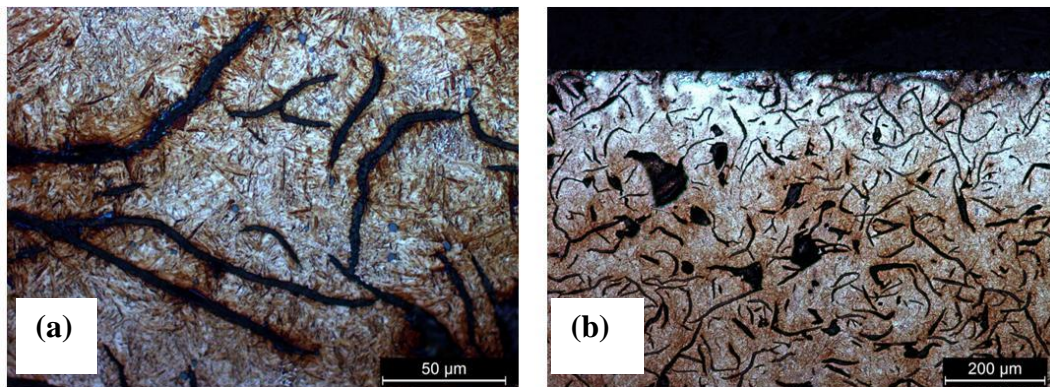


Figure 8.4.1. a) Martensitic microstructure of heat treated disc, b) The decarburized surface of the heat treated disc.

8.4.1 Friction and wear behaviour of heat-treated cast iron disc

Fig.8.4.2 displays the friction coefficient and the average contact temperature during wear test using different disc conditions i.e., untreated, heat treated and heated treated + ground disc. The average steady-state values of friction coefficient, attained after about 4000 m of sliding, are listed in Table 8.4.1.

Table 8.4.1: Average pin temperature and friction coefficient attained after 4000m of sliding.

| Type of disc | T_{max} [$^{\circ}C$] | μ |
|-----------------------|---------------------------|-------|
| Untreated | 28-30 | 0.5 |
| Heat treated | 23 | 0.3 |
| Heat treated + ground | 32 | 0.4 |

The heat-treated disc have a reduction in the friction coefficient value with respect to the untreated disc and also if the heat treated disc is further ground, the decrease in frictional behavior is quite limited. The recorded average contact temperature was not proportional to the coefficient of friction. The highest values of the contact temperature were achieved by the heat-treated + ground specimen, which showed an intermediate friction coefficient.

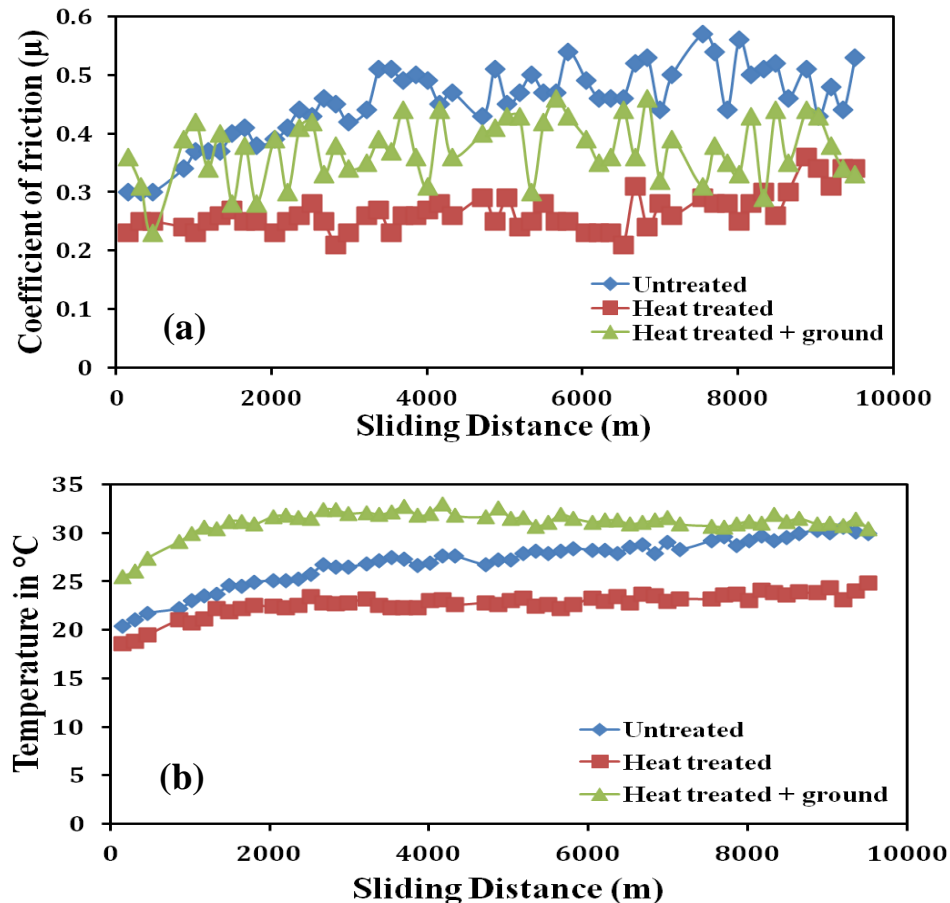


Figure 8.4.2: Evolution of the friction coefficient (a) and of the average contact temperature (b) during wear tests.

Fig. 8.4.3 shows the surface profile obtained perpendicularly to the wear scar to evaluate the wear volume of the heat treated disc. In Table 8.4.2, the experimental wear rates and the specific wear coefficients, for pin and discs are listed.

From the table 8.4.2, the wear rate of both the pin and the disc are one order of magnitude lower than the untreated condition. The specific wear rates range between 10^{-15} and 10^{-14} m^2/N , indicating that a mild form of wear was present in all disc conditions [Straffelini et al.,2015].

Fig.8.4.4 compared the specific wear rate of the three different disc and M2 pin. The best performance is displayed by the heat-treated + ground disc characterized by the highest hardness in the contact region (Table 8.4.3). This result can be attributed to the high hardness of the disc achieved by the heat treatment. The reduction in wear of the disc is accompanied by a reduction in wear of the pin.

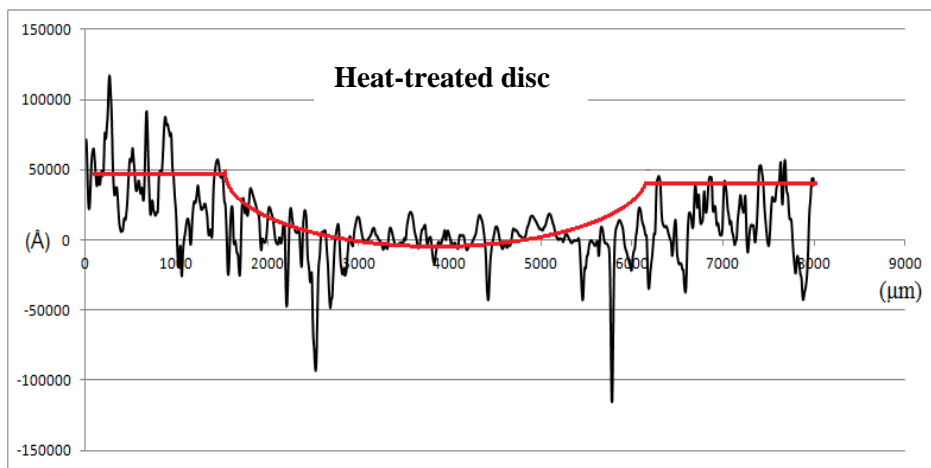


Figure 8.4.3: Surface profile across the wear track of heat treated disc.

Table 8.4.2: Wear rates of the pin and different discs.

| Type of the disc | Wear Rate [mm ³ /mm]x10 ⁻⁷ | | Specific Wear Coefficient [m ² /N] x 10 ⁻¹⁴ | |
|-----------------------|---|------|--|------|
| | Pin | Disc | Pin | Disc |
| Untreated | 5.78 | 4.39 | 1.20 | 0.91 |
| Heat Treated | 2.44 | 2.54 | 0.51 | 0.52 |
| Heat Treated + Ground | 1.22 | 0.65 | 0.25 | 0.13 |

Table 8.4.3: Treated disc surface hardness.

| Disc | Area of measurement | HV 0.05 |
|--------------|---------------------|----------|
| Untreated | Surface and core | 287 ± 37 |
| Heat Treated | Surface | 717 ± 48 |
| | Core | 957 ± 30 |

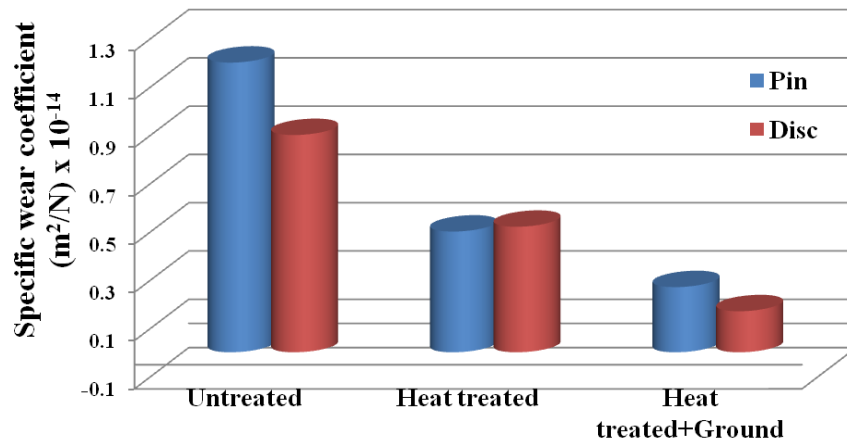


Figure 8.4.4: Comparison of specific wear coefficient, K_w , of the M2 pin and different discs.

8.4.2 SEM observation of the wear tracks on heat-treated cast iron disc

Fig.8.4.5 a) shows the microstructure of the pin used for test against untreated disc. The friction plateaus formed have the higher degree of coverage on the pin surface. There are clear evidence of two distinguish friction plateaus, primary plateaus- less compacted and secondary plateaus - more compacted. EDXS analysis highlighted higher concentration of Fe in primary plateau, while Cu is dominant in the well compacted secondary plateau. The compacted friction layer formed at the surface of pin stabilized friction and reduce wear, copper content has an important role in this issue [Lee et al., 2013]. The composition of primary plateaus are mainly Fe, Cu, Zr, Ba, Al, as concern the composition of secondary plateaus is a mixture of oxides coming from both surfaces of pin and disc. The highest extend is for iron oxides originated from the thermal oxidation of cast iron disc, but also zirconium oxides and silicates from the pin. Cu concentration differs in these two types of friction plateaus, it is in a higher extend in well compacted plateau than in less compacted one.

For heat treated disc, the friction plateaus formed (Fig.8.4.5 b) have the less degree of coverage on the pin surface than in the case of untreated disc tests. Chemical composition provided by EDX prove the same composition as for untreated disc.

The heat treated + ground disc and corresponding pin microstructures are shown in fig.8.4.5 c). Friction layer formed at the surface of the pin has a lower extend, primary and secondary plateau are hardly identified (fig.8.4.5 c).

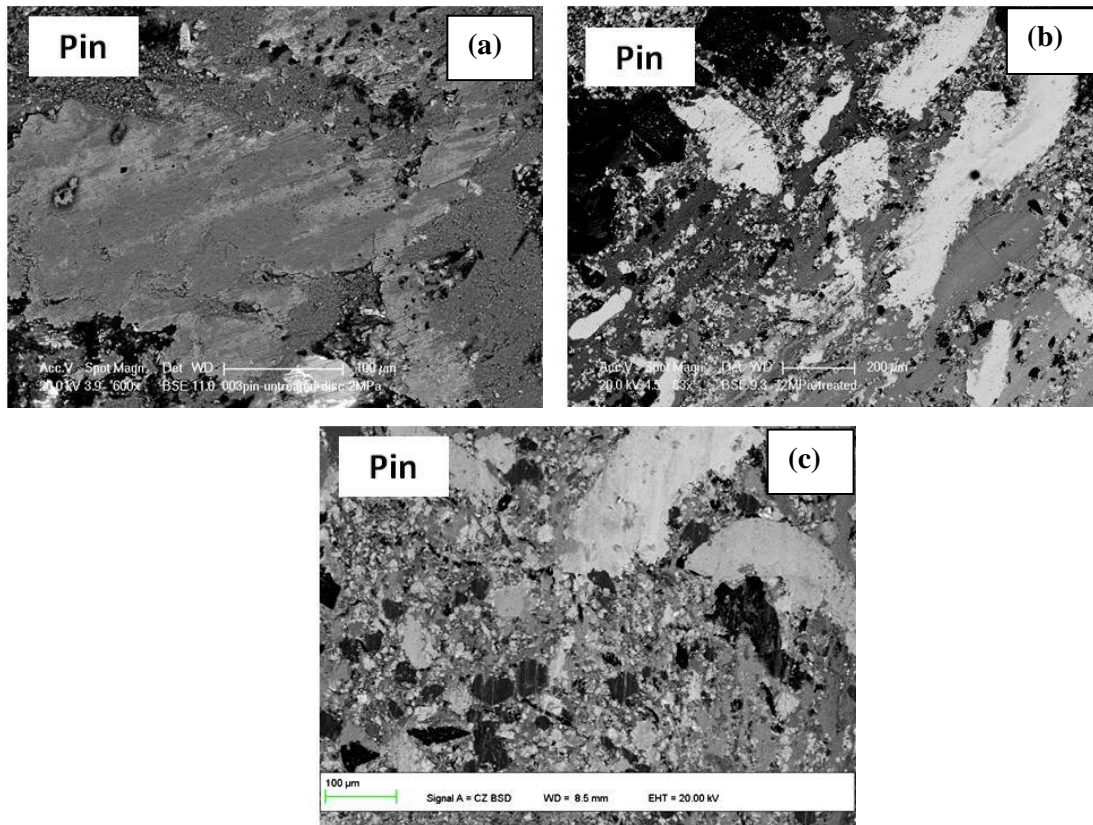


Figure 8.4.5: SEM micrographs of the wear tracks on the pin surface after sliding against the untreated (a), the heat-treated (b) and the heat treated and grinded disc (c).

The worn surfaces of the counterface cast iron discs were also observed. Fig. 8.4.6 shows the wear track for the untreated disc. EDX results show that the area which is indicated by point 1 in fig. 8.4.6 is graphite lamellae emerge at the disc surface. However in point 2, an accumulation of wear debris occurs. The EDXS analyses revealed that the debris originate from both the friction materials and the cast iron disc. Similar debris accumulations were observed close to the surface graphite lamellae in the heat-treated and heat-treated + ground specimens. According to Eriksson et al.,2002, the wear of the counterface disc is tribo-oxidative in nature, with the formation of iron oxides (both magnetite and hematite) that exert an abrasive action on the pin surface and may also transfer onto it entering the friction layer.

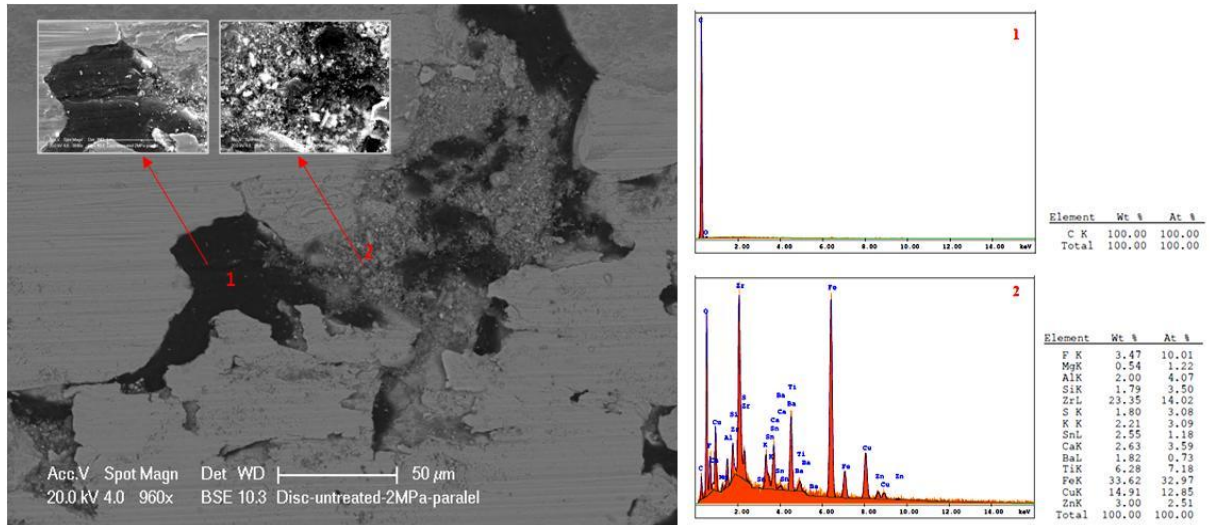


Figure 8.4.6: SEM planar view of the wear surface of the untreated cast iron disc. The picture shows a region where the graphite lamellae emerge (point 1) at the surface and there is an accumulation of wear fragments from the friction material (point 2) and corresponding EDX spectra of the highlighted regions.

The cross sectional investigation of the pins determines the main features of the friction layer. Fig. 8.4.7 shows the SEM images of the cross section of pin surface of untreated disc. The presence of friction layer coverage was higher observed on the pin used against the untreated disc with respect to heat treated conditions. On these friction layer EDXS analysis was performed to get information about the chemical composition (Table 8.4.4) and results shows almost all the element of the brake pin are present along with high addition of iron, which originated from the tribo-oxidation wear of the counterface cast iron disc.

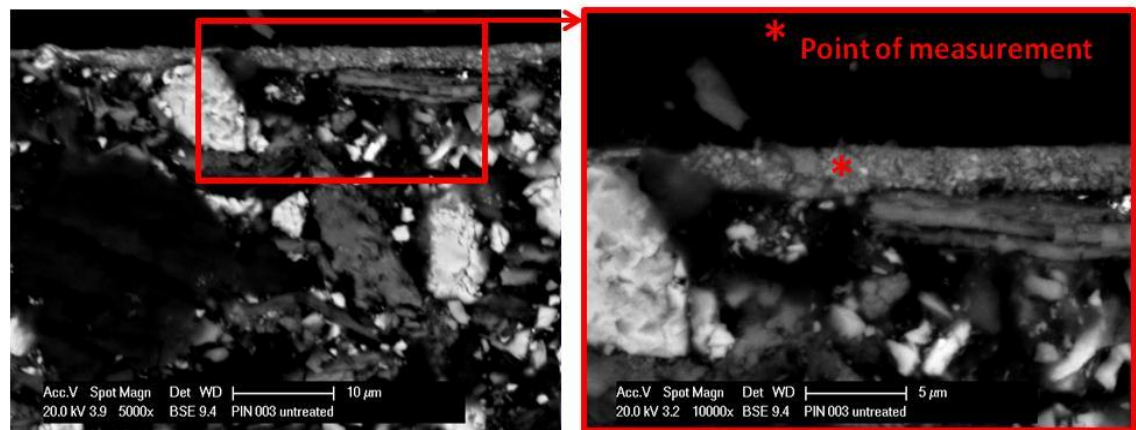


Figure 8.4.7: Cross sectional SEM micrographs of the friction layer on the pin after sliding against the untreated disc. Low (S_x) and higher (D_x) magnification.

Table 8.4.4: Chemical composition of the friction layer based on EDXS.

| Element | wt % |
|---------|------|
| Al | 3.4 |
| Si | 3.2 |
| Zr | 22.9 |
| K | 4.5 |
| Ca | 2.9 |
| Ti | 15.7 |
| Fe | 28.3 |
| Cu | 10.3 |
| Zn | 10 |

Fig. 8.4.9 shows the SEM images of the cross section of pin surface of heat treated disc and heat treated + ground disc respectively. In both heat treated discs, the friction layer was present over small regions only. The EDX analysis shows a very similar data (table 8.4.4) have been obtained for the friction layers formed on the pin tested against the heat treated discs and shows almost all of the elements of the virgin pad are present, with the important addition of iron, that originates from the wear of the counterface cast iron disc.

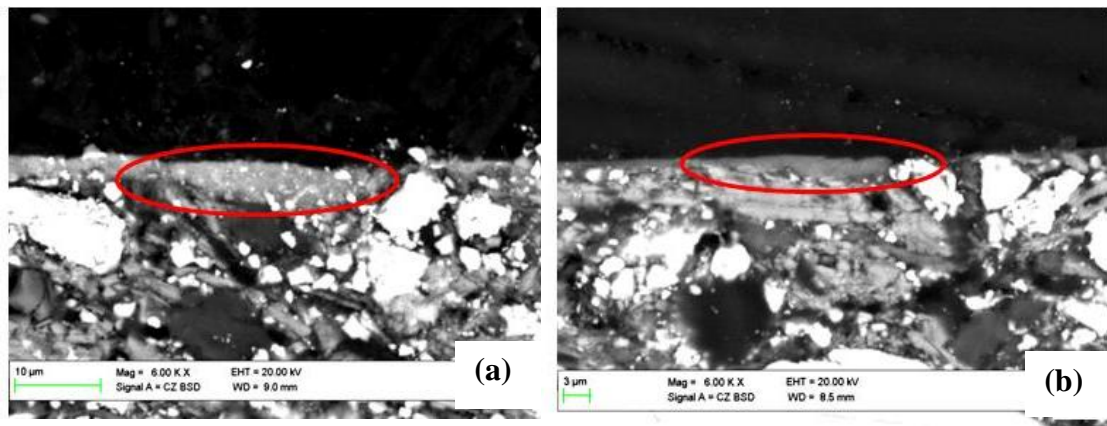


Figure 8.4.8: Cross sectional view of the pins against a) Heat treated, b) Heat treated and ground.

The results in section 8.4 show how a conventional heat-treatment of the cast iron disc provides a noticeable decrease in the wear rate of both the pin and the corresponding cast iron disc (fig. 8.4.3). From the table 8.4.2, it has been concluded that the specific wear coefficient of the friction material (M2 pin) and the corresponding untreated cast iron disc (approximately 10^{-14} m^2/N) decreases down to 10^{-15} m^2/N for the heat-treated and ground disc i.e., decrease in the wear of the pin and the disc, after the disc heat-treatment. The heat treatment of discs i.e., heat treated and ground discs, decreases the value of friction behavior when compared to the untreated disc and have no direct proportionality between the evolution of friction coefficient and the corresponding average contact temperature.

As Table 8.4.1 and Fig. 8.4.3, summarized the steady-state friction coefficient for the untreated disc, which is equal to 0.5, in agreement with literature data for similar types of low metallic friction materials [Day et al.,2014]. From the friction test results of heat-treated + ground disc, there is a reduction in the coefficient of friction to 0.4, which occurred due to the strong increase in disc hardness that greatly reduces the abrasive interactions at the contacting asperities.

The SEM results provide useful information in predicting such reduction in wear and friction behavior of heat treated disc. SEM observation revealed the presence of surface oxide on the heat treated disc may have reduced the average shear stress at the asperity contacts during sliding [Kong et al.,1995], which could be one of the reason for such reduction in friction behavior, as confirmed from the heat treated + ground disc, when the surface oxide was removed, the friction coefficient rose to about average value of 0.35 (fig.8.4.2). The average temperature rise in the contact region due to sliding is directly proportional to the dissipated frictional power, given by the product of the friction coefficient, the applied load and the sliding velocity, and inversely proportional to the thermal conductivities of the mating materials [Sraffellini et al.,2015, Lim et al.,1987].

When using the heat-treated disc, the lowest temperature rise during sliding was detected (Fig. 8.4.2 b), in agreement with the observed lowest friction coefficient (Fig. 8.4.2a). Whereas, the heat-treated and ground disc displayed the highest contact temperature, despite of the intermediate value of the friction coefficient. This occurrence can be better explain by the effect of the heat-treatment on the thermal conductivity of the cast iron disc. Martensitic microstructures in ferrous alloys feature a lower thermal conductivity than the same alloy in the annealed or heat-treated and tempered conditions [Kuepferle et al.,2015, Wilzer et al.,2012].

However, the presence of carbon atoms in solid solution in martensite strongly reduce the electronic component of heat conduction. In addition to this, the reduction in the phononic component of heat conduction is due to the increase in the dislocation density caused by the tetragonal distortion of the crystal lattice exerted by carbon atoms [Wilzer et al.,2012].

Table 8.4.2 shows the progressive decrease in the specific wear coefficient for the cast iron disc in passing from the untreated to the heat-treated and then heat-treated and ground conditions, this decrease in the specific wear coefficient have a coherency with the evolution of the disc surface hardness, as shown in table 8.4.3. A decrease in the tribo-oxidative wear of disc occurred when the disc alloy matrix develop the surface oxides layer and therefore an increased surface hardness give ability to the disc to sustain the surface oxide layer [Day et al.,2014].The increased hardness of the disc also lower down the wear rate of the pin material. This behavior can be explained considering the active wear mechanisms. As known and also shown in paragraph analysis of wear tracks are characterized by the formation of friction layers. Particles detached from the pad and tribo-oxidative wear of the counterface cast iron disc, were agglomerated and compacted during sliding, being influenced by pressure and temperature. In such a way secondary plateau is formed (fig. 8.4.7) and disruption of such plateaus produce wear debris by adhesion or by brittle contact. This behavior is typical for this tribological pin-on-disc system and shown by number of authors [Osterle et al.,2001, Eriksson et al.,2002]. In this respect, the abrasive action of loose iron oxides helps in the formation of the friction layer through the formation of small particles (mainly Zirconium oxides) able to enter the friction layer, in agreement with a our previous investigation. Therefore an increase in the surface hardness of the disc results in a lower production of loose iron oxide which further lower down the surface damage by abrasion of the friction material and therefore the formation of a wide covering friction layer and thus decrease in the wear rate of the M2 friction pin.

Chapter 9

Concluding Remarks

9.1 Conclusions

In the present work, a characterization protocol for wear products has been developed and wear mechanisms that underlies the pin-on-disc experiments have been investigated. The study has been conducted on two different brake friction materials (M1 & M2) sliding against a cast iron counterface, both at room and, at higher temperatures. The effect of specific heat treatments of the cast iron disc on the wear behaviour has been also considered. To study the tribological phenomena, two different types of tribometers have been used:

- Simple Pin-on-disc tribometer (Frictional heating)
- High temperature pin-on-disc tribometer (External heating)

If we see the overall results of the different *Cases*, we highlight very promising conclusions in the following paragraphs, interesting for further developments of the research of novel friction materials and to reduce the PM emission in the atmosphere. The effect of the composition on the tribological characteristics of friction materials M1 and M2 were studied and also the wear resistance and coefficient of friction for both friction materials were investigated. The tribological outcome from different cases i.e., *Case I* is the wear behavior of M1 & M2 at room temperature, *Case II* is the characterization procedures adopted for wear debris, *Case III* includes high temperature wear behaviors of M1 & M2 friction materials and *Case IV* is the specific heat treatments of the cast iron disc, as discussed below:

- As regards the composition, M2 friction material shows the presence of potassium titanate, zirconium oxide and copper which decrease the coefficient of friction under testing conditions for which the wear behavior of M1 material is dominated by MgO and ZnO with a consequent rise in friction coefficient.
- The evolution of the friction coefficient with sliding distance and temperature shows that M2 has a steady and uniform trend over entire period of the test where as M1 displayed a unsteady and high fluctuations of friction coefficient.
- The wear resistance of M2 pin is high as compared to the M1 pin.
- Wear rate of M1 is much higher as one degree of magnitude than the M2 friction material.
- Wear mechanisms involves at room temperature are tribo-oxidation and three body abrasive wear.

The main aspects of a characterization protocol developed is to study wear products involving disc brake materials, as illustrated in *Case II* (section 8.2). The goal was to use in an optimized way, based on the kinds of available samples, instrumentation and related methodologies in order to get comparatively fast responses useful to identify wear mechanisms and, thereby, improve materials properties from the functional and environmental point of view. The main challenges of the study raise from the broad compositional and dimensional range of the wear debris and, on some occasions, the need to analyze critically limited amounts of particles.

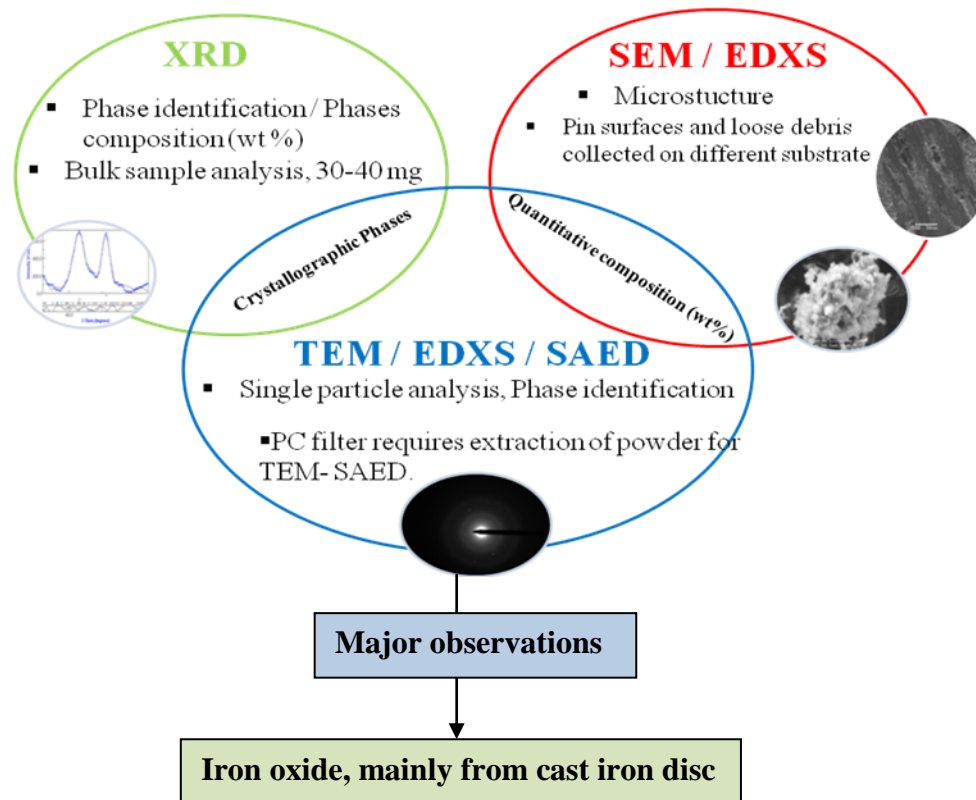


Figure 9.1.1: *Reliable combination of characterization tools for particulate matters.*

Fig. 9.1.1 shows the smart and reliable combination of the results obtained from different techniques, although not necessarily on exactly the same specimens, turned out to be very important for the success of the approach, proved by the fact that the results could be profitably used to identify the main wear mechanisms active under the different wear testing conditions. The particles considered in *Case II* belong to the broad category of PM, which is a major concern for its environmental and health implications. Impactor dust collectors of the same or similar kind as the one employed in this investigation are also used in laboratory tests and on field monitoring for environmental studies, a field that may therefore benefit from the proposed PM analysis methodology.

In my view, the proposed experimental approach could be profitably employed also in other contexts, like environmental and health monitoring, as far as particulate matter, even from other sources than brake systems, is concerned.

Apart from the reliable characterization protocol development for efficient and in optimized characterization of wear debris, another major outcome of *Case II* is the large percentage of iron oxides in wear debris, which are due to the wearing of counterpart cast iron disc.

The focus of *Case III* is the effect of temperature on the pin-on-disc wear behavior of a M1 & M2 friction materials. Tests were conducted at disc temperatures ranging from 25°C (room temperature) up to a maximum of 350°C, in order to study how thermal evolution of the components of the friction materials, in particular the decomposition of the organic binder, influences the main wear mechanisms. These were inferred from the analyses of the wear tracks left after the tests on the surface of the pin and disc specimens. Raman spectroscopy and SEM coupled with EDXS were the main experimental tools used for this purpose. The following main conclusions can be drawn for *Case III*:

- The TGA results of M1 & M2 friction materials shows that the major thermal decomposition of the phenolic binder starts in between 230°C-350°C with a maximum decomposition rate.
- Friction layer progressively decreases for M2 at higher temperature. Friction layer at higher temperatures were absent in M1 pins.
- A transition in wear rate from mild to severe wear is observed in passing from 170°C to 200°C disc temperature for M2, whereas for M1, the wear values has one degree higher magnitude than M2 i.e., under the same working condition i.e., 2MPa and 1.3 m/s (PV), the wear performance of the M2 pin is far superior than the M1 pin.
- Friction behavior for M1 & M2 pin at higher temperature is more stable and uniform, which is due to the presence of thin carbon film on the friction plateaus, acting as a lubricant.
- Carbonaceous products are present on worn surfaces of the pin specimens, referable to different carbon based structures.
- A carbonaceous friction layer formed at higher temperature, has more weight percentage of carbon then the other element, which is due to the decomposition of resin binder, analyzed at characterization of friction layer by XRD and Raman spectra.
- For M1, wear mechanisms involved at high temperature pin-on-disc test are higher percentage of three body abrasive wear + thermal tribo-oxidation + higher percentage of adhesive wear. For M2 friction material, higher percentage of three body abrasive wear + thermal tribo-oxidation + lower percentage of adhesive wear.

Although results obtained under relatively extreme conditions, as compared to those faced in real brake systems, the study highlight some critical aspects of the tribological behavior of brake materials that can be taken into account in the development of better performing brake systems.

Pin-on-disc tests were employed (*Case IV*) to investigate the role of heat-treatment of a cast iron disc in dry sliding against a low-metallic friction material. The main results are as follows:

- Wear rates of both discs i.e., heat-treated disc and heat-treated and ground disc and M2 pin were reduced by almost one order of magnitude when compared it to untreated disc test.
- The decrease in wear rate of heat treated disc is due to its increased surface hardness.
- Reduction in the steady-state friction coefficient when considering untreated disc ($\mu=0.5$) to heat treated ($\mu=0.3$) and heat treated and ground disc ($\mu=0.4$).
- The heat-treated and ground disc displayed the highest temperature rise during test with intermediate friction coefficient, among other disc samples. This was attributed to the decrease in the thermal conductivity induced by the martensitic microstructure.

Fig. 9.1.2 and table 9.1.1, shows the overall findings of every *Cases* in a synthetic way.

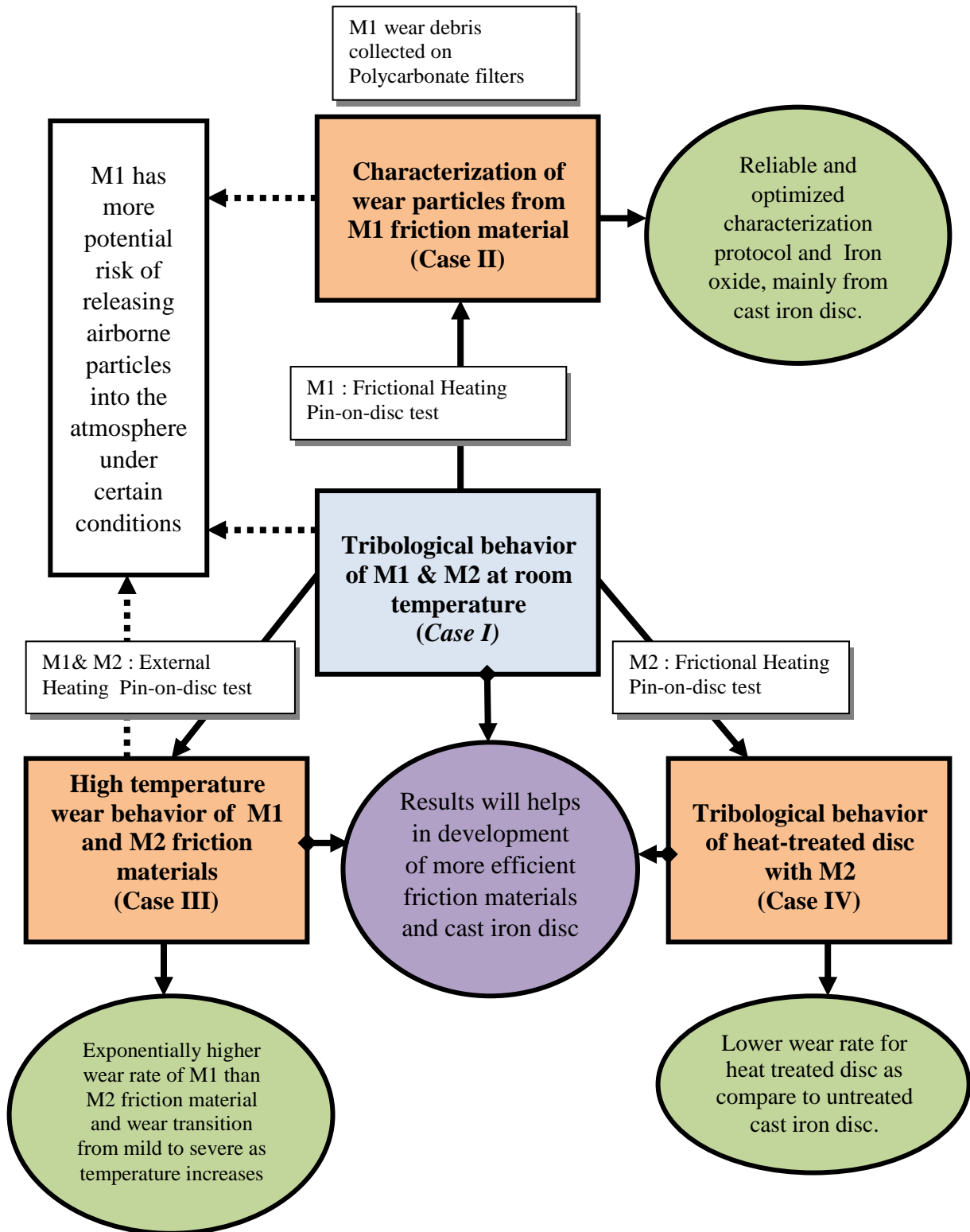


Figure 9.1.2: Flow chart describing major findings of each one of the tribological Cases.

Table 9.1.1: Major results highlights of each one of the tribological Cases.

| Cases | Friction Materials | Major highlights |
|----------|--------------------|--|
| Case I | M1 & M2 | <ul style="list-style-type: none"> • At room temperature, wear rate of M1 is higher than the M2 friction material. • Three body abrasive wear and tribo-oxidation wear mechanisms in M1 & M2. • Formation of compacted friction plateaus for M2 and delamination of friction plateaus for M1 due to hard particles. |
| Case II | M1 | <ul style="list-style-type: none"> • Major phases present in the wear debris of M1 at room temperature is MgO, ZnO and Fe₃O₄. • Most of the Iron oxides in the wear debris were from cast iron disc. • Pin-on-disc rig can be used to produce wide range of wear debris from micron - nanometer. |
| Case III | M1 & M2 | <ul style="list-style-type: none"> • Decomposition of phenolic resin at higher temperatures. • Decomposed product i.e., carbon spread on the friction plateaus. • Absence of friction layer for M1 at higher temperatures. • Decrement in the friction layer coverage for M2 as temperature increases. • Wear rate of M1 is much higher than M2 at elevated temperatures. • Friction behavior for M1 & M2 pin at higher temperature is more stable and uniform. • For M1, wear mechanism involved, higher percentage of three body abrasive wear + thermal tribo-oxidation + higher percentage of adhesive wear. • For M2, wear mechanism involved, higher percentage of three body abrasive wear + thermal tribo-oxidation + lower percentage of adhesive wear. |
| Case IV | M2 | <ul style="list-style-type: none"> • Wear and friction behavior of heat treated cast iron disc is lower compared to untreated iron disc. • The decrease in wear rate of heat treated disc is due to its increased surface hardness. |

9.2 Future developments

The results presented herewith validate the experimental protocol that has been developed, and that can be effectively adopted for the characterization of wear debris, irrespective of the total amount of powders actually available.

On the other hand, the samples analyzed within the work would require further methodological developments. The results allow us to put forward some guidelines for future developments:

- The samples that have been considered so far are mostly wear debris, i.e., particulate matter of different grain size.
- Other important wear products are wear tracks both on pads/pins and discs. Preliminary observations, mostly SEM-EDXS, XRD and Raman, have been conducted on planar and cross sectional samples obtained from pins. The results turn out to be extremely important for a full characterization of the wear systems and will be definitely pursued further for a better understanding and modeling of the wear mechanisms. Therefore, observations and analyzes will be carried out even on discs.
- An important aspect we will consider is the statistical relevance of the chemical, morphological and crystallographic data, obtained with the techniques considered in the present thesis. This is a critical aspect particularly as concerns single particle analyzes and, in general, measurements involving a limited number of powder particles.
- For high temperature wear test future work could be collection methodology of high temperature wear debris since with our high temperature wear test rig has a limitation for collection of wear debris at elevated temperature.
- As far as the friction material is concerned, the formation of a well compacted friction layer could be advisable to stabilize friction, reduce wear and also reduce the particle emission. In material M2, Zr-oxides were found to play an important role in the formation of the friction layer with the presence of copper that seem to aid in increasing the layer cohesion. A possible route to further favor this process is the use of Zr-oxide particles with reduced average size and already inter mixed with a thin copper layer. This objective might be achieved with an optimized ball milling of this two ingredients.
- Heat treated pin-on-disc test results turn out to be extremely important and open the door for further development or modification of the disc. Wear examination of different types of treated disc is highly recommended for the development of the novel brake pad-disc system.

Appendixes

Appendix A: *Abbreviations and definitions*

ASTM = American Society for Testing and Materials
BSE = backscattered electrons
CCSEM = computer controlled scanning electron microscopy
DII = Department of Industrial Engineering, University of Trento, Italy (existing from 2013)
DICAM = Department of Civil, Environmental and Mechanical Engineering, University of Trento, Italy (existing from 2013)
EC = elemental carbon
EDXS = energy dispersive x-ray spectroscopy
EEA = european environment agency
EM = electron microscopy
EPA = environmental Protection Agency of the United States of America (USA)
ESEM = environmental scanning electron microscopy
HEI = health effects institute
ISO = international organization for standardization
LVSEM = low vacuum scanning electron microscopy
MAUD = materials analysis using diffraction
OM = optical microscopy
PC = polycarbonate
PoD = pin-on-disc machine
PM = particulate matter
PM10 = particulate matter with an aerodynamic diameter lower than 10 μm (which includes also PM2.5)
PM2.5 = particulate matter with an aerodynamic diameter lower than 2.5 μm
PTFE = teflon
SAED = selected area electron diffraction
SE = secondary electrons
SEM = scanning electron microscopy
SPA = single particle analysis
STEM = scanning transmission electron microscopy
TEM = transmission electron microscopy
UAAA = ultrafine anthropogenic, atmospheric aerosols
UF = ultrafine (referred to particles with diameter smaller than 0.1 μm)
UFPM = ultrafine particulate matter (referred to particles with diameter smaller than 0.1 μm)
USEPA = United States Environmental Protection Agency
WHO = World Health Organization
XRD = x-ray diffraction
XRF = x-ray fluorescence

Appendix B: *List of scientific publications*

1

Wear debris materials from brake systems: environmental and health issues

R. Ciudin, P. C. Verma, S. Gialanella & G. Straffelini
Department of Industrial Engineering, University of Trento, Italy

Abstract

The environmental and health concerns related to Particulate Matter (PM) released in the environment from different sources have attracted increasing attention in recent years. The present paper is focused on the PM pollution coming from the wear of automotive brake systems. Generally, brake pads have a complex composition containing even more than 30 different components, some of them more polluting than others. The extent of such emissions depends on their physical and chemical properties and on the tribological interactions with the counter face disc during the braking stages. The main topic of the ongoing research regards the potential impact of the emitted PM on the human health, depending on the mechanisms of formation and toxicity of the particles. Since specific epidemiological studies indicated a link between airborne PM and adverse health effects experienced by urban populations throughout the world, it is important to reduce emissions of pollutants at source, i.e. in the present context, brake systems. The EU funded REBRAKE project is one of the many international research projects that are tackling the problem of wear debris emissions from brakes. The first results achieved by REBRAKE team are presented and discussed with regard to the updated situation as emerging from a detailed review of the present knowledge on this topic.

Keywords: REBRAKE project, brake wear, particulate matter, environmental impact, health impact, pin-on-disc, wear testing.

1 Introduction

In order to decrease the impact on human health and on environment, it is important to reduce emissions of pollutants at source. Particulate Matter (PM) released in the environment from industry and traffic have attracted increasing



WIT Transactions on Ecology and The Environment, Vol 191, © 2014 WIT Press
www.witpress.com, ISSN 1743-3541 (on-line)
doi:10.2495/SC141202



Contents lists available at ScienceDirect

Wear

journal homepage: www.elsevier.com/locate/wear

Braking pad-disc system: Wear mechanisms and formation of wear fragments



Piyush Chandra Verma^a, Luca Menapace^a, Andrea Bonfanti^b, Rodica Ciudin^a, Stefano Gialanella^a, Giovanni Straffelini^{a,*}

^a Dipartimento di Ingegneria Industriale, Università di Trento, Via Sommarive 9, 38122 Trento, Italy

^b Brembo S.p.A., via Europa, 2, 24040 Stezzano (Bg), Italy

ARTICLE INFO

Article history:

Received 2 August 2014
Received in revised form
19 November 2014
Accepted 20 November 2014
Available online 29 November 2014

Keywords:

Brake systems
Wear tests
Pin-on-disc
Wear debris
Friction coefficient

ABSTRACT

The tribological phenomena that occur in brake systems are interesting even in other respects than just the braking action. One important issue, that is gaining increasing importance over the last years, concerns the environmental impact of wear debris produced by the braking action. In this context, the present study is focussed on the tribological behaviour of a commercial friction pad material dry sliding against a cast iron disc. Pin-on-disc tests were conducted at room temperature under mild wear conditions, as concerns load and rotating speed. The effect of some components of pad material, in particular of copper, on the dynamic of formation of tribological layer and wear debris is presented. The results obtained so, although referring to quite a simpler system than real brake systems, still may provide interesting indications, for instance in view of the development of novel brake pad materials and braking control systems.

© 2014 Elsevier B.V. All rights reserved.

1. Introduction

Brake pads are an important part of braking systems for all those vehicles that are equipped with disc brakes. Brake pads are made of a steel backing plate with a friction material bound onto the surface facing the disc. Brake pads convert the kinetic energy of the vehicle into thermal energy by friction.

The performances of brakes are controlled to an important extent by the composition and microstructure of the pad material. Industrial pads usually contain a large number of different constituents, such as ceramic particles and fibres, minerals, metallic chips and fibres, solid lubricants and elastomers, all bound by, for instance, a phenolic resin [1,2]. In fact, brake material should maintain a relatively high, stable and reliable friction coefficient over a wide range of braking conditions, temperature and humidity. Metals, such as copper, steel and brass are used in order to affect the frictional characteristics and relevant wear behaviour of involved materials by a suitable selection of their type, morphology and hardness [3–5].

Nowadays, brake material manufacturers are regularly testing materials to develop new formulations for brake pads that might respond more efficiently to the end users demands for materials featuring steady frictional coefficient [6,7], low wear rates [8–10],

reduced emission of particulate matter (PM) in the atmosphere (hazardous debris) [11–13], and noise [7,9,11]. Particular attention has been recently paid to the environmental related problems, due to the release of fine particles produced by brake wear. For example, it has been estimated that around 35% of the brake pad wear is emitted as airborne PM, and 86% of these particles are smaller than 2.5 μm [11]. The wear processes that take place at the interface between braking disc and pad are responsible for the production of the wear debris that is possibly released in the environment. Such processes are quite complex, reflecting the complex composition of brake pad materials, that may contain up to 30 different constituents held together by a phenolic resin [1,2]. Several investigations carried out so far have shown that wear processes are characterized by the formation of a friction layer, also called third body or mechanically-mixed layer, which bears the contact load and strongly influences the actual frictional and wear behaviour [14–16]. In particular, it has been shown that wear initially induces the detachment of particles from the phenolic matrix close to large and hard constituents, which thus form protruding primary plateaus. The components that may form such plateaus were found to be typically larger than 100 μm, and with hardness values greater than that of the counterface disc material, typically pearlitic cast iron. Tough pad constituents too, such as steel fibres and highly strain-hardened copper or brass particles, are involved in the formation of such primary plateaus [17]. Subsequently, micrometric and submicrometric wear particles tend to accumulate close to such plateaus, where they are even compacted to some extent, depending on the contact pressure and sliding shear stresses. In this

* Corresponding author. Tel.: +39 0461282458; fax: +39 0461281977.
E-mail address: giovanni.straffelini@ing.unitn.it (G. Straffelini).



Contents lists available at ScienceDirect

Tribology International

journal homepage: www.elsevier.com/locate/triboint

Wear debris from brake system materials: A multi-analytical characterization approach



Piyush Chandra Verma^a, Mattia Alemani^b, Stefano Gialanella^{a,*}, Luca Lutterotti^a, Ulf Olofsson^c, Giovanni Straffelini^a

^a Department of Industrial Engineering, University of Trento, 38123 Trento, Italy

^b Brembo SpA, Stezzano, Italy

^c Department of Machine Design, KTH, Royal Institute of Technology, 100 44 Stockholm, Sweden

ARTICLE INFO

Article history:

Received 26 March 2015

Received in revised form

1 August 2015

Accepted 9 August 2015

Available online 22 August 2015

Keywords:

Wear debris

Frictional sliding

Scanning electron microscopy

Transmission electron microscopy

ABSTRACT

In this work a streamline characterization protocol for debris coming from wear tests on materials used for disc brake assemblies is presented. An important aspect of the methodology concerns powder collection involving aluminum foil, for a gravitational collection, and polycarbonate filters of an impactor, on which particles are selectively trapped, according to their size. The protocol is based on the application of scanning and transmission electron microscopy, X-ray spectroscopy, X-ray and selected area electron diffraction. The aim of the study was to identify selection parameters, like specimen availability and average particle size, for an effective and smart application of the techniques.

© 2015 Elsevier Ltd. All rights reserved.

1. Introduction

Brakes dissipate energy by converting rotational motion into heat. Disc brakes slow the rotational motion of automobile wheels with friction caused by a brake pad pushing against a brake disc. During this operation, both brake pad and counterface disc wear out, releasing huge amount of wear debris in the surrounding atmosphere. These hazardous wear debris need to be addressed in order to reduce their potentially hazardous effects on human health and, in general, on the environmental conditions. For this reason, one of the main guidelines for the development of new materials for disc brake systems for road vehicles is the reduction of wear debris release. Indeed, this aspect is becoming more and more important in view of the increasing percentage of emissions due to vehicular traffic coming from non-exhaust sources [1], like road surface [2,3], tires [2,4–8] and, of course, the mentioned brake systems [9–11], whose contribution to particulate matter (PM) concentration is equaling exhaust component [12,13]. In this respect, the study of wear products from real brake assemblies is providing not only paramount information to understand the main active wear mechanisms, but also data on potential health and environmental threats that brake contribution to atmospheric PM may have [14,15]. On the other hand, to get the actual composition and

features of wear particles released in the atmosphere is very challenging, considering the diffuse character of this pollutant source, resuspension effects [16] and the possible changes introduced by interactions with the environment and with other PM components. Therefore, although conventional [17] and novel [18,19] environmental monitoring approaches are providing more and more reliable data, the lab test route still stands as a very effective tool to test brake materials concerning their tribological behavior. Their main aspects can be identified thanks to the experimental characterization of the wear products, i.e., debris and tracks that can be found after the test on the surface of pad material and counterface disc.

The aim of this study was to establish an experimental protocol suitable for characterizing particles coming from laboratory pin-on-disc wear tests, involving brake disc materials, collected on different substrates. All materials characterization techniques involved in the study required specific sample preparation procedures, that are important parts of the streamline characterization protocol implemented and optimized in view of its systematic application also to PM collected in other environmental monitoring contexts.

2. Experimental details

2.1. Sample collection and preparation procedures

Tests were performed using a pin-on-disc machine with a horizontal rotating disc and a deadweight-loaded pin (see Fig. 1 condition 1). A fixed sliding speed of 13 m/s (corresponding to

* Corresponding author.

E-mail addresses: piyushchandra.verma@unitn.it (P.C. Verma), mattia_alemani@brembo.it (M. Alemani), stefano.gialanella@unitn.it (S. Gialanella), luca.lutterotti@unitn.it (L. Lutterotti), ulfo@md.kth.se (U. Olofsson), giovanni.straffelini@unitn.it (G. Straffelini).

<http://dx.doi.org/10.1016/j.triboint.2015.08.011>

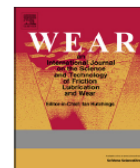
0301-679X/© 2015 Elsevier Ltd. All rights reserved.



ELSEVIER

Contents lists available at ScienceDirect

Wear

journal homepage: www.elsevier.com/locate/wear

Role of the friction layer in the high-temperature pin-on-disc study of a brake material



Piyush Chandra Verma^a, Rodica Ciudin^a, Andrea Bonfanti^b, Pranesh Aswath^c,
Giovanni Straffelini^a, Stefano Gialanella^{a,*}

^a Dipartimento di Ingegneria Industriale, Università di Trento, via Sommarive 9, Povo, 38123, Trento, Italy

^b Brembo S.p.A., Via Europa, 2, 24040 Stezzano (Bg), Italy

^c College of Engineering, University of Texas at Arlington, 416 Yates Street, Rm. 624, Arlington, TX 76019, USA

ARTICLE INFO

Article history:

Received 24 August 2015

Received in revised form

4 November 2015

Accepted 5 November 2015

Keywords:

High-temperature wear tests

Friction coefficient

Severe wear

Mild wear

Brake materials

Degradation phenolic resin

ABSTRACT

The tribological behavior of a commercial brake pad material, wear tested under dry sliding conditions against a cast iron counterface disc with a pin-on-disc apparatus, was investigated. Wear tests were conducted at the following disc temperatures: 25 °C, 170 °C, 200 °C, 250 °C, 300 °C and 350 °C. Above 170 °C a transition from mild to severe wear was observed. At 25 °C and 170 °C, the friction layer on the pin surface consists of primary and compacted secondary plateaus. At 200 °C and above, a progressive reduction of the pin surface coverage by the secondary plateaus, that are barely present after the 350 °C test, is observed. Wear tracks on the discs derive from wear fragments due to the tribo-oxidation of the disc itself and from the wearing out of the pin material. The observed tribological behavior is very much influenced by the thermal degradation of the phenolic binder of the friction material, confirmed by thermogravimetric analyses, conducted on purpose on the pin material. Raman spectroscopy indicated the presence of carbonaceous products on the high temperature worn out pin surface. Although referring to rather extreme and simplified sliding conditions, the results obtained in this study provide useful indications on the role of the thermal stability of the organic component.

© 2015 Elsevier B.V. All rights reserved.

1. Introduction

Brake materials transform the kinetic energy of the vehicle into thermal energy by friction between pad materials and metal, usually cast iron, disc [1]. Heat is then dissipated through exchange mainly with the environment and during braking, temperature may even rise tremendously in the contact regions. Wear behavior at the elevated temperatures resulting from the braking conditions, is highly dependent on the ingredients of the friction materials. These are to be selected in order to guarantee suitable braking conditions, high temperature stability and, consequently, reduced wear rates. However, at high temperatures, the degradation of friction material is a major issue, mostly associated with the thermal decomposition of phenolic resins, widely used as binders for friction materials [2–4]. They embed the ingredients effectively over most of the operational regimes, thanks to a good combination of mechanical properties, such as high hardness, compressive strength, creep resistance, and very good wetting capability. However, these resins are sensitive to heat and humidity, which

cause serious threat to frictional, wear behavior at elevated temperatures, notwithstanding the common practice to add to the formulation suitable, carbon-based stabilizers, like graphite, coal, etc. [5,6]. Therefore, binder decomposition is blamed for various brake operational drawbacks, with specific studies displaying the importance of the heat resistance and mechanical strength of the binder in the wear behavior of brake materials.

Thermal decomposition of the phenolic resins involves several reactions, depending on the actual formulation and thermal history of the material. Temperatures falling in the 250–475 °C interval are reported for the onset of the main transformations involved with the resin decomposition [7,8]. Another important aspect affecting the tribological behavior of sliding wear systems is the trapping of wear debris in between the sliding surfaces [9–13], leading to the formation of the so-called friction layer, or friction film, that is paramount in determining the friction behavior of the mating surfaces in sliding contact [14–17]. Jacko et al. [18] concluded that “when stable friction films, commonly called friction layers, are readily formed for a given friction couple, a stable friction level and low wear rates can be maintained at various temperatures, as long as the friction film is not destroyed”. The wear processes, that occur at the pad and disc interface, display several steps, including the formation of the primary plateaus,

* Corresponding author.

E-mail address: stefano.gialanella@unitn.it (S. Gialanella).

<http://dx.doi.org/10.1016/j.wear.2015.11.004>

0043-1648/© 2015 Elsevier B.V. All rights reserved.



Contents lists available at ScienceDirect

Wear

journal homepage: www.elsevier.com/locate/wear

Wear behavior of a low metallic friction material dry sliding against a cast iron disc: Role of the heat-treatment of the disc



Giovanni Straffelini^{a,*}, Piyush Chandra Verma^a, Ibrahim Metinoz^b, Rodica Ciudin^a, Guido Perricone^b, Stefano Gialanella^a

^a Department of Industrial Engineering, University of Trento, Trento, Italy

^b Brembo S.p.A., Bergamo, Italy

ARTICLE INFO

Article history:

Received 30 May 2015

Received in revised form

26 November 2015

Accepted 28 November 2015

Available online 11 December 2015

Keywords:

Heat-treatment

Sliding wear

Friction

Contact temperature

Cast iron

Friction material

ABSTRACT

In commercial automotive braking systems, consisting of a friction pad dry sliding against a pearlitic cast iron disc, the wear of the disc contributes significantly to the overall wear. In the present work, pin-on-disc sliding tests were carried out for determining the role of conventional heat-treatment conducted on cast iron discs on the friction and wear behavior of the above coupling. Wear rates of both disc and friction materials were reduced by almost one order of magnitude when the disc is preliminarily heat-treated and then ground to remove the surface decarburized layer that forms during the thermal cycle. Heat-treatment and heat-treatment plus grinding resulted also in the decrease of the friction coefficient, which was comparatively lower for the ground samples. The friction and wear behavior along with the contact temperature evolutions were rationalized according to the actual materials characteristics, as resulting from the different treatments.

© 2015 Elsevier B.V. All rights reserved.

1. Introduction

The optimal performances of the pad-disc braking system depend on the properties of the friction material and of the counterface disc [1]. During braking, the kinetic energy of the moving vehicle is converted into thermal energy. The disc provides an appropriate friction coefficient during sliding against the friction pad. Moreover, it ensures an important contribution to the cooling of the system, since the largest fraction of the frictional heat abandons the system through the disc [2]. The discs in automotive braking systems are typically made of pearlitic grey cast iron. This material has several advantages and interesting features. It shows good dry sliding behavior against different counterface materials due to its relatively high hardness and for the presence of graphite lamellae, protruding from the disc surface during sliding, providing a self-lubricating effect [3,4]. The lamellar morphology of graphite also improves the thermal conductivity of the material, and, consequently, its resistance to thermal stresses associated with the braking action [5]. Finally, cast iron discs are relatively cheap, another important element for mass production components. On the other hand, the pearlitic cast iron disc greatly contributes to the overall wear of a braking system

[1,6]. Recent investigations have demonstrated that wear debris from the discs are an important fraction of particulate matter (PM) emissions in the environment [7], mostly concerning particles with an average size below 20 μm [7,8].

So far, most experimental investigations on the reduction of the wear in braking systems have been especially focused on the optimization of the friction materials, by selecting suitable ingredients and relevant concentrations [9–11]. The present research is focused instead on the cast iron disc. According to literature reports, several alternative approaches can be followed. Thornton et al. [12] have recently shown that a deep cryogenic treatment may increase the wear resistance of pearlitic cast iron when sliding against a bearing steel counterface. Also conventional heat-treatments increase wear resistance of cast iron dry sliding against a steel counterface [13]. These treatments include the usual quenching plus tempering and austempering, recommended to obtain a comparatively more ductile cast iron material [14,15]. The laboratory experimental results are definitely promising and provide solid indications that excellent wear performances can be achieved by adopting a suitable treatment that may induce the formation of a hard phase in the alloy matrix, which creates the conditions for a mild tribo-oxidative wear and shifts to highest loads the occurrence of a severe adhesive wear [3].

In the present work, the role of a conventional heat-treatment on the dry sliding behavior of a cast iron material, for brake discs,

* Corresponding author. Tel.: +39 0461282458; fax: +39 0461281977.
E-mail address: giovanni.straffelini@ing.unitn.it (G. Straffelini).

<http://dx.doi.org/10.1016/j.wear.2015.11.020>

0043-1648/© 2015 Elsevier B.V. All rights reserved.

Paper under peer review process

- Giovanni Straffelini, Segey Verlinski, **Piyush Chandra Verma**, Stefano Gialanella, Giorgio Valota. Wear and contact temperature evolution in pin-on-disc tribotesting of low-metallic friction material sliding against pearlitic cast iron. Under review in **Tribology Letters**.

Appendix C: *Participation to conferences, schools and workshops*

- **Conference proceeding: Euro brake – 2015, International congress centre, Dresden Germany, May 4-6, 2015. www.eurobrake.net**

EB2015-EFP-03

CHARACTERIZATION OF WEAR PARTICLES AND TRACKS FROM DISC BRAKE MATERIALS: A MULTIANALYTICAL APPROACH.

¹Chandra Verma, Piyush*, ²Alemani, Mattia, ¹Gialanella, Stefano, ³Olofsson, Ulf, ¹Straffelini, Giovanni

¹Department of Industrial Engineering, University of Trento, Italy

²Brembo SpA, Italy

³Royal Institute of Technology – KTH, Stockholm, Sweden

KEYWORDS – Wear testing, debris collection, electron microscopy, single particle analysis, X-ray diffraction, wear mechanism.

ABSTRACT - The characterization of wear debris and tracks is paramount to understand the dominant wear mechanisms active in tribological systems. In this paper we present the main aspects of a streamline characterization protocol we have implemented to characterize wear products, particularly disc brake materials, obtained in different ways and from different wear rigs.

The protocol is based on the smart application of different materials characterization tools, like X-ray diffraction, scanning and transmission electron microscopy, energy dispersive spectroscopy. It is validated by studying wear debris and tracks obtained under different experimental conditions with the aim of identifying the main wear mechanisms.

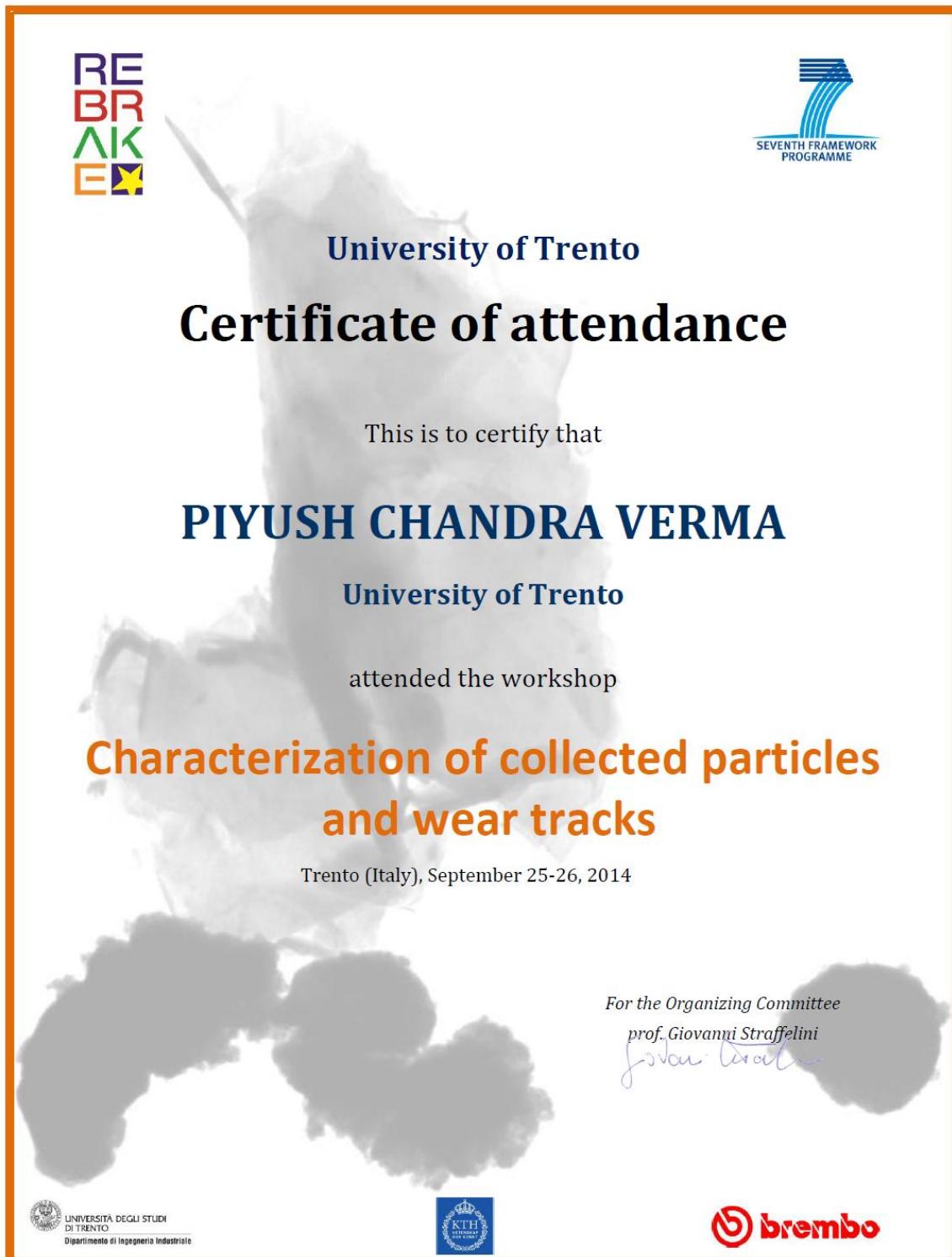
A discussion on the best practice for experimental testing, even as concerns the statistical significance of the data, is presented. In this respect the proposed experimental approach may be profitably employed even in other contexts, like environmental and health monitoring, as far as particulate matter, even from other sources than brake systems, is concerned.

INTRODUCTION – The development of new materials for disc brake systems for road vehicles is nowadays conducted not only in the attempt to improve brake performances but also to reduce the release in the environment of the wear debris produced by the tribological events involved with the braking action. Indeed, this aspect is becoming more and more important in view of the increasing percentage of emissions due to vehicular traffic coming from non-exhaust sources, like road and tires consumptions and the mentioned wearing out of brake discs and pads (1-2). In this respect, the study of wear products from real brake assemblies is providing not only paramount information to understand the main active wear mechanism, but also data on potential health and environmental threats that brake contribution to atmospheric particulate matter (PM) may have (3). On the other hand, to get the actual composition and features of, particularly, wear particles released in the atmosphere is very challenging, considering the diffuse character of this pollutant source and the possible changes introduced by interactions with the environment and with other PM components. Therefore, although conventional (4) and novel (5-6) environmental monitoring approaches are providing more and more reliable data, the lab test route still stands as a very effective tool to test brake materials concerning their tribological behaviour. Their main aspects can be identified thanks to the experimental characterization of the wear products, i.e., debris and tracks that can be found after the test on the surface of pad material and counterface disc. In view of the complexity of this sort of specimens a multi-analytical approach is very much recommended for the characterization of wear tracks and debris (7-8), these latter even as concerns the nanometric range (9-10). In fact, the finer fraction of wear debris from brake systems is attracting interest and raising concern owing to their sanitary and environmental implications (11).

- **Workshop: IEEE Italy School of Career Boosting, February 10-14, 2014, Trento-Italy.**



- Workshop on characterization of collected particles and wear tracks, September 25-26, 2014, Trento-Italy.



- **Workshop on Testing of friction materials and possibilities for evaluation of wear particles emission, December 1st, 2014, Stezzano-Italy.**



EC Seventh Framework Programme
Project Co-funded by the European Commission
Grant agreement no.: 324385
Call identifier: FP7-PEOPLE-2012-IAPP
Project Start Date: 01/03/2013



REBRAKE

50% Reduction of Brake Wear Particulate Matter

Workshop

Testing of friction materials and possibilities for evaluation of wear particles emission

Date: 1st December, 2014

Venue: Brembo S.p.a. - Stezzano- Italy

Partners: Brembo; UniTN; KTH

Appendix D: *Research internships*

- One week research internship at Brembo S.p.A, Stezzano-Italy.



This document certifies that Mr. Piyush Chandra Verma, PhD student in the Department of Industrial engineering (UNITN), has participated in the research experiments, namely Dyno-bench test and SEM observation of wear debris, conducted in R&D department of BREMBO S.p.A.
The stay of the student in the Brembo S.p.A. was from 09/02/2015 – 13/02/2015 (one week).

13/02/2015

The supervisor : Guido Perricone

A handwritten signature in blue ink, appearing to read 'Guido Perricone', is written over a horizontal line.

| BREMBO S.p.A. | Sede legale | Sede amministrativa e uffici | | |
|---------------|--|--|---|--|
| | Via Brembo, 25 24035 CURNO Bergamo (Italy) | Viale Europa, 2 24040 STEZZANO Bergamo (Italy) | Tel. +39 035 605 1111 Fax +39 035 605 2300 Cap. Soc. € 34.727.914 Export M BG 020900 | R.E.A. 134667 Registro Imprese BG Codice Fiscale e Partita IVA n° 00222620163 |

- **Three month of research internship at University of Texas at Arlington, USA.**



To whom it may concern:

I hereby certify that Mr. Verma (*surname*) Piyush Chandra (*name*) has taken part in research activity in the Materials Science and Engineering Department, in the College of Engineering at The University of Texas at Arlington as a doctoral student from June 15th to Sept. 15th 2015.

A handwritten signature in black ink, appearing to read 'Pranesh B. Aswath', written over a horizontal line.

Dr. Pranesh B. Aswath
Professor of Materials Science and Engineering and
Associate Dean, College of Engineering

Date: Sept 16th 2015

References

- S. Abbasi, J. Wahlstrom, L. Olander, C. Larsson, U. Olofsson, U. Sellgren, A study of airborne wear particles generated from organic railway brake pads and brake discs, *Wear* 273 (2011) 93–99.
- Abbasi S, Jansson A, Olander L, Olofsson U, Sellgren U., A pin-on-disc study of the rate of airborne wear particle emissions from railway braking materials. *Wear* 284-285 (2012) 18-29.
- Abd Rahim AbuBakar, Huajiang Ouyang, Wear prediction of friction material and brake squeal using the finite element method, *Wear* 264 (2008) 1069-1076.
- Adachi, S., Kawamura, K. and Takemoto, K. A trial on the quantitative risk assessment of man-made mineral fibers by the rat intraperitoneal administration assay using the JFM standard fibrous samples. *Indust. Health* 39 (2001) 168–74.
- Amato F, Schaap M, Denier van der Gon HAC, Pandolfi M, Alastuey A, Keuken M et al. Short-term variability of mineral dust, metals and carbon emission from road dust resuspension. *Atmos Environ* 74 (2013) 134-40.
- Amato F, Cassee FR, van der Gon HACD, Gehrig R, Gustafsson M, Hafner W et al. The challenge of traffic non-exhaust emissions. *J Hazard Mat* 275 (2014) 31-6.
- Anastasio, C., Martin, S.T. Atmospheric nanoparticles, *Nanoparticles and the Environment* (2001) 293–349.
- A. Soderberg, S. Andersson, Simulation of wear and contact pressure distribution at the pad-to-rotor interface in a disc brake using general purpose finite element analysis software, *Wear* 267 (2009) 2243-2251.
- A.E. Anderson, Brake system performance-effect of fiber types and concentrations Proceedings of fibers in linings symposium, The Asbestos Institute, Montreal, Quebec (1987) 2-57.
- A.E. Anderson, Friction and wear of automotive brakes, *ASM Handbook* 18 (1992) 569-577.
- A.R. Riahi, A. T. Alpas, Wear map for grey cast iron, *Wear* 255 (2003) 401-409.
- Archard, J. F., Contact and rubbing of flat surfaces, *Journal of Applied Physics*, 24 (8) (1953)18-28.
- Archard, J. F., Friction between metal surfaces, *wear* (113) 1 (1986) 54.
- A.S.M.A. Haseeb, Md. Aminul Islam, Md. Mohar Ali Bepari, Tribological behavior of quenched and tempered, and austempered ductile iron at the same hardness level, *Wear* 244 (2000) 15-19.
- Avallone, E. A. and Baumeister III, T. *Marks Handbook for Mechanical Engineers*, 10th edition, (1997) 6–142 (McGraw-Hill, New York).
- Barlow, T.J., Boulter, P.G., McCrae, I.S., Sivell, P., Harrison, R. M., Carruthers, D., Stocker, J., Non-Exhaust Particulate Matter Emissions From Road Traffic: Summary Report. Prepared for: Project Record: CPEA23, (2007).
- Bertolotti G, Gialanella S. Review: use of conifer needles as passive samplers of organic pollutants in air quality monitoring. *Analytical Methods* 6 (2014) 6208-22.
- Bharat Bhushan, *Introduction to tribology*, John Wiley & son, publication (2002).
- K. Bode, G.P. Ostermeyer, A comprehensive approach for the simulation of heat and heat-induced phenomena in friction materials, *Wear* 311 (2014) 47-56.
- Booher, B. V. Pultrusion method of making brake linings. US Pat. 5156787, (1992) (United States Patent and Trademark Office).
- Brinzey, A. E. Friction materials with universal core of non-asbestos fibres. US Pat. 5041471, (1991) (United States Patent and Trademark Office).
- B. Breur, K.H. Bill, *Brake Technology Handbook*, SAE International; Pennsylvania (2008).
- Buseck, P.R., Adachi, K., Nanogeoscience: nanoparticles in the atmosphere, *Elements*, 4, 6 (2008) 389-394,.

- Camatini M, Crosta G, Dolukhanyan T, Sung C, Giuliani G, Corbetta G et al. Microcharacterization and identification of tire debris in heterogeneous laboratory and environmental specimens. *Mater Charact* 46 (2001) 271-83.
- CEN 16414. Biomonitoring with mosses – Accumulation of atmospheric contaminants in mosses collected in situ: from the collection to the preparation of samples (2014).
- Ceramic fibres (respirable size). Tenth Report on Carcinogens, US Department of Health and Human Services, (2002).
- Chrysotile asbestos. Priority Existing Chemical Report 9, National Industrial Chemicals Notification and Assessment Scheme, Commonwealth of Australia (1999) 8.
- Ciudin R, Verma P C, Gialanella S, Straffelini G. Wear debris materials from brake systems: environmental and health issues. *Proc. 9th international Conf. on Urban Regeneration and Sustainability (The Sustainable City IX)*; Wit Press, Southampton (2014) 1423-34.
- Critchley, J. P., Knight, G. J. and Wright, W. W. *Heat Resistant Polymers* (1983) 21–29 (Plenum Press, New York).
- Cuesta A, Dhamelincourt P, Laureyns J, Martinez-Alonso A, Tascon JMD. Raman microprobe studies on carbon materials, *Carbon* 32 (1994) 1523-1532.
- D Chan and G W Stachowiak, Review of automotive brake friction materials, *Proc. Instn Mech. Engrs Vol. 218 Part D: J. Automobile Engineering*, 953-966.
- Dahl A, Gharibi A, Swietlicki E, Gudmundsson A, Bohgard M, Ljungman A et al. Traffic-generated emissions of ultrafine particles from pavement-tire interface. *Atmos Environ* 40 (2006) 1314-23.
- Dall OM, Beddows DCS, Gietl JK, Olatunbosun OA, Yang X, Harrison RM. Characteristics of tyre dust in polluted air: Studies by single particle mass spectrometry (ATOFMS). *Atmos Environ* 94 (2014) 224-30.
- Day, *Braking of road vehicles*, Oxford, UK, Butterworth-Heinemann (2014).
- Denier van der Gon HAC, Gerlofs-Nijland ME, Gehrig R, Gustafsson M, Janssen N, Harrison RM et al. The policy relevance of wear emissions from road transport, now and in the future-an international workshop report and consensus statement. *J Air Waste Manag Assoc* 63 (2013) 136-49.
- Dyson A. , Patterns of wear in reciprocating motion, *Wear* 65 (2) (1980) 243-257.
- EEA EMEP/CORINAIR Emission Inventory Guidebook European Environment Agency, 2005. <http://reports.eea.europa.eu/EMEP/CORINAIR4/en>
- ELPI+ - features and specifications. Retrieved from [http://www.dekati.com/products/Fine Particle Measurement/ELPI+™](http://www.dekati.com/products/Fine_Particle_Measurement/ELPI+™). Dekati (2014).
- EN 12341. Determination of the PM10 fraction of suspended particulate matter. Reference method and field-test procedure to demonstrate reference equivalence of measurement methods (1999).
- Eriksson, M., Bergman, F. and Jacobson, S. Surface characterization of brake pads after running under silent squealing conditions. *Wear* 232 (1999) 163–167.
- Mikael Eriksson, Staffan Jacobson, Tribological surfaces of organic brake pads, *Tribology International* 33 (2000) 817-827.
- Mikael Eriksson , John Lord, Staffan Jacobson, Wear and contact conditions of brake pads: dynamical in situ studies of pad on glass, *Wear* 249 (2001) 272-278.
- Eriksson, M., Bergman, F. and Jacobson, S. On the nature of tribological contact in automotive brakes. *Wear* 252 (2002) 26–36.
- E. Rabinowicz, L.A. Dunn, P.G. Russell, A study of abrasive wear under three-body conditions, *Wear* 4 (5) (1961) 345-355.
- EU Directive 2008/50/EC of the European Parliament and of the Council of 21 May (2008) on Ambient Air Quality and Cleaner Air for Europe.

- European Environment Agency (EEA report). Air Quality in Europe – (2013) report, No 9, doi:10.2800/92843, Denmark. 2013. www.europa.eu
- European Environment Agency EMEP/EEA air pollutant emission inventory guidebook, Technical Report No 12/2013 (2013).
- Fatima Eddoumy, Haytam Kasem, Houcine Dhieb, Josephus Gerardus Buijnsters, Philippe Dufrenoy, Jean-Pierre Celis, Yannick Desplanques, Role of constituents of friction materials on their sliding behavior between room temperature and 400°C, *Materials and Design* 65 (2015) 179-186.
- Garg, B.D., Cadle, S.H., Mulawa, P.A., Groblicki, P.J., Laroo, C. & Parr, G.A., Brake wear particulate matter emissions, *Environ Sci Technol*, 34(21) (2000) 4463–4469.
- Gasser, M., Riediker, M., Mueller, L., Perrenoud, A., Blank, F., Gehr, P., Rothen-Rutishauser, B., Toxic effects of brake wear particles on epithelial lung cells in vitro, *Particle and Fibre Toxicology* 6 (2009) 30.
- Geiger, A., Cooper, J. Overview of Airborne Metals Regulations, Exposure Limits, Health Effects, and Contemporary Research, Cooper Environmental Services LLC, Portland. (2010) <http://www.epa.gov>
- Georges F, Sykes J, Decomposition characteristics of a char-forming phenolic polymer used for ablative composites, *Nat. Aeronautics Space Admin.* (1967) NASA TN D-3810.
- G.M. Ingo, M. D’Uffizi, G. Falso, G. Bultrini, G. Padeletti, Thermal and microchemical investigation of automotive brake pad wear residues, *Thermochimica Acta* 418 (2004) 61-68.
- G.P. Ostermeyer, On the dynamics of the friction coefficient, *Wear* 254 (2003) 852–858.
- G.P. Ostermeyer, M. Muller, Dynamic interaction of friction and surface topography in brake systems, *Tribology International* 39 (2006) 370-380.
- G.P. Ostermeyer, M. Muller, Cellular automata method for macroscopic surface and friction dynamics in brake systems, *Tribology International* 40 (2007) 942–952.
- G.P. Ostermeyer, K. Bode, A comprehensive approach for the simulation of heat and heat-induced phenomena in friction materials, *Wear* 311(2014) 47-56.
- G. Straffelini, A simplified approach to the adhesive theory of friction, *Wear* 249 (2001) 78-84.
- G. Straffelini, M. Pellizzari, L. Maines, Effect of sliding speed and contact pressure on the oxidative wear of austempered ductile iron, *Wear* 270 (2011) 714-719.
- G. Straffelini, L. Maines, The relationship between wear of semimetallic friction materials and pearlitic cast iron in dry sliding, *Wear* 307 (2013) 75-80.
- G. Straffelini, *Friction and wear – Methodologies for designing and control*, Springer Verlag (2015).
- G. Straffelini, *Friction and wear, methodologies for Design and Control*, Springer (2015).
- Gunawardana C, Goonetilleke A, Egodawatta P, Dawes L, Kokot S. Source characterization of road dust based on chemical and mineralogical composition. *Chemosphere* 87 (2012) 163-70.
- Gustafsson M, Blomqvist G, Gudmundsson A, Dahl A, Swietlicki E, Bohgard M et al. Properties and toxicological effects of particles from the interaction between tyres, road pavement and winter traction material. *Sci Total Environ* 393 (2008) 226-40.
- Helland, A., Wick, P., Koehler, A., Schmid, K. & Som, C. Reviewing the environmental and human health knowledge base of carbon nanotubes, *Environmental Health Perspectives* 115, 8 (2007) 1125-1131.
- HEI - Panel on the Health Effects of Traffic-Related Air Pollution, *Traffic-related Air Pollution: A Critical Review of the Literature on Emissions, Exposure, and Health Effects*. HEI Special Report, 17. Health Effects Institute, Boston, MA (2010).
- HEI - Review Panel on Ultrafine Particles, *Understanding the Health Effects of Ambient Ultrafine Particles*, HEI Perspectives 3, Health Effects Institute, Boston, MA (2013).
- Hell, M., Jaworek, W., Huppatz, W. and Wieser, D. Friction lining, especially for brakes and clutches, and a method for producing a friction lining. US Pat. 6481555 (2002) (United States Patent and Trademark Office).

- Honga U.S., Junga S.L., Choa K.H., Choa M.H., Kimb S.J., Jang H. Wear mechanism of multiphase friction materials with different phenolic resin matrices, *Wear* 266 (2009) 739-744.
- Holman, J. P. Heat Transfer, 8th edition, pp. 641–642 (McGraw-Hill, Singapore).
- Hulskotte JHJ, Roskam GD, Denier van der Gon HAC. Elemental composition of current automotive braking materials and derived air emission factors. *Atmos Environ.* 99 (2014) 436-45.
- Iijima, A., Sato, K., Yano, K., Tago, H., Kato, M., Kimura, H., Furuta, N., Particle size and composition distribution analysis of automotive brake abrasion dusts for the evaluation of Sb sources of airborne particulate matter, *Atmospheric Environment* 41 (2007) 4908–4919.
- Jiaren Jiang, F.H. Stott, M.M. Stack, A mathematical model for sliding wear of metals at elevated temperatures, *Wear* 181-183 (1995) 20-31.
- Jiaren Jiang, F.H. Stott, M.M. Stack, The effect of partial pressure of oxygen on the tribological behaviour of a nickel-based alloy, N80A, at elevated temperatures, *Wear* 203-204 (1997) 615-625.
- Jiaren Jiang, F. H. Stott and M. M. Stack, The role of triboparticulates in dry sliding wear, *Tribology International*, 31 No.5 (1998) 245-256.
- Jang, H. and Kim, S. J. The effects of antimony trisulphide and zirconium silicate in the automotive brake friction material on friction characteristics. *Wear* 239 (2000) 229–236.
- Jang, H., Lee, J. S. and Fash, J. W. Compositional effects of the brake friction material on creep groan phenomena. *Wear* 251 (2001) 1477–1483.
- J.R. Laguna-Camacho, G. Juárez-Morales, C. Calderón-Ramón, V. Velázquez-Martínez, I. Hernández-Romero, J.V. Méndez-Méndez, M. Vite-Torres, A study of the wear mechanisms of disk and shoe brake pads, *Engineering Failure Analysis* 56 (2015) 348-359.
- Kamioka, N., Tokumura, H. and Yoshino, T. Friction material containing BT resin dust. US Pat. 5384344, 1995 (United States Patent and Trademark Office).
- Kane, J. F. and Mowrer, N. R. Phenolic resin compositions with improved impact resistance. US Pat. 5736619, (1998) (United States Patent and Trademark Office).
- Kobayashi, M. Non-asbestos friction materials. US Pat. 6413622 (2002) (United States Patent and Trademark Office).
- Komori, T., Miyake, S. and Senoo, Y. Brake friction material. US Pat. 4954536 (1990) (United States Patent and Trademark Office).
- H. Kong, E.S. Yoon, O.K. Kwon, Self-formation of protective oxide films at dry sliding mild steel surfaces under a medium vacuum, *Wear* 181-183 (1995) 325-333.
- Kim, S. J., Cho, M. H., Lim, D.-S. and Jang, H. Synergistic effects of aramid pulp and potassium titanate whiskers in the automotive friction material. *Wear* 251 (2001) 1484–1491.
- Kimura, K., Goto, Y., Torii, N., Katagiri, H., Miyazawa, H. and Motoyoshi, Y. Friction material for dampers and process for producing the same. US Pat. 5830566 (1998) (United States Patent and Trademark Office).
- K. Hirasata, K. Hayashi, Y. Inamoto, Friction and wear of several kinds of cast irons under severe sliding conditions, *Wear* 263 (2007) 790-800.
- K.H. Liew, U. Nirmal, Frictional performance evaluation of newly designed brake pad materials, *Mater. Des.* 48 (2013) 25-33.
- J. Kuepferle, J. Wilzer, S. Weber, W. Theisen, Thermo-physical properties of heat-treatable steels in the temperature range relevant for hot-stamping applications, *J. Mater. Sci.* 50 (2015) 2594-2604.
- Kukutschova, J., Roubíček, V., Malachová, K., Pavlíčková, Z., Holusab, R., Kubackovac, J., Mickac, v., MacCrimmond, D., Filip, P., Wear mechanism in automotive brake materials, wear debris and its potential environmental impact, *Wear* 267 (2009) 807–817.
- Jana Kukutschova, Václav Roubíček, Miroslav Maslán, Dalibor Jancík, Václav Slovák, Katerina Malachová, Zuzana Pavlíčková, Peter Filip, Wear performance and wear debris of semimetallic automotive brake materials, *Wear* 268 (2010) 86-93.

- Kukutschova, J., Moravec, P., Tomasek, V., Matejka, V., Smolík, J., Schwarz, J., Seidlerová, J., Safárová, K., Filip, P., On airborne nano/micro-sized wear particles released from low-metallic automotive brakes, *Environmental Pollution*, 159 (4) (2011) 998-1006.
- K. Kato, Micro-mechanisms of wear- wear modes, *Wear* (153) (1992) 277-295.
- Keiner W., Werning H., GG15HC high carbon grey iron. An ideal material for brake discs and drums. *Konstrulieren and Glesten* (15) 4 (1990).
- J.L. Labar, Consistent indexing of a (set of) SAED pattern(s) with the Process Diffraction program, *Ultramicroscopy* 103 (2005) 237-249.
- J.L. Labar, Electron Diffraction Based Analysis of Phase Fractions and Texture in Nanocrystalline Thin Films, Part I: Principles, *Microsc. Microanal.* 14 (4) (2008) 287-295.
- J. wahlstrom, A study of airborne wear particles from automotive disc brakes, Phd thesis (2009).
- J. Bijwe, P.V. Gurunath, Friction and wear studies on brake-pad materials based on newly developed resin, *Wear* 263 (2007) 1212-1219.
- J.R. Laguna-Camacho, G. Juárez-Morales, C. Calderón-Ramón, V. Velázquez-Martínez, I. Hernández-Romero, J.V. Méndez-Méndez, M. Vite-Torres, A study of the wear mechanisms of disk and shoe brake pads, *Engineering Failure Analysis* 56 (2015) 348–359.
- Lamport, R. A., Biermann-Weaver, J. M., Jain, V. K. and Shih, P. Resin mixture for friction materials. US Pat. 5753018 (1998) (United States Patent and Trademark Office).
- Lee S, Kwak J, Kim H, Lee J. Properties of roadway particles from interaction between the tire and road pavement. *Int. J. Automot. Technol. Manag.* 14: (2013)163.
- S.C. Lim, M.F. Ashby, Wear mechanisms maps, *Acta Mater.* 35 (1987) 1-24.
- Londahl, J., Massling, A., Pagels, J., Size-resolved respiratory-tract deposition of fine and ultrafine hydrophobic and hygroscopic aerosol particles during rest and exercise, *Inhal. Toxicol.* 19(2) (2007) 109-116.
- L. Lutterotti, *Nuclear Inst. and Methods in Physics Research B* 268, 334 (2010).
- L. Lutterotti, S. Matthies, H.R. Wenk, A.J. Schultz and J. Richardson, *J. Appl. Phys.* 81, 594 (1997).
- M.A. Moore, Abrasive wear of brittle solids, *Wear* (60) 1(1980) 123-140.
- Marzocchi, A., Jannarelli, A. E. and Garrett, D.W. Friction materials for brake linings and the like. US Pat. 3967037 (1976) (United States Patent and Trademark Office).
- McClellan, R. O., Setting ambient air quality standards for particulate matter, *Toxicology* 181-182 (2002) 329-347.
- M.G. Jacko, P.H.S. Tsang, S.K. Rhee, Automotive linings evolution during the past decade, *Wear* 100 (1984) 503-515.
- M.G. Jacko, P.H.S. Tsang, S.K. Rhee, Wear debris compaction and friction film formation of polymer composites, *Wear* 133 (1989) 23-38.
- M.H. Cho, S.J. Kim, D. Kim, H. Jang, “Effects of ingredients on tribological characteristics of a brake lining: an experimental case study”, *Wear* 258 (2005) 1682–1687.
- Mihir Patel, Cristy Leonor Azanza Ricardo, Paolo Scardi, Pranesh B. Aswath, Morphology, structure and chemistry of extracted diesel soot—Part I: Transmission electron microscopy, Raman spectroscopy, X-ray photo electron spectroscopy and synchrotron X-ray diffraction study, *Tribology International* 52 (2012) 29-39.
- Mosleh, M., Blau, P.J., Dumitrescu, D., Characteristics and morphology of wear particles from laboratory testing of disk brake materials, *Wear* 256 (11) (2004) 1128-34.
- Monika Kristkova, Peter Filip, Zdenek Weiss, Rudolf Peter, Influence of metals on the phenol–formaldehyde resin degradation in friction composites, *Polymer Degradation and Stability* 84 (2004) 49-60.
- M. Khrushchov, Principles of abrasive wear, *Wear* (28) 1 (1974) 69-88.
- Mukesh K., J. Bijwe, Influence of different types of binder in non-asbestos-organic brake lining materials: A case study on inertia brake dynamometer, *J. Engineering Tribology* 228 (5) (2014) 584-592.

- Alemani, Mattia, Perricone Guido, Olofsson Ulf, Söderberg Anders, Wahlström Jens, Ciotti Alessandro, A proposed dyno bench test cycle to study particle emissions from disc brakes, Eurobrake conference, Dresden Germany (2015) EB2014-SE-001.
- Nakagawa, M., Yamashita, Y., Ibuki, M. and Kishimoto, H. Friction material and method of manufacturing such material. US Pat. 5268398 (1993) (United States Patent and Trademark Office).
- Nel, A., Xia, T., Madler, L. & Li, N., Toxic potential of materials at the nanolevel, *Science* 311, 5761 (2006) 622–627.
- N.K. Myshkin, M.I. Petrokovets, A.V. Kovalev, “Tribology of polymers: Adhesion, friction, wear, and mass-transfer”, *Tribology International* 38 (2005) 910–921.
- N.S.M. EL-Tayeb, K.W. Liew, V.C. Venkatesh, Evaluation of new frictional brake pad materials. Proc. International Conference on Manufacturing Science and Technology, ISBN 983-42051-1-2, Malacca-Malaysia, 28-30 August (2006) 380-383.
- Oberdörster, G., Oberdörster, E., Oberdörster, J. Nanotoxicology: an emerging discipline evolving from studies of ultrafine particles, *Environmental Health Perspectives* 113, 7 (2005) 823–839.
- Ohya, K. and Kimbara, H. Disc brake pad. US Pat. 4944373 (1990) (United States Patent and Trademark Office).
- U. Olofsson, L. Olander, A. Jansson A, A study of airborne wear particles generated from a sliding contact, *Journal of Tribology* vol. 131(4) (2009).
- Olofsson U, Olander L, Jansson A. Towards a model for the number of airborne particles generated from a sliding contact. *Wear* 267 (2009) 2252-56.
- W. Osterle, M. Griepentrog, Th. Gross, I. Urban, Chemical and microstructural changes induced by friction and wear of brakes, *Wear* 251 (2001) 1469–1476.
- W. Osterle, I. Urban, Friction layers and friction films on PMC brake pads, *Wear* 257 (2004) 215-226.
- W. Osterle, Ingrid Urban, Third body formation on brake pads and rotors, *Tribology International* 39 (2006) 401-408.
- W. Osterle, H. Kloß, I. Urban, A.I. Dmitriev, Towards a better understanding of brake friction materials, *Wear* 263 (2007) 1189-1201.
- W. Osterle, I. Dorfel, C. Prietzel ,A comprehensive microscopic study of third body formation at the interface between a brake pad and brake disc during the final stage of a pin-on-disc test, *Wear* 267 (2009) 781–788.
- W. Osterle, C. Prietzel, H. Kloß, A.I. Dmitriev, On the role of copper in brake friction materials, *Tribology International* 43 (2010) 2317-2326.
- W. Osterle, A.I. Dmitriev, G. Orts-Gil, T. Schneider, H. Ren, X. Sun, Verification of nanometre-scale modelling of tribofilm sliding behaviour, *Tribology International* 62 (2013) 155-162.
- Pant P, Harrison RM. Estimation of the contribution of road traffic emissions to particulate matter concentrations from field measurements: a review. *Atmos Environ* 77 (2013) 78-97.
- Peter Filip, Zdenek Weiss, David Rafaja, On friction layer formation in polymer matrix composite materials for brake applications, *Wear* 252 (2002) 189-198.
- Soydan Ozcan, Peter Filip, Wear of carbon fiber reinforced carbon matrix composites: Study of abrasive, oxidative wear and influence of humidity, *CARBON* 62 (2013) 240-247.
- Piyush Chandra Verma, Luca Menapace, Andrea Bonfanti, Rodica Ciudin, Stefano Gialanella, Giovanni Straffelini, Braking pad-disc system: Wear mechanisms and formation of wear fragments, *Wear* 322-323 (2015) 251-258.
- P.J. Blau, Fifty years of research on the wear of metals, *Tribology International* 30 (5) (1997) 321-331.
- P.V. Gurunath, J. Bijwe, Friction and wear studies on brake-pad materials based on newly developed resin, *Wear* 263 (2007) 1212-1219.
- P.W. Lee, P. Filip, Friction and wear of Cu-free and Sb-free environmental friendly automotive brake materials, *Wear* 302 (2013) 1404-1413.

- Quinn, T.F.J., Sullivan J.L., Rowson D.M., Origins and development of oxidational wear at low temperatures, *Wear* (94) (1984) 175-191.
- Querol X, Alastuey A, Viana MM, Rodriguez S, Artinano B, Salvador P et al. Speciation and origin of PM10 and PM2.5 in Spain. *Journal of Aerosol Science* 35 (9) (2004) 1151-72.
- S. Ramousse, J.W. Hoj, O.T. Sørensen, Thermal characterization of brake pads, *J. Therm. Anal. Calorim.* 64 (2001) 933-943.
- Riediker M, Devlin RB, Griggs TR, Herbst MC, Bromberg PA, Williams RW. Cardiovascular effects in patrol officers are associated with Fine particulate matter from brake wear and engine emissions. Part. *Fibre Toxicol* 1 (1) (2004) 2.
- Roemer, W., Hoek, G., Brunekreef, B., PM₁₀ elemental composition and acute respiratory health effects in European children (PEACE project), *Pollution Effects on Asthmatic Children in Europe*, *Eur Respir J* 15(3) (2000) 553-559.
- Ruth Hinrichs, M.A.Z. Vasconcellos, Werner Österle, Claudia Prietzel, A TEM snapshot of magnetite formation in brakes: The role of the disc's cast iron graphite lamellae in third body formation, *Wear* 270 (2011) 365-370.
- Samuels, G. J. Friction composition and friction element fabricated therefrom. US Pat. 5516816 (1996) (United States Patent and Trademark Office).
- Sanders, P. G., Xu, N., Dalka, T. M. & Maricq, M. M., Airborne brake wear debris: Size distributions, composition, and a comparison of Dynamometer and vehicle tests, *Environmental Science and Technology*, 37(18) (2003) 4060-4069.
- Schlesinger, R. B., Kunzli, N., Hidy, G. M., The health relevance of ambient particulate matter characteristics: coherence of toxicological and epidemiological inferences, *Inhal Toxicol*, 18(2) (2006) 95-125.
- Sehlstedt, M., Forsberg, B., Westerholm, R., Boman, C., Sandström, T., The Role of Particle Size and Chemical Composition for Health Risks of Exposure to Traffic Related Aerosols - A Review of the Current Literature, Final report 071212.
- Seong Jin Kim, Ho Jang, Friction and wear of friction materials containing two different phenolic resins reinforced with aramid pulp, *Tribology International* 33 (2000) 477-484.
- S. Narayanan, L.S. Schadler, Mechanisms of kink band formation in graphite/epoxy composites: A micromechanical experimental study, *Compos. Sci. Technol.*, 59 (1999) 2201-2213.
- S.K. Rhee, Wear mechanics for asbestos-reinforced automotive friction materials, *Wear* 29 (1974) 391-393.
- Rhee, S. K., Wear equation for polymers sliding against metal surfaces, *Wear*, 16 (1970) 431-445.
- Smith, W. N. and Boyd, P. Carbonaceous friction materials. US Pat. 5965658 (1999) (United States Patent and Trademark Office).
- Spurny K. R., On the physics, chemistry and toxicology of ultrafine anthropogenic, atmospheric aerosols (UAAA): new advances, *Toxicol Lett* 96-97 (1998) 253-261.
- Squadrito, G. L., Cueto, R., Dellinger, B., Quinoid redox cycling as a mechanism for sustained free radical generation by inhaled airborne particulate matter, *Free Radic Biol Med* 31(9) (2001) 1132-1138.
- E. Suzuki, High - resolution scanning electron microscopy of immunogold-labelled cells by the use of thin plasma coating of osmium", *Journal of Microscopy* 208 (3) (2002) 153-157.
- Takahasi, K., Yoshida, M., Hagiwara, Y., Kondoh, K., Takano, Y. and Yamashita, Y. Titanium and/or titanium alloy sintered friction material. US Pat. 5922452 (1999) (United States Patent and Trademark Office).
- Taylor, A. J., Taylor, S. K., Hubbard, D. A. and Lotfipour, M. Friction pads for use in disc brakes. US Pat. 5725077 (1998) (United States Patent and Trademark Office).
- Terzano, C., Di Stefano, F., Conti, V., Graziani, E. & Petroianni, A., Air pollution ultrafine particles: Toxicity beyond the lung, *European Review for Medical and Pharmacological Sciences*, 14 (10) (2010) 809-821.
- Thematic Strategy on Air Pollution - Commission of the European Communities (2005) www.central2013.eu

- Thorpe, A., Roy, M. H., Sources and properties of non-exhaust particulate matter from road traffic: A review, *Science of the Total Environment*, 400 (2008) 270-282.
- R. Thornton, T. Slatter, A.H. Jones, R. Lewis, The effects of cryogenic processing on the wear resistance of grey cast iron brake discs, *Wear* 271 (2011) 2386-2395.
- Rongping Yun, Peter Filip, Yafei Lu, Performance and evaluation of eco-friendly brake friction materials, *Tribology International* 43 (2010) 2010-2019.
- USEPA - United States Environmental Protection Agency (2012).
- Vaclav Roubicek a, Helena Raclavska a, Dagmer Juchelkova a, Peter Filip, Wear and environmental aspects of composite materials for automotive braking industry, *Wear* 265 (2008) 167-175.
- Vlastimil Matejka, Zhezhen Fu, Jana Kukutschova, Shicheng Qi, Shengling Jiang, Xiaoa Zhang, Rongping Yun, Miroslav Vaculik, Marie Heliova, Yafei Lu, Jute fibers and powderized hazelnut shells as natural fillers in non-asbestos organic non-metallic friction composites, *Materials and Design* 51 (2013) 847-853.
- Wahlin, P., Berkowicz, R., Palmgren, F., Characterization of traffic-generated particulate matter in Copenhagen, *Atmospheric Environment*, 40 (12) (2006) 2151-2159.
- Warren, R. *Ceramic-Matrix Composites*, (1992) 2 (Blackie, New York).
- WHO - World Health Organization, 2000. Particulate Matter, Chapter 7.3; WHO Regional Publications, European Series: Copenhagen, Denmark (2012) 1-40.
- J. Wilzer, S. Weber, Ch. Escher, W. Theisen, On the relationship of heat treatment, microstructure, mechanical properties, and thermal conductivity of tool steels, *TOOL* (2012): Proceedings of the 9th international tooling conference, developing the world of tooling, Leoben.
- Wirth, D. Eggleston, R. Whitaker, A fundamental tribochemical study of the third body layer formed during automotive friction braking, *Wear* 179 (1-2) (1994) 75-81.
- W.L. Guesser, et al., Production experience with compacted graphite iron automotive components, in: Proceedings of the AFS Congress, Dallas, 2001.
- Wahlström J, Söderberg A, Olander L, Jansson A, and Olofsson U., A pin-on-disc simulation of airborne wear particles from disc brakes. *Wear* 268 (2010) 763-769.
- Wahlström J, Olander L, and Olofsson U., A pin-on-disc study of automotive disc brake materials focusing on airborne wear particles. *Journal of Tribology* (2010). Paper Id: TRIB-10-1122.
- Wahlström J, Gventsadze D, Olander L, Kutelia E, Gventsadze L, Tsursumia O, and Olofsson U, A pinon-disc investigation of nanoporous composite-based and conventional brake pad materials focusing on airborne wear particles, *Tribology International*, 44 (12) (2011) 1838-1843.
- J. Wahlström, U. Olofsson, A. Jansson and L. Olander, Airborne Wear Particles Emissions from Commercial Disc Brake Materials – Passenger Car Field Test, *TRITA – MMK 2008:21 ISSN 1400-1179* (2008).
- X. Xin, C. Guangxu, L. Feiqing, Research progress of friction properties for fibre reinforced resin matrix composite materials, *J. Mater. Sci. Eng.*, 23 (3) (2005) 457–461.
- Yamashita, Y., Nakagawa, M., Ibuki, M. and Kishimoto, H. Friction material for making brake pads. US Pat. 5266395 (1993) (United States Patent and Trademark Office).
- Yesnik, M. A. Friction material comprising powdered phenolic resin and method of making same. US Pat. 5529666 (1996) (United States Patent and Trademark Office).
- R. Yun, P. Filip, Y. Lu, Performance and evaluation of eco-friendly brake friction materials, *Trib. Int.* 43 (2010) 2010-2019.